NASA CR-86096

R-613

APPLICATION OF INERTIAL NAVIGATION AND MODERN CONTROL THEORY TO THE ALL-WEATHER LANDING PROBLEM

by
Charles Broxmeyer, Duncan MacKinnon
and Paul Madden

June 1968

INSTRUMENTATION LABORATORY

MASSACHUSETTS INSTITUTE OF TECHNOLOGY

Cambridge 39, Mass.

R-613

APPLICATIONS OF INERTIAL NAVIGATION AND MODERN CONTROL THEORY TO THE ALL-WEATHER LANDING PROBLEM

by

Charles Broxmeyer
Duncan MacKinnon
Paul Madden

June 1968

INSTRUMENTATION LABORATORY
MASSACHUSETTS INSTITUTE OF TECHNOLOGY
CAMBRIDGE, MASSACHUSETTS 02139

Submitted by _____
Deputy Associate Director

Approved by _____
Associate Director

Approved by _____
Deputy Director

ACKNOWLEDGMENTS

The authors wish to acknowledge the sponsorship of Robert Pawlak, of the Electronics Research Center of the National Aeronautics and Space Administration, whose interest in the applications of inertial navigation to all-weather landing resulted in the establishment of the project reported herein. We are also indebted to Paul Fahlstrom of the Federal Aviation Agency whose interest in the problem was also instrumental in establishing the project.

We wish to acknowledge the contribution of Eugenia Freiburghouse in programming and running the simulations.

This report was prepared under DSR Project 55-30500, sponsored by the Electronics Research Center of the National Aeronautics and Space Administration through Contract NAS 12-602 with the Instrumentation Laboratory of Massachusetts Institute of Technology in Cambridge, Massachusetts.

The publication of this report does not constitute approval by the National Aeronautics and Space Administration of the findings or the conclusions contained therein. It is published only for the exchange and stimulation of ideas.

R-613

APPLICATIONS OF INERTIAL NAVIGATION AND MODERN CONTROL THEORY TO THE ALL-WEATHER LANDING PROBLEM

ABSTRACT

This report investigates (a) the implications of inertial navigation for the automatic landing problem, and (b) the attainment of system performance criteria through the application of certain nonlinear control system techniques.

A procedure based on estimation theory is developed for systematically correcting measured position and velocity data using Instrument Landing System (ILS) radio beams as absolute references. The corrected inertial data provides the basis for the design of improved lateral and vertical position control systems.

Additional improvements to the control system design are achieved by the addition of nonlinear reference flight path generation (utilizing the theory of optimal control) and simultaneous control of several reference variables.

It is shown, by comparison with conventional systems, that the above design concepts yield improved response characteristics and minimize the sensitivity to external disturbances.

In addition to the lateral and vertical channel control problems, the flare-out and decrab control problems have been considered.

A comprehensive automatic landing system has been synthesized and digitally simulated using the dynamics of the Boeing B-2707 Phase IIC Supersonic Transport. The vehicle model includes important nonlinear terms and the effect of an unsteady atmosphere. The improved landing system characteristics are compared with those of a landing system of conventional configuration which has been designed for the same vehicle.

by C. Broxmeyer
D. MacKinnon
P. Madden

June 1968

TABLE OF CONTENTS

TABLE OF CONTENTS (Cont)

TABLE OF CONTENTS (Cont)

TABLE OF CONTENTS (Cont)

CHAPTER 1

INTRODUCTION

1.1 Introduction

Routine all-weather landing of transport aircraft is one of the outstanding unsolved problems of present-day technology. The importance of the problem and its implications both for passenger safety and for economic operation of airlines have been recognized for decades. Now that the jumbo-type transport and the supersonic transport are soon to be introduced into passenger service the problem of all-weather landing may be considered to be a critical factor limiting the full employment of these aircraft.

Over the past ten years, important strides have been made in the direction of the goal of all-weather landing. Of these, the most important has undoubtedly been the actual implementation of aircraft control systems which use Instrument Landing System (ILS) information and which have successfully performed thousands of automatic landings. An outstanding example is the system developed by the Blind Landing Experimental Unit (BLEU) of the Naval Aircraft Establishment, United Kingdom (see ref (1)). It is highly probable that the basic concepts of control in what might be termed a classical automatic landing system such as the BLEU system will provide the conceptual framework for the systems that will eventually be adopted. It does not appear, however, that systems exist which will provide the invariable accuracy, reliability and independence from external disturbances, which will be mandatory for routine all-weather landing of transport aircraft.

The point of view of the study described in this report is twofold. The study is concerned with the implications of inertial navigation technology for the all-weather landing problem. As a corollary, the study is concerned with the application of control theory, both classical and modern, for the effective utilization of the inertial equipment. The study is directed particularly towards the development of an all-weather landing system for the supersonic transport (SST). The SST presents a particularly challenging landing problem as a result of its high approach speed and its aerodynamic characteristics. It should be emphasized, however, that the results of the study may be applied to any aircraft.

Over the past twenty years, an increasingly sophisticated technology of inertial navigation and guidance systems has grown up. This technology has been grounded on the continuous development of extremely precise reference components, principally floated gyros and accelerometers and a parallel development of support technology, such as gimbal structures, angular encoders, and thermal control systems. The concurrent advances in computer technology have been indispensible to the rapid advances made in inertial systems. The developments in inertial navigation and guidance have been almost entirely motivated by military requirements. While the utility of inertial navigation systems for commercial aircraft has been recognized, the participation of commercial aircraft users in inertial navigation development has been a minor factor because of the costs involved. It is now considered, however, that the accuracy, reliability and production costs of inertial navigation equipment originally developed for military purposes are such that they are appropriate for commercial use. Plans for the large commercial transports soon to be introduced invariably include one or more inertial navigation systems per aircraft. It is planned, for example, that the SST will carry three inertial navigation systems.

Search of the available literature fails to show that any significant application of inertial navigation technology has been made to the automatic landing problem. A primary purpose of the present study, as noted, has been to demonstrate, by computer simulation, the implications of inertial navigation for the automatic landing problem. On the basis of work performed to date it is believed that significant advantages will accrue from appropriate use of inertial navigation equipment. This contention is fully described and documented in the subsequent chapters.

1.2 Conventional Automatic Landing Systems*

The landing of a transport aircraft, whether automatic or pilot controlled, can be broken into the following phases:

1. Acquisition by the aircraft of the line defined by the intersection of the localizer and glide slope beams.
2. Traverse of the reference line to a point about seventy feet from the ground.
3. Pitch-up of the aircraft to reduce the velocity at the time of impact with the ground. This phase is called FLAREOUT.

*See refs (1), (2), and (3)

4. Yaw of the aircraft to align the longitudinal axis with the vertical plane containing the velocity vector. The velocity vector must be oriented in the direction of the runway center line. This phase is called DECRAB.

5. Touchdown of the aircraft.

6. Rollout along the runway.

In a pilot-controlled landing, items 1 through 6 are accomplished by the pilot through:

1. Inspection of an instrument which displays the localizer and glide-slope receiver outputs. Ideally the instrument displays angular deflections of the aircraft from the planes of the localizer beam and the glide slope beam. The apexes of the angles measuring the deflections are at the localizer antenna, which is usually about a thousand feet beyond the far end of the runway, and at the glide-slope antenna which is along the runway and is usually about a thousand feet from the near end. The relationships are illustrated in Fig. 1.2-1.

2. Inspection of visual cues from other instruments and from the local geography.

Below an altitude of one hundred feet visual contact must be established with the runway, if this has not been accomplished before. If visual contact is not established, the pilot executes a missed-approach procedure.

In an automatic approach and landing, the typical procedure followed is:

1. The pilot sets the aircraft to intercept the localizer beam at a point about three miles beyond the outer marker. The intercept angle is nominally 45 degrees. Utilizing the signal from the localizer receiver, the aircraft control system enables capture of the localizer beam by the aircraft.

2. When the signal from the glide-slope receiver is sufficiently small the pilot engages the glide-slope control system, and the glide-slope beam is captured by the aircraft. The aircraft is now automatically flying a course which intersects the runway at an angle of about three degrees.

3. Below altitudes of about 100 feet, the glide-slope beam is not considered to be reliable. At this altitude the glide-slope channel is disconnected and the aircraft is maintained at a fixed pitch angle to an altitude of about 70 feet. Pitch control below 100 feet is determined by the output of a radio altimeter.

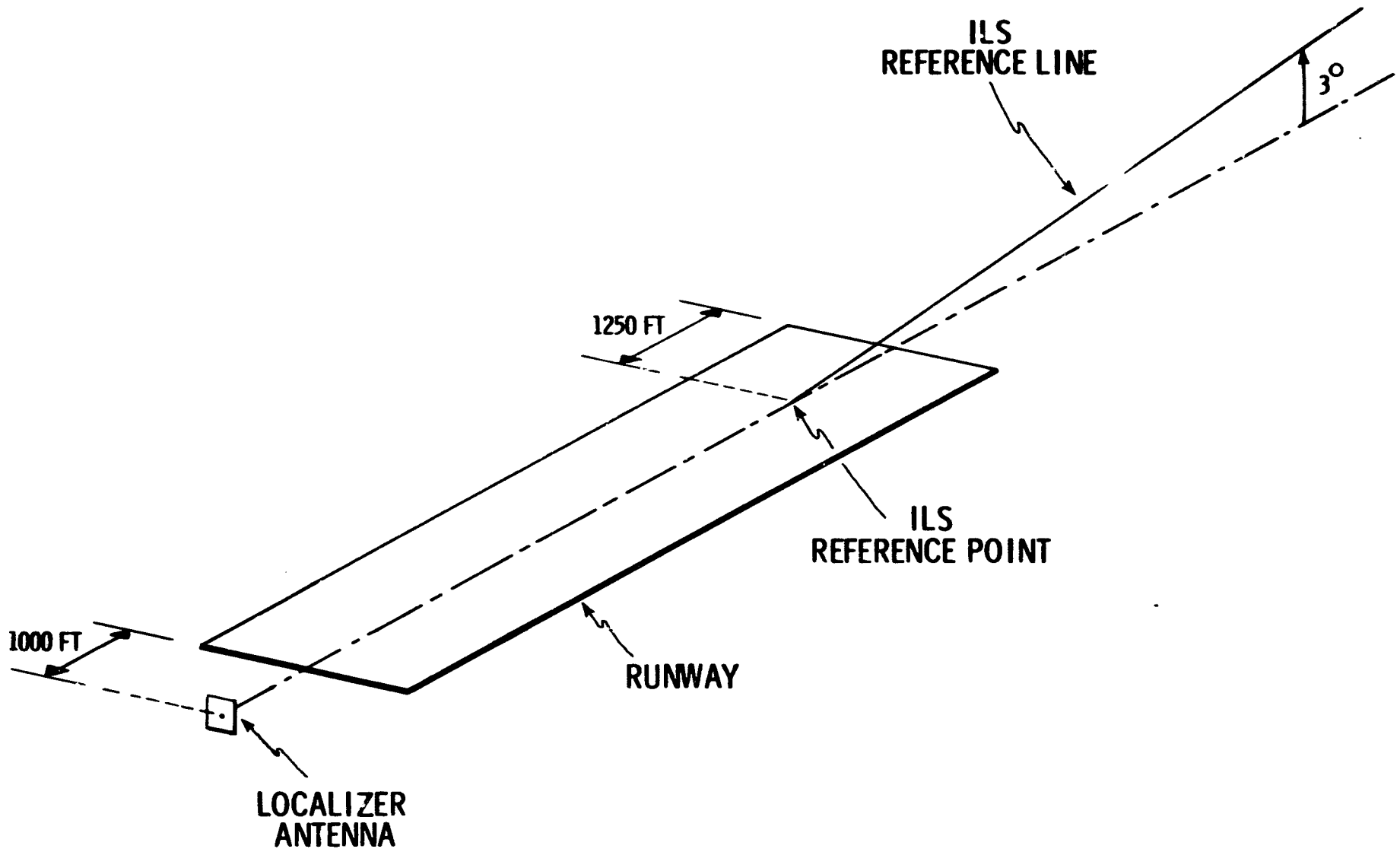

Fig. 1.2-1 ILS system geometry.

4. At an altitude of about 70 feet, the flareout maneuver begins, and at a lower altitude the decrab maneuver is initiated.
5. Just prior to touchdown, the pilot disconnects the localizer signal and establishes manual control of aircraft lateral motion.
6. After touchdown the pilot completes the rollout manually.

The primary means of automatic control are seen to depend on the outputs of the localizer receiver, glide-slope receiver and radio altimeter.

During traverse of the reference path, the outputs of the localizer and glide-slope receivers serve as error signals as shown in Fig. 1.2-2. Each receiver output is processed by a device called a coupler, and the output of the coupler is applied as an input to the aircraft autopilot. The coupler normally provides three functions:

1. Direct connection of the error signal to the autopilot through a variable gain.
2. Integration (or phase lag).
3. Differentiation (or phase lead).

Items 1, 2 and 3 are standard techniques conventionally applied to closed-loop systems. The purpose of the integration is to improve the low-frequency response by allowing the system to reach a settled state, without error, in the presence of a steady perturbation such as a trim error or windshear. The purpose of the phase lead is to stabilize the system and otherwise improve the dynamic performance. A detailed discussion of a conventional automatic landing system is presented in Appendix A ; while part of Chapter 2 contains a simplified discussion of a conventional lateral position control system.

1.3 Performance Criteria for Automatic Landing Systems

Before the question of improving a system is approached, it is important to establish the exact nature of the indices which will be used to measure performance. These criteria should reflect the qualities which are normally desirable in flight control systems. In addition, special performance measures must be introduced which pertain to the problems peculiar to automatic landing. A set of measures which reflect these goals are:

1. Sensitivity to environmental disturbances.
2. Accuracy of flight relative to a desired reference trajectory.
3. Control effector activity caused by noise.
4. Physical limitations imposed by the aircraft structure.
5. Human factors.

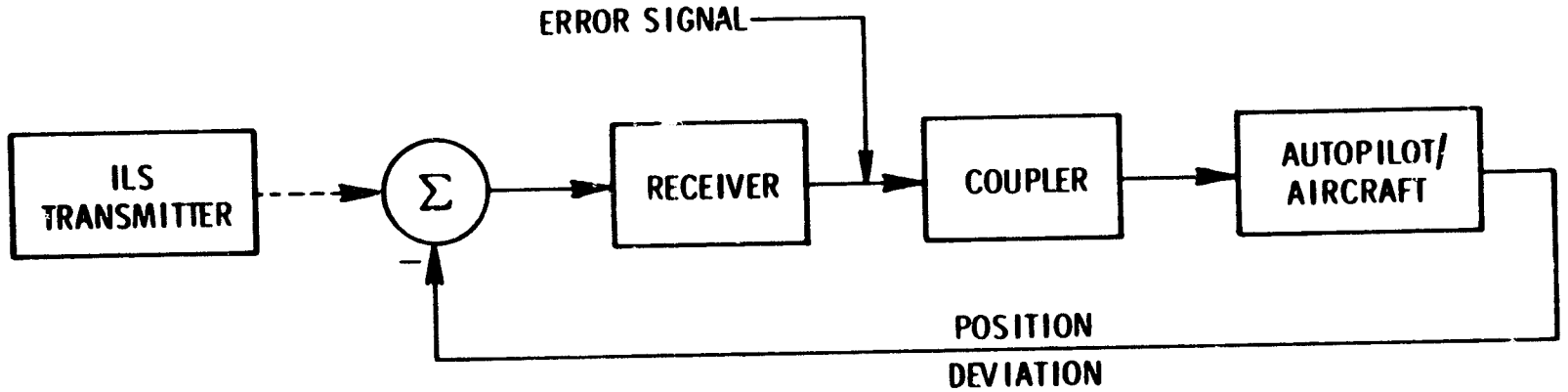

Fig 1.2-2 Simplified block diagram of an automatic landing system.

The first two performance measures deal specifically with landing accuracy. A reduction in the effects of external disturbances ensures that landings may be repeated with small dispersion in spite of large changes in ambient atmospheric conditions. The ability to track a desired path accurately is obviously a particularly important item and will undoubtedly provide a key to winning the confidence of aircrews and the acceptance of the new automatic landing systems by the airlines. Accurate path tracking also provides the greatest margin of safety, since a comparatively small deviation from the path may be interpreted as an incipient failure and an appropriate warning transmitted to the pilot.

Control effector activity resulting from noise levels in the sensors which provide the information for control-loop closure must be restricted to a fairly low level to reduce wear on the effectors, decrease drag and limit undesired inputs into the pilots controls.

The control system must also operate without exceeding the structural limitations of the vehicle. This implies control within a particular flight envelope and special care to ensure that the flexible bending modes of the vehicle are not excited.

Human factors are particularly important in a passenger aircraft. Restrictions on variables such as roll, roll rate and vertical acceleration must be incorporated into the design. An automatic landing system should optimize items 1 through 5 while working within these restrictions.

The above criteria may be interpreted as a set of specific performance requirements applicable to each control stage of an automatic landing. Such a set of specific requirements is given in Table 1.3-1.

Table 1.3-1

List of Specific Performance Requirements

Phase	Requirement
Acquisition	1. Acquire the ILS localizer and glide-slope centers as quickly as possible with minimum overshoot. 2. Perform this maneuver within the restrictions imposed on roll and roll rate.
ILS Reference Line Tracking	1. Minimize the error between the actual path of the aircraft and the ideal location of the ILS reference line.
Flareout	1. Minimize the error between a desired vertical velocity profile and the actual vertical velocity profile.
Decrab	1. Minimize the lateral components of aircraft velocity and position at touchdown. 2. Minimize the angular difference between a vertical plane through the runway center line and the aircraft's longitudinal axis at touchdown. 3. Attempt to achieve zero roll angle at touchdown.
Rollout	1. Minimize the distance between the path of the aircraft and the runway center line.

1.4 Methods of Improving Automatic Landing System Performance

To the end of satisfying the performance criteria discussed in the preceding section, this report introduces the following five concepts:

1. Inertial stabilization of the aircraft control system.
2. Inertial filtering of the ILS reference beams.
3. Nonlinear trajectory generation.
4. Command signal processing.
5. Generalized trajectory control.

Items 1 through 5 can be discussed independently, but will in general react with each other and with other control system aspects such as the response functions of accessible and inaccessible elements of the control system. In particular, items 1 and 2 have significant implications for the following important item from conventional control theory:

6. Open-loop gain maximization.

1.5 Open-Loop Gain

Two important criteria discussed in Section 1.3 are minimization of the effect of environmental disturbance on the system and ability to follow a desired trajectory precisely. It is known from control theory that, in general, both goals are reached by requiring the open-loop gain of the system to be as large as possible. For the simple control system shown in Fig. 1.5-1 the open-loop gain is the modulus of the open-loop transfer function

$$Y(s) = G(s)\,H(s)$$

at an arbitrary reference frequency $s = i\omega_o$. The open-loop transfer functions for the lateral and longitudinal control systems are defined precisely in the subsequent chapters.

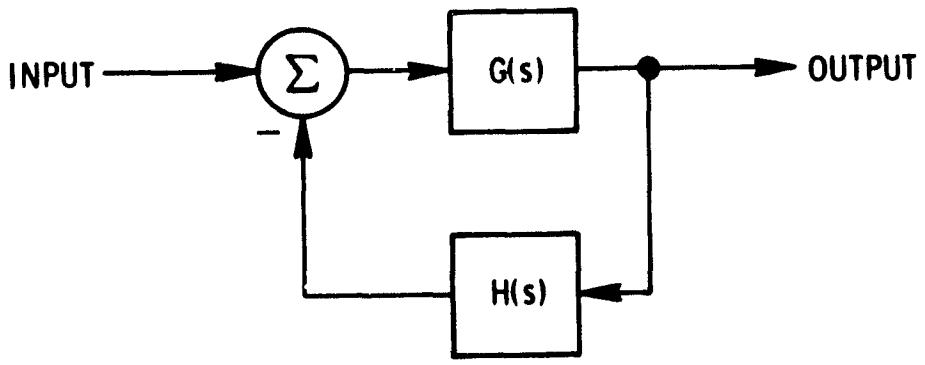

Fig. 1.5-1 Simple feedback control system.

The items which limit the open-loop gain are

1. The basic dynamic characteristics of the aircraft and its effectors.

   For a given fixed element in any control system, there is a limit on the open-loop gain that can be achieved within reasonable physical constraints such as insensitivity to parameter changes and operation inside saturation levels. The above limitations apply in the noise-free case.

2. The nature of the signals which are available for control purposes.

   The aircraft displacement measured by the ILS receiver is noisy because of imperfections of the ILS beam structure. Noise is reduced by a filter in the ILS receiver, and a time lag is thereby introduced in the position information. Furthermore, an additional time lag must be introduced in the stabilization signal derived from the receiver output. The lags limit the open-loop gain that can be achieved in a stable system.

3. The permissible control effector activity resulting from sensor noise.

   Residual noise in the position and stabilization signals further restricts the gain because of the limitations that must be placed on effector activity.

4. Limitations on the magnitudes of variables, such as roll and roll rate, imposed by human factors.

   The magnitudes of the aircraft state variables have strong dependence on open-loop gain.

It is clear from the above discussion that the achievement of a significant improvement in automatic landing system performance depends on the possibility of obtaining precise, noise-free, lag-free information describing the state of the aircraft.

1.6 Inertial Stabilization of the Control System

It was noted in Section 1.2 that stabilization of a conventional automatic landing system is accomplished by operating on the ILS receiver output to produce

a lagged velocity signal and feeding this signal forward into the control system.

An inertial navigation system normally computes north and east velocity components. The velocity components can be resolved, or the inertial platform can be reoriented, to produce an unlagged lateral velocity signal to replace the stabilization signal obtained from the localizer receiver. The inertially-computed velocity is virtually noise free although it may contain a bias error.

In the vertical plane an analogous velocity signal can be obtained from an inertial system to stabilize the longitudinal control channel.

Although inertial navigation systems do not normally compute acceleration, a lagged acceleration can be determined inertially, in directions normal to the ILS reference line, and fed into the control system as an additional stabilizing input. The resultant system is illustrated in Fig. 1.6-1.

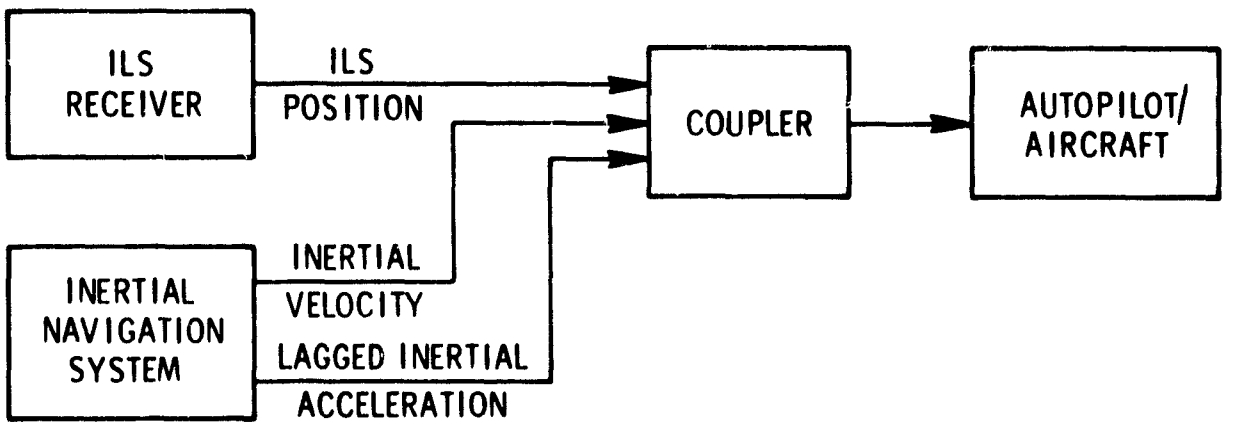

Fig. 1.6-1 Inertially-stabilized control system.

In the noise-free case, the availability of the above information permits significant increases in the open-loop gains of the two control channels. In the physical case it would not be practicable to implement the high gains because of the noise introduced into the system by the ILS position reference signal. Full use of the inertial equipment, however, as outlined in the next section, will permit the realization of a high-gain control system.

1.7 Inertial Filtering

Although the ILS beam structure contains noise, as shown in detail in ref 2, it has small bias error and is drift free. The inertially-generated position on the other hand is relatively noise free but may have a large bias error and is subject to low-frequency drift.

By suitably operating on the outputs of both the inertial system and the ILS receiver, corrected inertial position and velocity can be obtained which are significantly better than can be obtained from either device alone. The method will be

referred to as inertial filtering. In Chapter 3 two methods of inertial filtering are presented, and the implications for precise vehicle control are illustrated.

1.8 Command Signal Processing, Nonlinear Trajectory Generation and Generalized Trajectory Control

The impact of an increase in open-loop gain on certain other areas of the control problem must now be considered.

Saturation limits are always present in control systems. In an aircraft, saturation occurs in the form of rate and magnitude limitations on aerodynamic control surface travel, for example. The effect of the saturation is primarily reflected in limitations on the maximum angular acceleration and rate of change of acceleration that can be achieved. Higher gains tend to operate the effectors closer to saturation limits. Thus it is particularly important to investigate the implications of saturation on the improved control system design.

In Section 4.2 it is shown that effector saturation leads to an open-loop condition which increases the vehicle sensitivity to disturbances. Thus it is desirable to avoid situations which result in saturation. The effectors may be driven to their limits by signals arising from

1. Disturbances acting on the vehicle.
2. Reference inputs.

Saturation from the first source is controlled by reducing the magnitude of the open-loop gain. Thus an additional source of restrictions on the size of the adjustable gains is introduced. The second source of saturation may be controlled by two techniques which will be referred to as (1) command signal processing, and (2) nonlinear trajectory generation.

In a conventional automatic landing system, the command signal is the output of the ILS receiver and the reference is the ILS reference line. If the bandwidth of the receiver output is too high, the control system may be driven into saturation. Command signal processing is a technique for limiting bandwidth by applying an operator to the command signal. For small signals the output of the operator follows the input. The operator is designed so that the magnitude of the output and of selected derivatives of the output are limited. Examples of command signal processors are shown in the subsequent chapters.

In a conventional automatic landing system, the reference trajectory may be considered to be a step function, since an instantaneous translation of the vehicle to the ILS reference line would reduce the position error to zero. If the reference trajectory is modified from a step function to a trajectory designed to

reflect the contraints imposed upon vehicle behavior by saturation, it is apparent that saturation can be avoided. The above technique is referred to as nonlinear trajectory generation.

The process of nonlinear trajectory generation yields, in addition to the primary control variable which is position reference, other variables such as the roll and roll rate corresponding to the reference trajectory. The additional reference variables can be fed into the control system and compared with the corresponding measured variables for more precise control of the trajectory than can be obtained from a position reference alone. This process will be called generalized trajectory control.

1.9 Summary

This chapter has defined the problem of improving automatic landing system performance and has outlined the methods by which the improved performance is to be sought. Six concepts, listed in Section 1.4, have been isolated as having important potential for improvement of performance. The first two items listed involve the introduction of new (inertial) information into the system. The third, fourth and fifth items are new control system principles. The sixth item is a classical control system concept which has an important bearing on the problem.

In the following chapters the implications of the six concepts are explored in detail through system synthesis and confirming simulation. In Chapters 2 and 3 the inertial applications are introduced through the use of a simplified model of the aircraft and control system. In the subsequent simulations a precise formulation of the SST dynamics is employed.

CHAPTER 2

INERTIAL STABILIZATION

2.1 Introduction*

This chapter contains an introduction to the subject of stabilization of the aircraft control system through the use of output velocity and acceleration from an inertial navigation system. A contrast is made with a control system of conventional type. To keep the discussion simple and expose the essential aspects of the control problem, a number of simplifying assumptions are imposed. These are

1. Simplified aircraft dynamics.
2. Noise-free ILS.
3. Unlagged acceleration available.
4. Error-free inertial system.

The assumptions are not essential and are removed in the detailed development given in the subsequent chapters.

For both the conventional and inertially-stabilized systems, assumptions 1 through 4 lead to higher gains than are achievable in practice. The development, however, clearly illustrates the relative advantages of the inertially-stabilized system.

2.2 Aircraft Lateral Approach Dynamics

Lateral control of an aircraft is primarily achieved by modification of the roll angle. The precise behavior of the aircraft, under autopilot control, depends on the autopilot configuration and the aircraft dynamics. In this chapter an autopilot has been assumed which forces the yaw rate to be a specified function of the roll angle, thus insuring a coordinated turn in a non-accelerated air mass. As a result, the laws governing the behavior of the vehicle are particularly simple.

The force structure acting on the vehicle under the above circumstances is illustrated in Fig. 2.2-1. Rotation of the lift vector L through a roll angle ϕ results in a horizontal component of force F_y.

*This chapter is a summary of the material contained in the technical proposal which led to the current study.

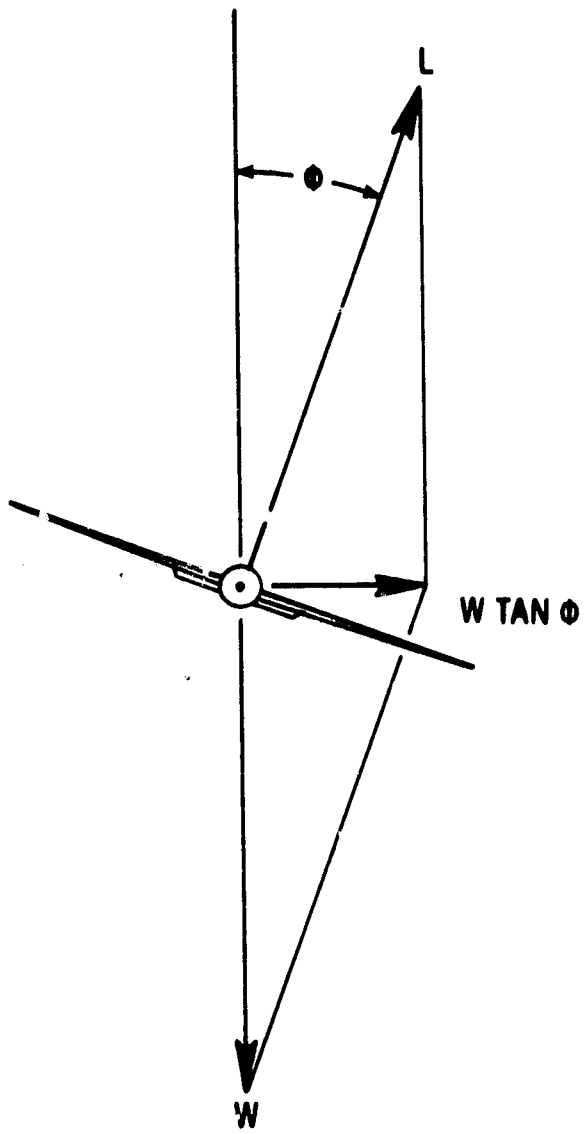

Fig. 2.2-1 Forces acting on an aircraft in a coordinated turn.

$$F_y = w \tan \phi \tag{2.2-1}$$

where w is the weight of the aircraft. In order to preserve equilibrium, this force is balanced by a centrifugal force:

$$F_y = \frac{w}{g} \frac{v_p^2}{R} \tag{2.2-2}$$

where R is the instantaneous radius of curvature of the flight path, v_p is the instantaneous velocity component along the longitudinal stability axis of the aircraft and g is the gravitational constant.

Solving Eqs (2.2-1) and (2.2-2) for R yields:

$$R = \frac{v_p^2}{g \tan \phi} \tag{2.2-3}$$

The yaw rate is

$$\dot{\psi} = \frac{v_p}{R}$$

$$= \frac{g \tan \phi}{v_p} \approx \frac{g}{v_p} \phi \tag{2.2-4}$$

The approximation (2.2-4) is valid for the small roll angles which would occur in the case of aircraft operated in accordance with commercial vehicle procedures.

Let a nominal flight path with azimuth ψ_o be defined as illustrated in Fig. 2.2-2. Then the component of aircraft velocity perpendicular to this path is given by:

$$\dot{y} = v_y = v_p \sin (\psi - \psi_o) \tag{2.2-5}$$

The lateral displacement relative to the localizer course is given by integration of v_y.

$$y = y(t_1) + \int_{t_1}^{t} v_y \, dt \tag{2.2-6}$$

For $\psi_o = 0$ the simplified aircraft dynamics may be summarized in the form

$$\dot{\psi} = \frac{g}{v_p} \phi \tag{2.2-7}$$

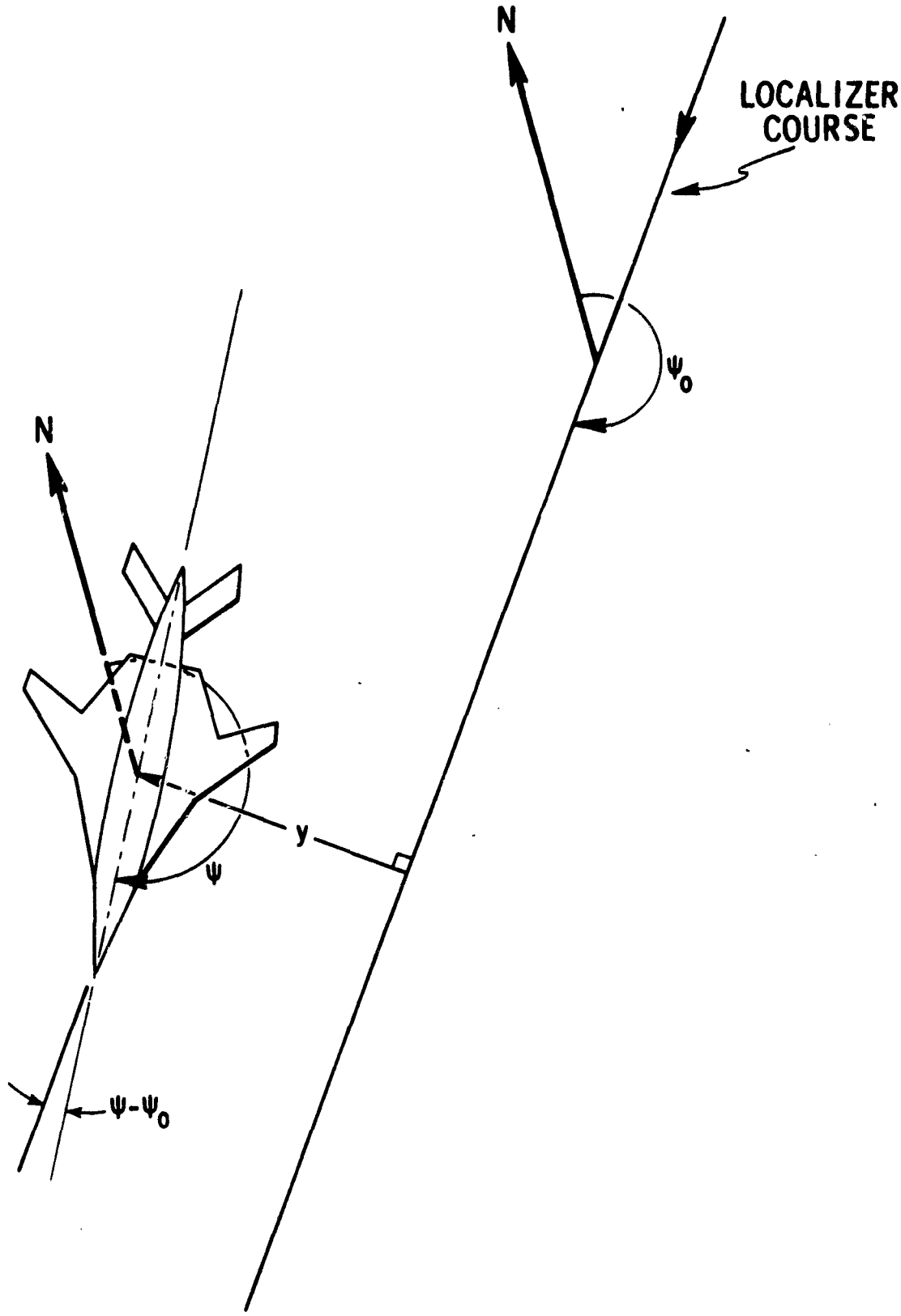

Fig 2.2-2 Aircraft flight path geometry.

$$\dot{y} = v_p \psi \tag{2.2-8}$$

When an aircraft flies through an environment subject to stochastic variations in lateral acceleration such as gusting, or deterministic variations such as windshear, the aircraft experiences acceleration. The total lateral acceleration may be approximated in the form

$$\ddot{y} = v_p \dot{\psi} + \dot{w}_y \tag{2.2-9}$$

The first term on the right-hand side is the rate of change of velocity resulting from change of heading, and the second term is air-mass lateral acceleration, where it is assumed that sideslip is negligible. When $w_y \neq 0$, Eq (2.2-9) replaces Eq (2.2-8).

2.3 Aircraft Roll Characteristics

In order to analyze and simulate the lateral control problem, it is necessary to define the relationship between desired roll angle and actual roll angle. This relationship is, in general, determined by the properties of the coupler/autopilot/airframe combination and may be specified by an appropriate set of differential equations. It is known that the relationship can be approximated by a second-order system of the form*

$$\frac{\phi}{\phi_c} = \frac{\omega_\phi^2}{s^2 + 2\omega_\phi \zeta_\phi s + \omega_\phi^2} \tag{2.3-1}$$

The validity of Eq (2.3-1) has been assumed for the preliminary analysis.

A list of typical parameters for the transfer function (2.3-1) is presented in Table 2.3-1 (ref 2). Analysis and simulation studies for this chapter were performed using the parameters for the Boeing 707.

*ref (3) page 17

Table 2.3-1 Transfer Function Parameters

Aircraft	Autopilot	Natural Frequency ω_ϕ rad/sec	Damping Factor ζ_ϕ
C-131	Sperry A12	1.7	0.9
707	Bendix	1.8	1.2
F86	Lear F5	1.8	0.5
B47	Sperry A12	1.2	0.9

2.4 ILS Receiver Characteristics

The lateral position information control is generated by the instrument landing system receiver. Two elements of the ILS system performance have a strong impact on control system design. The first is the filter that is used to smooth the position output signal of the receiver. For purposes of dynamic analysis, the receiver-filter combination may be approximated by a simple time lag. The second important item is the measurement by the receiver of angular rather than position deviations from the desired path. The measurement results in an inverse change in position loop gain as a function of distance from the localizer antenna. The receiver may be modeled by a transfer function of the form:

$$\frac{\theta_{ILS}}{y} = \frac{1/R}{s\tau_f + 1} \qquad (2.4\text{-}1)$$

where R is the range to the localizer antenna, τ_f is the characteristic receiver time constant, y is the aircraft position deviation and θ_{ILS} is the measured angular deviation. The variation in gain associated with Eq (2.4-1) can be corrected if R is known and for the purpose of this simplified analysis is ignored by writing

$$\frac{y_{ILS}}{y} = \frac{1}{s\tau_f + 1} \qquad (2.4.2)$$

A typical value, $\tau_f = 0.40$ seconds, was chosen for this investigation (see ref 3). As noted, the effect of spatial deformation of the reference path is not considered in the preliminary analysis, but is carefully considered in the subsequent develop-

ment.

2.5 Conventional Lateral Control of Aircraft Path

A simplified model of a conventional automatic landing system is illustrated in Fig. 2.5-1. The roll angle command signal is generated by operating on the ILS receiver output with a pure gain K_y, a proportional plus integral compensator with gain K_{iy}, and a lead network of gain $K_{\dot{y}}$. The lead network time constant τ_v, serves to eliminate some of the noise introduced by differeniation of the receiver output. Integral compensation serves to eliminate steady-state errors while the lead network improves damping and permits use of a somewhat higher value of position loop gain.

The gains K_y and $K_{\dot{y}}$ are selected for satisfactory time-domain dynamic response characteristics while the integral compensator gain is increased until the dynamic response starts to deteriorate. As a result, it is usually possible to ignore the integral compensator during dynamic analysis.

The maximum values of K_y and $K_{\dot{y}}$ are determined by the parameters τ_f, τ_v, ω_ϕ, and ζ_ϕ associated with the aircraft, the autopilot and the ILS receiver. The simulation results presented in Section 2.7 demonstrate that these restrictions are quite severe. The effect of the limitations is particularly highlighted by the response of the system to disturbances as indicated in Section 2.8.

2.6 An Inertially-Stabilized Control System

The gain restriction of the conventional automatic landing system depends on the time lags associated with the ILS receiver and the lead network. Suppose that inertially-measured velocity is available. Then the velocity time constant can be completely eliminated. If inertially-measured acceleration is available, additional stabilization can be obtained from this source.

The inertially-stabilized control system is illustrated in block diagram form in Fig. 2.6-1. Position information is derived from the ILS receiver as before. Now, however, velocity and acceleration signals from the inertial system are used to provide damping. For the configuration illustrated, it can be shown that the Nyquist limitation on the position gain K_y is virtually eliminated. It is stressed that in the practical case the gains will, of course, be limited by considerations such as high frequency dynamics ignored in the simplified model, the permissible aircraft dynamic range, inertial system errors, lag in the computed acceleration signal and noise of the localizer beam.

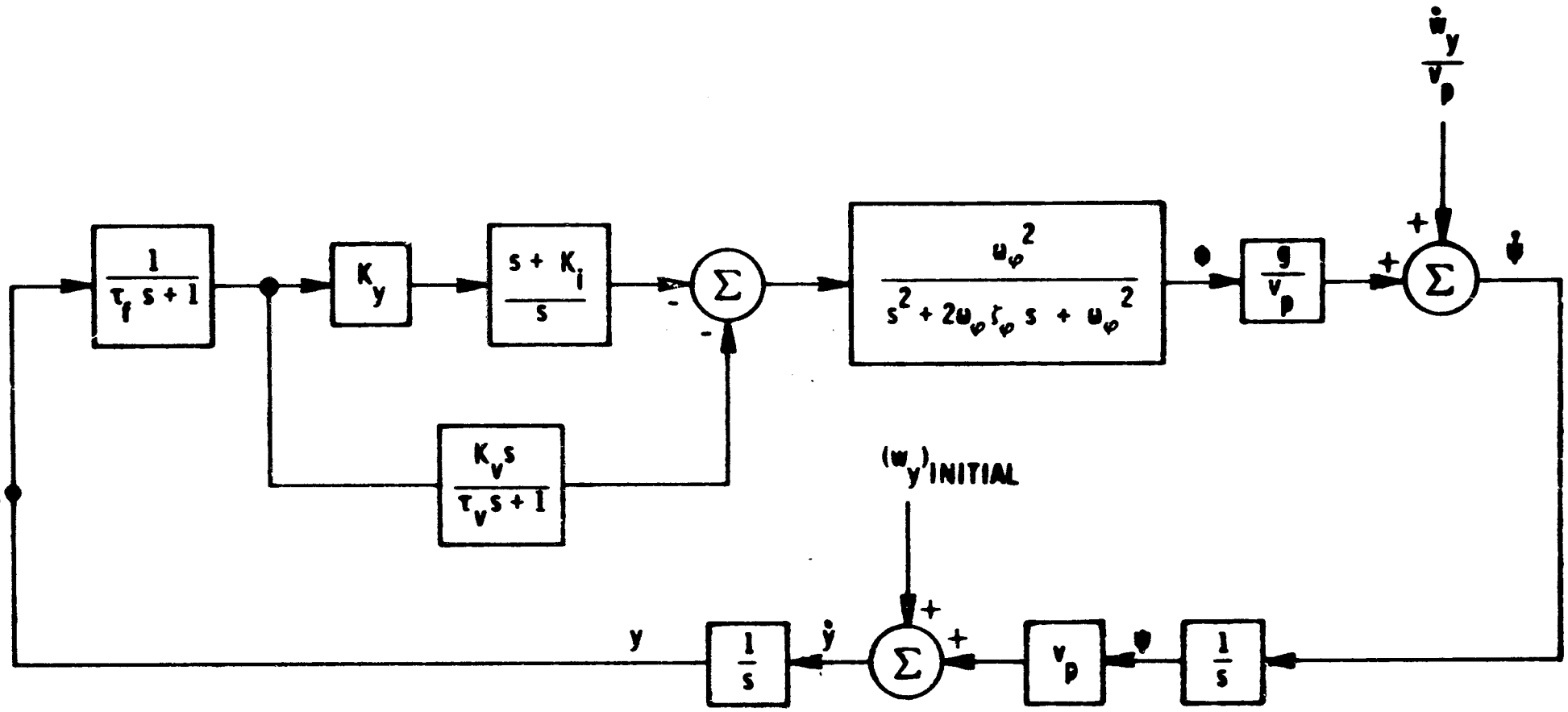

Fig. 2.5-1 Simplified model of a conventional automatic landing system.

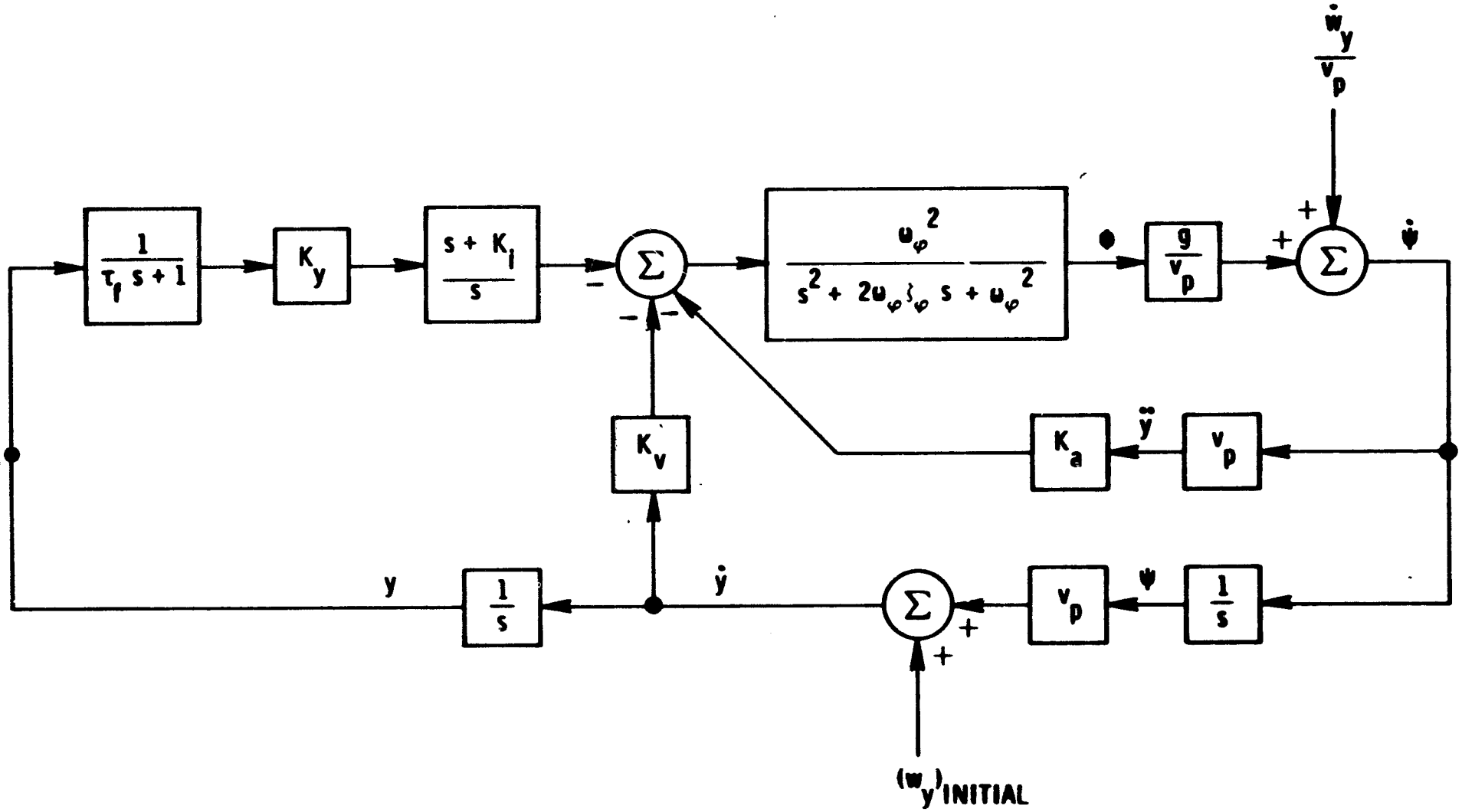

Fig. 2.6-1 Simplified model of an inertially-stabilized automatic landing system.

2.7 Simulation of Aircraft Lateral Control System

To select gain parameters for the systems diagrammed in Figs. 2.5-1 and 2.6-1, the following procedure was used:

1. The roll angle transfer function parameters given in Table 2.3-1 for the Boeing 707 and the receiver time constant 0.4 sec were taken as constraints.

2. The vehicle longitudinal velocity and the windshear were taken to be, respectively,

$$v_p = 200 \text{ ft/sec}$$

$$\dot{w}_y = 0$$

3. For each system, the gain $K_{\dot{y}}$ was selected by opening the position loop and observing the velocity response $\dot{y}$ to an initial condition $\dot{y}(0)$. The responses selected were those having fast settling time with negligible overshoot. The responses are shown in Figs. 2.7-1 and 2.7-2 and the results indicate the significantly larger open-loop velocity gain which may be achieved using inertial system data.

4. Utilizing the parameter values obtained in 3 the position loops were closed and the open-loop position gains were varied. The results are shown in Figs. 2.7-3 and 2.7-4. The increase in inertially-aided position gain is apparent from these results.

5. Values of gain K_{iy} for the integral compensation were determined in a manner similar to that used in 3 and 4. In this case it is important to minimize the effect of integral compensation on the dynamic response of the system. The results are shown in Figs. 2.7-5 and 2.7-6.

Parameters selected by the above procedure are summarized in Table 2.7.1

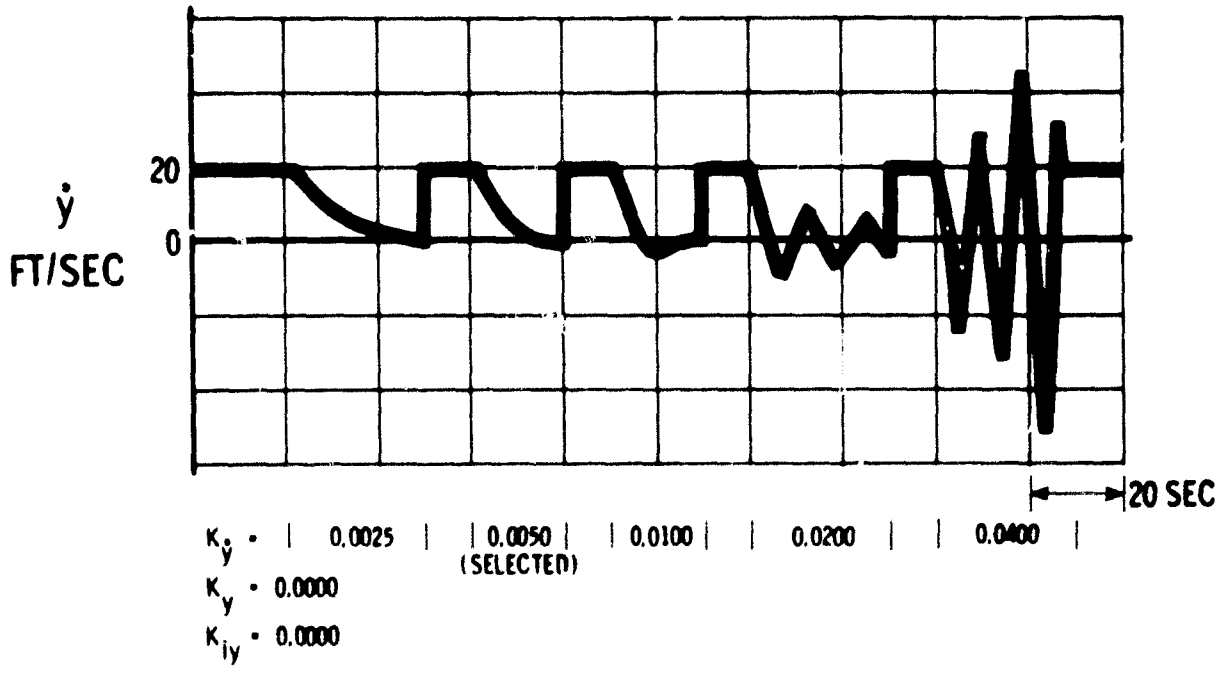

Fig. 2.7-1 Conventional system velocity responses.

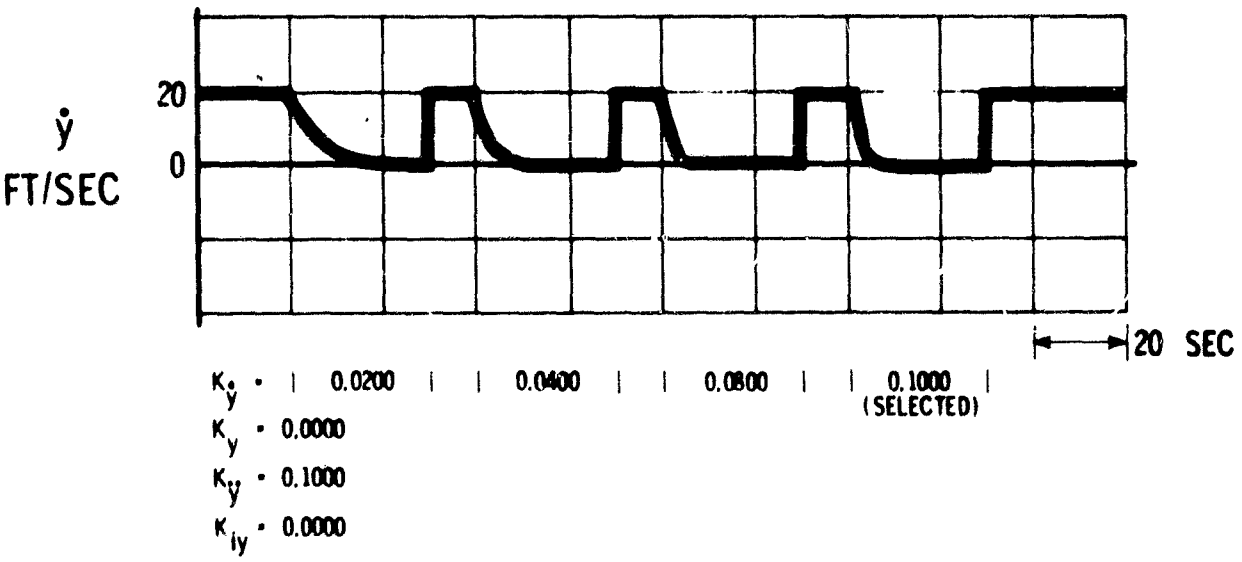

Fig. 2.7-2 Inertially-stabilized system velocity responses.

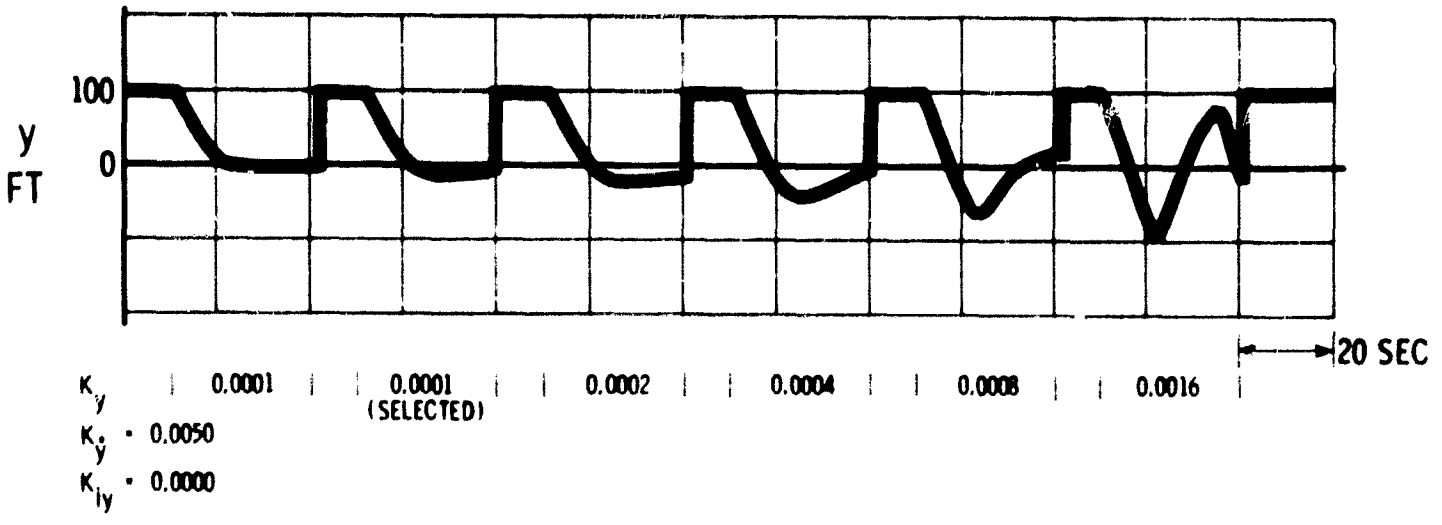

Fig 2.7-3 Conventional system position responses.

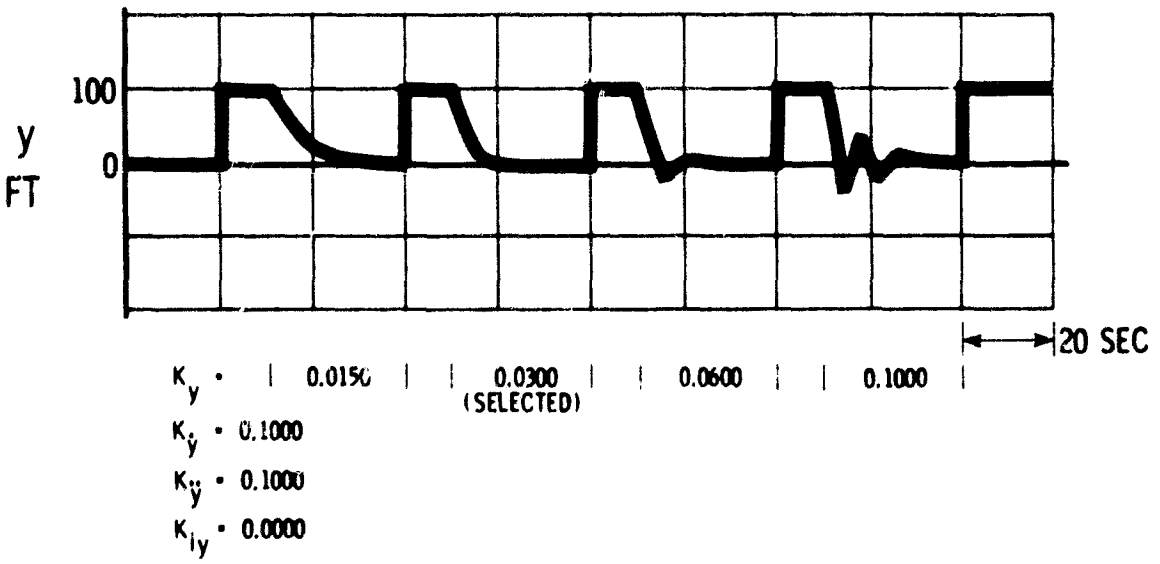

Fig. 2.7-4 Inertially-stabilized system position responses.

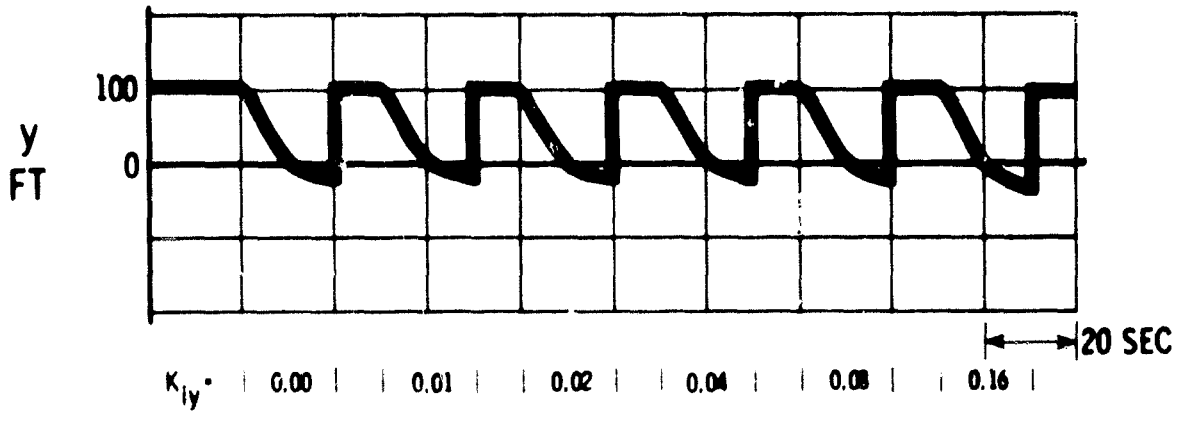

Fig. 2.7-5 Conventional system position responses with integral compensation.

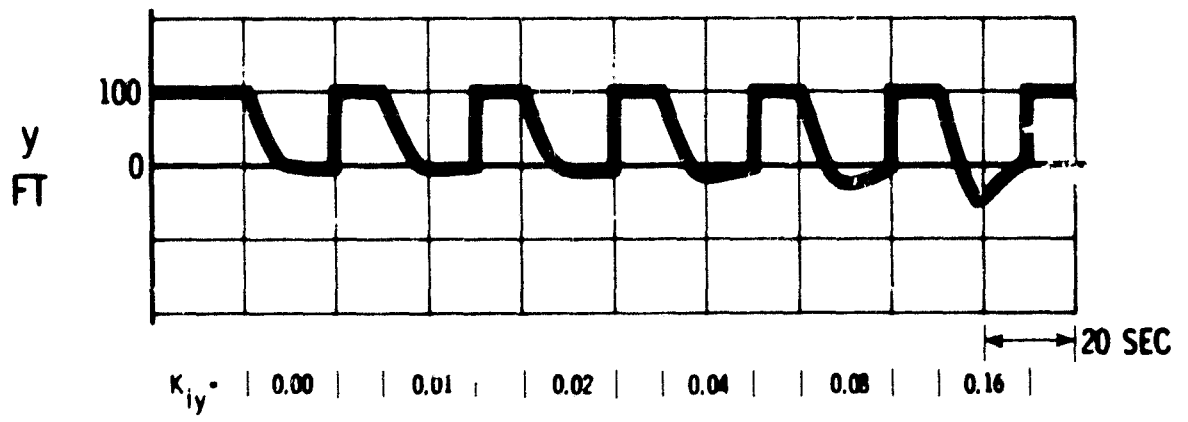

Fig. 2.7-6 Inertially-stabilized system responses with integral compensation.

Table 2.7-1

Summary of Automatic Landing System Simulation Gains

GAIN	CONVENTIONAL SYSTEM	INERTIALLY-STABILIZED SYSTEM
$K_{\dot{y}}$ rad/ft/sec^2	----	0.1000
K_y rad/ft/sec	0.0050	0.1000
K_y rad/ft	0.0001	0.0300
K_{iy} sec	0.05	0.02
ω_ϕ rad/sec	1.8	1.8
ζ_ϕ	1.2	1.2

The results of the above preliminary work are summarized in Fig. 2.7-7 where selected responses, without integral compensation ($K_{iy} = 0$), to an initial lateral position error of 100 feet are compared. The corresponding changes in the system variables roll, heading angle and lateral velocity, are also indicated. While these responses are qualitatively similar, the responses of the two systems to environmental disturbances are quite different.

Open-loop frequency response characteristics are shown in Fig. 2.7-8 for the parameters in Table 2.7-1. The responses shown are those obtained when the control loops shown in Fig. 2.5-1 and 2.6-1 are broken at point "A." The improvement in gain at all frequencies, obtained through the use of inertially-measured information, is reflected in a large increase in bandwidth as indicated in the closed-loop response functions shown in Fig. 2.7-9.

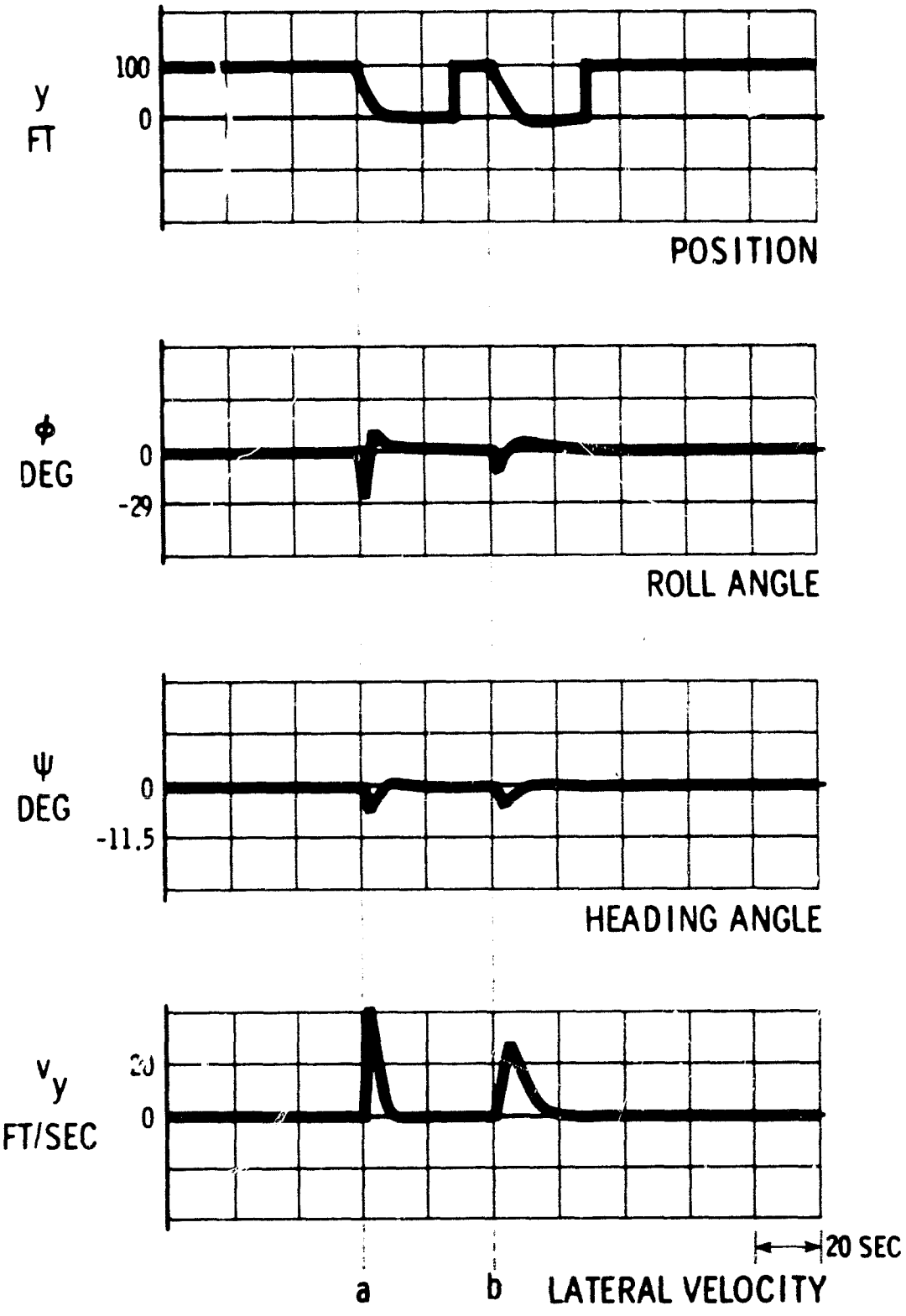

Fig. 2.7-7 Position responses of the inertially-stabilized (a) and conventional (b) systems with selected gains.

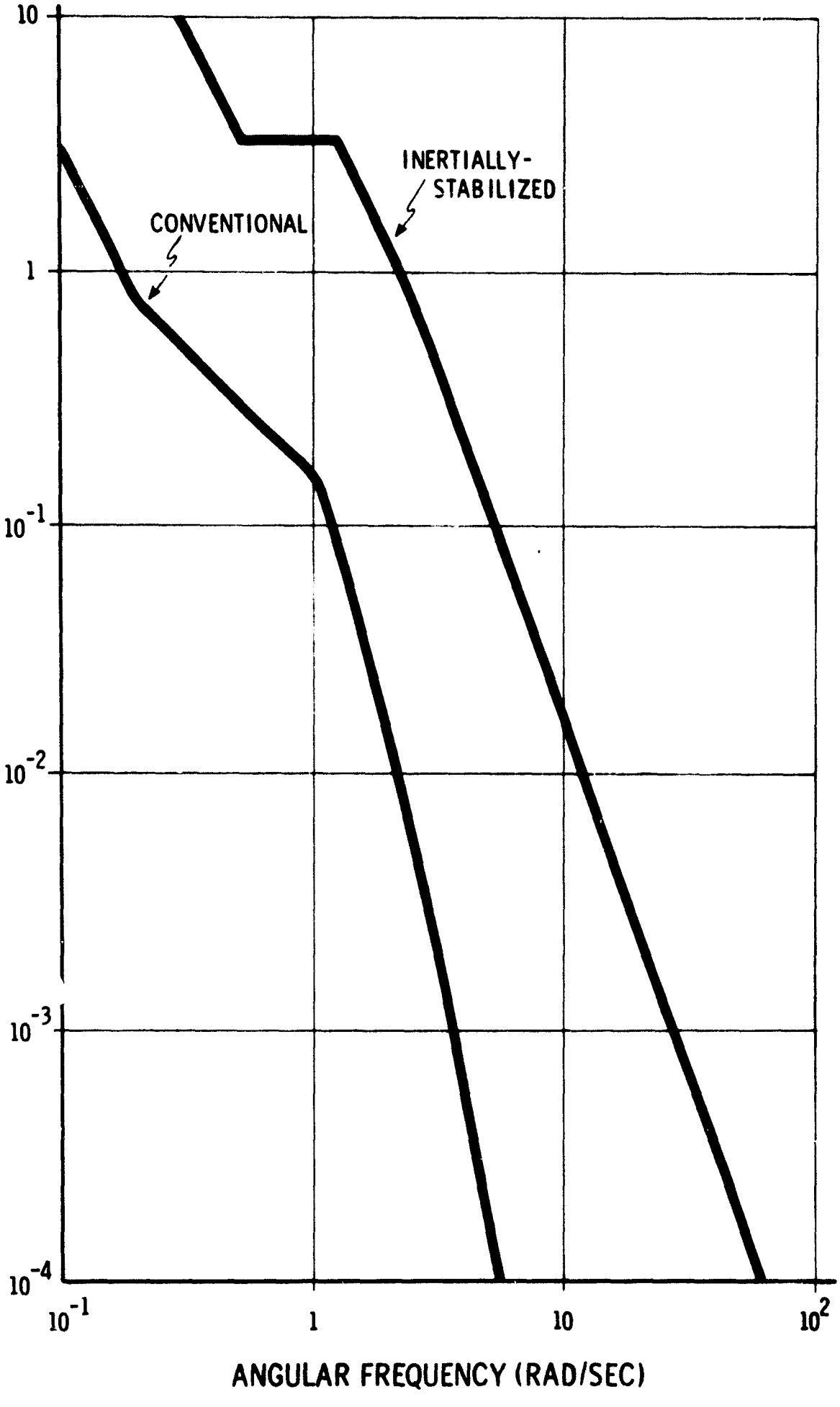

Fig. 2.7-8 Open-loop magnitude characteristics of the position control systems.

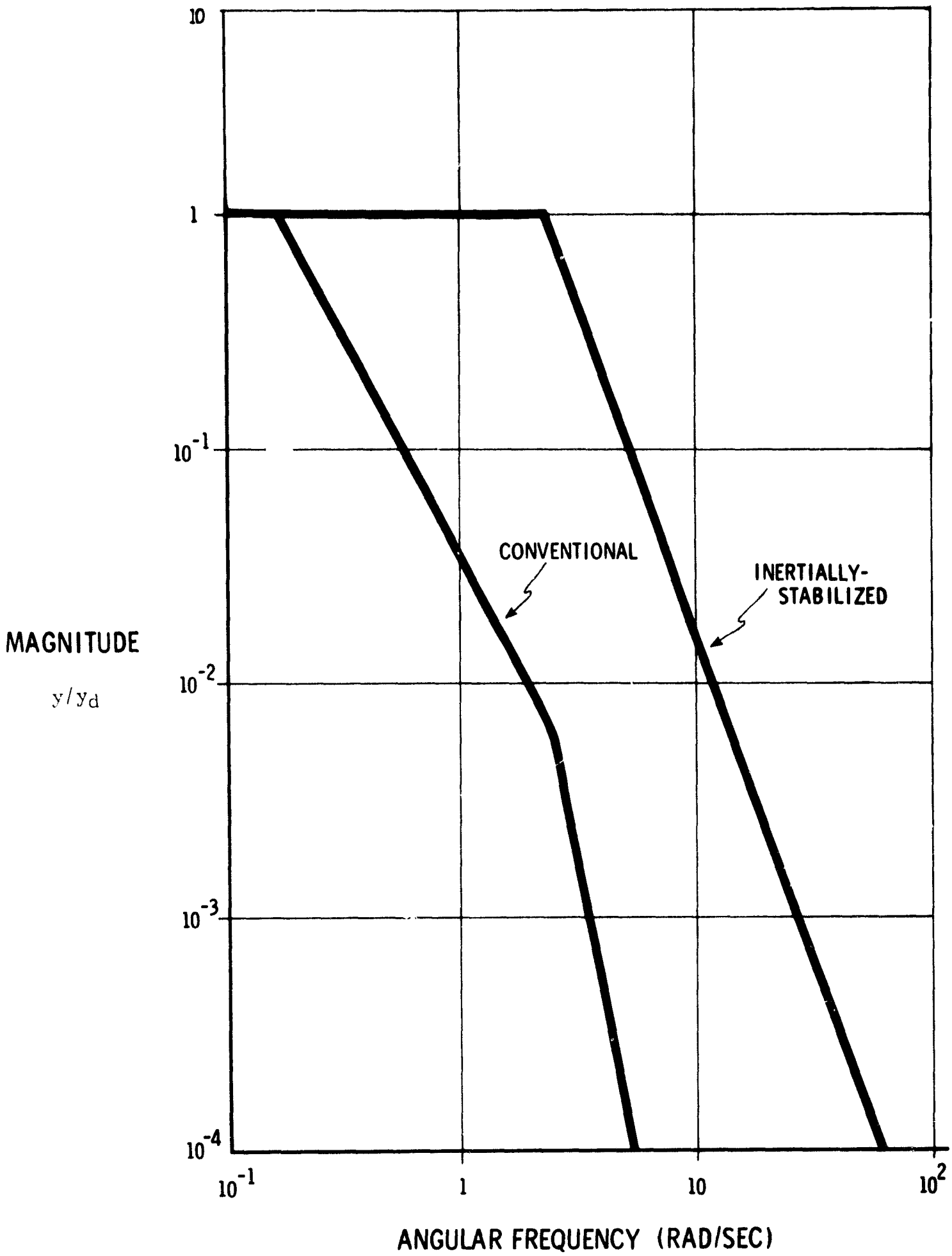

Fig. 2.7-9 Closed-loop position response magnitude characteristics.

2.8 Lateral Behavior in the Presence of Environmental Disturbances

Figure 2.8-1 is a simplified version of the diagram in Fig. 2.6-1. The transfer function relating the variation in lateral position to the disturbance can be obtained from the diagram. The transfer function is

$$\frac{y}{\dot{w}_y} = \frac{1}{s^2 + (L\omega_\phi^2 g/s^2 + 2\omega_\phi \zeta_\phi s + \omega_\phi^2)} \qquad (2.8.1)$$

where L is the transfer function of the receiver/coupler. From this expression it is apparent that the magnitude of the transfer function L should be as large as possible to minimize the change in y for a specified rate of change of air mass velocity $\dot{w}_y$.

The frequency response characteristics relating position to air mass acceleration input are shown, for the conventional and inertially-stabilized landing systems, in Fig. 2.8-2. The parameters listed in Table 2.7-1 define the curves. The asymptotic behavior of the characteristics at low and high frequencies, respectively, is

$$\lim_{\omega \to 0} \frac{y}{\dot{w}_y} = \begin{cases} \frac{1}{K_y g} & (K_{iy} = 0) \\ 0 & (K_{iy} \neq 0) \end{cases} \qquad (2.8\text{-}2)$$

$$\lim_{\omega \to 0} \frac{y}{\dot{w}_y} = 0 \qquad (2.8\text{-}3)$$

Of particular interest is the response of the vehicle to stochastic disturbances such as wind gusting. Most of the wind gust spectral energy is confined to frequencies below two ra ans per second. Noting that the magnitude response of the inertially-aided system to disturbances is approximately 1/20 that of the conventional system in this frequency range, it is apparent that the total lateral response power component due to wind gusts is reduced by a factor of 400 by the utilization of inertial data. This is a very significant improvement.

An important deterministic source of lateral position error is wind shear, a gradient of wind velocity with altitude. For the case whe e the direction of wind is transverse to the localizer direction, the acceleration of the local air mass is the product of the gradient $\partial w_y/\partial z$ of the transverse wind velocity and the rate of descent $\dot{z}$.

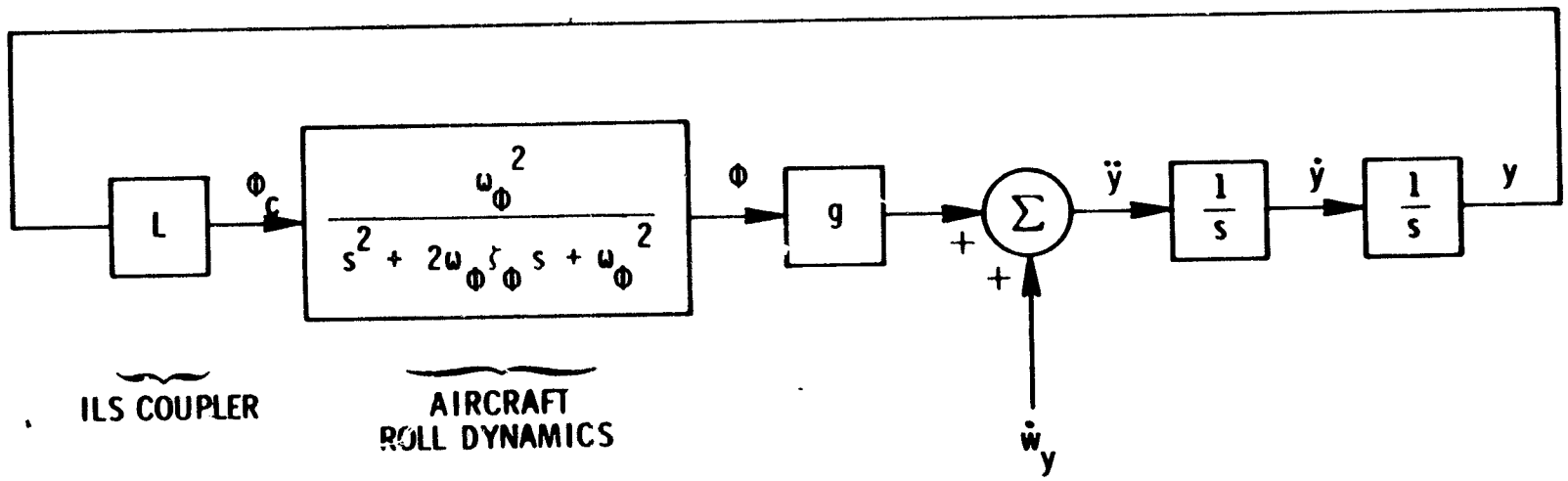

Fig. 2.8-1 Linear model of a lateral position control system.

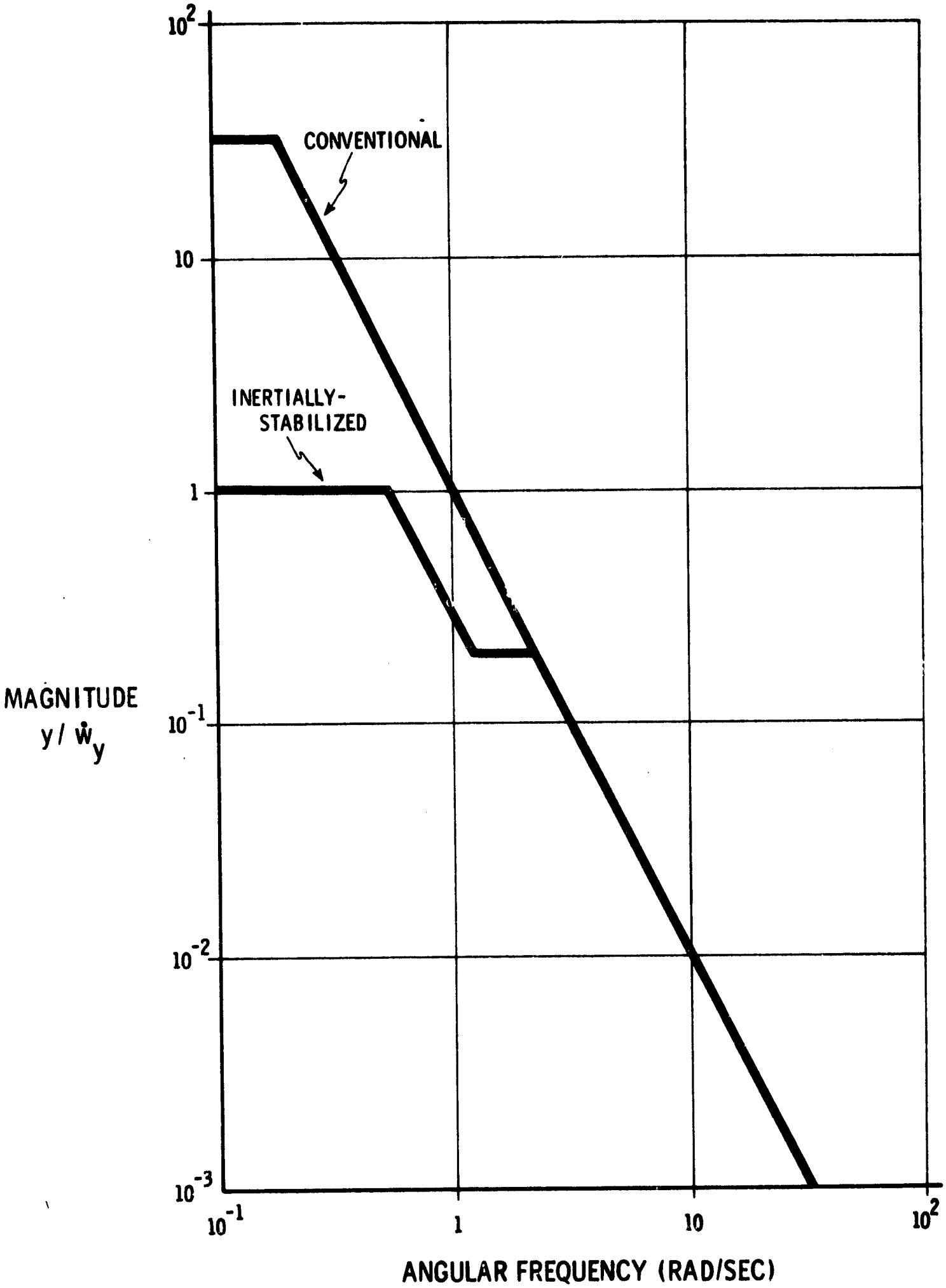

Fig. 2.8-2 Magnitude characteristics relating position response to air mass acceleration.

If Eq (2.8-1) is rewritten in the form

$$\frac{y}{\dot{w}_y} = H \tag{2.8-4}$$

then, when $(\partial w_y/\partial z)\dot{z}$ is constant, the limiting value of y is given by the final value theorem

$$\lim_{t \to \infty} y = \lim_{s \to 0} H(s) \frac{\partial w_y}{\partial z} \dot{z} \tag{2.8-5}$$

When integral compensation is not employed ($K_{iy} = 0$)

$$\lim_{t \to \infty} y = \frac{\frac{\partial w_y}{\partial z}}{K_y g} \dot{z} \tag{2.8-6}$$

Thus the steady-state error in position is inversely proportional to the open-loop position gain and directly proportional to the rate of change of air mass velocity.

The responses of a conventional, and an inertially-stabilized, automatic landing system to a constant air mass acceleration of 0.270 ft/sec^2 (resulting from an assumed wind shear gradient of 8 knots/100 ft and an assumed rate of descent of 2.0 ft/sec), were investigated using the analog simulation diagrams illustrated in Figs. 2.5-1 and 2.6-1 and the parameter values listed in Table 2.7-1. The results of the investigation without integral compensation ($K_{iy} = 0$) are illustrated in Figs. 2.8-3 and 2.8-5. Figures 2.8-4 and 2.8-6 illustrate the results for $K_{iy} \neq 0$. It will be noted that magnitude scales have been considerably reduced. The large reduction in error is a result of the increase in position loop gain allowed by introduction of the inertially-obtained information.

In the case where integral compensation is used ($K_{iy} \neq 0$), the steady-state error is:

$$\lim_{t \to \infty} y = 0 \tag{2.8-7}$$

While the application of proportional plus integral compensation does indeed result in zero steady-state error, the dynamic response characteristics may still be quite unsatisfactory as illustrated in Fig. 2.8-1. Tabulated response characteristics may be found in Table 2.8-1.

Table 2.8-1

Response Characteristics in an Air Mass
Subject to Constant Acceleration

SYSTEM	$\dot{w}_y = \left(\frac{\partial w_y}{\partial z}\right)\dot{z}$	Position loop gain K_{y_g} rad/sec^2	K_{iy} rad sec/ft	lim y $t \to \infty$	max y
CONVEN-TIONAL SYSTEM	0.270 ft/sec^2	0.00322	0.00	84.00 ft	84.00 ft
	0.270 ft/sec^2	0.00322	0.05	0.00 ft	35.00 ft
INERTIALLY-STABILIZED SYSTEM	0.270 ft/sec^2	0.90000	0.00	0.30 ft	0.30 ft
	0.270 ft/sec^2	0.90000	0.02	0.00 ft	0.26 ft

2.9 Implications of High Gains in Feedback Control Systems

The results presented in the preceding section have demonstrated that a significant improvement in performance can be achieved by increasing the gains associated with the automatic landing lateral control system. In the case considered, inertial system data in the form of vehicle lateral velocity and acceleration relative to the ILS course is used to increase the position loop gain by a factor of 280 for the model considered. Some implications of the large increase in gain are now considered.

In any investigation of lateral control of an aircraft, careful attention must be paid to limitations placed on the dynamic operating characteristics of the vehicle. Typical limitations are imposed by maximum lifting surface loadings, effector characteristics and passenger comfort. The limits may be interpreted in terms of restrictions on the magnitudes of the roll angle ϕ and the roll angular rate $\dot{\phi}$ for example. The difficulties associated with the limits can be illustrated as follows. Consider the case where the aircraft is in unaccelerated flight parallel to the localizer course and integral compensation is not used. The commanded roll angle ϕ_c is then equal to:

$$\phi_c = -K_y y_{ILS} \qquad (2.9\text{-}1)$$

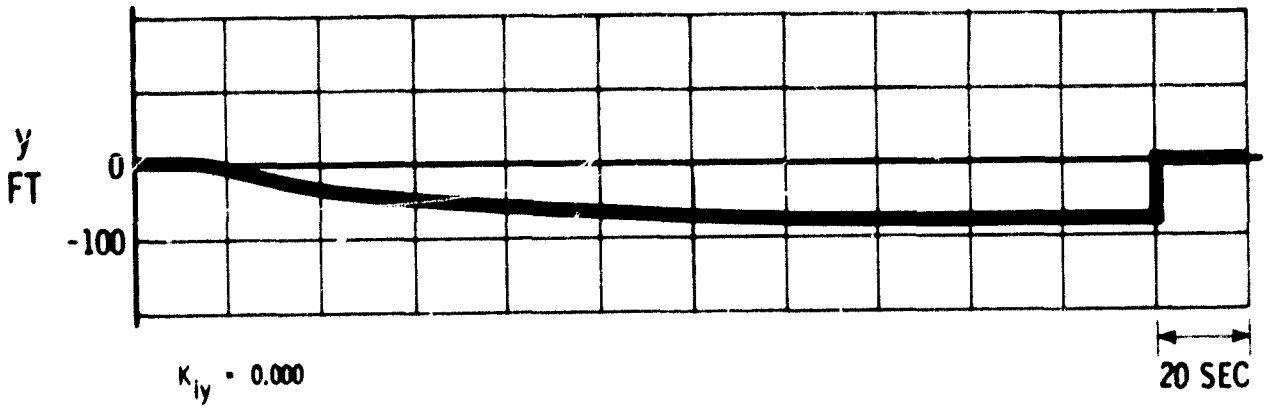

Fig. 2.8-3 Wind shear response of conventional system without integral compensation.

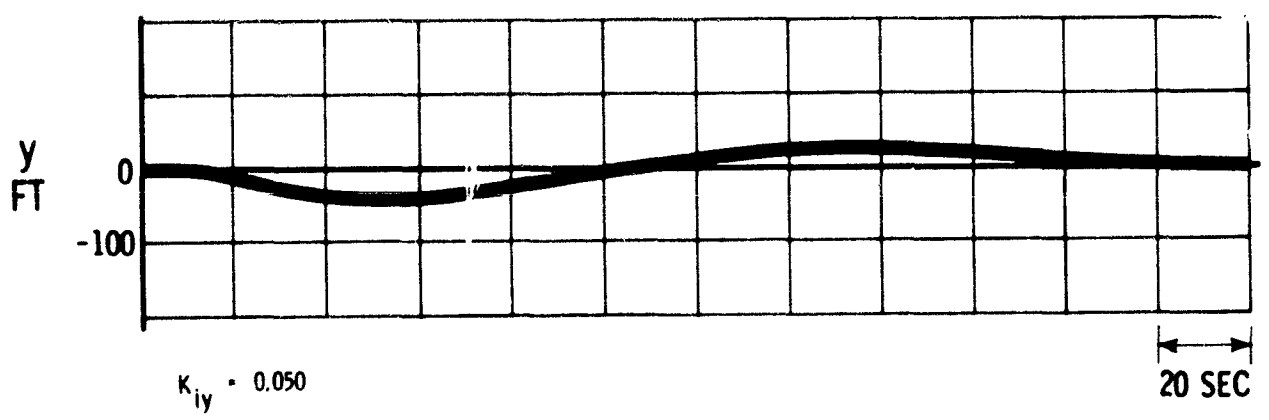

Fig. 2.8-4 Wind shear response of conventional system with integral compensation.

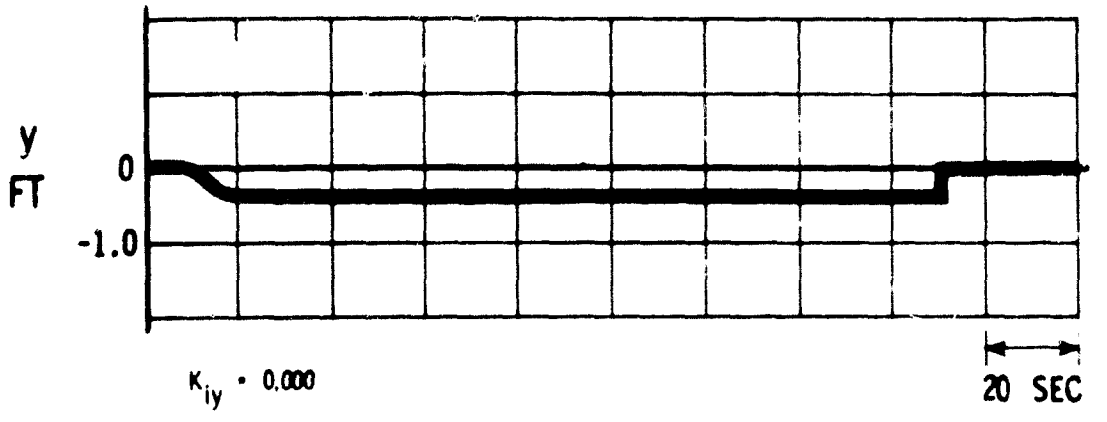

Fig. 2.8-5 Wind shear response of inertially-stabilized system without integral compensation.

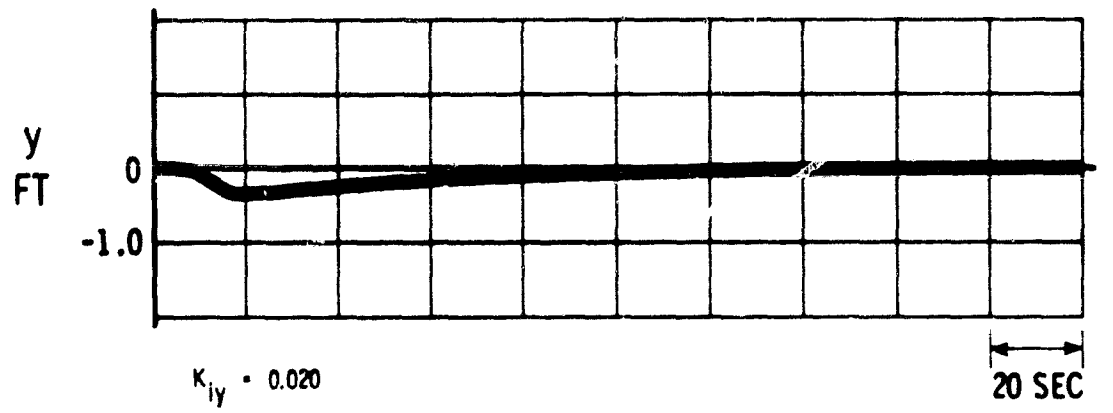

Fig. 2.8-6 Wind shear response of inertially-stabilized system with integral compensation.

Since the ILS receiver time constant τ_f is small, this equation may be written:

$$\phi_c \approx -K_y y \tag{2.9-2}$$

If it is assumed that the system behaves in a linear fashion, the maximum value of actual roll angle ϕ is related to the maximum commanded roll angle in Eq. (2.9-2) by:

$$(\phi)_{maximum} = -\alpha K_y y \tag{2.9-3}$$

where α is a positive constant. Let the limit on roll angle magnitude be ϕ_m. The maximum permissible lateral displacement is then given by:

$$(y)_{maximum} = \frac{\phi_m}{\alpha K_y} \tag{2.9-4}$$

Thus it is apparent that dynamic restrictions can incur severe limitations on permissible course deviations if a purely linear approach is used in conjunction with high loop gains.

The general case is, of course, much more complicated and leads to restrictions on all the state variables associated with the mathematical model of the vehicle.

Another significant problem arises when saturation occurs, as discussed in Chapter 1. In essence, saturation of an element in a closed control loop reduces the loop gain to zero. As a result, the sensitivity of the loop to disturbances increases. This of course leads to undesirable perturbations in the flight path, as long as the condition of saturation persists.

The problems outlined above may be solved by operating on the lateral position data, in order to make it acceptable for presentation to the automatic landing system. In Chapter 4 generalizations of the control system configuration are presented which relieve the problems of restriction of the state variables and of effector saturation.

2.10 Summary

The conclusions arrived at in the previous sections are summarized here. By utilization of inertial data for the assumed simplified model it was possible to:

1. Increase the position loop gain by a factor of 280.
2. Reduce the lateral displacement power component due to wind

gusts by approximately 400 times.

3. Reduce the maximum perturbation due to a constant air mass acceleration by 135 times.

While these numbers do not present a completely realistic picture of the improvements which can be achieved in practice, they do, however, demonstrate that a significant potential for increase in performance exists. A comparison system performance based on a comprehensive vehicle-control system model is presented in Chapter 9.

CHAPTER 3

INERTIAL FILTERING AND CONTROL

3.1 Introduction

This chapter contains an exposition of two methods for combining the outputs of an inertial navigation system and an ILS receiver to obtain estimates of position and velocity which are better than could be obtained from either source alone. The estimates are applied to the aircraft control system in the manner described in Chapter 2. A comparison is made of conventional and inertially-stabilized systems when realistic ILS beam noise is considered.

Two methods of operating on the inertial and ILS information are introduced.

1. Method 1 - Minimization of the integral square of the difference between inertially-computed vehicle displacement and ILS-determined vehicle displacement over the trajectory flown by the aircraft. The method is applied to both the lateral and longitudinal channels, and simulation results are shown for the lateral channel.

2. Method 2 - Kalman Filtering Technique. As applied here the method minimizes the sum of the mean-square differences between the estimated and actual values of several variables over a hypothetical ensemble of trajectories. The estimation is based on information provided by the inertial and ILS systems. Simulation results are given for the lateral channel.

3.2 Errors of the Inertial System

The error analysis of inertial navigation systems has been exhaustively studied over many years and is very completely treated in the literature. The following general statements apply. If the inertial navigation system is undamped, which almost certainly would be the case in the application considered here, then the errors build up in a manner analogous to the buildup of oscillations in a linear oscillator. One oscillation mode, which will primarily affect the vertical errors, and the velocity errors, has an 84 minute period. Another oscillation mode has a period approximately equal to the time it takes for the vehicle to be carried once around the earth's axis. For a slowly-moving vehicle this time is twenty-four hours. For a

rapidly-moving vehicle such as the SST the period depends on the velocity of the vehicle in the east-west direction. The principal limitation on the performance of the inertial system is known to be gyro drift which excites the oscillation modes, and this fact has led to the expenditure of great effort in the development of extremely accurate gyros. There are less important sources of error such as accelerometer drift and gravity anomalies. In addition, there are secondary error sources such as heading sensitivity, a combination of thermal and magnetic effects which affect component performance through the changing environment that results from changes in the gimbal angles.

For the current problem the behavior of the navigation system is important over a time interval of about five minutes - the time between acquisition of the ILS path and touchdown. For a period of this length relatively simple approximations can be made to the inertial system errors.

It is assumed that prior to the time of arrival in the landing area the aircraft has been in the air for several hours. It is possible that a position error of some miles and a velocity error of some knots will have built up. Once a receiver output has been obtained from the ILS beam, an immediate correction can be made in the inertially-computed position, and the resulting position error should be of the order of several hundred feet.

For the additional time that it takes to land, the errors will be dominated by the errors at acquisition. There should, however, be little increase in inertial component-generated error during the landing process. An approximation to the inertially-determined position error during landing can therefore be obtained by considering the errors at acquisition to be initial condition errors.

Inertial navigation systems normally compute variables referred to a geographic reference frame, defined as a right-handed system with

x-north
y-east
z-vertical

A more natural system for the landing problem is a right-handed system with

x-along the ILS reference line
y-horizontal
z-contained in a vertical plane

In such a frame the lateral deviation of the aircraft from the reference path would be given by a coordinate y and the vertical deviation by a coordinate z.

In the frame defined above, the lateral position error δy would then be given by

$$\delta y = y_o + v_{yo} t \qquad (3-2-1)$$

where y_o and v_{yo} are the lateral position and velocity errors at some time $t = 0$ defined to occur after acquisition.

The effect of component error during the landing process can be taken into account by generalizing (3.2-1). Component error will cause vertical error and rate of change of vertical error, which introduce unwanted components of gravity and rate of change of gravity. In this case the position error is

$$\delta y = y_o + v_{yo}t + \tfrac{1}{2}\delta g t^2 + \tfrac{1}{6}\delta \dot{g} t^3 \qquad (3.2\text{-}2)$$

and, in general, a power series approximation will apply if the time t is sufficiently short.

In the current problem the simpler expression (3.2-1) will be used. A better approximation will be considered subsequently. The position output of the inertial system is therefore taken to be

$$y_i = y + y_o + v_{yo}t \qquad (3.2\text{-}3)$$

where y is the true position of the vehicle in the y direction.

In summary, the position output of the inertial system will be a smooth, virtually noise-free indication whose error will be dominated by initial conditions. The error will tend to drift with time.

3.3 Errors of the ILS System

The principal source of information on ILS beam errors that has been available to the authors is ref (4) which was prepared by the Bendix Corporation. Reference (4) was reprinted as an appendix of ref (3).

Since the localizer and glide-slope beams define geometrical entities in space, there is no drift except over very long periods of time. The beam errors are functions of position along the beam. The errors are of a random nature, although constant in time, and depend primarily on distortion of the transmitting antenna patterns by reflections from the surrounding terrain.

The unit of aircraft deflection from the ILS beam that is used conventionally is the microamp of receiver output current. Full current output of 150μa corresponds to an angle of about 2.0 degrees in the localizer case, and an angle of about 0.5 degrees in the glide-slope case. Inspection of the beam errors recorded in ref (4), which were determined by theodolite tracking of aircraft flying the ILS beams at various facilities, indicates that the beams usually have a bias of several μa and a spectrum of bends ranging from a wavelength of 100 feet to a wavelength of several thousand feet. Spectral analysis of beam errors shows considerable variation in the spectral distribution of various beams.

For the purposes of the studies which are reported in this document, beam noise was generated by computer. A typical example is shown in Fig. 3.3-1. The figure at the top in units of microamps is simulated white noise, operated upon by a simple time lag. The bottom figure shows the same noise in units of feet of error from the reference line.

Specifications on peak beam noise, as given in ref (4) are as follows:

Localizer

1. End of runway to middle marker ±5 μa.
2. Middle marker to outer marker - linear from ±5 μa to ±30 μa.
3. Beyond outer marker - ±30 μa.

Glide-Slope

1. End of runway to middle marker - ±20 μa.
2. Middle marker to outer marker - linear from ±20 μa to ±30 μa.
3. Beyond outer marker - ±30 μa.

The localizer noise shown in Fig. 3.3-1 and used in the simulation is a far more stringent input than the noise prescribed by the above specifications.

3.4 Method 1 - Lateral Channel Analysis

3.4.1 Definition of Estimated Position and Velocity

Ideally, the localizer receiver measures the angle θ, which can be defined as the angle between the vertical plane containing the ILS reference path and the line containing the aircraft and the localizer antenna. The output θ_{If} of the localizer receiver, however, depends on the localizer beam noise n_y and on the localizer receiver filter. The output can be characterized by the Laplace transform expression

$$\bar{\theta}_{If} = \frac{1}{s\tau_f + 1}\bar{\theta}_I \qquad (3.4\text{-}1)$$

where

$$\theta_I = \theta - n_y \qquad (3.4\text{-}2)$$

and the bar is used to indicate a Laplace transform.

The output of the inertial system, on the other hand, is given by Eq(3.2-3). If the range R to the localizer antenna is available an angle θ_i, which is the inertially-computed analog of θ_I, can be formed

$$\theta_i = \frac{y_i}{R} = \frac{y}{R} + \frac{y_o}{R} + \frac{v_{yo}t}{R} \qquad (3.4\text{-}3)$$

The inertial analog of θ_{If} is

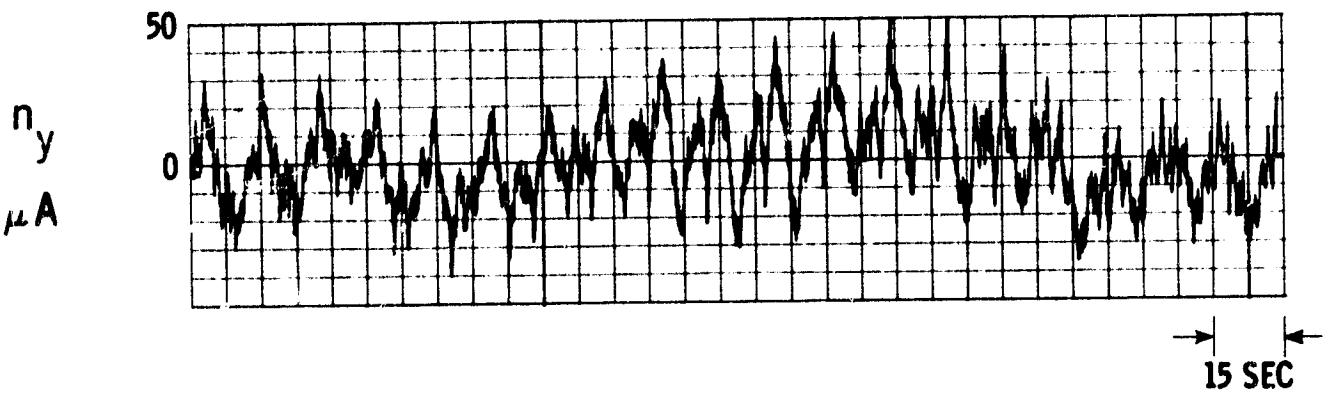

Fig. 3.3-1 a Simulated ILS noise (μA).

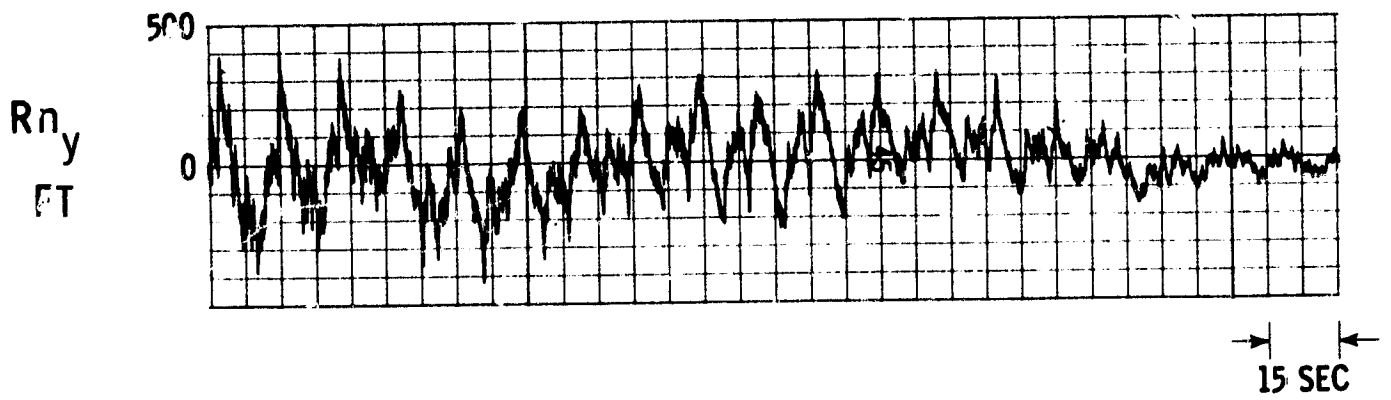

Fig. 3.3-1 b Simulated ILS noise (ft).

$$\bar{\theta}_{if} = \frac{1}{s\tau_f + 1}\bar{\theta}_i \qquad (3.4\text{-}4)$$

Consider the difference ϵ between the filtered output of the inertial system and the output of the localizer receiver.

$$\epsilon = \theta_{if} - \theta_{If} \qquad (3.4\text{-}5)$$

The quantity ϵ is independent of aircraft motion and depends only on the localizer noise n_y and on the inertial system initial conditions y_o and v_{yo}. This can be shown as follows:

$$\bar{\epsilon} = \frac{1}{s\tau_f + 1}(\bar{\theta}_i - \bar{\theta}_I) \qquad (3.4\text{-}6)$$

Since $y/R = \theta$

$$\bar{\epsilon} = \frac{1}{s\tau_f + 1}\mathcal{L}\left\{\frac{y_o}{R} + \frac{v_{yo}t}{R} + n_y\right\} \qquad (3.4\text{-}7)$$

where $\mathcal{L}\{\ \}$ indicates a Laplace transform.

The operations required to determine ϵ are shown in block diagram form in Fig. 3.4-1. As indicated above, the inertial system output is operated on by a filter identical with the localizer filter so that the dynamic effects of the two paths are the same.

The following procedure is now proposed. It is assumed that the computation of ϵ proceeds from time $t = 0$. It is assumed further that y_o and v_{yo} may be grossly in error - say several hundred feet for y_o and several knots for v_{yo}. Let corrections y_{oc} and v_{yoc} be defined at $t = 0$. Then a quantity ϵ' given by

$$\epsilon' = \frac{1}{s\tau_f + 1}\mathcal{L}\left\{\frac{y_o + y_{oc}}{R} + \frac{v_{yo} + v_{yoc}}{R}t + n_y\right\} \qquad (3.4\text{-}8)$$

should, in general, be less than ϵ. It is proposed to determine y_{oc} and v_{yoc} by the condition that the integral

$$I_y = \int_0^t \epsilon'^2\, dt \qquad (3.4\text{-}9)$$

be a minimum.

The procedure defined above will determine y_{oc} and v_{yoc}, the corrections which should have been made in y_i and v_{yi} respectively at $t = 0$. At some later time the corrected inertial quantities, if the error model (3.2-3) is assumed, are

$$\hat{y} = y_i + y_{oc} + v_{yoc}t \qquad (3.4\text{-}10)$$

$$\hat{v}_y = v_{yi} + v_{yoc}$$

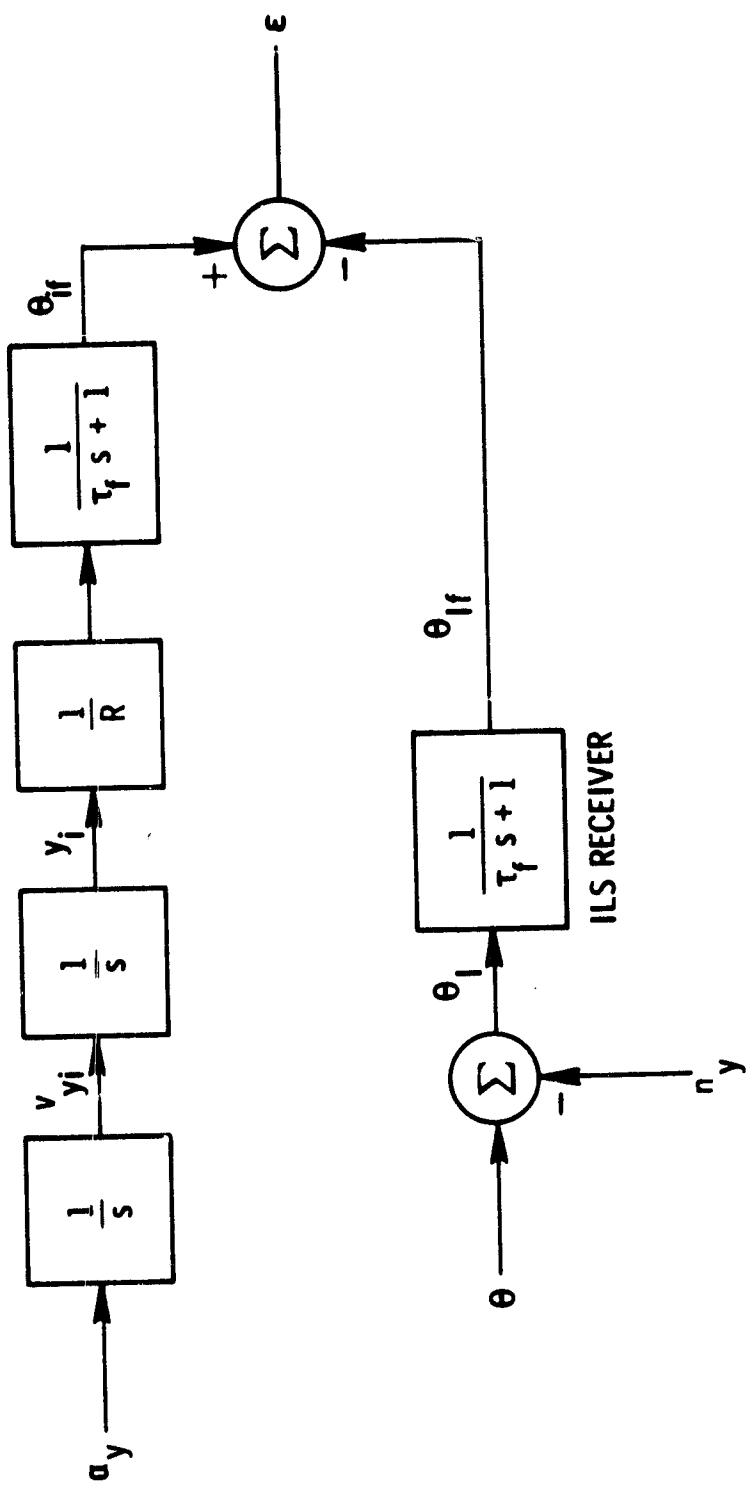

Fig. 3.4-1 Error computation.

The expressions $\hat{y}$ and $\hat{v}_y$ are then taken to be the best current estimates of y and v_y, respectively.

3.4.2 Minimization of the Performance Measure

Let θ_{if} be considered to have three components, dependent respectively on y, y_o and v_{yo}. Then

$$\theta_{if} = u + v + w \tag{3.4-11}$$

where

$$\begin{aligned} u &= \frac{1}{s\tau_f + 1}\mathcal{L}\left\{\frac{y}{R}\right\} \\ v &= \frac{1}{s\tau_f + 1}\mathcal{L}\left\{\frac{y_o}{R}\right\} \\ w &= \frac{1}{s\tau_f + 1}\mathcal{L}\left\{\frac{v_{yo}t}{R}\right\} \end{aligned} \tag{3.4-12}$$

The quantities u, v, and w satisfy the differential equations

$$\begin{aligned} \tau_f \dot{u} + u &= \frac{y}{R} \\ \tau_f \dot{v} + v &= \frac{y_o}{R} \\ \tau_f \dot{w} + w &= \frac{v_{yo}t}{R} \end{aligned} \tag{3.4-13}$$

The equations for v and w can be normalized by the following procedure. Put

$$\begin{aligned} v &= v_n y_o \\ w &= w_n v_{yo} \end{aligned} \tag{3.4-14}$$

Then v_n and w_n satisfy

$$\begin{aligned} \tau_f \dot{v}_n + v_n &= \frac{1}{R} \\ \tau_f \dot{w}_n + w_n &= \frac{t}{R} \end{aligned} \tag{3.4-15}$$

and are independent of y_o and v_{yo}. The initialization of Eqs (3.4-15) is determined by the following procedure. It is assumed that at t = 0, the output of the filter acting on the inertial position is set equal to its input. Then

$$\theta_{if}(0) = \theta_{i}(0) \tag{3.4-16}$$

and

$$\begin{aligned} u(0) &= \frac{y(0)}{R(0)} \\ v(0) &= \frac{y_o}{R(0)} \\ w(0) &= \frac{v_{yo}t}{R(0)} = 0 \end{aligned} \tag{3.4-17}$$

It follows that

$$\begin{aligned} v_n(0) &= \frac{1}{R(0)} \\ w_n(0) &= 0 \end{aligned} \tag{3.4-18}$$

From Eqs (3.4-1), (3.4-2), (3.4-5) and (3.4-11)

$$\begin{aligned} \epsilon &= \theta_{if} - \theta_{If} \\ &= (u + v + w) - (u - n_{yf}) \\ &= v + w + n_{yf} \\ &= v_n y_o + w_n v_{yo} + n_{yf} \end{aligned} \tag{3.4-19}$$

Let corrections y_{oc} and v_{yoc} produce a corrected error

$$\begin{aligned} \epsilon' &= v_n(y_o + y_{oc}) + w_n(v_{yo} + v_{yoc}) + n_{yf} \\ &= v_n y_{oc} + w_n v_{yoc} + \epsilon \end{aligned} \tag{3.4-20}$$

The integral square of ϵ' is

$$I_y = y_{oc}^2 \int_0^t v_n^2\,dt + v_{yoc}^2 \int_0^t w_n^2\,dt + 2y_{oc} \int_0^t v_n\,\epsilon\,dt + 2v_{yoc} \int_0^t w_n\,\epsilon\,dt$$
$$+ 2y_{oc}v_{yoc} \int_0^t v_n w_n\,dt + \int_0^t \epsilon^2\,dt \qquad (3.4\text{-}21)$$

The integral I_y is a minimum when

$$\frac{\partial I_y}{\partial y_o} = 0 \qquad \frac{\partial I_y}{\partial v_{yo}} = 0 \qquad (3.4\text{-}22)$$

The condition (3.4-22) yields

$$-\int_0^t v_n\,\epsilon\,dt = y_{oc} \int_0^t v_n^2\,dt + v_{yoc} \int_0^t v_n w_n\,dt$$
$$-\int_0^t w_n\,\epsilon\,dt = y_{oc} \int_0^t v_n w_n\,dt + v_{yoc} \int_0^t w_n^2\,dt \qquad (3.4\text{-}23)$$

Solution of Eq (3.4-23) for y_{oc} and v_{yoc} gives

$$y_{oc} = \frac{dA - bB}{b^2 - ad} \qquad (3.4\text{-}24)$$

$$v_{yoc} = \frac{aB - bA}{b^2 - ad}$$

where

$$A = \int_0^t v_n\,\epsilon\,dt \qquad B = \int_0^t w_n\,\epsilon\,dt \qquad (3.4\text{-}25)$$

and

$$a = \int_0^t v_n^2\,dt \qquad b = \int_0^t v_n w_n\,dt \qquad c = \int_0^t w_n^2\,dt \tag{3.4-26}$$

A block diagram of the resultant estimation system is shown in Fig. 3.4-2.

The above procedure determines y_{oc} and v_{yoc} by minimizing the integral square of the difference between the filtered inertially-computed angle off the localizer path and the radio-determined angle off the localizer path. The resultant corrected inertial position measures the distance of the aircraft from a plane through the noisy localizer reference. All angular errors along the path were given the same weight. Since the specifications on localizer accuracy are more stringent as the runway is approached, it may be appropriate to weight the integrand of Eq (3.4-9) more heavily near the runway so that the more accurate radio input has a greater effect. For the beam noise illustrated in ref (4), however, there did not seem to be an advantage in weighting the integrand of Eq(3.4-9) as a function of range.

3.5 Method 1 - Lateral Channel Simulation Results

The method of estimating position and velocity described above has been tested on the aircraft and control system model developed in Chapter 2. The cases considered are as follows:

1. Conventional system.
2. System with ILS position input and uncorrected inertial velocity and acceleration inputs.
3. System with corrected inertial position and velocity inputs, and acceleration input.

In all cases the localizer beam was assumed to have the error indicated in Fig. 3.3-1. This error model is considerably more stringent than the beam errors illustrated in ref (4), as indicated earlier.

Case 1

For the conventional system (no inertial navigation system) Fig. 3.5-1 illustrates the roll angle ϕ, the heading angle ψ, the lateral velocity v_y and the lateral position error y. The peak roll angles ϕ are quite high, which indicates that the gain K_y is higher than would be practical in an operational system flying a beam as noisy as the one assumed. The results are, however, useful in comparing the three cases, and the stringent beam noise will empha-

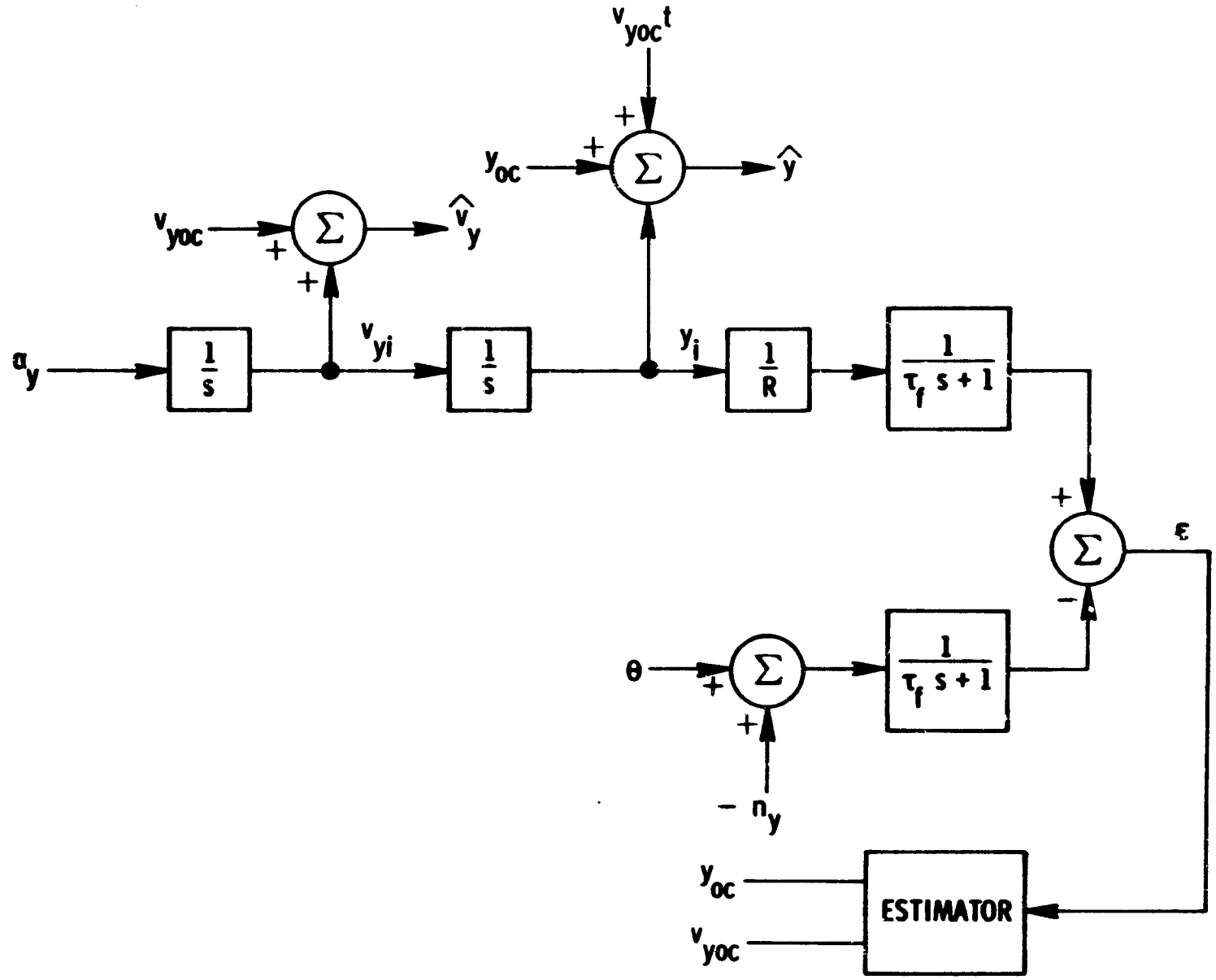

Fig. 3.4-2 Block diagram of estimation system.

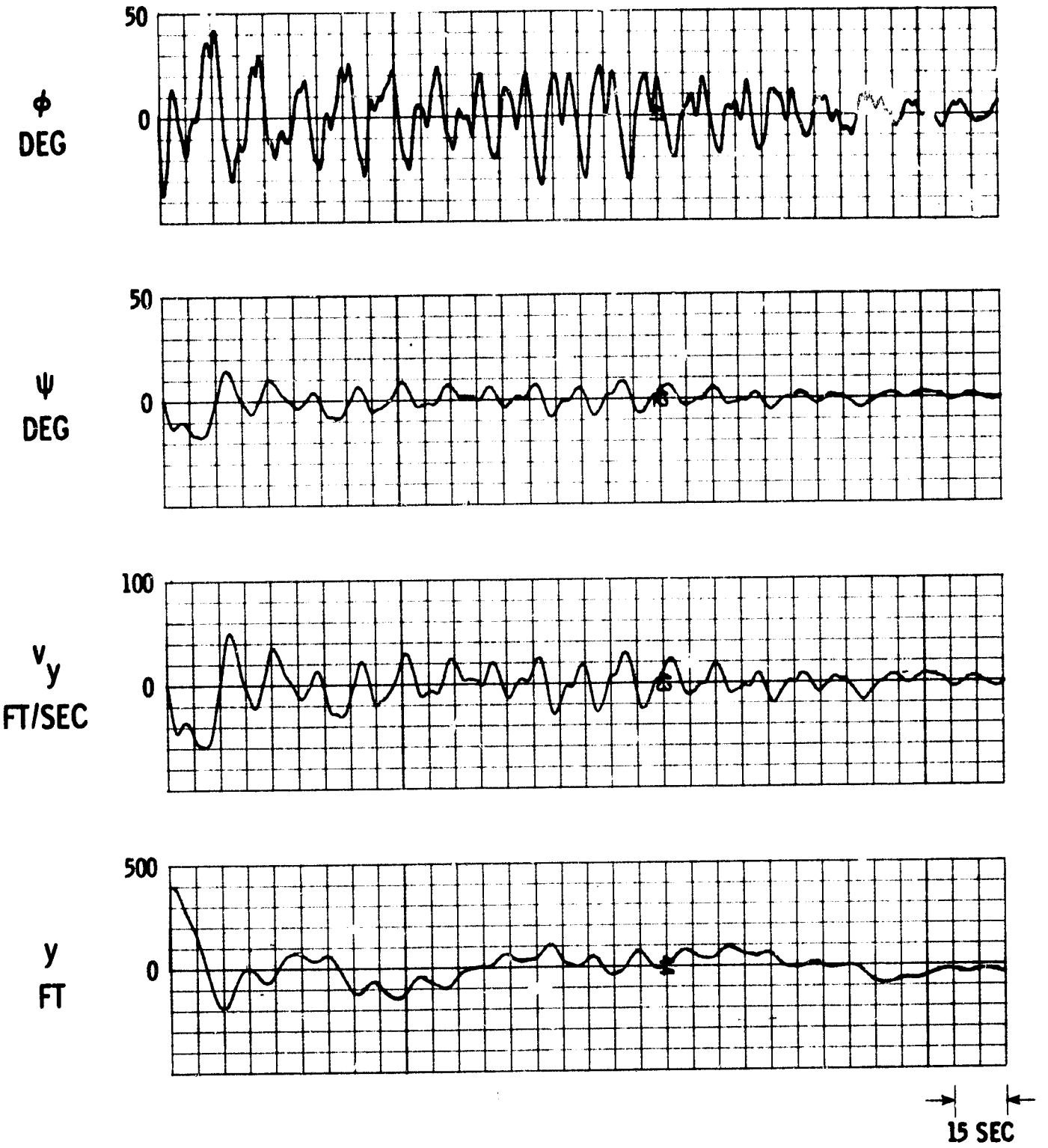

Fig. 3.5-1 Responses of conventional system (Case 1).

size the drastic improvement obtained in Case 3. It will be noticed that the aircraft tends to follow the average value of the beam noise.

Case 2

For the high gain system with ILS position reference and uncorrected inertial velocity and acceleration feedback (as described in Chapter 2), the results are shown in Fig. 3.5-2. In this case the aircraft lateral position error is about the same as in Case 1. The peak roll angles, however, have become even higher. The inertial inputs therefore, with higher gain, appear to have deteriorated the roll performance with no compensating benefit in position accuracy. It will be recalled, however, that the prime motivations for a high-gain system were the ability to attenuate external disturbances, as shown in Fig. 2.8-6 and 2.8-7, and the ability to follow the position reference precisely. The effect of noise in the position reference will be to increase the system responses as Fig. 3.5-2 clearly shows. It can be concluded that when beam noise is considered, the control system discussed in Chapter 2 is not sufficient in itself to produce an acceptable system.

Case 3

In Case 3, the aircraft was controlled with estimated inertial position y and stabilized with estimated inertial velocity v_y and acceleration a_y. The inertial navigation system was assumed to have a position error of 400 ft. and a velocity error of 2 ft/sec at t = 0. Figure 3.5-3 shows the system responses, and Fig. 3.5-4 shows the error in the estimated velocity and position. After an initial transient, the estimates converge to a fraction of a ft/sec and to peaks of less than 100 ft respectively. The ILS position reference error shown in Fig. 3.3-1 has effectively been replaced by the negative of the position error signal $\hat{y} - y$.

It will be noticed that a drastic improvement has occurred in the roll angle excursion, which is now quite acceptable after 20 seconds. The aircraft position deflection is now much smoother than in the two preceeding cases, and the accuracy at touchdown is better. Since the estimation procedure required about 25 seconds to converge, the estimated variables were not introduced at t = 0. The initial references were set to be pure inertial. The estimated references were phased in after convergence, replacing the pure inertial references over a period of about 20 seconds.

The above results demonstrate the considerable improvement attainable from appropriate utilization of the inertial information.

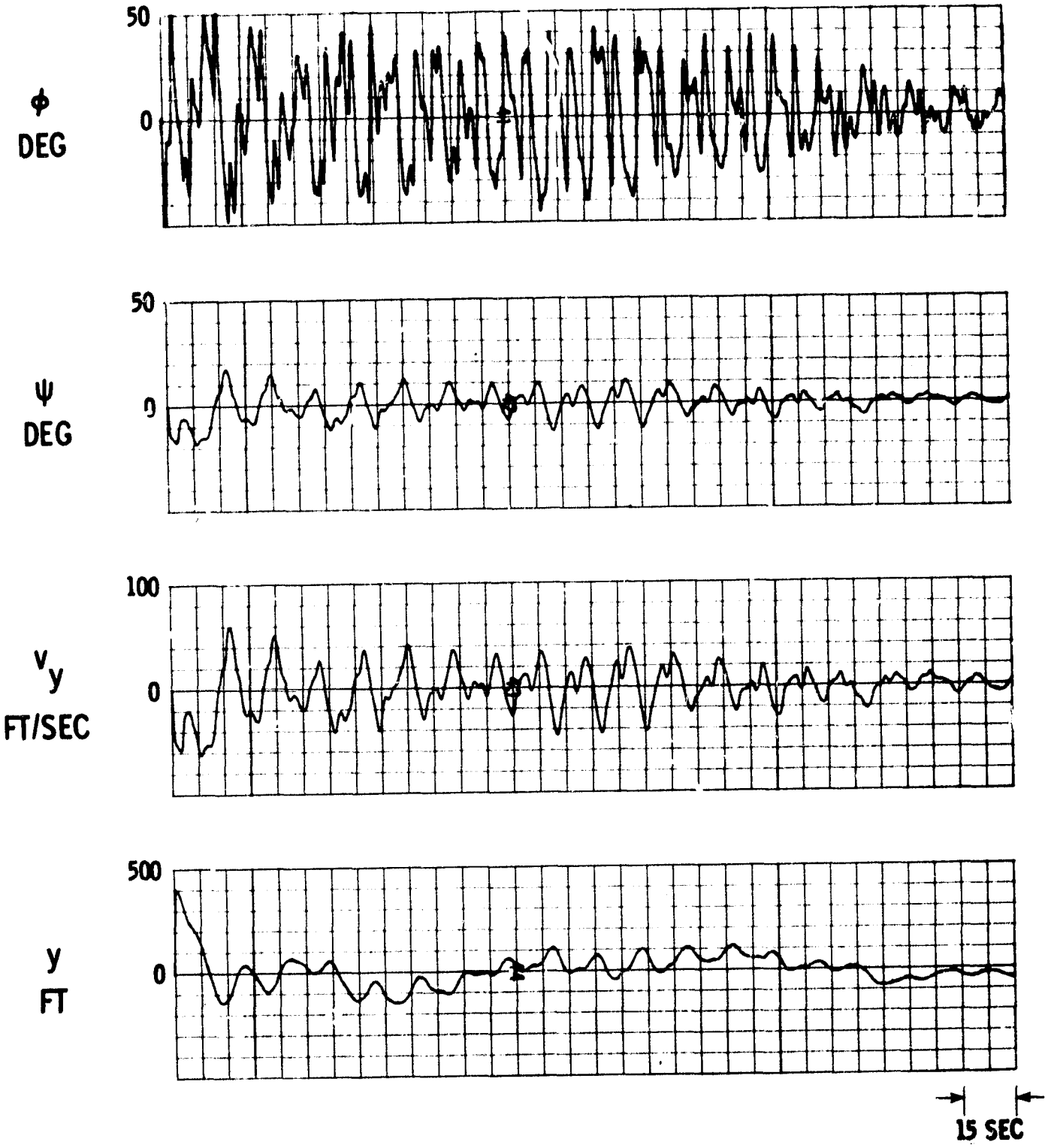

Fig. 3.5-2 Responses of inertially-stabilized system (ILS position reference - Case 2).

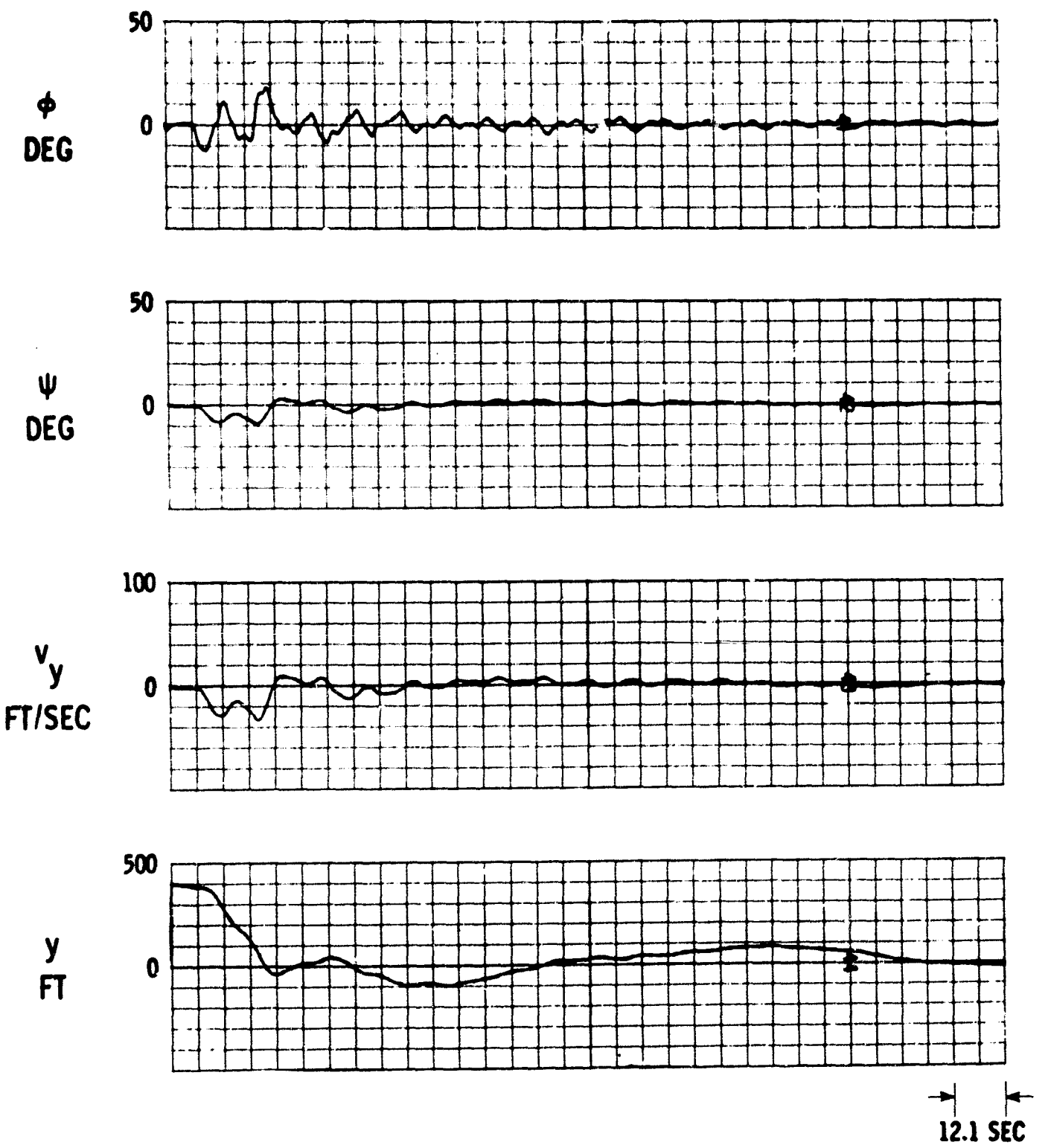

Fig. 3.5-3 Responses of inertially-stabilized system (corrected inertial position reference - Case 3).

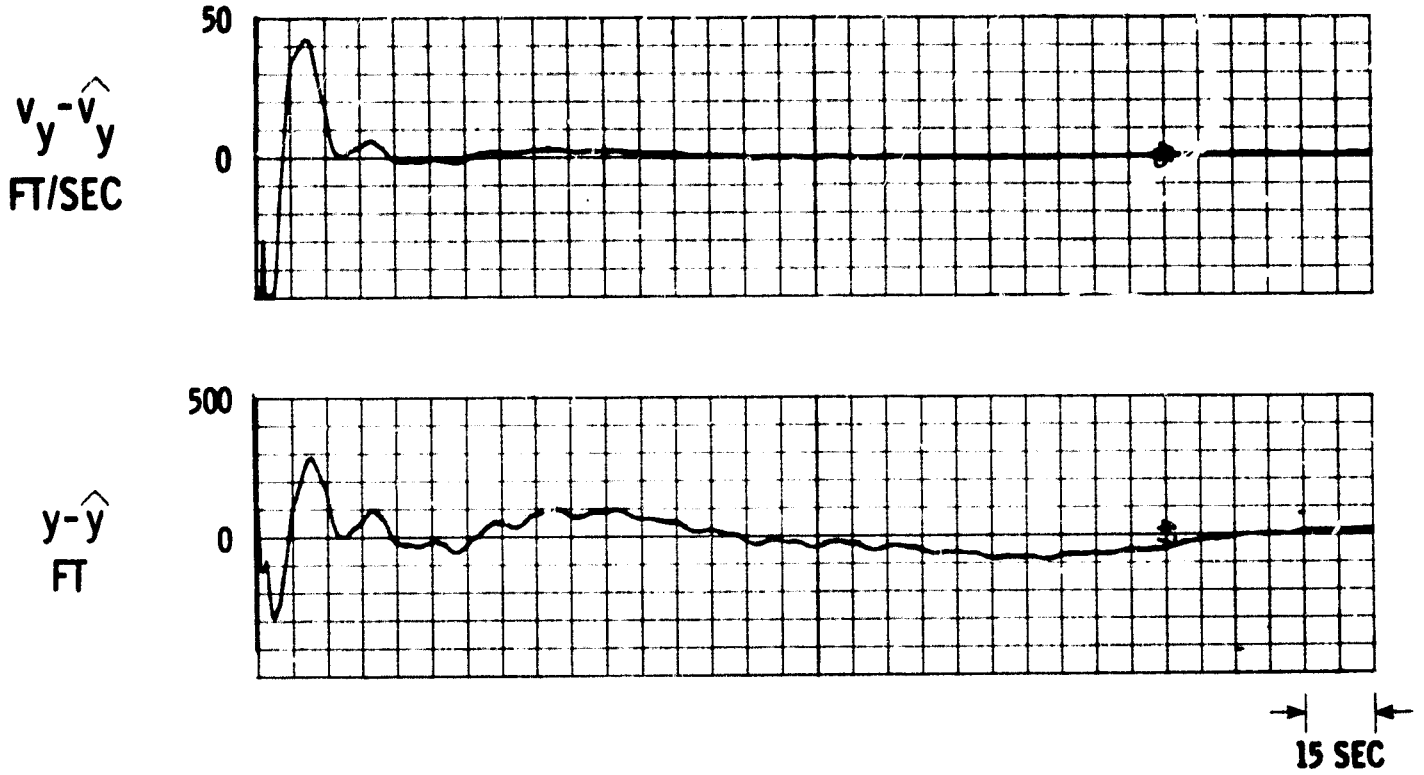

Fig. 3.5-4 Velocity and position estimation error.

3.6 Method 1 - Longitudinal Channel

The position and velocity to be computed are in the vertical plane along an axis normal to the ILS reference line. The positive direction is downward. An accelerometer with input axis aligned with the reference axis will sense the specific force

$$f_z = g_z - a_z \tag{3.6-1}$$

where g_z is the component of gravity along the axis. To compute the position and velocity of the vehicle along the reference axis, it is necessary to compensate the gravity term, thus isolating the acceleration a_z, so that position can be determined by integration.

In general, g_z will not be compensated perfectly because of lack of knowledge of the local variation of gravity or because of imperfection of system mechanization, and position and velocity errors dependent on the compensation error δg will arise. The simplest assumption is that δg is constant, although this assumption is by no means necessary.

The assumption $\delta g = \text{const}$ leads to the following expression for inertially computed position along z

$$z_i = z + z_o + v_{zo}t + \frac{1}{2}\delta g\, t^2 \tag{3.6-2}$$

In analogy with Eq (3.4-3) the inertially-determined angular deflection can be written in the form

$$\theta_{zi} = \frac{z}{R} + \frac{z_o}{R} + \frac{v_{zo}t}{R} + \frac{1}{2}\frac{\delta g}{R}t^2 \tag{3.6-3}$$

where R is now the distance to the glide-slope antenna. The subsequent development is analogous to the development of the preceding section. The results can be summarized as follows:

The estimated variables are

$$\begin{aligned} \hat{z} &= z_i + z_{oc} + v_{zoc}t + \frac{1}{2}\delta g_{oc}t^2 \\ \hat{v}_z &= v_{zi} + v_{zoc} + \delta g_{oc}t \\ \hat{\delta g} &= \delta g_{oc} \end{aligned} \tag{3.6-4}$$

The computed initial condition corrections are

$$\begin{bmatrix} z_{oc} \\ v_{zoc} \\ \delta g_{oc} \end{bmatrix} = -M_z^{-1} \begin{bmatrix} A_z \\ B_z \\ C_z \end{bmatrix} \tag{3.6-5}$$

where

$$M_z = \begin{bmatrix} a_z & b_z & c_z \\ b_z & d_z & e_z \\ c_z & e_z & f_z \end{bmatrix} \tag{3.6-6}$$

and

$$\begin{aligned} A_z &= v_{zn}\epsilon_z \\ B_z &= w_{zn}\epsilon_z \\ C_z &= m_{zn}\epsilon_z \end{aligned} \tag{3.6-7}$$

$$\begin{aligned} a_z &= v_{zn}^2 \\ b_z &= v_{zn}w_{zn} \\ c_z &= v_{zn}m_{zn} \\ d_z &= w_{zn}^2 \\ e_z &= w_{zn}m_{zn} \\ f_z &= m_{zn}^2 \end{aligned} \tag{3.6-8}$$

The quantities v_{zn}, w_{zn} and m_{zn} satisfy

$$\dot{v}_{zn} = \frac{1}{\tau_{fz}}\left(\frac{1}{R} - v_{zn}\right)$$

$$\dot{w}_{zn} = \frac{1}{\tau_{fz}}\left(\frac{t}{R} - w_{zn}\right) \qquad (3.6\text{-}9)$$

$$\dot{m}_{zn} = \frac{1}{\tau_{fz}}\left(\frac{1}{2}\frac{t^2}{R} - m_{zn}\right)$$

The error ϵ_z is the difference between the filtered, inertially-determined angular deflection θ_{zif} and the output of the glide-slope receiver θ_{zIf}

3.7 Method 2 - Lateral Channel Analysis

3.7.1 Introduction

Since the publication on 1960 and 1961 of important papers on linear filtering and prediction R. E. Kalman and others (see refs (22) and (23)) an extensive literature has grown up on what is now generally referred to as Kalman Filter Theory. In this section an application of the theory is made to the problem of filtering ILS beam signals when information from an inertial navigation system is available. In Appendix B an exposition of the theory sufficient for the applications of this section is given.

The technique to be described is a powerful formalism for improving, sequentially, the accuracy of knowledge of the state of a system when certain measurements are made. The system is represented by a set of differential equations. For a given physical situation, however, Kalman filtering is not an automatic process for improving accuracy. There is usually considerable latitude of choice in how a physical system is described by a set of equations. The results obtained will depend on setting the problem up in appropriate fashion so that best use of the available information is achieved.

3.7.2 General Filter Equation

It is assumed that a system is represented by the matrix differential equation

$$\dot{x} = Fx + n \qquad (3.7\text{-}1)$$

where n is white noise. A vector z is measured periodically and is related to x by

$$z = Hx + u \tag{3.7-2}$$

where u is a measurement error. The sequence of values of u are uncorrelated. Prior to a measurement the estimated value of x is $\hat{x}'$. Following the measurement an improved estimate $\hat{x}$ is computed.

Let the autocorrelation function of n be given by

$$\Phi_n = Q\delta(\tau) \tag{3.7-3}$$

and the expected value of the sum of the squares of the measurement errors be represented by R_u.

$$R_u = \mathcal{E}\,(uu_T) \tag{3.7-4}$$

The covariance matrix E is defined as the expectation of the product $(\hat{x} - x)(\hat{x} - x)_T$. In applications an initial estimate of E must be provided. The subsequent values of E are specified by the filtering process.

The improved value of $\hat{x}$, following the measurement is given by

$$\hat{x} = \hat{x}' + E'H_T(HE'H_T + R_u)^{-1}(z - H\hat{x}') \tag{3.7-5}$$

The covariance matrix is updated, following the measurement, by

$$E = E' - E'H_T(HE'H_T + R_u)^{-1}HE' \tag{3.7-6}$$

Between measurements, the value of $\hat{x}$ is extrapolated by using Eq (3.7-1) with the assumption of zero noise.

$$\dot{\hat{x}} = F\hat{x} \tag{3.7-7}$$

The covariance matrix is extrapolated between measurements by

$$\dot{E} = FE + EF_T + Q \tag{3.7-8}$$

The above process insures that the trace of E is a minimum.

3.7.3 Application to ILS Beam Filtering

Consider the interconnected inertial and ILS system illustrated schematically in Fig. 3.7-1. The equations of the system are

$$\dot{v}_{yi} = a_y \tag{3.7-9}$$

$$\dot{y}_i = v_{yi}$$

$$\begin{aligned} \tau_f \dot{\theta}_{if} + \theta_{if} &= \theta_i \\ \tau_f \dot{\theta}_{If} + \theta_{If} &= \theta_I \end{aligned} \tag{3.7-10}$$

and

$$\begin{aligned} \theta_i &= \frac{y_i}{R} \\ \theta_I &= \theta - n \\ \epsilon_y &= \theta_{if} - \theta_{If} \end{aligned} \tag{3.7-11}$$

The system is precisely the same as the one treated by Method 1. It is assumed, as before, that v_{yi} differs from its correct value by a constant, and that y_i has an initial condition error. The quantity to be measured and operated upon is ϵ_y; however, ϵ_y is now to be sampled periodically rather than continuously.

Since v_{yi} differs from its correct value by a constant

$$\delta \dot{v}_{yi} = \frac{d}{dt}(v_{yi} - v_y) = 0 \tag{3.7-12}$$

Also

$$\delta \dot{y}_i = \delta v_i \tag{3.7-13}$$

and

$$\begin{aligned} \tau_f \dot{\epsilon}_y + \epsilon_y &= \theta_i - \theta + n_y \\ &= \delta\theta_i + n_y \end{aligned} \tag{3.7-14}$$

The inertially-measured angular deflection is

$$\delta\theta_i = \frac{\delta y_i}{R} \tag{3.7-15}$$

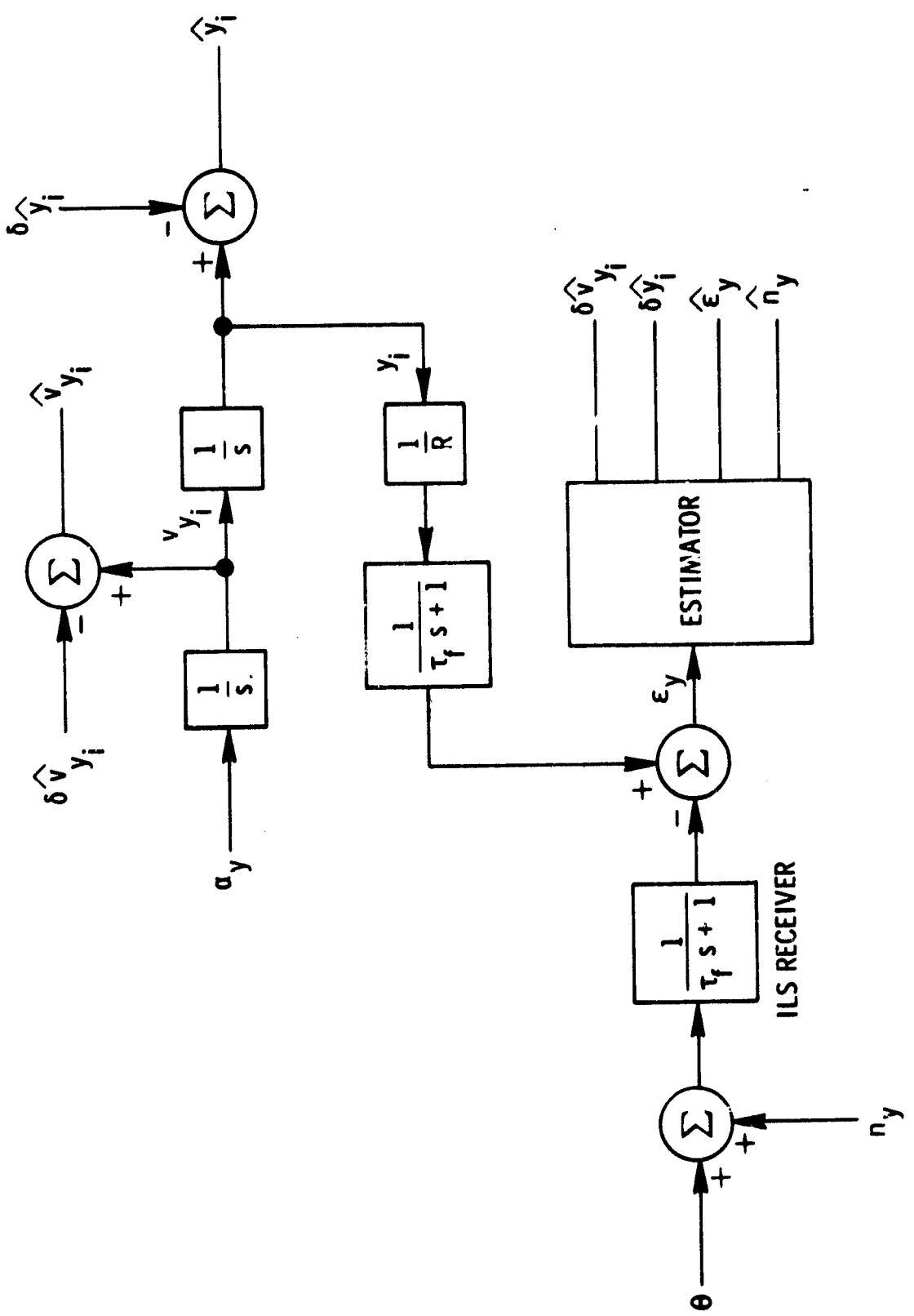

Fig. 3.7-1 Block diagram of estimation system employing Kalman filter.

The formulation (3.7-1) requires that n_y be white noise. The noise contribution of the ILS beam, however, is band limited and cannot be represented by a white-noise model. Accordingly, the following artifice is used. The beam noise is assumed to be suitably represented by the output of a low-pass filter excited by white noise. The filter output is taken as an additional state variable, and the resultant system can be assumed to be excited by white noise. This idea was first put forth by Bode and Shannon in their 1950 exposition of Wiener's theory of filtering and prediction (see ref (7)). For the current problem, the ILS noise is represented by n_y where

$$\dot{n}_y = -\frac{1}{\tau_n} n_y + n_w$$

where n_w is white noise.

The resultant set of equations is

$$\begin{aligned} \delta\dot{v}_{yi} &= 0 \\ \delta\dot{y}_i &= \delta v_i \\ \epsilon_y &= \frac{1}{\tau_f}\left(\frac{\delta y_i}{R} - \epsilon_y + n_y\right) \\ \dot{n}_y &= -\frac{1}{\tau_n} n_y + n_w \end{aligned} \qquad (3.7\text{-}16)$$

In the notation of Eqs. (3.7 - 1) and (3.7 -2)

$$F = \begin{bmatrix} 0 & 0 & 0 & 0 \\ 1 & 0 & 0 & 0 \\ 0 & \frac{1}{\tau_f R} & -\frac{1}{\tau_f} & \frac{1}{\tau_f} \\ 0 & 0 & 0 & -\frac{1}{\tau_n} \end{bmatrix} \qquad (3.7\text{-}17)$$

$$H = [0 \;\; 0 \;\; 1 \;\; 0] \qquad (3.7\text{-}18)$$

The measurement of ϵ_y is assumed to be made perfectly so that $R_u = 0$. From the generalized Kalman filter equations, and the

representations for F and H derived above, the following special forms can be obtained explicitly. Between measurements, the estimated state vector is extrapolated by

$$\begin{aligned}
\dot{\delta v}_{yi} &= 0 \\
\dot{\delta y}_i &= \delta \hat{v}_i \\
\dot{\hat{\epsilon}}_y &= \frac{1}{\tau_f}\left(\frac{\delta \hat{y}_i}{R} - \hat{\epsilon}_y + \hat{n}_y\right) \\
\dot{\hat{n}}_y &= -\frac{1}{\tau_n} n_y
\end{aligned} \tag{3.7-19}$$

The covariance matrix is extrapolated by

$$\begin{aligned}
\dot{E}_{11} &= 0 \\
\dot{E}_{12} &= E_{11} \\
\dot{E}_{13} &= \frac{1}{\tau_f R} E_{12} - \frac{1}{\tau_f} E_{13} + \frac{1}{\tau_f} E_{14} \\
\dot{E}_{14} &= -\frac{1}{\tau_n} E_{14} \\
\dot{E}_{22} &= 2E_{12} \\
\dot{E}_{23} &= E_{13} + \frac{1}{\tau_f R} E_{22} - \frac{1}{\tau_f} E_{23} + \frac{1}{\tau_f} E_{24} \\
\dot{E}_{24} &= E_{14} - \frac{1}{\tau_n} E_{24} \\
\dot{E}_{33} &= \frac{2}{\tau_f R} E_{23} - \frac{2}{\tau_f} E_{33} + \frac{2}{\tau_f} E_{34} \\
\dot{E}_{34} &= \frac{1}{\tau_f R} E_{24} - \left(\frac{1}{\tau_f} + \frac{1}{\tau_n}\right) E_{34} + \frac{1}{\tau_f} E_{44} \\
\dot{E}_{44} &= -\frac{2}{\tau_n} + Q
\end{aligned} \tag{3.7-20}$$

Immediately following a measurement of ϵ_y, the estimates are updated by

$$\delta\hat{v}_{yi} = \delta\hat{v}'_{iy} + \frac{E'_{13}}{E'_{33}} (\epsilon_y - \hat{\epsilon}'_y)$$

$$\delta\hat{y}_i = \delta\hat{y}'_i + \frac{E'_{23}}{E'_{33}} (\epsilon_y - \hat{\epsilon}'_y) \qquad (3.7\text{-}21)$$

$$\hat{\epsilon}_y = \epsilon_y$$

$$\hat{n}_y = \hat{n}'_y + \frac{E'_{34}}{E'_{33}} (\epsilon_y - \hat{\epsilon}'_y)$$

and the elements of the covariance matrix are updated by

$$E_{11} = E'_{11} - \frac{E'^2_{13}}{E'_{33}}$$

$$E_{12} = E'_{12} - \frac{E'_{13}E'_{23}}{E'_{33}}$$

$$E_{13} = 0$$

$$E_{14} = E'_{14} - \frac{E'_{13}E'_{34}}{E'_{33}}$$

$$E_{22} = E'_{22} - \frac{E'^2_{23}}{E'_{33}} \qquad (3.7\text{-}22)$$

$$E_{23} = 0$$

$$E_{24} = E'_{24} - \frac{E'_{23}E'_{34}}{E'_{33}}$$

$$E_{33} = 0$$

$$E_{34} = 0$$

$$E_{44} = E'_{44} - \frac{E'^2_{34}}{E'_{33}}$$

3.8 Method 2 - Lateral Channel Simulation Results

Figure 3.7-2 shows results analogous to those obtained for Case 3 of Section 3.4, i.e., Fig. (3.5-3). The aircraft was controlled with estimated position $\hat{y}$ and stabilized with estimated velocity $\hat{v}_y$ and acceleration a_y. The initial condition errors were the same as for Case 3. It will be noted that the results are quite similar, except for the finite corrections made at the sampling times.

3.9 Summary

This chapter completes the development, begun in Chapter 1, of methods for introducing inertially-measured information into the control system. It has been demonstrated that the feedback of inertial information, the benefits of which were demonstrated for the noise-free case in Chapter 2, is complemented in the noisy case by inertial filtering of ILS beam noise. The simulations show considerable reduction in error amplitudes, particularly in roll angle amplitude.

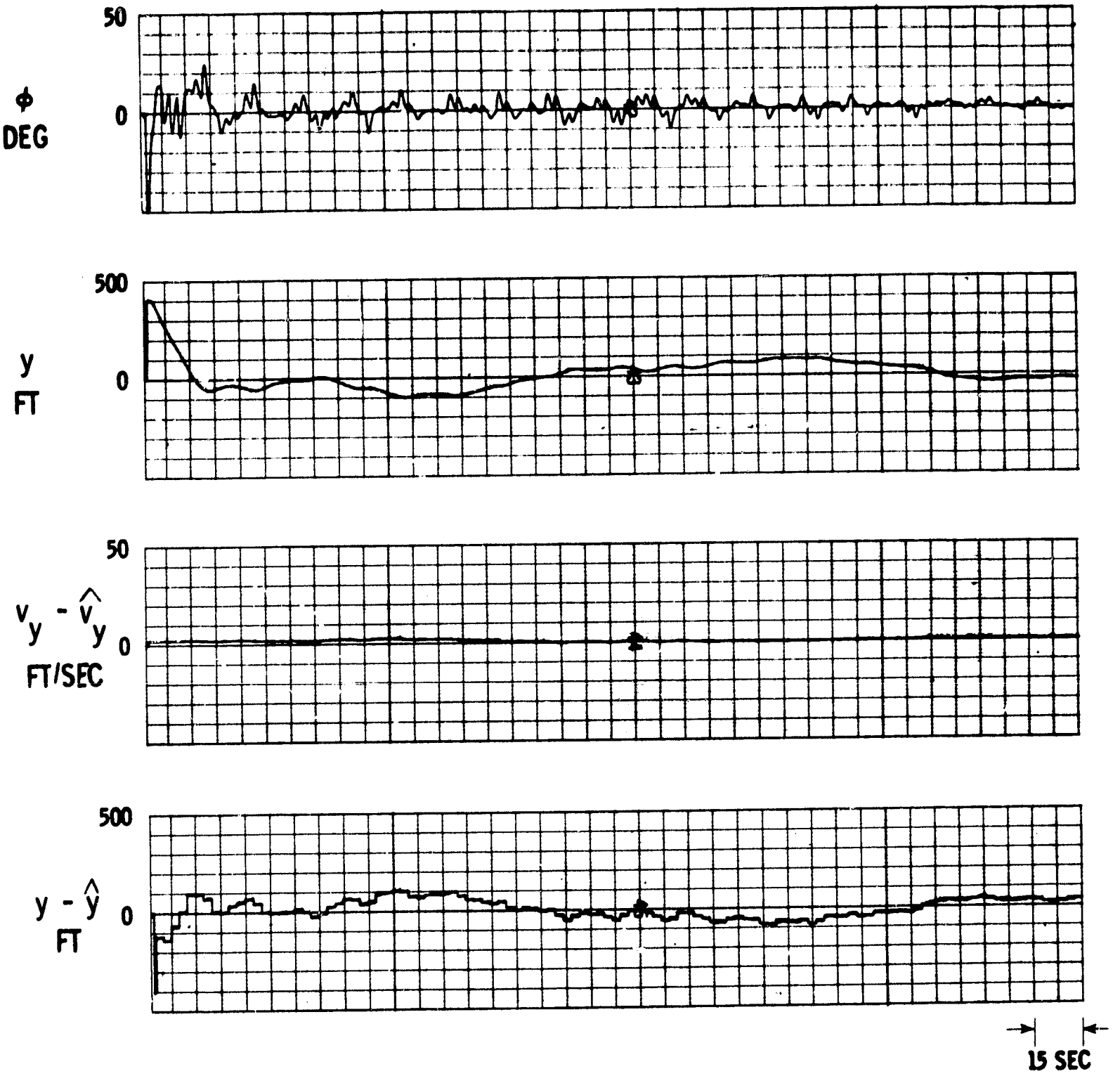

Fig. 3.7-2 Responses of inertially-stabilized system.

CHAPTER 4

OPTIMIZING TRAJECTORY PERFORMANCE

4.1 Introduction

The data derived from the inertial navigator, updated by the ILS system, provides comparatively noise-free information describing the position, velocity and acceleration of the vehicle in earth-fixed coordinates. Full utilization of the new information requires a fundamental reappraisal of the quality of the automatic landing system. Thus it is important to consider certain basic aspects of the control system properties at this point.

Perhaps the most significant measure of control system performance is ability to follow precisely a desired trajectory in space. This property is particularly important in an automatic landing system and will undoubtedly provide the key to acceptance by the airlines and aircrew. Improved trajectory response may be achieved in three ways:

1. Increasing the open-loop gain to reduce dynamic errors and the effects of disturbances.
2. Tailoring the trajectory to match the characteristics of the controlled vehicle.
3. Generalized trajectory control.

Approaches 1, 2 and 3 are now considered in detail.

4.2 Accuracy Improvement and Sensitivity Reduction

The processed inertial system data provides relatively noise-free position, velocity and acceleration data. The position and velocity data is free from lags which characterize the information provided by the ILS system. The acceleration information is subject to a small lag* which does not seriously impair its usefulness as a feedback variable. As a result, the limitations im-

* Since the accelerometers generate incremental velocity information which must be processed to extract acceleration data.

posed by noise and dynamic lags are relaxed and a significant increase in gain can be effected as demonstrated in Chapter 2. The impact of these changes is now carefully considered.

A block diagram of a typical control system is shown in Fig. 4.2-1. The object of the control system is accomplished if the controlled variable C follows the reference input R. The system is subject to disturbances D which interfere with the control process. The fixed elements in the control system are G_1 and G_2 while G_0 and H are subject to modification.

The transfer function between C and R is

$$\frac{C}{R} = \frac{G_0 G_1 G_2}{1 + G_0 G_1 G_2 H} \qquad (4.2\text{-}1)$$

The dynamic response characteristics of the system depend upon the location of the zeros of the denominator. The location of the zeros may be modified by altering the transfer functions G_0 and H. The zeros are normally located to yield an overdamped step response. The rapidity of the response is primarily determined by the crossover frequency of the open-loop transfer function $G_0 G_1 G_2 H$. It is desirable to have the bandwidth as wide as possible; however, the bandwidth is usually limited by considerations such as noise and physical constraints in the actual system.

The effect of external disturbances must always play an important role in control system design. Such effects are considered by examining the transfer function between the controlled input C and the disturbance D.

$$\frac{C}{D} = \frac{G_2}{1 + G_0 G_1 G_2 H} \qquad (4.2\text{-}2)$$

Since G_2 is fixed, the magnitude of the component of C resulting from a disturbance is reduced if the magnitude of the open-loop transfer function $G_0 G_1 G_2 H$ is increased.

The ability to follow a trajectory precisely in space is a prime requirement for an automatic landing system. Control system accuracy is measured by examining the relationship defining the error between the desired and actual responses

$$E = R - C \qquad (4.2\text{-}3)$$

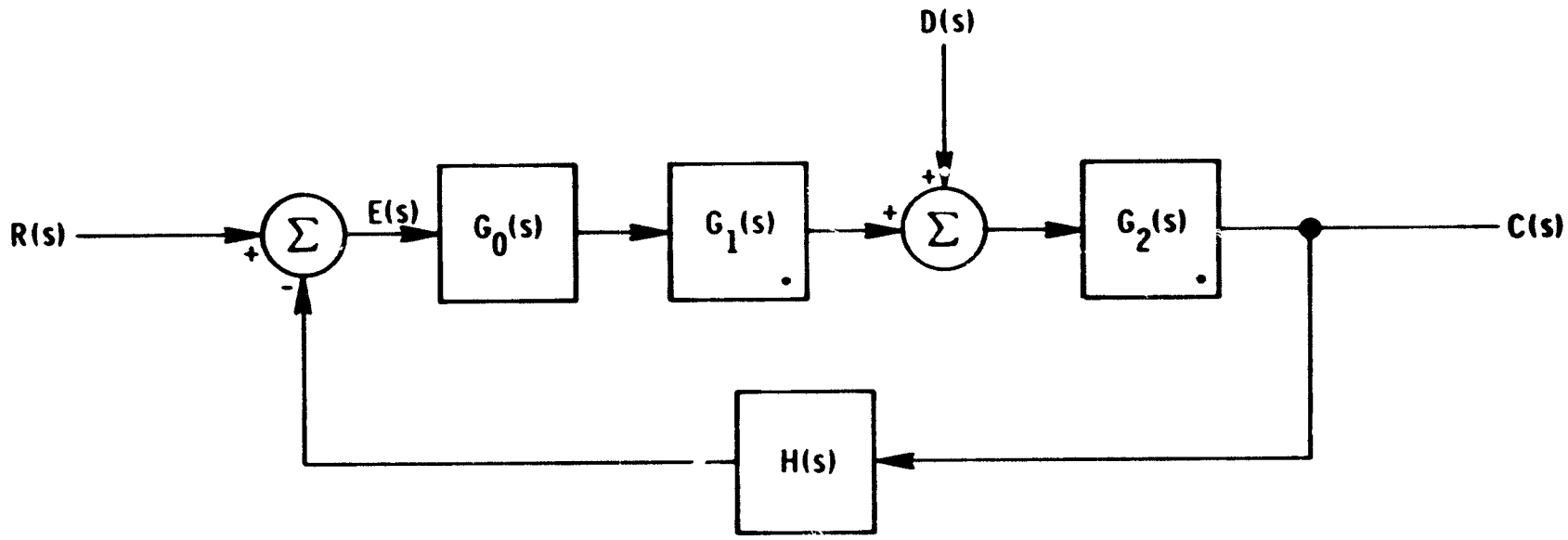

FIXED ELEMENTS OF THE CONTROL SYSTEM

Fig. 4.2-1 Block diagram of a control system with a reference input, R(s), a controlled output, C(s) and a disturbance input, D(s).

and the reference input R.

$$\frac{E}{R} = \frac{1}{1 + G_0G_1G_2H} \tag{4.2-4}$$

It is apparent that an increase in the magnitude characteristics of $G_0G_1G_2H$ reduces the error E. Thus an increase in the open-loop magnitude reduces the sensitivity to disturbances and improves accuracy simultaneously. While it is evident that a considerable improvement is obtained by increasing the open-loop gain, other considerations must be illuminated before a completely satisfactory design is achieved.

4.3 Trajectory Generation

Increased gains decrease the sensitivity of a linear control system to external disturbances, reduce cross-axis coupling and result in a more precise response to a desired trajectory. However, gains cannot be increased indefinitely as a result of considerations such as stability, noise and system nonlinearities. Saturation, in particular, presents a serious problem negating the beneficial effects of enlarged gains and impairing the ability of the vehicle to follow a trajectory precisely.

The most common form of saturation occurs in the effectors which produce the moments and forces required to effect changes in vehicle state. All the aerodynamic effectors of the SST have magnitude and rate limitations. Effector saturation is particularly serious, resulting in an essentially open-loop condition as long as it persists. The effect of saturation is studied by examining the transfer functions of a system linearized about its current operating point. Consider the block diagram in Fig. 4.2-1 and let G_1 represent the effector transfer function. Saturation in effector magnitude or rate modifies G_1 to

$$G_1 = 0 \tag{4.3-1}$$

As a result, the transfer functions relating C to R and C to D become:

$$C/R = 0 \tag{4.3-2}$$

$$C/D = G_2 \tag{4.3-3}$$

Thus reference control is momentarily lost and the sensitivity of the system to disturbances is increased by the factor $1 + G_0G_1G_2H$. It is therefore desirable to

eliminate or prevent saturation.

Saturation may be excited by three sources:

1. Reference commands to the control system.
2. External disturbances acting on the vehicle.
3. The combination of reference commands and external disturbances.

Saturation arising from disturbances is controlled by reducing the magnitude of the open-loop transfer function. Thus the magnitude of the environmental disturbances imposes further restrictions on open-loop gain. Saturation resulting from reference inputs is restricted by processing the reference signal. This aspect is now considered in detail.

The problem of input signal processing may be formulated within the Theory of Optimal Control. For example, consider the linearized dynamical system

$$\dot{x} = f_x x + f_m m \tag{4.3-4}$$

where

x is an n-dimensional state vector
m is an m-dimensional input
f_x is an n x n matrix
f_m is an n x m matrix

The state vector is subject to a set of limits of the form*

$$|x| \leq L_x \tag{4.3-5}$$

$$|\dot{x}| \leq L_{\dot{x}}$$

L_x and $L_{\dot{x}}$ are n-dimensional vectors. The absence of a limit on a particular element of x is signified by setting the corresponding element of L equal to ∞. The problem may be defined as follows:

*The inequality sign signifies that $|x_i| \leq |L_{xi}|$ $i = 1, 2, \ldots, n$

Problem Definition: Find a control m and the corresponding trajectory x, which minimizes the integral performance index

$$J = \int_0^T x' Mx \, dt \tag{4.3-6}$$

subject to the nonholonomic constraint

$$\dot{x} = f_x x + f_m m \tag{4.3-7}$$

and the hard constraints

$$\left.\begin{aligned} |x| &< L_1 \\ |\dot{x}| &< L_2 \end{aligned}\right\} \tag{4.3-8}$$

where

$$\left.\begin{aligned} L_1 &< L_x \\ L_2 &< L_{\dot{x}} \end{aligned}\right\} \tag{4.3-9}$$

The matrix M is positive semi-definite.

The object of the optimization is to transfer the vehicle to the vicinity of a terminal state while satisfying the limits imposed by Eq (4.3-8). The inequalities (4.3-9) are introduced to allow for the effects of disturbances on the system by providing some range between undisturbed operating values and saturation constraints.

The solution of this problem is complicated by the presence of the magnitude constraints. As a result, a two-point boundary problem must be formulated and solved. While the optimal control approach produces the best answer, the resulting computational complexity usually leads to a solution which requires a special-purpose, hybrid computer if real-time control is desired. These problems have discouraged the application of optimal-control techniques.

To circumvent the computational difficulties the following approximate technique for generating solutions to the problem defined above is presented. The

method is particularly suited to vehicle control problems. Consider the simplified vehicle control system shown in Fig. 4.3-1. The desired terminal state may be set equal to

$$x_1 = m_c \tag{4.3-}$$

$$x_2 = 0 \tag{4.3-11}$$

The control input is the variable m_d. The effector output x_2 is subject to saturation

$$|x_2| \leq L_0 \tag{4.3-12}$$

$$|\dot{x}_2| \leq L_1 \tag{4.3-13}$$

These limits imply constraints on the vehicle state of the form

$$|\dot{x}_1| \leq |L_0 K_1| \tag{4.3-14}$$

$$|\ddot{x}_1| \leq |L_1 K_1| \tag{4.3-15}$$

Suppose that the natural frequency of the system in Fig. 4.3-1

$$\omega = \left[\frac{K_0 K_1}{T_0}\right]^{1/2} \tag{4.3-16}$$

is large compared to the bandwidth of the input m_c, and the damping ratio

$$\xi = \frac{1}{2}\left(\frac{1}{T_0 K_0 K_1}\right)^{1/2} \tag{4.3-17}$$

is greater than 1. Then the output satisfies

$$\begin{aligned} x_1 &\approx m_d \\ x_2 &\approx \frac{\dot{m}_d}{K_1} \end{aligned} \tag{4.3-18}$$

provided that

$$|\dot{m}_d| \leq |L_0 K_1| \tag{4.3-19}$$

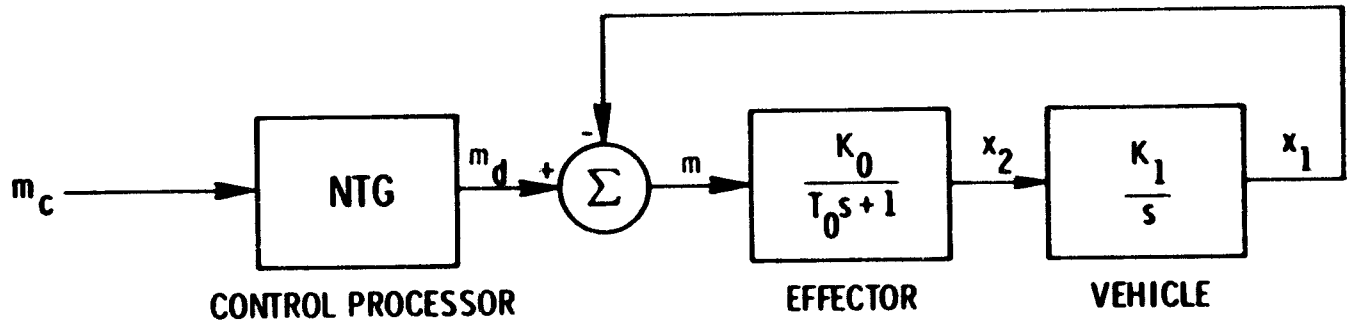

Fig. 4.3-1 Illustrative model of a trajectory control system. The value of x_1 should follow the value of m_d closely.

$$|\ddot{m}_d| \leq |L_1 K_1| \tag{4.3-20}$$

The variable m_d may be identified with the trajectory r. Thus the limits on the state variable x imply corresponding constraints on r if saturation within the control loop is to be avoided. A requirement is consequently established for a device which

1. Controls the bandwidth of the input signal.
2. Modifies the input signal by constraining the maximum amplitudes of its first and second derivatives.

A device having the desired properties is illustrated in Fig. 4.3-2. The device will be referred to as a nonlinear trajectory generator. A linearized model of the NTG is obtained by removing the magnitude limits. The transfer function then becomes

$$\frac{m_d}{m_c} = \frac{K_1}{s^2 + K_2 K_1 s + K_1} \tag{4.3-21}$$

The bandwidth of the transfer function is modified by varying the natural frequency ω_t and is normally equal to the crossover frequency of the open-loop transfer function of the control system. The natural frequency depends upon the value of K_1

$$\omega_t = K_1^{1/2} \tag{4.3-22}$$

The damping ratio ξ_t is normally larger than 1

$$\xi_t = \frac{K_2 K_1^{1/2}}{2} \tag{4.3-23}$$

or

$$K_2 = \frac{2\xi_t}{K_1^{1/2}} \tag{4.3-24}$$

The limits impose the following constraints on the outputs of the NTG

$$|m_d| \leq S_0 \tag{4.3-25}$$

$$|\dot{m}_d| \leq S_1 \tag{4.3-26}$$

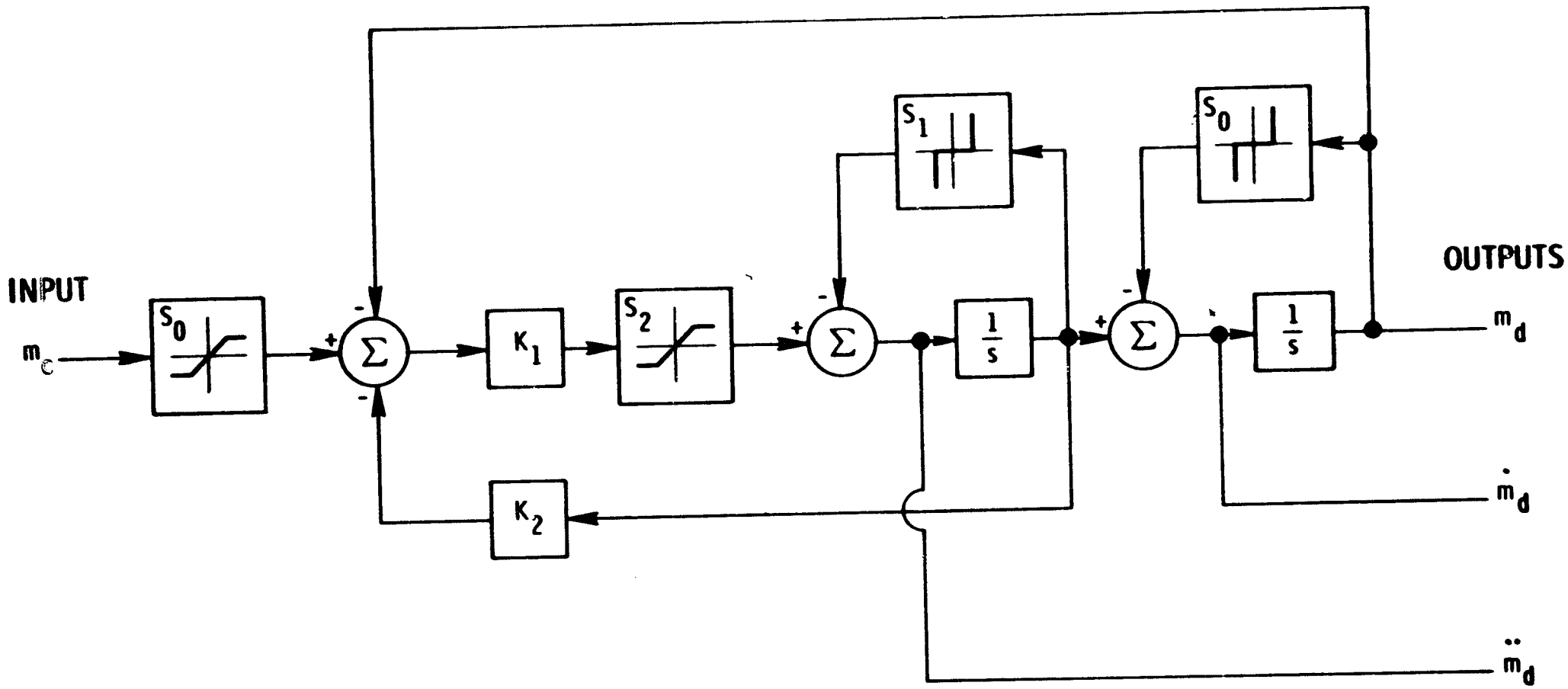

Fig. 4.3-2 Block diagram representation of a second-order nonlinear trajectory generator (NTG).

$$|\ddot{m}_d| \leq S_2 \tag{4.3-27}$$

Saturation of m_d automatically sets $\dot{m}_d$ equal to zero; similarly, saturation of $\dot{m}_d$ sets $\ddot{m}_d$ to zero. Thus the requirements imposed by saturation are satisfied. The availability of first and second derivatives of the output plays an important role in the construction of control systems capable of precisely following a trajectory, as is shown later in the sections on vertical and lateral control system synthesis.

4.4 Generalized Trajectory Control

The closed-loop transfer function between the reference input R and the controlled output of Fig. 4.2-1 was stated earlier to be

$$\frac{C}{R} = \frac{G_0G_1G_2}{1 + G_0G_1G_2H} \tag{4.4-1}$$

It is of interest to consider the asymptotic behavior of this transfer function as the magnitude of the open-loop transfer function varies. Two cases are of interest

(a) $$G_0G_1G_2H \ll 1$$

$$\frac{C}{R} \rightarrow G_0G_1G_2 \tag{4.4-2}$$

(b) $$G_0G_1G_2H \gg 1$$

$$\frac{C}{R} \rightarrow \frac{1}{H} \tag{4.4-3}$$

In the first case it is apparent that the advantages of feedback are lost if the open-loop magnitude is significantly less than one. In the second case the output C will not equal the input R unless H is identically one. This problem may be avoided by operating on the input with H so that Eq (4.4-1) becomes

$$\frac{C}{R} = \frac{G_0G_1G_2H}{1 + G_0G_1G_2H} \tag{4.4-4}$$

Consequently, precision trajectory control is achieved by producing a modified control signal which is a linear transformation of the desired trajectory. Typically, H has the form

$$H = 1 + K_{\dot{x}}s + K_{\ddot{x}}s^2 \qquad (4.4\text{-}5)$$

where $K_{\dot{x}}$ and $K_{\ddot{x}}$ are constants. The form of H in the present application implies that the first and second derivatives of the reference signal must be generated to provide the correct compensation. However, differentiation of the input can be avoided by utilizing the signals available from the nonlinear trajectory generator. The signals from the nonlinear trajectory generator are shown in Fig. 4.3-2 and this utilization is indicated in Fig. 4.4-1. The input R_c to the control system has the required form

$$\begin{aligned} R_c &= R_d + K_{\dot{x}}\dot{R}_d + K_{\ddot{x}}\ddot{R}_d \\ &= \left[1 + K_{\dot{x}}s + K_{\ddot{x}}s^2\right] R_d \\ &= HR_d \end{aligned} \qquad (4.4\text{-}6)$$

The subsequent chapters will consider, in detail, the application of the above techniques to improve system quality.

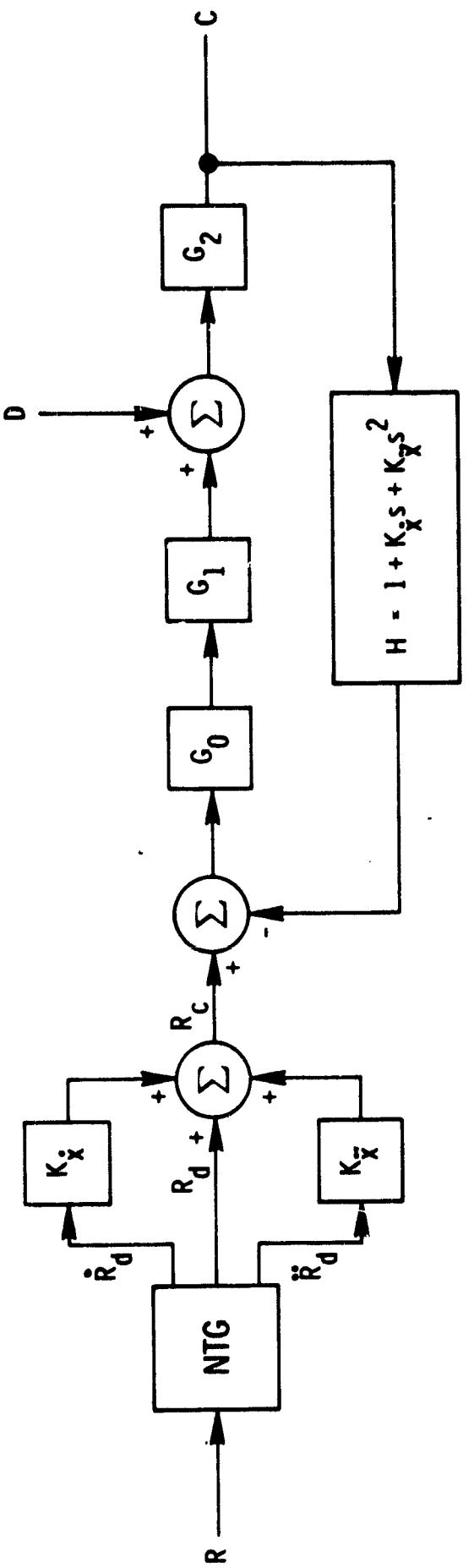

Fig. 4.4-1 Block diagram of a control system incorporating generalized trajectory control.

CHAPTER 5

LATERAL AND VERTICAL CONTROL SYSTEM DESIGN

5.1 Introduction

The fundamental control problem during an automatic landing involves guidance of the aircraft with respect to a path defined by the runway and glide-slope geometry. This chapter contains an exposition of a set of lateral and longitudinal control systems which appear to have significant advantages over systems currently in use.

These control problems will be studied in an earth-fixed reference frame with origin at the point where the glide slope intersects the runway center line. The x-axis lies along the center line, y is horizontal while z is directed downward.

5.2 Lateral Position Control

One of the most important requirements for an automatic landing system is the ability to provide precision guidance with respect to a vertical plane containing the runway center line. Position and velocity relative to the plane are determined by combining information from the ILS localizer signal with data from an inertial navigation system discussed in Chapters 2 and 3. The purpose of the lateral control system is to utilize the position and velocity information to guide the aircraft along an appropriate trajectory relative to the reference.

The primary lateral control variable in coordinated flight (no sideslip angle) is the roll angle of the aircraft. The lateral acceleration under these circumstances may be written:

$$\ddot{y} \approx g \tan \phi \qquad (5.2\text{-}1)$$

The analysis, therefore, will be initiated by a discussion of roll angle control.

5.3 Roll Angle Control System

Attitude control about the aircraft's longitudinal axis is achieved by deflecting the vehicle's ailerons and spoilers, thus exciting a nonsymmetric lift distribution along the transverse axis and producing a resultant x-axis moment. The variation in lift results in a nonsymmetric drag profile resulting in a yawing

moment and an accumulating sideslip angle β. This undesirable effect is generally controlled by generating a counter yaw moment with the rudder. The rudder deflection is linearly related to lateral body axis acceleration which is sensed by a body-mounted accelerometer. The accelerometer output is given by:

$$a_y = \dot{v} + r\, v_p - g \cos\theta \sin\phi \qquad (5.3\text{-}1)$$

where

a_y is the specific force along the y-body axis (ft/sec^2).

$\dot{v}$ is the acceleration of the vehicle along the y-body axis (ft/sec^2).

r is the yaw rate (rad/sec).

v_p is the path velocity (ft/sec).

g is the gravitational constant (32.2 ft/sec^2).

θ, ϕ are pitch and roll Euler angles, respectively.

The roll control system design is based on the transfer characteristics between aileron deflection and roll rate ($\beta = 0$) which are illustrated in Fig. 5.3-1.* At high frequencies the ailerons produce a moment proportional to their deflection. As a result, the roll rate p is proportional to the integral of the aileron deflection. At low frequencies the accumulation in roll rate reduces the moment produced by the ailerons so that the p becomes proportional to aileron deflection.

The effector characteristics are modeled by a simple first-order time lag with a time constant, T_{ail}, of 0.05 seconds.

A linearized model of the roll control system is shown in Fig. 5.3-2. Roll angle and roll-rate gains were selected to yield good damping characteristics and a conservative crossover frequency as shown in Fig. 5.3-3. The resultant closed-loop frequency response is given in Fig. 5.3-4, and the step response of the corresponding linear system is shown in Fig. 5.3-5.

The final design was obtained by integrating a Boeing-designed lateral stability augmentation system (SAS) with appropriate roll-rate gain modifications to account for the roll damping already incorporated in the SAS. The SAS provides the necessary sideslip control for coordinated flight.

Sideslip control is achieved by using the accelerometer output Eq (5.3-1) corrected by heading rate information and feedforward coupling from the aileron command to provide the required rudder deflection. The complete design is shown

* The transfer functions are derived in Appendix C.

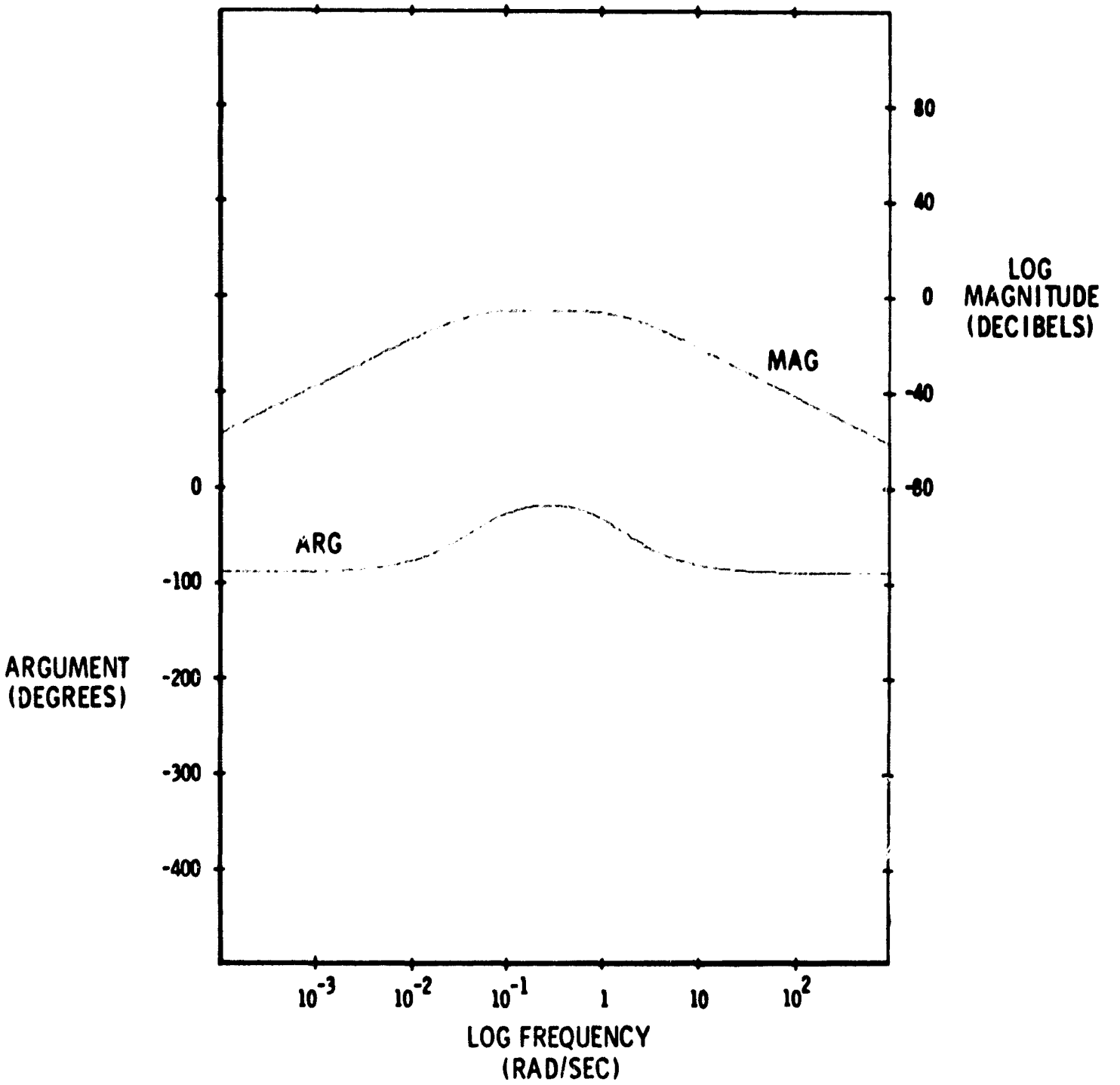

Fig. 5.3-1 Transfer function relating roll rate to aileron deflection, $\left(\frac{p}{\delta_a}\right)_{\beta = 0}$.

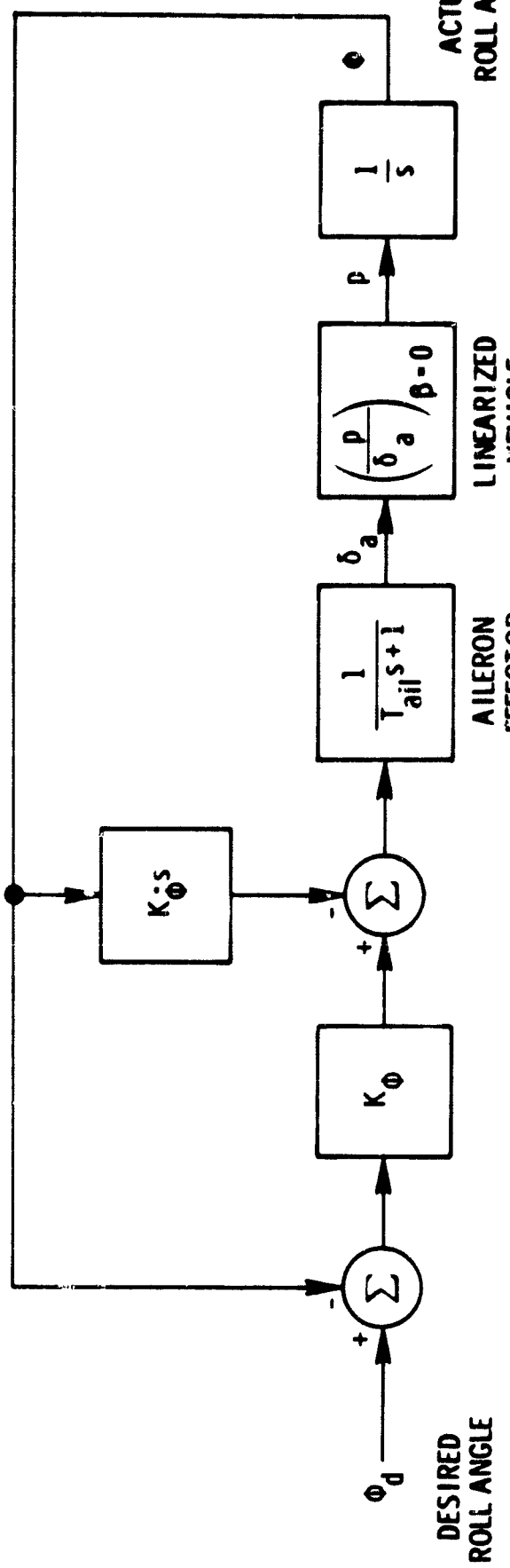

Fig. 5.3-2 Linear model of the roll angle control system.

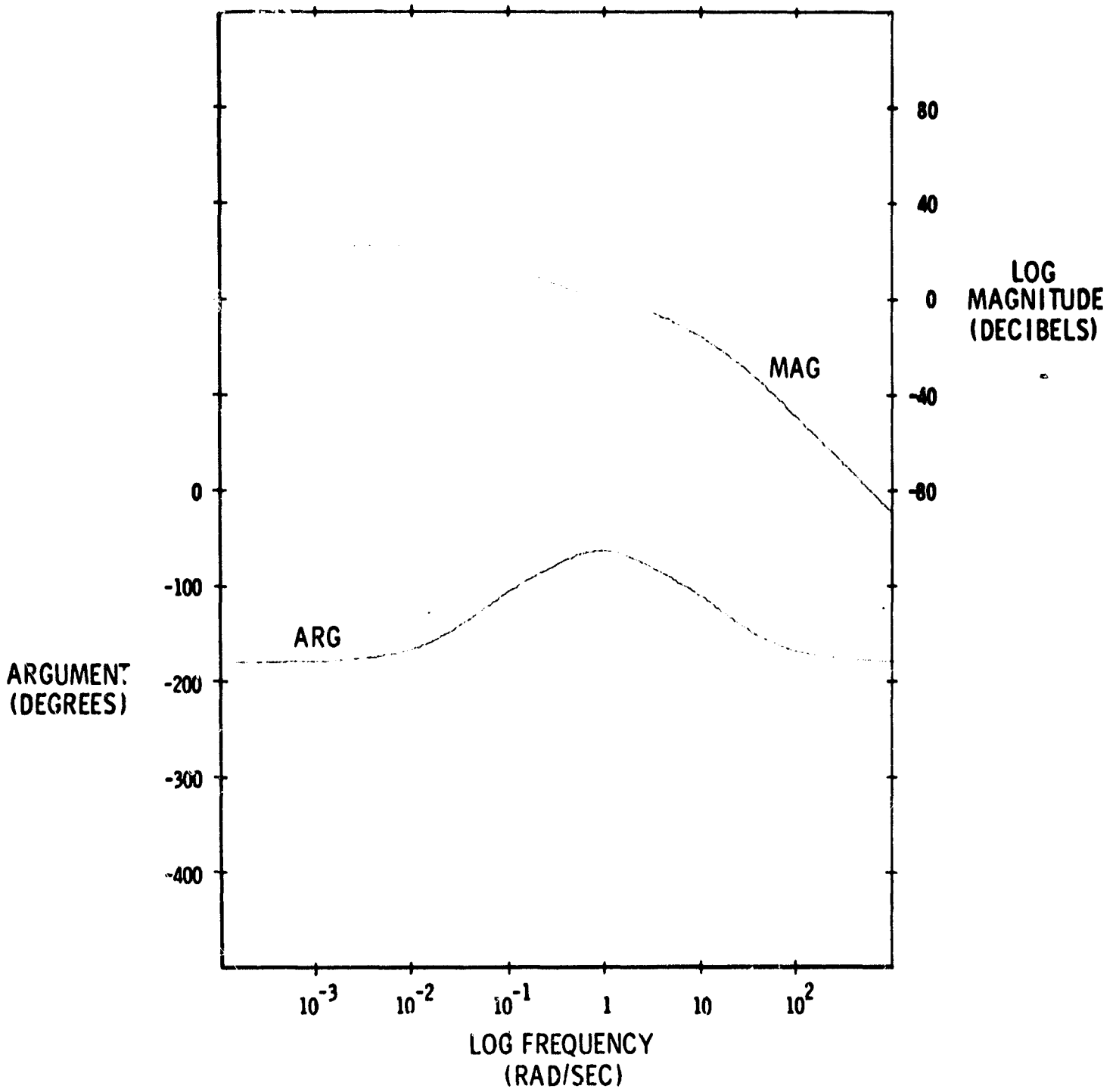

Fig. 5.3-3 Open-loop transfer function for the roll angle control system.

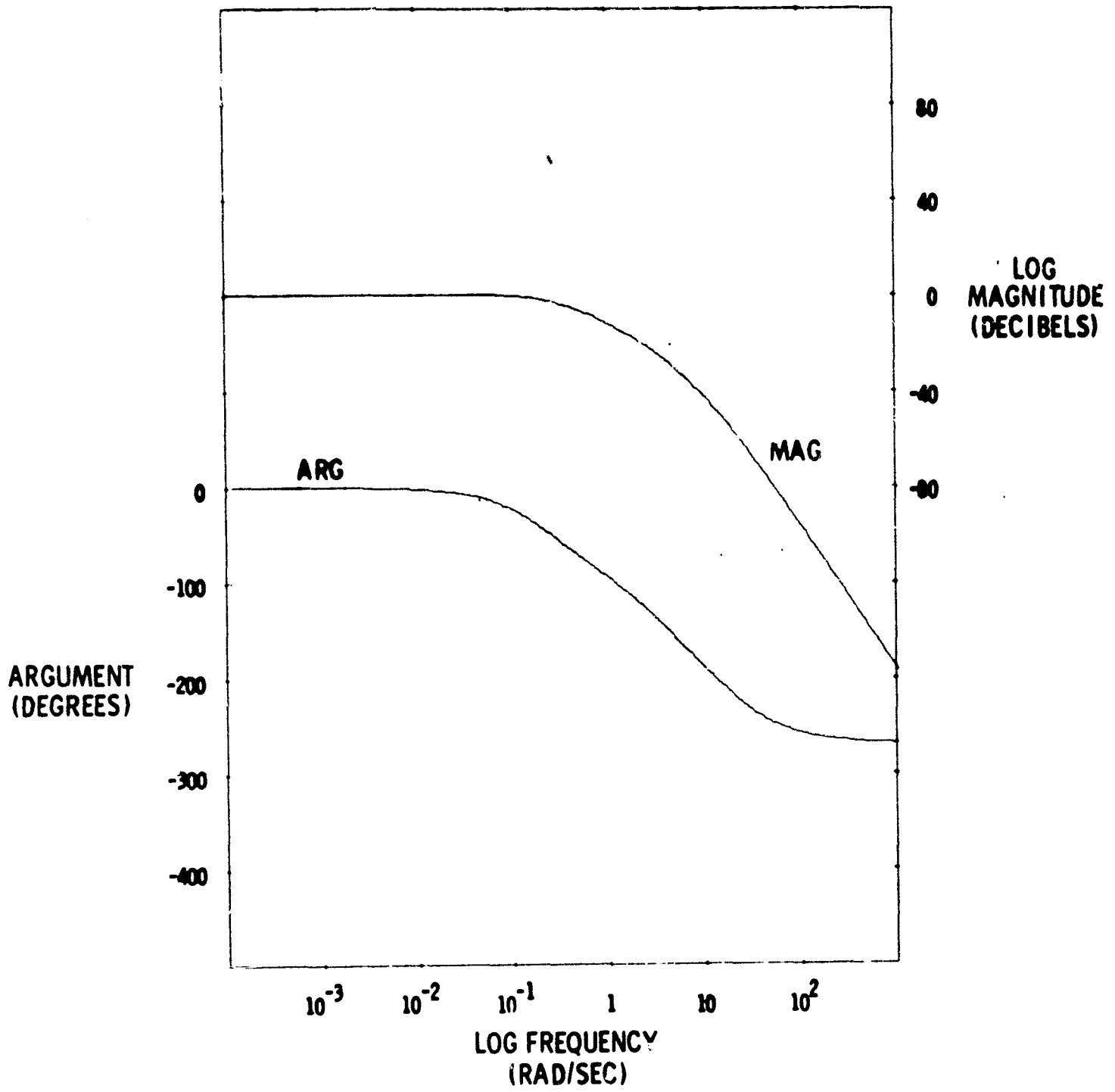

Fig. 5.3-4 Closed-loop frequency response of the roll angle control systems, $\frac{\phi}{\phi_d}$.

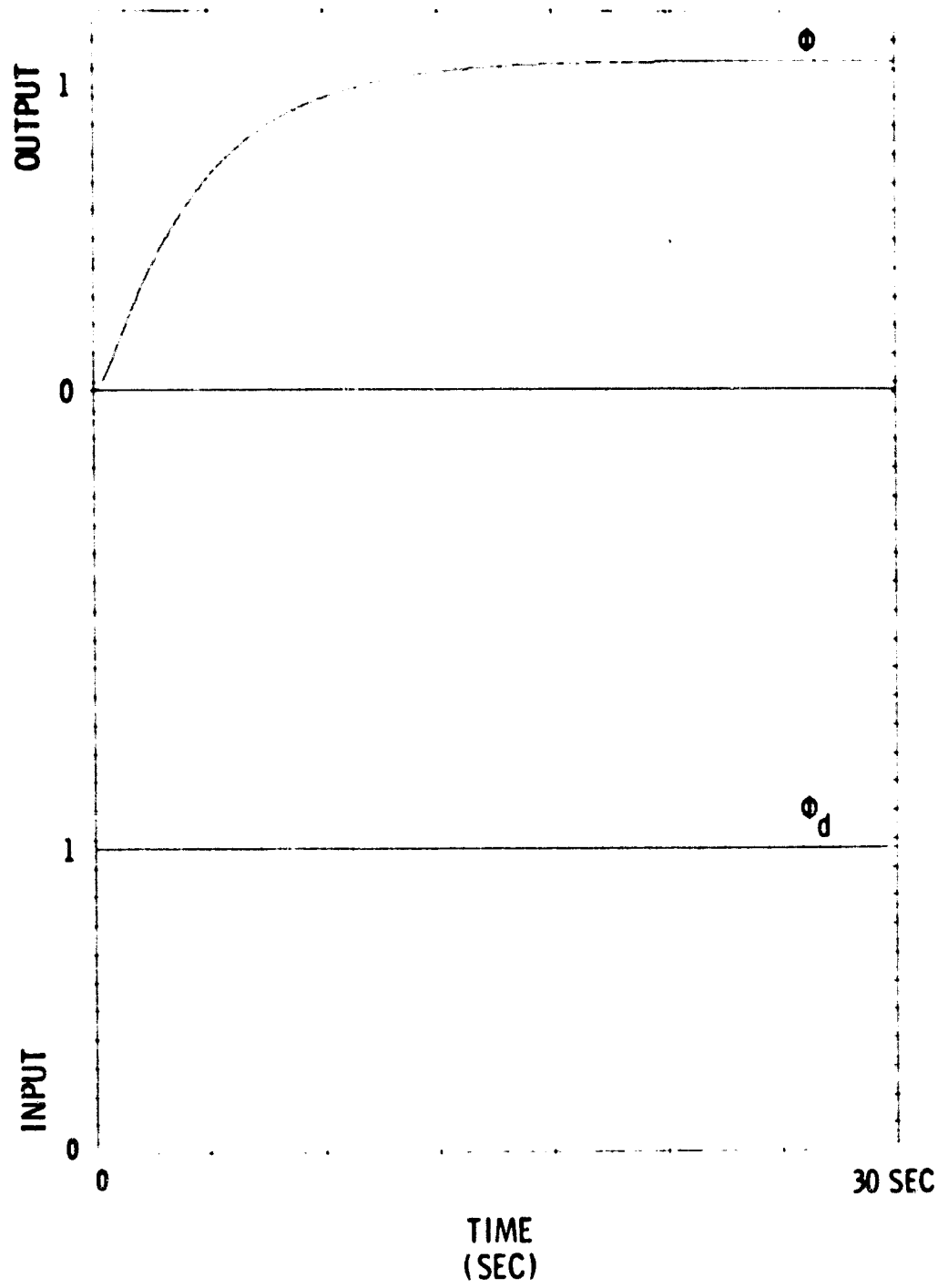

Fig. 5.3-5 Response of the linearized roll control system to a unit-step input.

in Fig. 5.3-6. The parameters shown on the diagram are defined and listed in Table 5.3-1.

5.4 Linear Analysis of a Lateral Position Control System

A simplified linear model of a lateral control system is shown in Fig. 5.4-1. The model utilizes the linear roll angle control system illustrated in Fig. 5.3-2 and is thus based on the assumption of coordinated turns. Under these circumstances the vehicle equations are particularly simple, and the lateral acceleration $\ddot{y}$ may be written:

$$\ddot{y} \approx g\,\phi \tag{5.4-1}$$

where

g is the gravitational constant ($g = 32.2$ ft/sec^2).

ϕ is the roll angle (radians).

Trajectory control is achieved by the closure of a position control loop on the filtered inertial position y. Dynamic response requirements are satisfied by the closure of additional loops on processed inertial velocity $\dot{y}$, lateral acceleration $\ddot{y}$ and approximate acceleration rate $g\,\dot{\phi}$.

The forward-loop transfer function is written:

$$G_y = K_y \frac{g\phi}{s^2 \phi_d} \tag{5.4-2}$$

The open-loop transfer function is given by:

$$G_y H_y = K_y \frac{g\phi}{s^2 \phi_d} \left[1 + \frac{K_{\dot{y}}}{K_y} s + \frac{K_{\ddot{y}}}{K_y (T_a s + 1)} s^2 + \frac{K_{\dddot{y}}}{K_y} g\,\dot{\phi} \right] \tag{5.4-3}$$

and is shown in Fig. 5.4-2

where

K_y is the adjustable position feedback gain.

$K_{\dot{y}}$ is an adjustable velocity feedback gain.

$K_{\ddot{y}}$ is an adjustable acceleration feedback gain.

$K_{\dddot{y}}$ is an adjustable acceleration rate feedback gain.

T_a is the time constant of a first-order lag associated with the acceleration feedback loop.

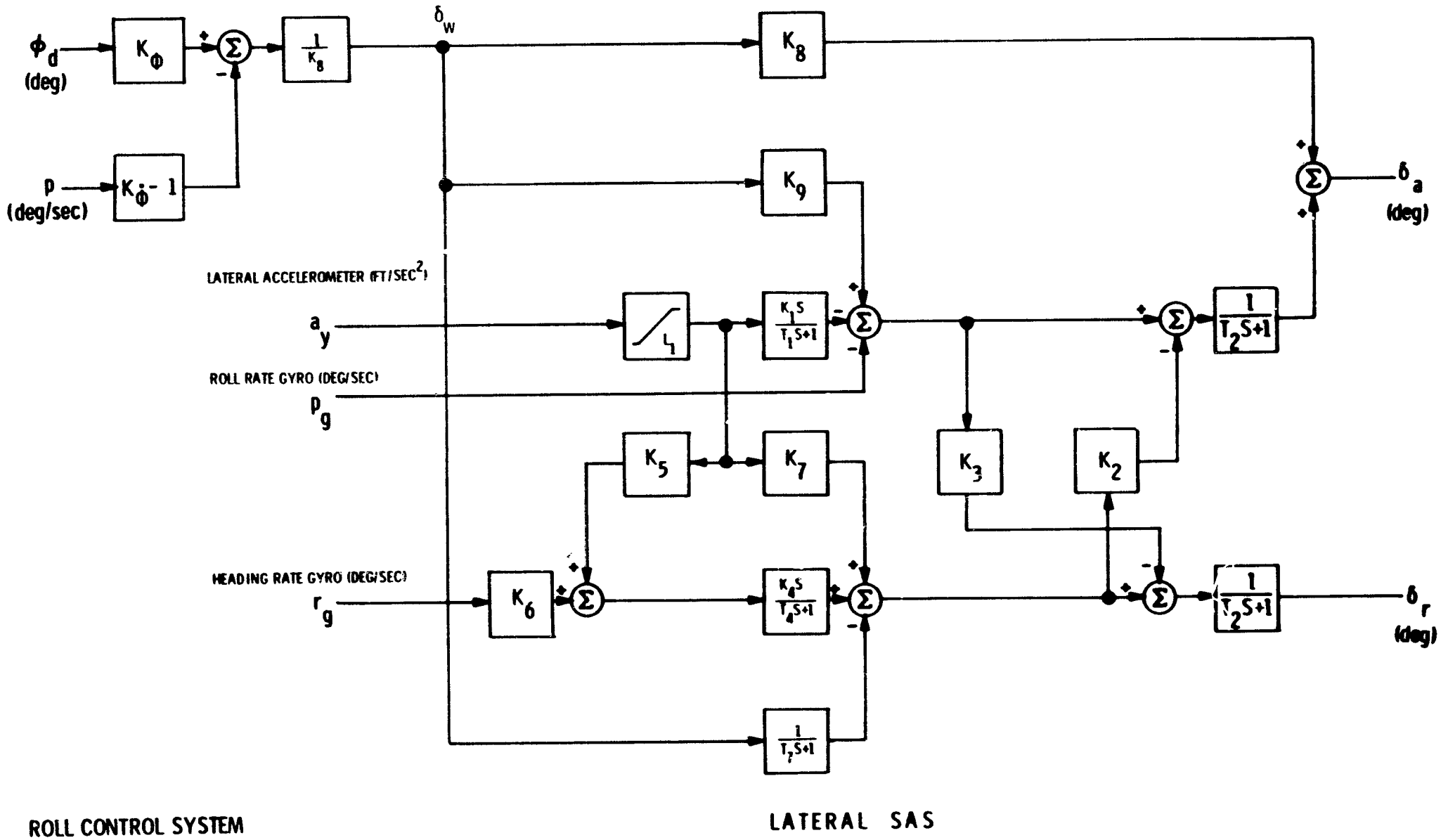

Fig. 5.3-6 Roll angle control system with lateral SAS.

Table 5.3-1 Roll Angle Control System Parameters

PARAMETER	VALUE
K_{ϕ}	1.000
$K_{\dot{\phi}}$	2.000
K_1	3.000
K_2	0.170
K_3	0.374
K_4	2.000
K_5	2.000
K_6	3.000
K_7	2.000
K_8	0.666
K_9	0.534
T_1	1.000
T_2	0.500
T_4	2.000
T_7	1.000
L_1	10.000

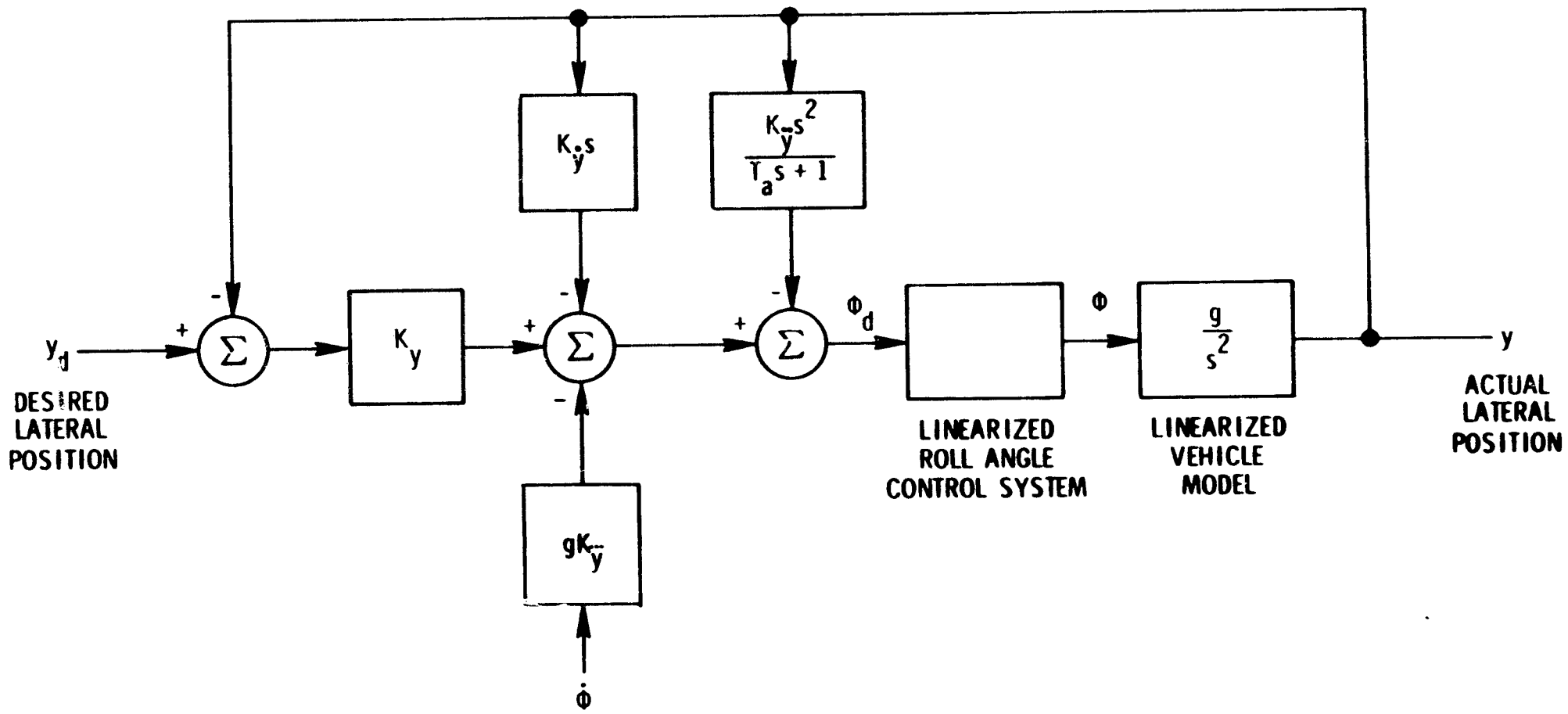

Fig. 5.4-1 Linearized model of lateral control system.

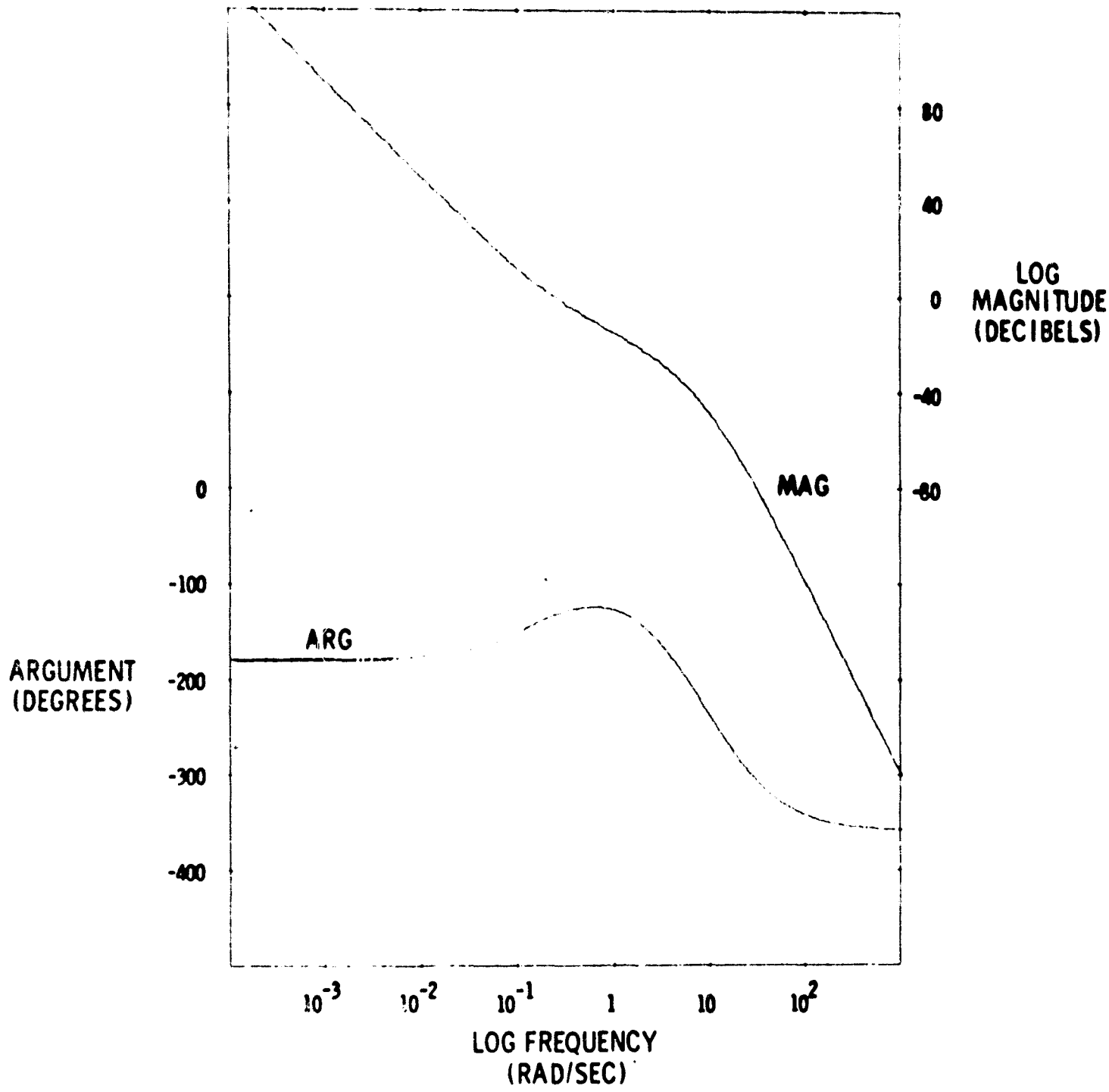

Fig. 5.4-2 Open-loop transfer function of the linearized lateral control system.

The simple lag in the acceleration loop reflects the fact that a pure acceleration signal is not available from most inertial systems. The corresponding closed-loop transfer function:

$$\frac{y}{y_d} = \frac{G_y}{1 + G_y H_y} \tag{5.4-4}$$

is illustrated in Fig. 5.4-3. The unit-step response of the illustrated linear system appears in Fig. 5.4-4. Parameter values appear in Table 5.8-1. Some practical problems are now considered.

5.5 Compensation for Steady Lateral Errors

If an aircraft is moving through an air mass having a low-frequency component of acceleration $\dot{w}_y$ perpendicular to the desired flight path, the aircraft heading angle must change in continuous fashion in order to maintain a zero velocity component perpendicular to the path. The relationship between wind velocity and crab angle with respect to the path is given by:

$$\psi_c = -\sin^{-1}\left(\frac{w_y}{v_p}\right) \tag{5.5-1}$$

Equation (5.5-1) implies that the heading rate must obey the relationship:

$$\dot{\psi}_c = -\frac{\dot{w}_y}{v_p \cos \psi_c} \tag{5.5-2}$$

Thus if $\dot{w}_y$ is constant, a constant heading rate must be maintained:

$$\dot{\psi}_c = \frac{g \tan \phi}{v_p} \tag{5.5-3}$$

In the system shown in Fig. 5.4-1 this heading rate may only be maintained if a position error e_y exists:

$$e_y = \frac{\phi}{K_y} \tag{5.5-4}$$

The steady-state error may be eliminated by the application of proportional plus integral compensation as shown in Fig. 5.5-1 . The output of the proportional plus integral compensator provides a signal equal to the error e_y plus a quantity proportional to the integral of the error. The integrator accumulates an output equal to ϕ/K_y. In the steady state e_y is zero, and the conditions for preservation of zero position error are satisfied. The value of integrator gain K_{iy} is selected through compromise between dynamic response degradation and static response improvement.

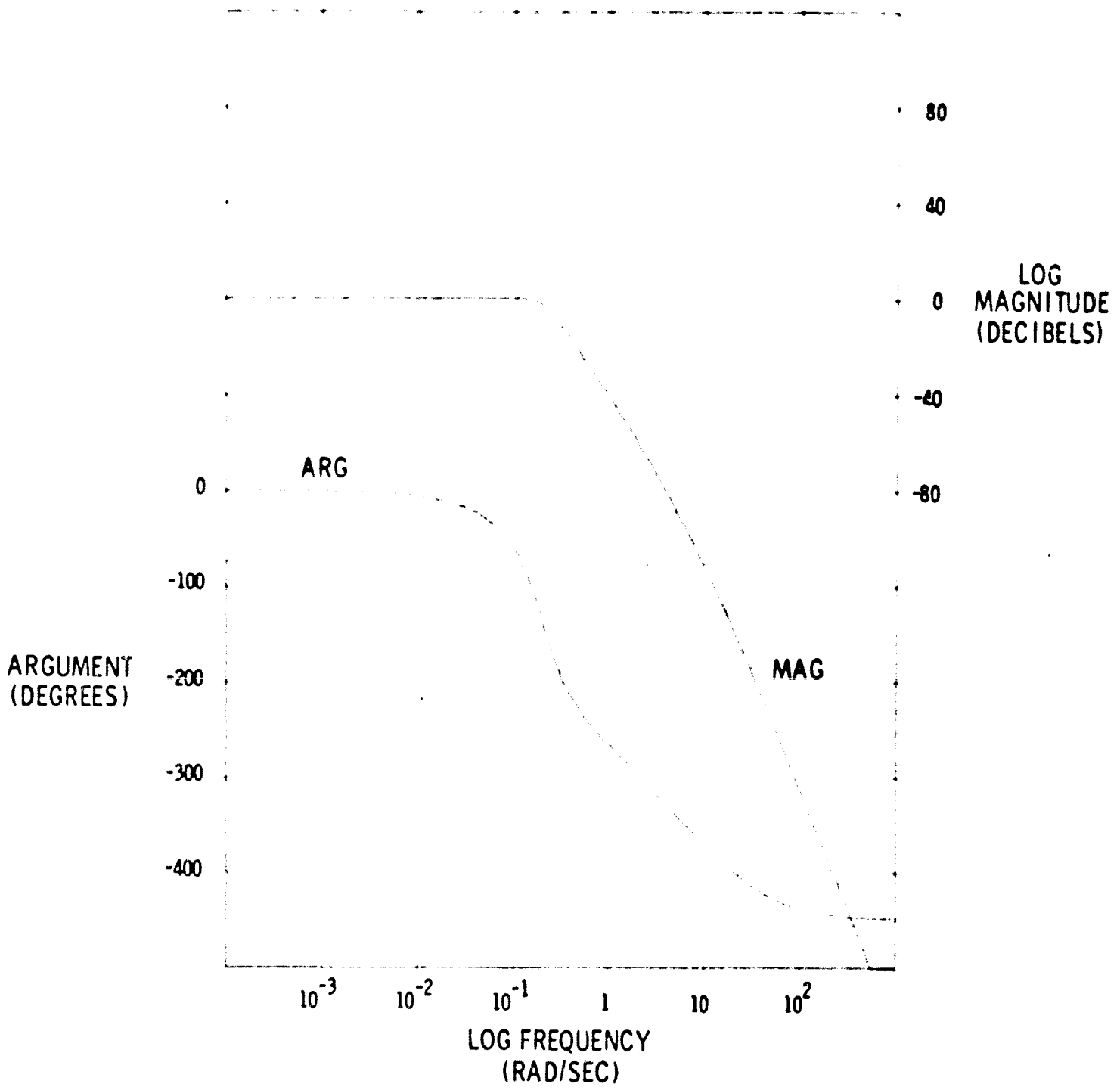

Fig. 5.4-3 Closed-loop transfer function $\frac{y}{y_d}$ for the linearized lateral control system.

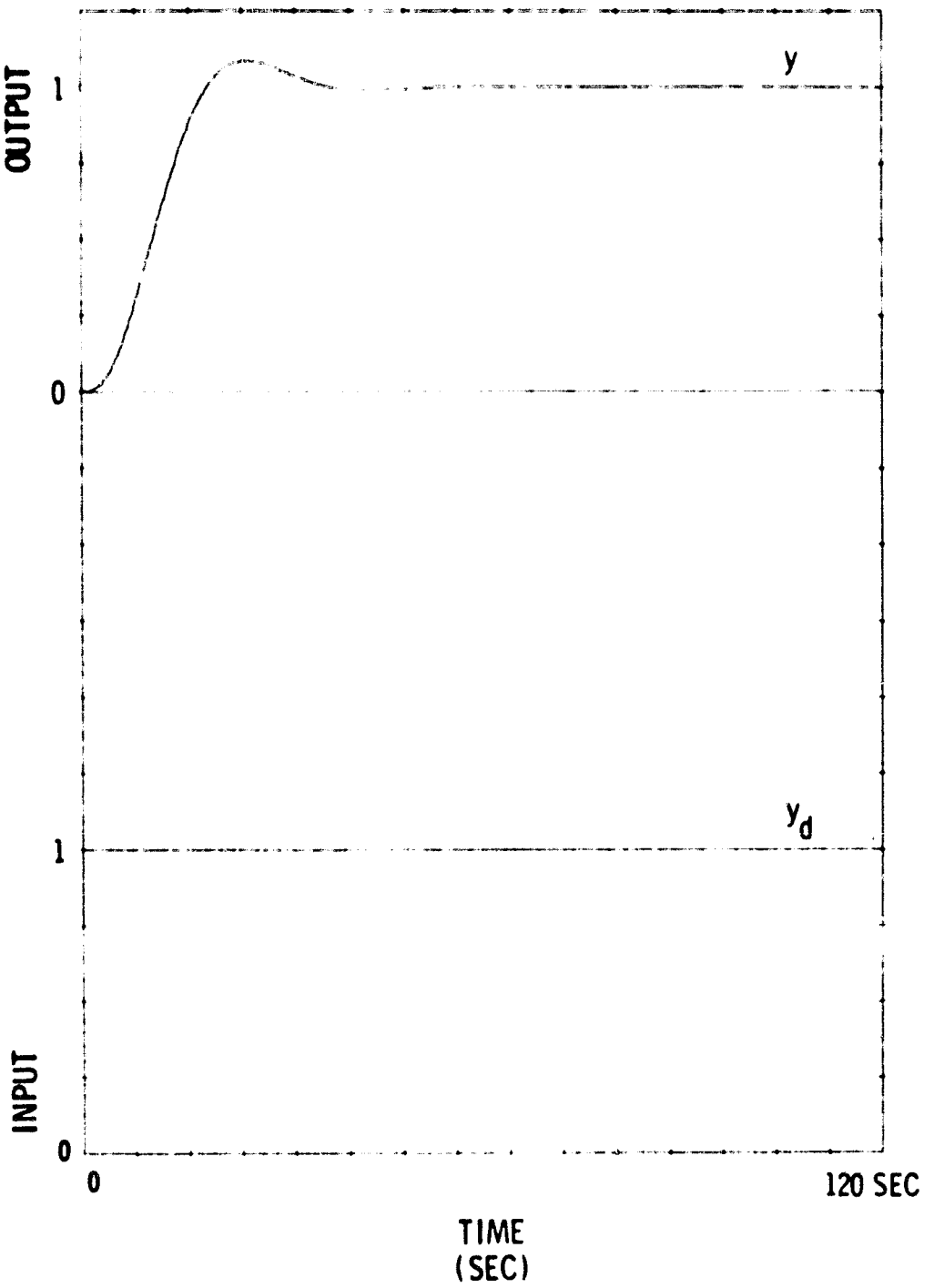

Fig. 5.4-4 Unit-step response of the linearized lateral control system.

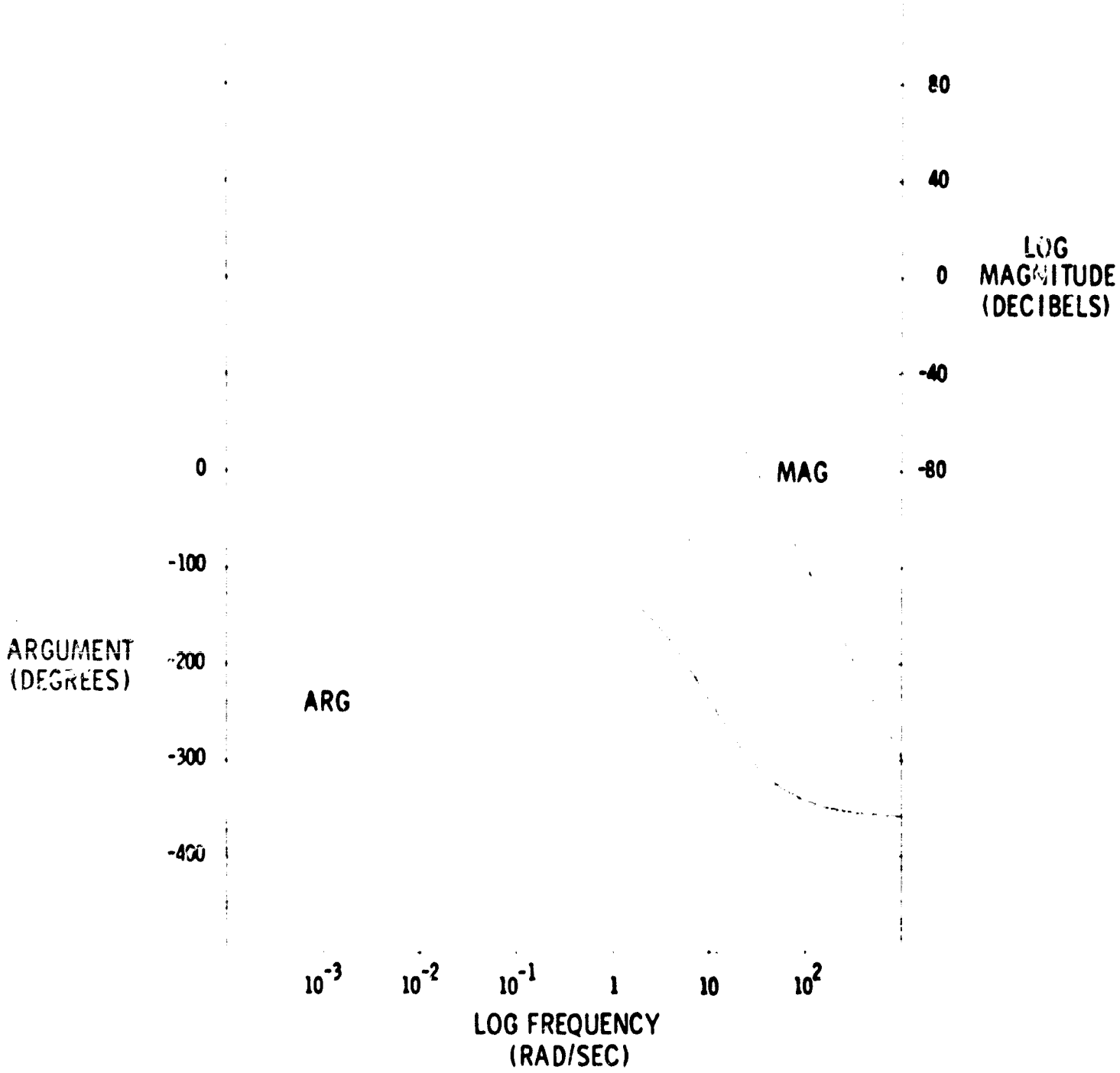

Fig. 5.5-1 Open-loop transfer function of the linearized lateral control system showing the effect of integral compensation.

The effect of the compensator on the open-loop transfer function is shown in Fig. 5.5-1.

5.6 Nonlinear Design Considerations for Lateral Control

The prime source of nonlinearity in the lateral control system arises from the requirements imposed by passenger comfort on the maximum roll angle and roll angular rate. The requirements impose restrictions on lateral acceleration and acceleration rate, which must be reflected in lateral trajectory synthesis. The desired lateral trajectory is described by the equations:

$$|\dot{y}_d| \leq v_p \sin |\psi_{max}| \tag{5.6-1}$$

$$|\ddot{y}_d| \leq \alpha_y \, g \tan |\phi_{max}| \tag{5.6-2}$$

where

ψ_{max} is the maximum path angle relative to the runway center line.

ϕ_{max} is the maximum roll angle.

α_y is a constant between 0 and 1.

The constant α_y is introduced to ensure that sufficient roll angular range is available to counteract environmental disturbances.

In addition to expressing these absolute limitations, the global dynamics of the trajectory should match those of the vehicle-control system in order to achieve precise tracking. The problem is solved by selection of the natural frequency ω_y and damping ζ_y of the nonlinear trajectory generator (NTG_y), as discussed in Section 4.3.

In addition to ensuring that the desired trajectory satisfies the restrictions imposed by the roll constraints, it is important to ensure that these limits will not be exceeded as a result of severe environmental disturbances. Absolute limiting of roll angle and roll angle rate is achieved by the introduction of a device which will be referred to as a command signal processor (CSP). The CSP is inserted between the commanded roll angle ϕ_c and the desired roll angle ϕ_d. The structure of the CSP is identical to that of the NTG shown in Fig. 4.3-2. The primary distinction lies in the selection of the dynamic parameters $\omega_{c\phi}$ and $\zeta_{c\phi}$ for the CSP. These are selected such that:

$$\omega_{c\phi} >> \omega_{\phi} \tag{5.6-3}$$

$$\zeta_{c\phi} \geq 1 \tag{5.6-4}$$

where

$\omega_{c\phi}$ is the natural frequency of CSP (rad/sec).

$\zeta_{c\phi}$ is the damping ratio of the CSP.

ω_{ϕ} is the natural frequency associated with the dominant roots of the roll angle control system.

As a result of these restrictions, it is apparent that the output ϕ_d will essentially equal the input ϕ_c providing the constraints imposed by CSP_{ϕ}

$$|\phi_d| \leq |\phi_{max}| \tag{5.6-5}$$

$$|\dot{\phi}_d| \leq |\dot{\phi}_{max}| \tag{5.6-6}$$

$$|\ddot{\phi}_d| \leq |\ddot{\phi}_{max}| \tag{5.6-7}$$

are not violated. Thus the limiting properties of the CSP may be introduced without affecting the loop gain of the lateral control system.

5.7 Velocity and Acceleration Control

In a control system where accurate trajectory control is the important goal, the requirements to achieve this goal should be examined. The value of y will continuously equal y_d if and only if

$$y = y_d \tag{5.7-1}$$

$$\dot{y} = \dot{y}_d \tag{5.7-2}$$

$$\ddot{y} = \ddot{y}_d \tag{5.7-3}$$

It is desirable to maintain the equalities (5.7-1), (5.7-2) and (5.7-3) as closely as possible if the trajectory error, the difference between y and y_d, is to be small. These goals may be achieved by generating the roll angular command in

the form

$$\phi_d = K_y \left(\frac{s + K_{iy}}{s}\right)\left(y_d - y\right) + K_{\dot{y}}\left(\dot{y}_d - \hat{\dot{y}}\right) + K_{\ddot{y}}\left(\ddot{y}_d - \frac{s}{T_a s + 1}\hat{\ddot{y}}\right) + K_{\dddot{y}} g\dot{\phi} + \phi_r \tag{5.7-4}$$

Thus the desired roll angle directly depends on the errors in the equalities and is modified to preserve trajectory precision. The low value of K_y, compared with $K_{\dot{y}}$ and $K_{\ddot{y}}$, would normally lead to a vehicle path which achieves velocity and acceleration accuracy at the expense of position error. This effect is controlled by the proportional plus integral compensator

$$G_{iy} = \frac{s + K_{iy}}{s} \tag{5.7-5}$$

which provides a monotone increasing weight to any residual position error as time increases. The control of acceleration is complicated by the presence of two measures of vehicle acceleration, lagged inertial acceleration and vehicle roll angle.

Since the lateral vehicle acceleration is approximately equal to

$$\ddot{y} = g \tan \phi \tag{5.7-6}$$

it is apparent that a desired acceleration $\ddot{y}_d$ requires a roll angle

$$\phi = \tan^{-1}\left(\frac{\ddot{y}_d}{g}\right) \tag{5.7-7}$$

The roll angle requirement is satisfied by generating a reference angle

$$\phi_r = \tan^{-1}\left(\frac{\ddot{y}_d}{g}\right) \tag{5.7-8}$$

which is added to the input ϕ_d of the roll CSP.

5.8 Lateral Control System Configuration

The structure of the lateral control system is shown in Fig. 5.8-1. The gains and parameters values associated with the NTG and CSP are given in Table 5.8-1. The roll control system, shown in block form, is described in detail in Section 5.3. A detailed analysis of the CSP and NTG is found in Section 5.6 and 4.3, respectively.

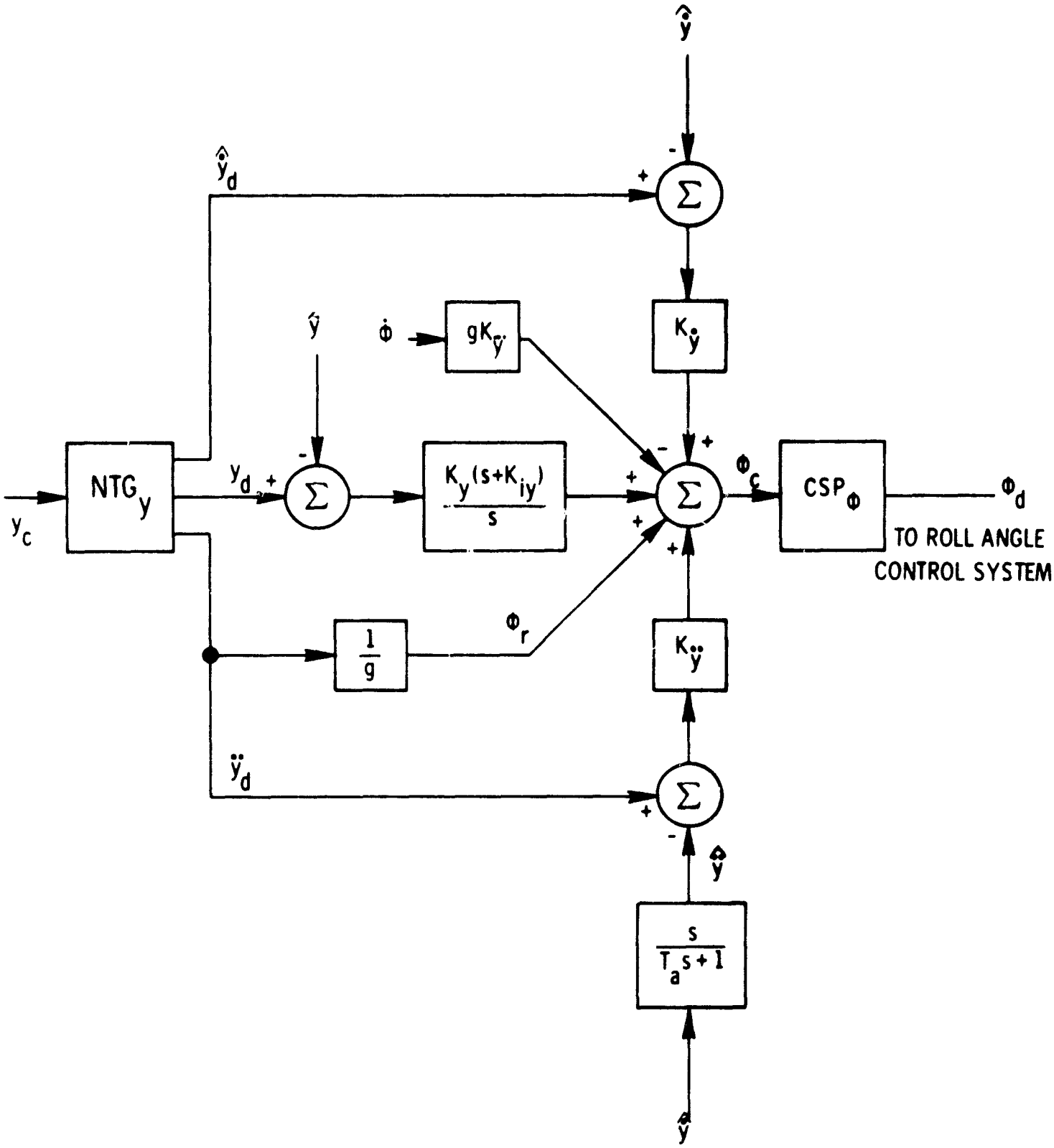

Fig. 5.8-1 Improved lateral position control system with nonlinear trajectory generation, roll command signal processing and inertial stabilization.

Table 5.8-1 Lateral Control System Parameters

GAINS		
K_y	Lateral position gain	0.051 deg/ft
$K_{\dot{y}}$	Lateral velocity gain	0.510 deg/ft/sec
$K_{\ddot{y}}$	Lateral acceleration gain	1.020 deg/ft/sec^2
$K_{\dddot{y}}$	Lateral acceleration rate gain	0.0310 deg/ft/sec^3
K_{iy}	Integral compensator gain	0.020 sec
CONSTANTS		
T_a	Lateral acceleration filter time constant	0.100 seconds
SATURATION LIMITS	IMPOSED BY VEHICLE LIMITS	IMPOSED BY NTG OR CSP
y	∞	∞
$\dot{y}$	±244.000 ft/sec	±244.000
$\ddot{y}$	±18.60 ft/sec^2	± 8.000 ft/sec^2
ϕ	± 30.000 degrees	±30.000 degrees
$\dot{\phi}$	±43.790 deg/sec	±10.000 deg/sec
$\ddot{\phi}$	±21.890 deg/sec^2	±10.000 deg/sec^2
NTG PARAMETERS		
ω_y	NTG_y natural frequency	0.200 rad/sec
ε_y	NTG_y damping ratio	1.000
ω_ϕ	CSP_ϕ natural frequency	8.660 rad/sec
ε_ϕ	CSP_ϕ damping ratio	4.330

5.9 Lateral Control System Response Characteristics

The response* of the lateral control system to a y position error and a zero initial y velocity is shown in Fig. 5.9-1. The variables shown correspond to those in Fig. 5.8-1. While the vehicle velocity $\hat{\dot{y}}$ and acceleration $\hat{\ddot{y}}$ are not precise duplicates of the desired velocity $\dot{y}_d$ and acceleration $\ddot{y}_d$, the error between the position responses $\hat{y}$ and y_d is quite small. The nonlinear character of the vehicle response to an initial y error ($\dot{y} = 0$) is illustrated in Fig. 5.9-2. Response nonlinearity is a result of the control imposed on maximum roll angle and rate.

5.10 Vertical Flight Path Control

Precise altitude control is also an important consideration in an automatic landing system design. The first vertical control phase occurs before localizer acquisition when the altitude is changed to h_{aq}, the altitude of intersection with the glide-slope center line at the termination of the ACQUISITION maneuver. Shortly before acquisition is terminated the desired vertical path is again altered to permit a smooth transition to a flight path coincident with the glide-slope center line which is followed until the terminal maneuvers, FLAREOUT and DECRAB.

The primary vertical control variable is the aircraft pitch angle θ. Thus the next section will consider the design of a pitch attitude control system.

A primary requirement for vertical guidance is effective flight path velocity control. Throughout this discussion it will be assumed that the aircraft is provided with an automatic throttle so that the airspeed is maintained at a constant value ($v_{as} \approx 244$ ft/sec, $u = 0$).

5.11 Pitch Angle Control System

Angular control about the transverse vehicle axis is effected by operating the auxiliary and main elevators. Such action produces a change in the lift provided by the horizontal stabilizer and resultant moment about the y body axis. The transfer function relating pitch rate to elevator deflection at constant speed ($u = 0$) is shown in Fig. 5.11-1. At high excitation frequencies the moment is proportional to elevator deflection. Thus the pitch rate is proportional to the integral of the elevator deflection at high frequencies. At low frequencies the increase in pitch rate due to elevator deflection reduces the deflection-produced moment resulting in a pitch rate proportional to δ_e.

The elevator deflection command is structured from the closure of a pitch angle control loop to provide the primary objective and a pitch rate feedback branch to obtain satisfactory response dynamics. Modest gains were selected to minimize the effect of sensor noise and to reduce the possibility of exciting the important body

* Obtained using the simulation described in Appendix D.

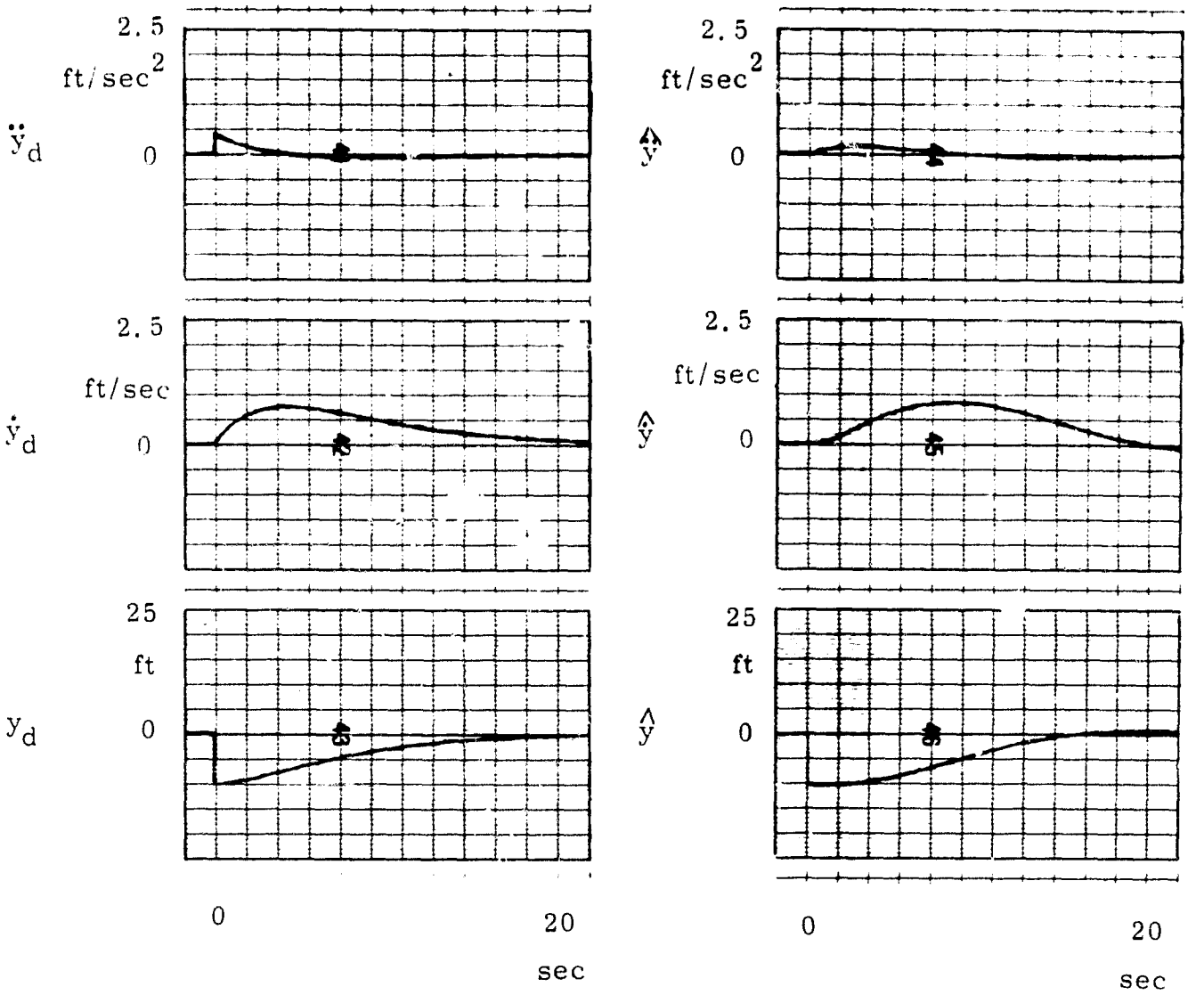

Fig. 5.9-1 Lateral control system response to a 10 ft initial displacement in y ($\dot{y} = 0$).

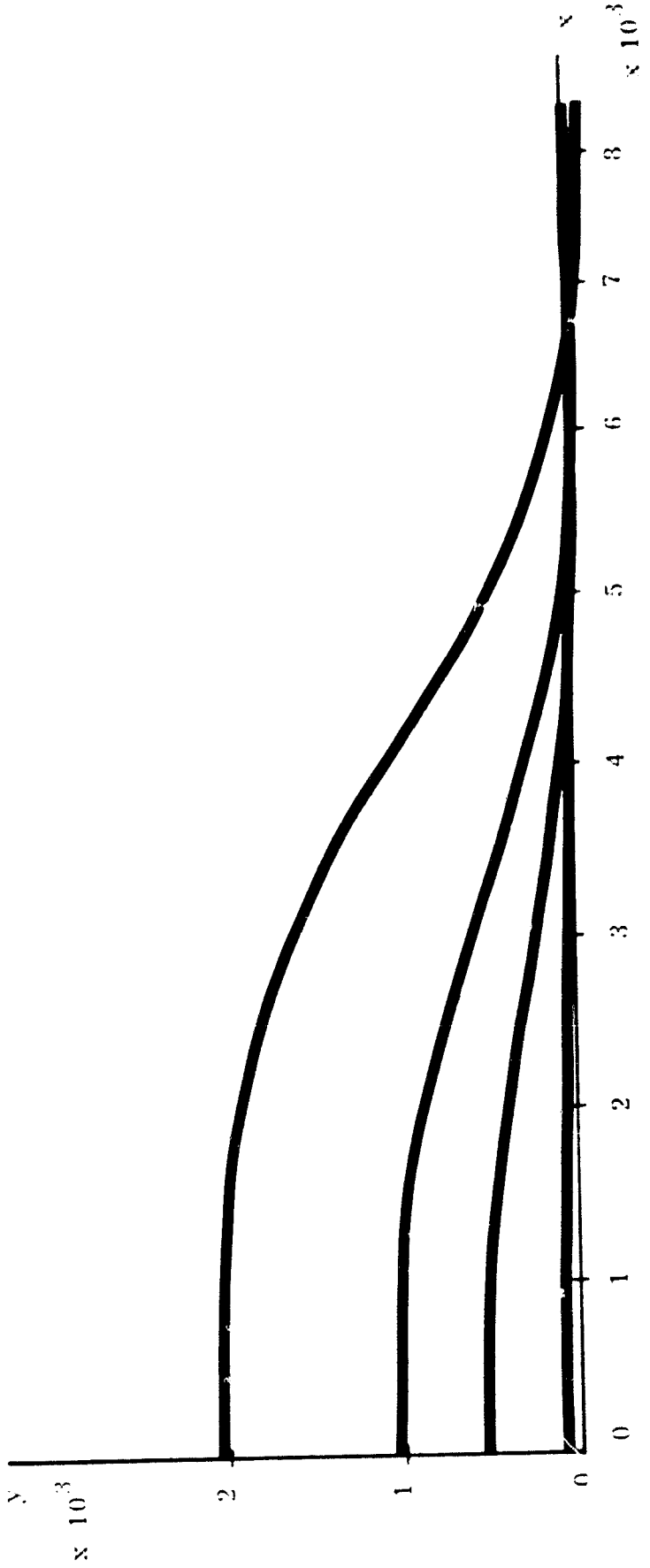

Fig. 5.9-2 Lateral position responses with y_c = 0 and initial values of y of 100, 500, 1000 and 2000 ft. The responses are essentially identical to the outputs of NTG_y. The nonlinear character of these responses is apparent.

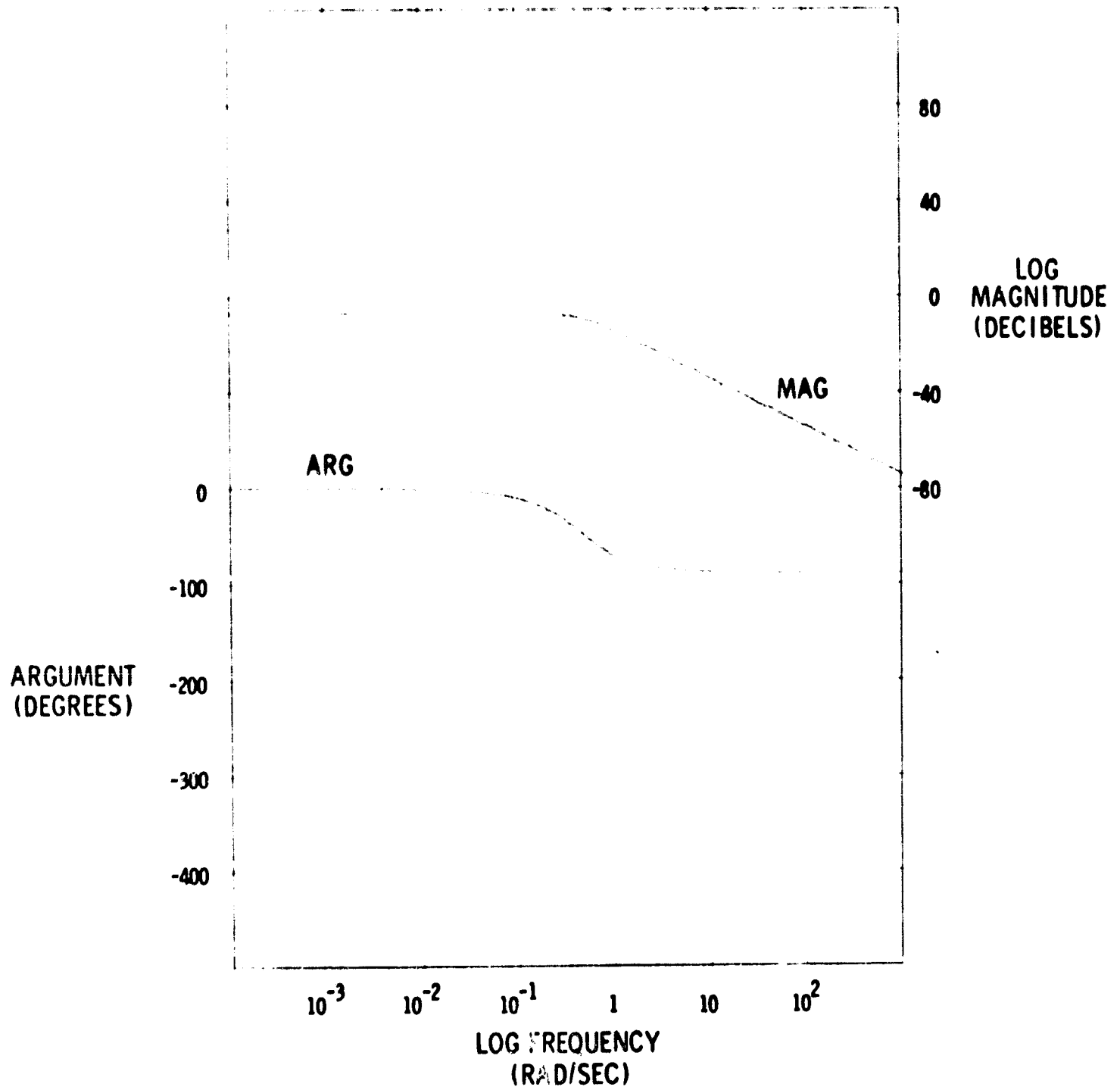

Fig. 5.11-1 Magnitude and phase characteristics of $\left(\frac{q}{\delta_e}\right)_{u=0}$.

bending modes. The elevator actuator is modeled by a simple first-order system with a 0.05 second time constant, T_{e1}. A simple linearized model is shown in Fig. 5.11-2

where

K_θ is an adjustable pitch angle feedback gain.

$K_{\dot\theta}$ is an adjustable pitch rate feedback gain.

The resultant open and closed-loop transfer functions are shown in Figs. 5.11-3 and 5.11-4. The response of the linear system to a unit step is shown in Fig. 5.11-5. The complete pitch angle control system is shown in Fig. 5.11-6, where magnitude and rate limits are incorporated into the elevator servomechanism. The parameters are defined in Table 5.11-1.

5.12 Linear Analysis of the Vertical Control System

If the flight path velocity is held constant, the vertical component of velocity $\dot z$ may be approximated by the linear relationship

$$\dot z = -v_p \gamma \qquad (5.12\text{-}1)$$

$$= -v_p (\theta - \alpha) \qquad (5.12\text{-}2)$$

where

$\dot z$ is the vertical velocity.

v_p is the flight path velocity.

γ is the path inclination angle.

θ is the pitch attitude.

α is the vertical slip angle.

Linear equations similar to those in Appendix C may be derived relating α to θ under the assumption that the velocity perturbation u is zero. Thus pitch angle becomes the primary control variable. The transfer function relating γ to θ is shown in Fig. 5.12-1. In the low frequency range changes in θ excite small changes in γ, and the transfer function approaches unity. At higher frequencies rapid changes in pitch produce large increments in the lift vector. The value of γ becomes proportional to the rate of change of θ, and a rising magnitude characteristic results.

A linear model of the vertical control system is shown in Fig. 5.12-2

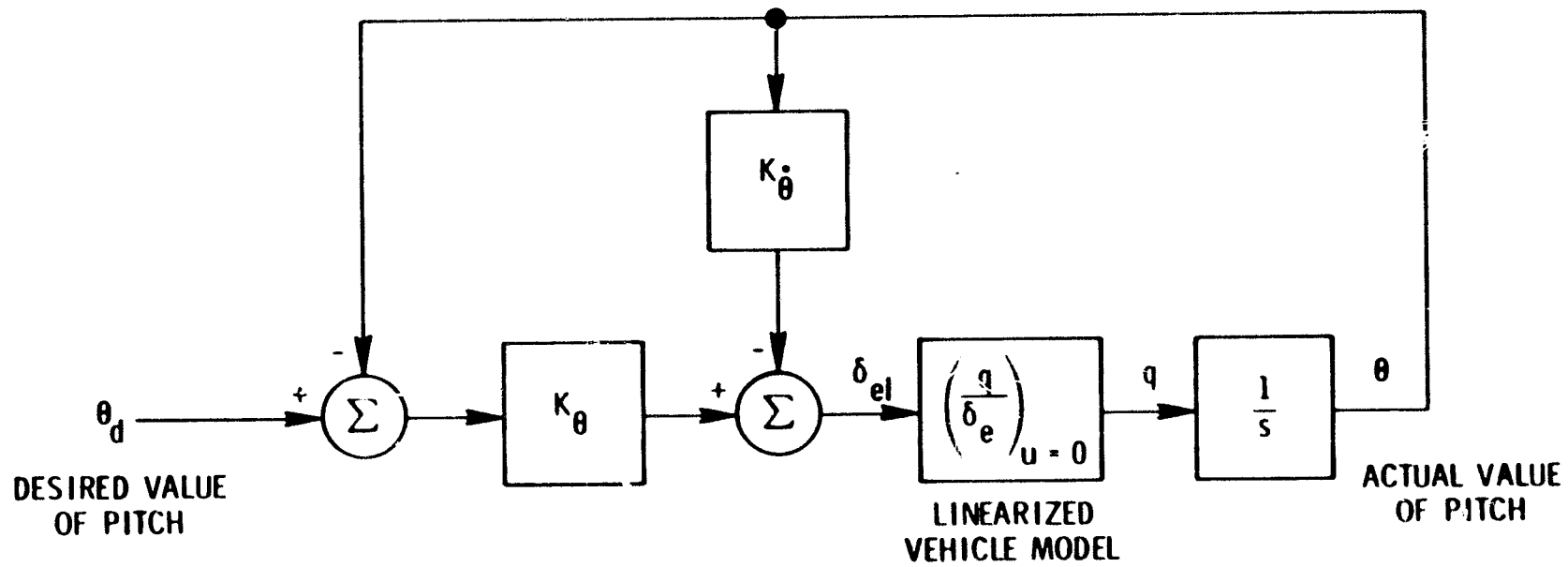

Fig. 5.11-2 Linearized model of a pitch attitude control system.

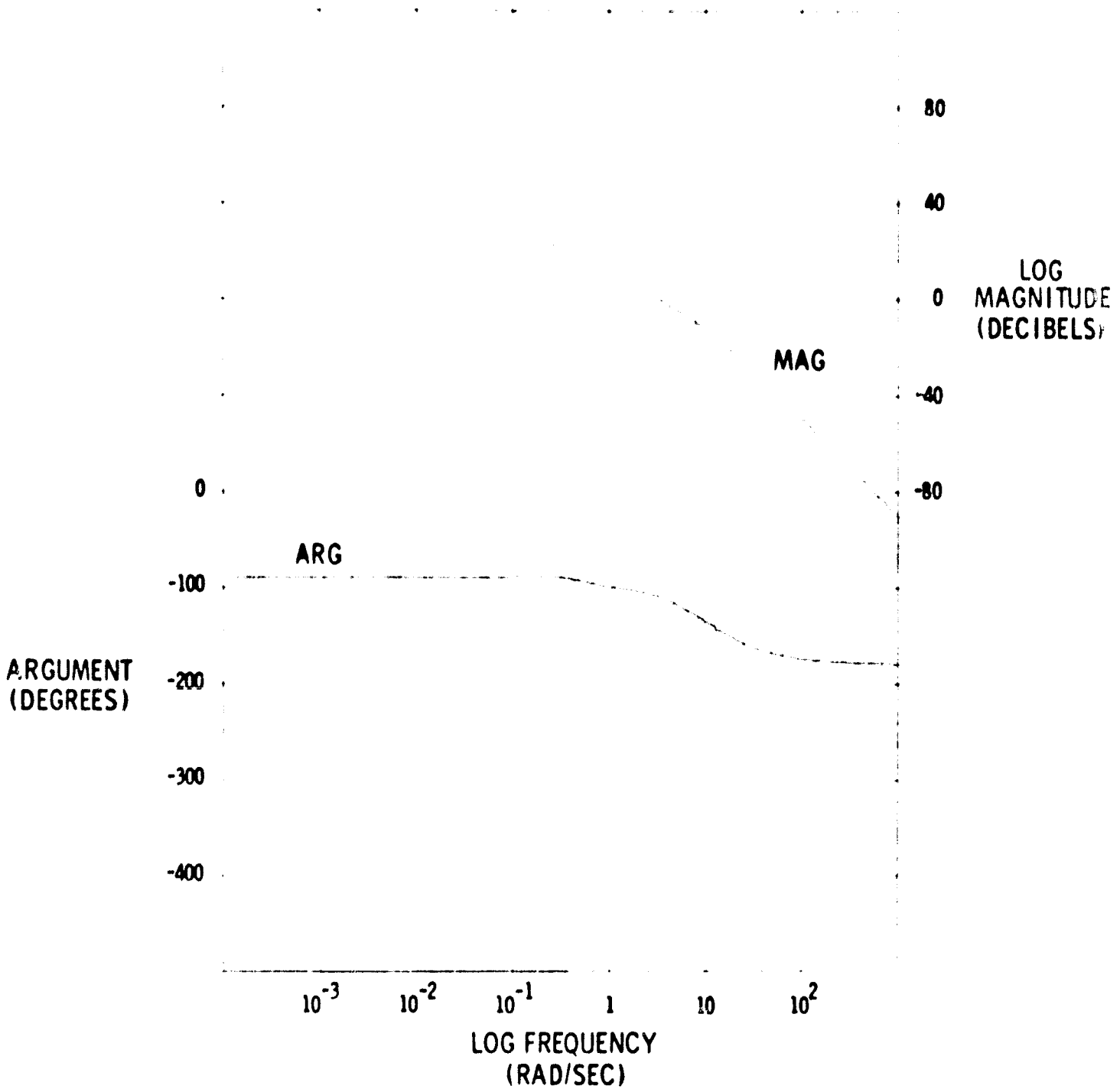

Fig. 5.11-3 Open-loop transfer function of the pitch control system.

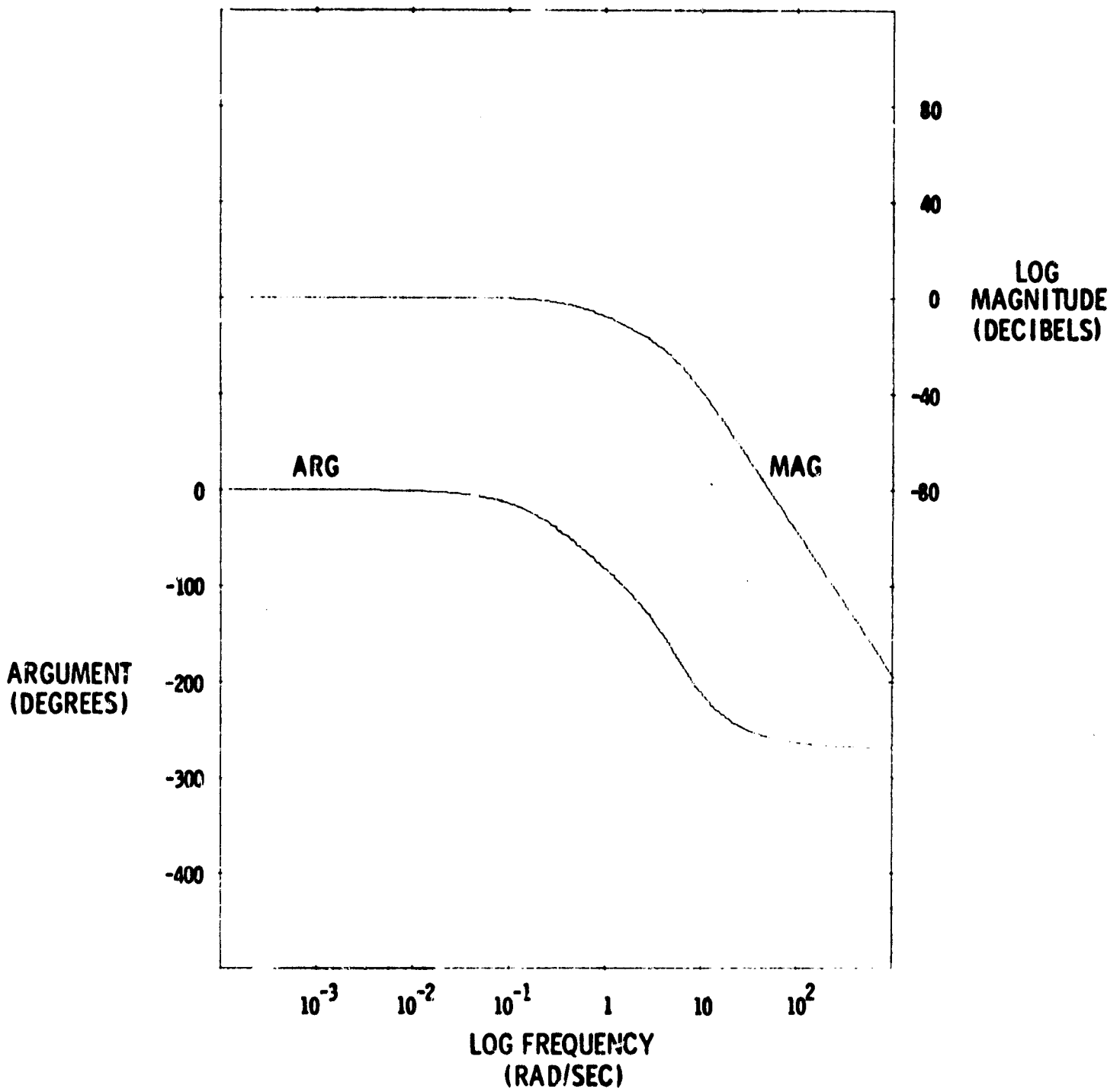

Fig. 5.11-4 Closed-loop transfer function of the pitch control system.

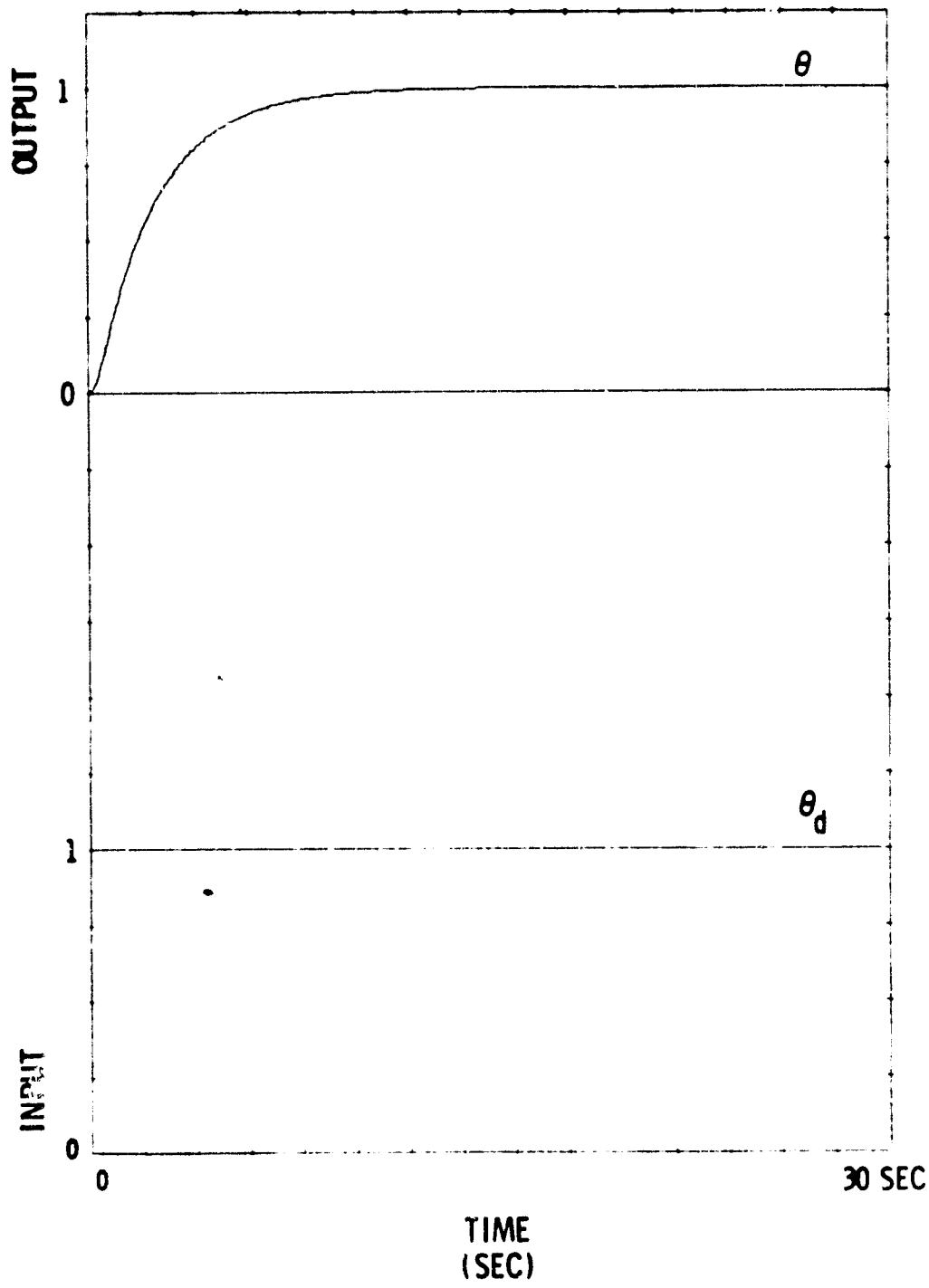

Fig. 5.11-5 Unit-step response of the linearized pitch angle control system.

Table 5.11-1 Pitch Angle Control System Parameters

GAINS		
K_θ	Pitch angle gain	7.100
$K_{\dot{\theta}}$	Pitch angular rate gain	16.250 sec
CONSTANTS		
T_e	Elevator model time constant	0.050 sec
SATURATION LIMITS		
L_o	Elevator angle limit	±30.000 deg
L_1	Elevator rate limit	±25.000 deg/sec

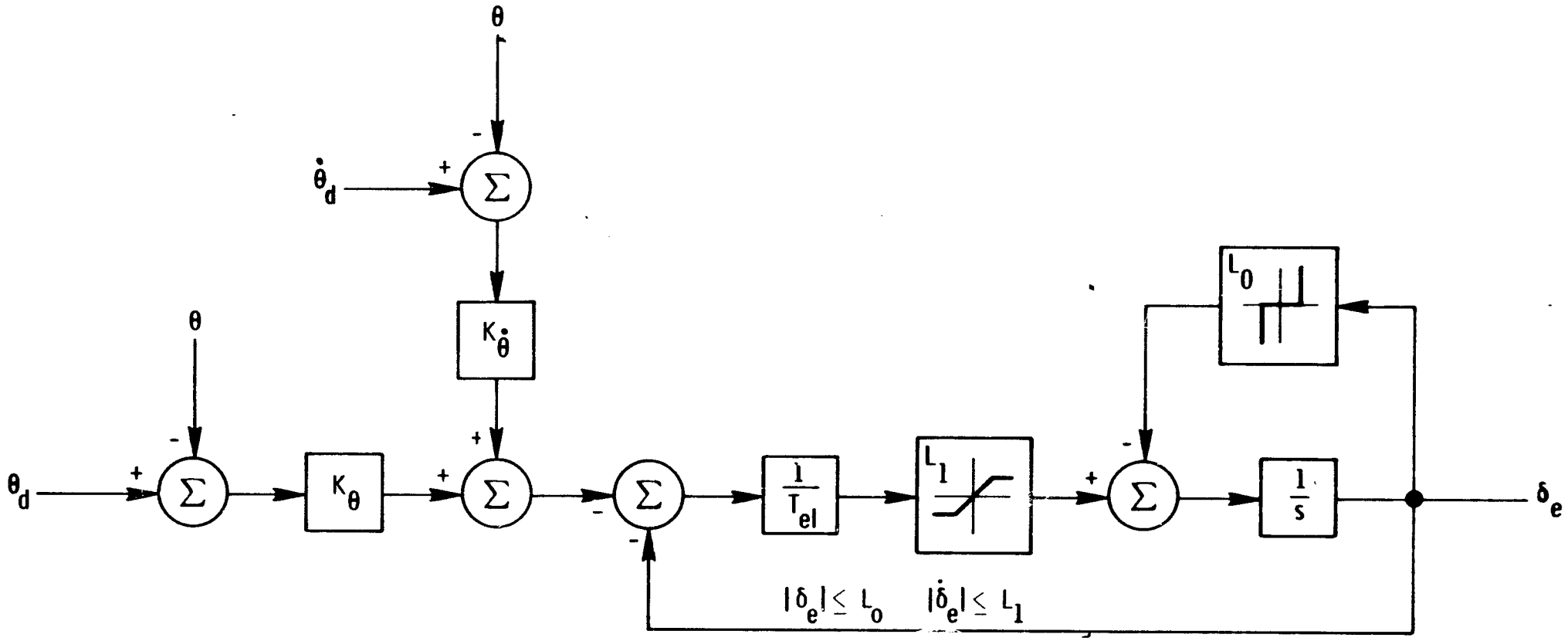

RATE AND MAGNITUDE LIMITED EFFECTOR

Fig. 5.11-6 Pitch attitude control system.

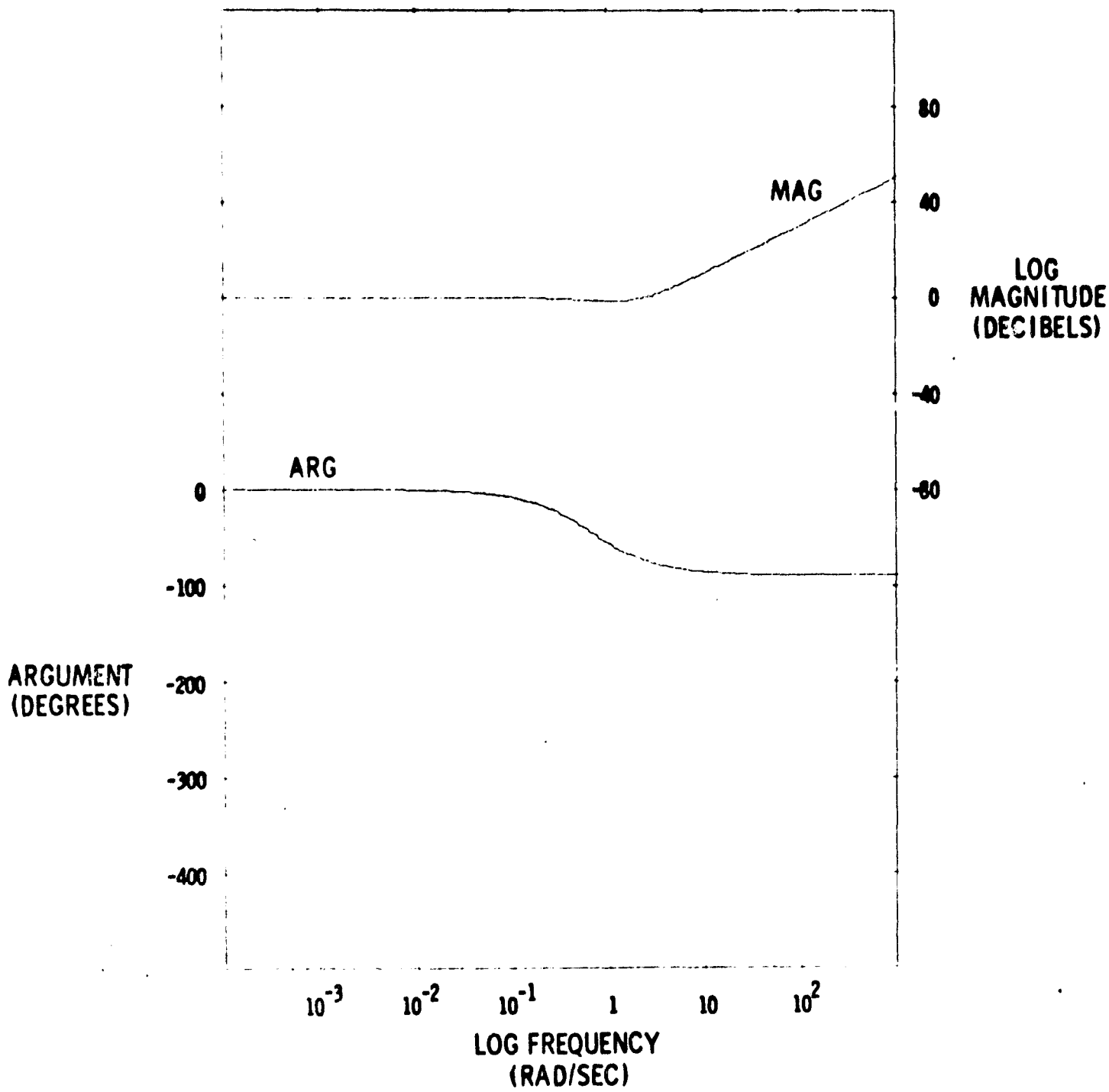

Fig. 5.12-1 Magnitude and phase characteristics of $\left(\frac{\gamma}{\theta}\right)_{u=0}$.

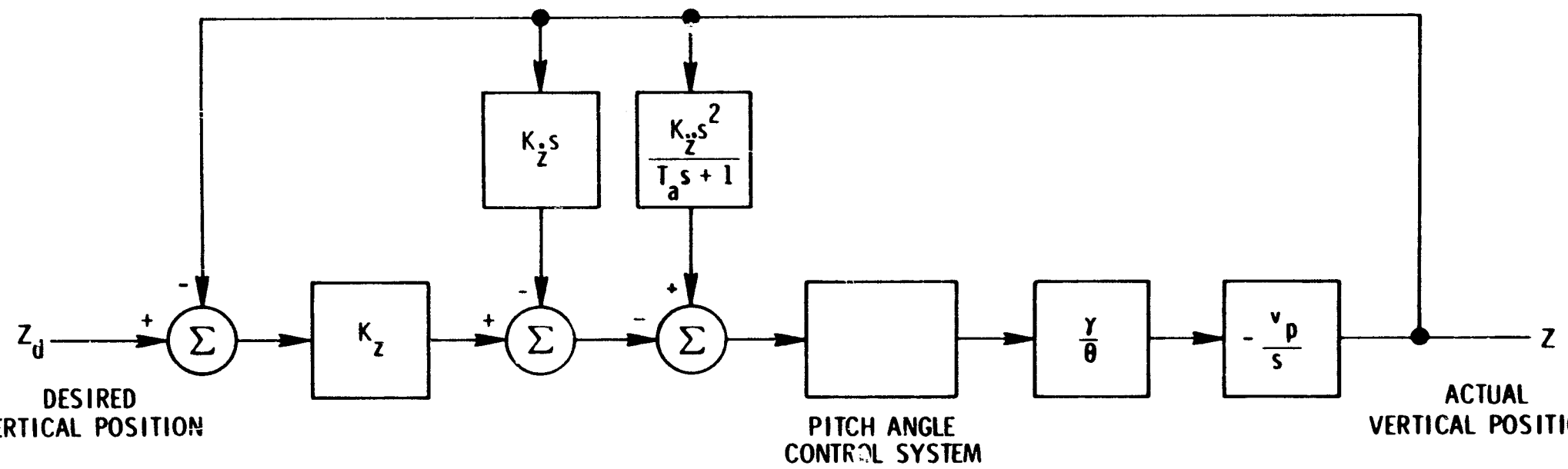

Fig. 5.12-2 Linearized model of a vertical position control loop.

where

K_z is an adjustable vertical position feedback gain.

$K_{\dot{z}}$ is an adjustable vertical velocity feedback gain.

$K_{\ddot{z}}$ is an adjustable acceleration feedback gain.

T_a is a time constant which reflects the fact that pure acceleration data is not available from most inertial systems.

The values are shown in Table 5.16-1.

The forward-loop transfer function is written

$$G_z = \frac{K_z v_p}{\theta_d} \qquad (5.12\text{-}3)$$

The open-loop transfer function is given by

$$G_z H_z = \left[\frac{K_z v_p}{\theta_d s}\right]\left[1 + \frac{K_{\dot{z}}}{K_z} s + \frac{K_{\ddot{z}} s^2}{K_z t_z s + 1}\right] \qquad (5.12\text{-}4)$$

The closed-loop transfer function is then

$$\frac{z}{z_d} = \frac{G_z}{1 + G_z H_z} \qquad (5.12\text{-}5)$$

The gains K_z, $K_{\dot{z}}$, $K_{\ddot{z}}$ were conservatively chosen based on sensor noise and dynamic response considerations. The open and closed-loop transfer functions are shown in Figs. 5.12-3 and 5.12-4. The unit-step response of the linear model appears in diagram 5.12-5. Some practical problems are considered at this point.

5.13 Compensation for Steady Vertical Errors

The instantaneous vertical component of velocity may be written

$$\dot{z} \approx -v_p \theta \qquad (5.13\text{-}1)$$

$$\approx -(v_{as} + w_b)\theta$$

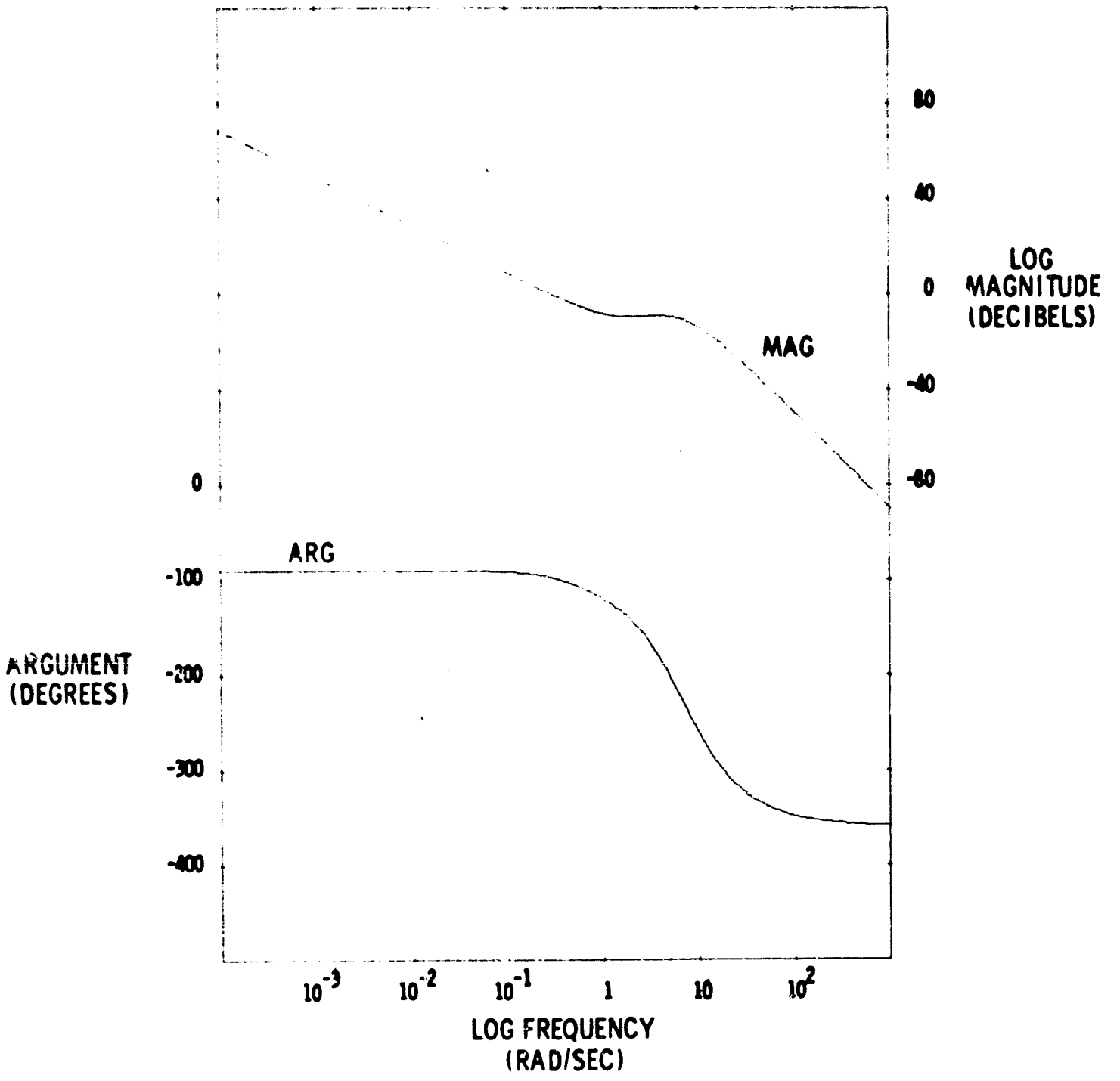

Fig. 5.12-3 Open-loop transfer function for the vertical control system.

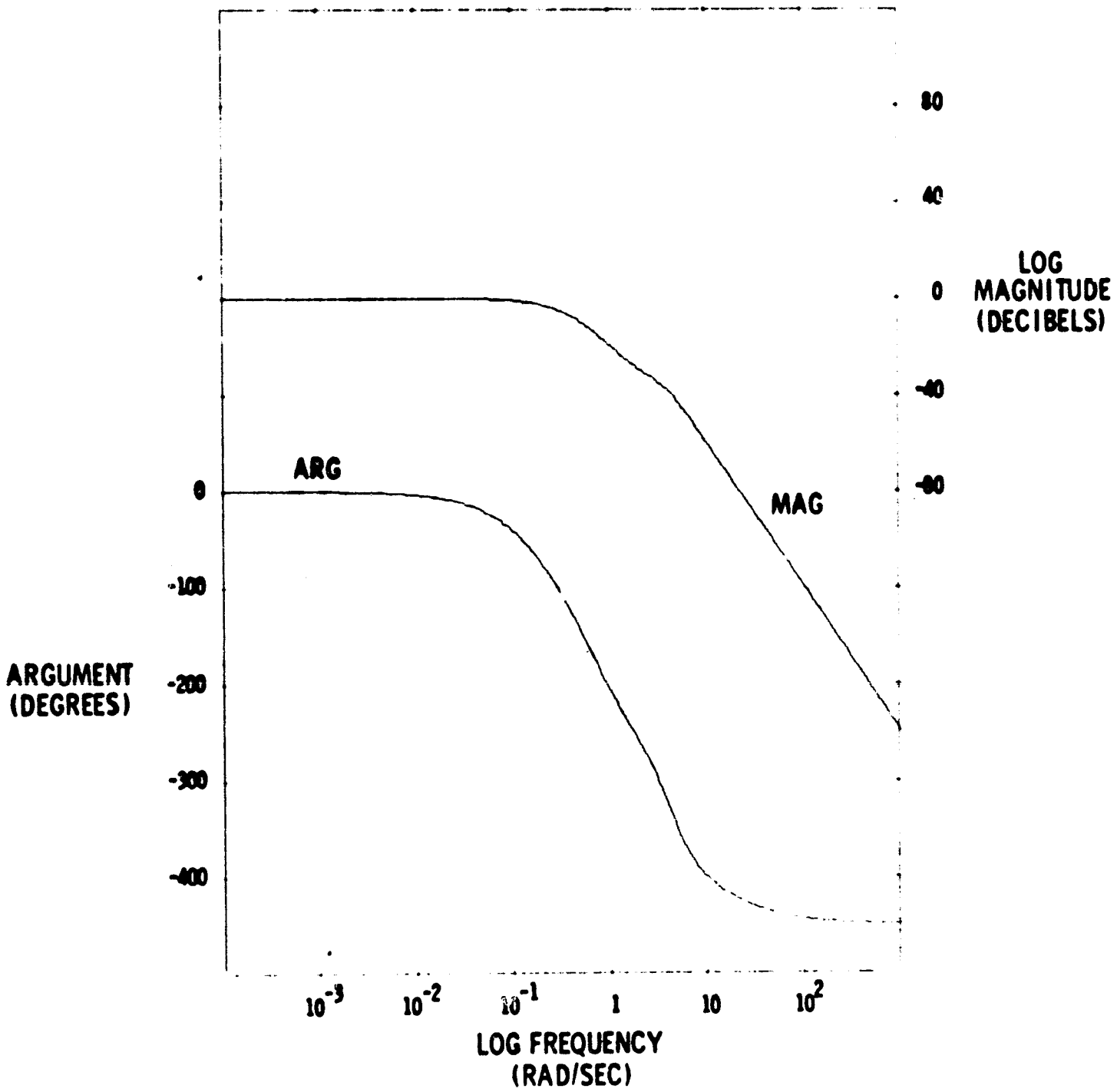

Fig. 5.12-4 Closed-loop transfer function $\frac{z}{z_d}$ for the vertical control system.

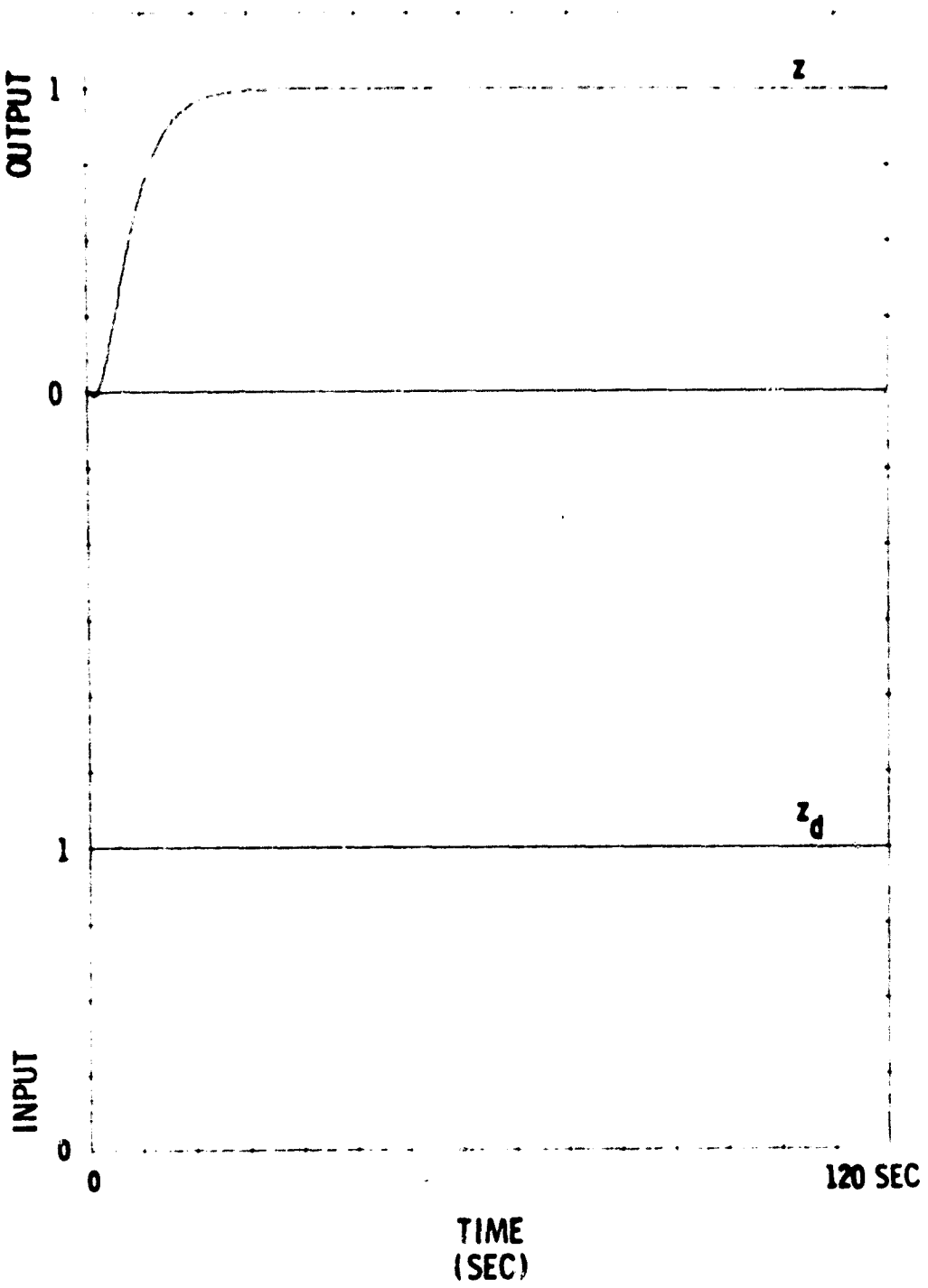

Fig. 5.12-5 Unit-step response of the linearized vertical control system.

where

v_{as} is the velocity of the aircraft relative to the air mass.

w_b is the component of wind velocity along the aircraft longitudinal axis.

Thus to maintain a constant rate of descent $\dot{z}_d$, the following must be true for θ:

$$\theta = \frac{-\dot{z}_d}{(v_{as} + w_b)} \tag{5.13-2}$$

The constant value of θ will be maintained in the quiescent state by a position error

$$e_z = \frac{\theta}{K_{iz}}$$

The position error can be eliminated by feeding forward a reference inpu θ_r to the summing junction

$$\theta_r = \frac{-\dot{z}_d}{v_{as} + w_b} \tag{5.13-4}$$

Unfortunately, it is difficult to compute the exact value of θ_r because of errors in the measurement of w_b. The problem may be avoided by utilizing a proportional plus integral compensator to remove residual error in θ_r as shown in Fig. 5.16-1. The compensator gain K_{iz} is selected by a compromise between deterioration of dynamic response and improvement of static characteristics. The effect of the compensator on open-loop response is shown in Fig. 5.13-1.

5.14 Nonlinear Design Considerations for Vertical Control

As a result of the relatively small changes in pitch attitude which occur during landing, pitch rate and magnitude do not impose serious restrictions on response. On the other hand, it is important to prevent rate and/or magnitude saturation in the elevator effector to minimize sensitivity to environmental disturbances. The magnitude restriction is reflected in a corresponding maximum vertical acceleration. Consequently, magnitude saturation may be controlled in an approximate fasnion by ensuring that

$$|\ddot{z}_d| \leq |\alpha_z \, v_p \, q_{max}| \tag{5.14-1}$$

where

q_{max} is the maximum pitching rate (radians/sec).

α_z is a positive constant between 0 and 1.

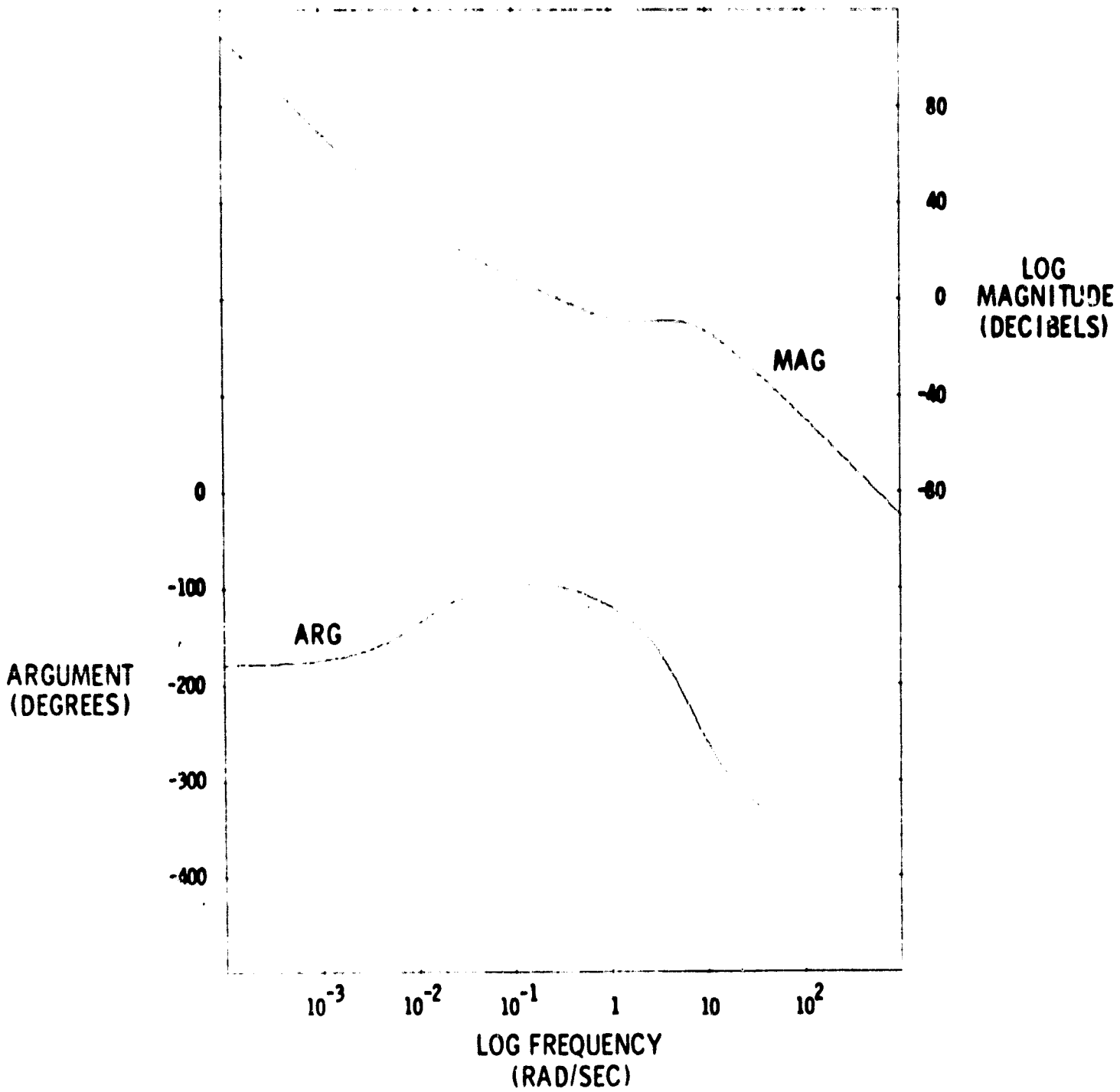

Fig. 5.13-1 Open-loop transfer function of the vertical control system showing the effect of integral compensation.

In addition to limiting acceleration it is customary to put some upper limit on rate of descent which would not be exceeded in normal operation.

$$|\dot{z}_d| \leq |\dot{z}_{max}| \tag{5.14-2}$$

In addition to restricting acceleration and velocity, it is important to match the general dynamics of the trajectory to the response characteristics of the vertical control system. This is accomplished by adjusting the natural frequency ω_z and damping ratio ζ_z of the second-order trajectory generator NTG_z, as discussed in Chapter 4.

5.15 Velocity and Acceleration Control

As discussed in Section 4.3, exact trajectory control requires

$$z = z_d \tag{5.15-1}$$

$$\dot{z} = \dot{z}_d \tag{5.15-2}$$

$$\ddot{z} = \ddot{z}_d \tag{5.15-3}$$

While it is not possible to achieve these goals exactly, improved performance may be obtained by structuring the control variable from corresponding error signals and a pitch reference input as shown in Fig. 5.16-1.

$$-\theta_c = K_z (z_d - \hat{z}) + K_{\dot{z}} (\dot{z}_d - \hat{\dot{z}}) + K_{\ddot{z}} (\ddot{z}_d - \frac{s}{T_a s + 1} \hat{\dot{z}}) - \theta_r \tag{5.15-4}$$

where

K_z is the vertical position gain (radians/ft).

$K_{\dot{z}}$ is the velocity gain (radians-sec/ft).

$K_{\ddot{z}}$ is the acceleration gain (radians-sec^2/ft).

θ_r is the pitch reference signal $\left(\theta_r = -\frac{\dot{z}_d}{v_p}\right)$.

The pitch rate is also referenced to an input variable

$$\dot{\theta}_r = -\frac{\ddot{z}_d}{v_p}$$

as shown in Fig. 5.16-1.

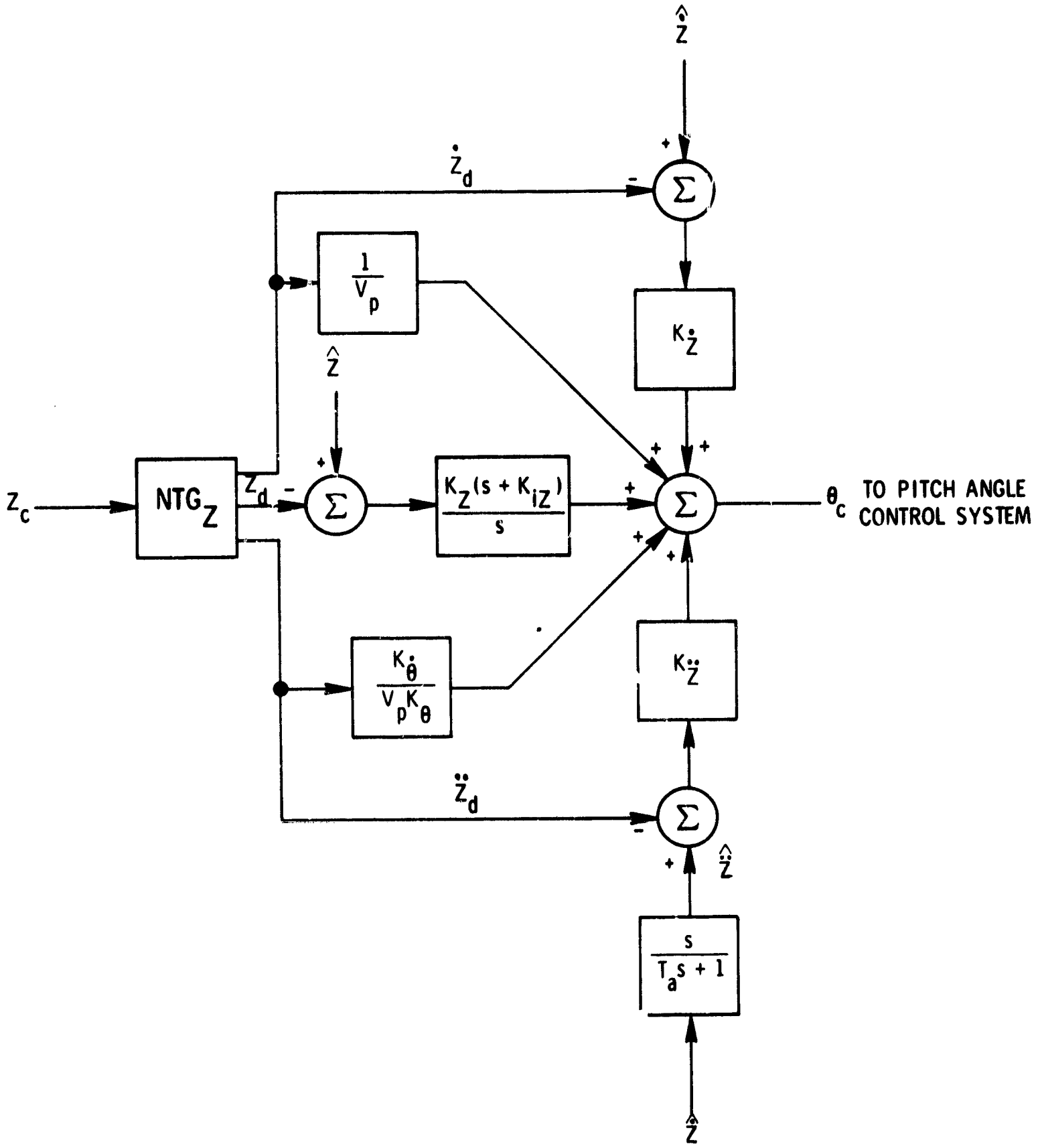

Fig. 5.16-1 Vertical position control system.

5.16 Vertical Control System Configuration

The final structure of the vertical control system is shown in Fig. 5.16-1. Table 5.16-1 lists the design values of the vertical gains and parameters. The pitch control system, which appears in block form, is described in Section 5.11. Detailed analysis of the NTG appears in Sections 5.6 and 4.3.

5.17 Vertical Control Systems Response Characteristics

The response* of the vertical control system to an initial z displacement ($\dot{z} = 0$) is shown in Fig. 5.17-1. A family of responses illustrating the nonlinear character of the controlled vertical trajectories are shown in Fig. 5.17-2.

Table 5.16-1 Vertical Control System Parameters

GAINS		
K_z	Vertical position gain	0.063 deg/ft
$K_{\dot{z}}$	Vertical velocity gain	0.246 deg/ft/sec
$K_{\ddot{z}}$	Vertical acceleration gain	0.156 deg/ft/sec^2
K_{iz}	Integral compensator gain	0.010 sec
CONSTANTS		
T_a	Vertical acceleration filter time constant	0.100 seconds
SATURATION LIMITS	**IMPOSED BY VEHICLE LIMITS**	**IMPOSED BY NTG**
z	-	
$\dot{z}$	-	±14.600 ft/sec
$\ddot{z}$	±25.1 ft/sec^2	±12.500 ft/sec^2
θ	-	-
$\dot{\theta}$	±5.90 deg/sec	-
$\ddot{\theta}$	±4.92 deg/sec^2	-
NTG PARAMETERS		
ω_z	NTG_z natural frequency	0.500 rad/sec
ζ_z	NTG_z damping ratio	1.000

* Obtained using the simulation described in Appendix D.

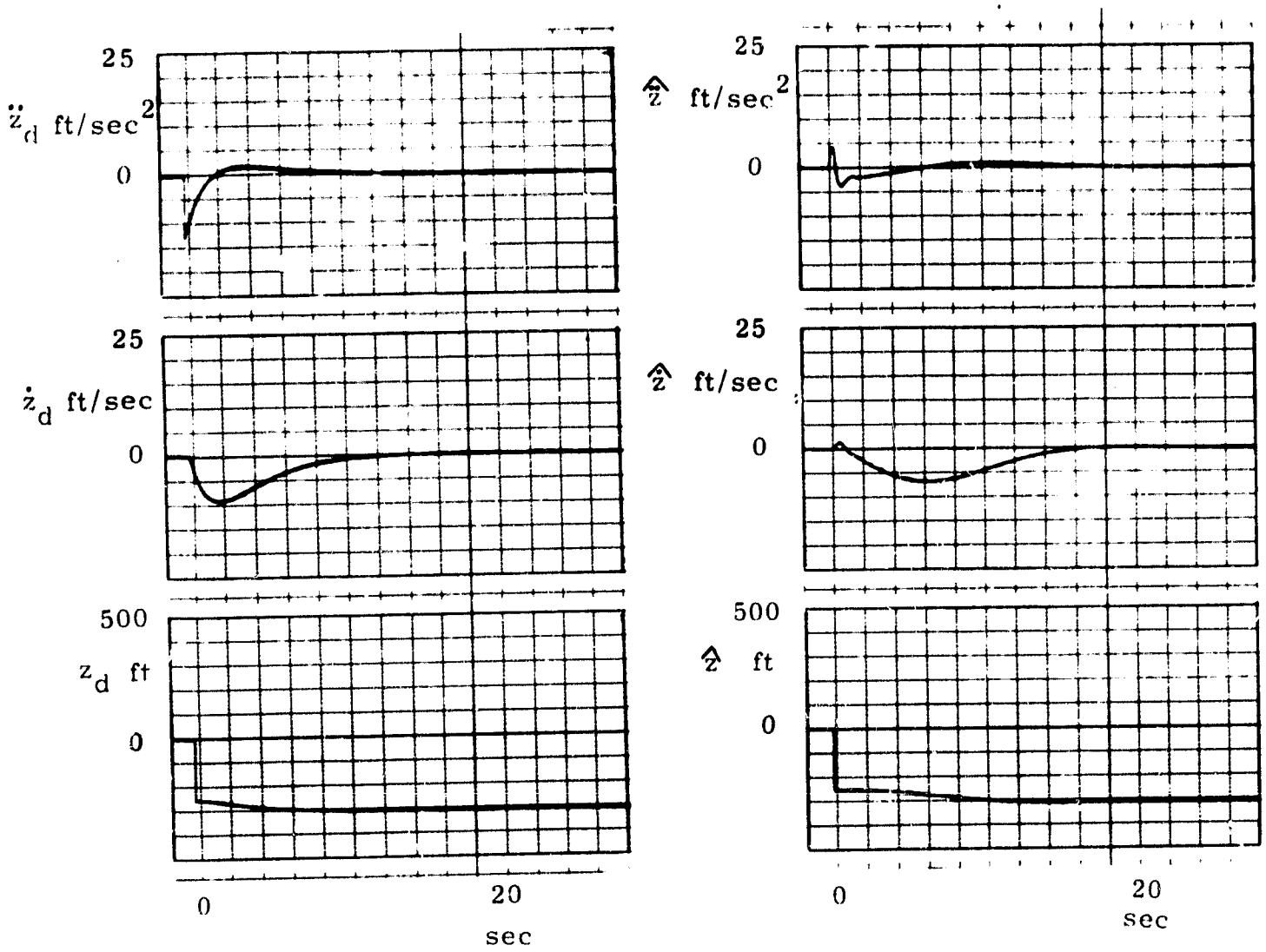

Fig. 5.17-1 Vertical control system response to a 50 ft change in vertical position command.

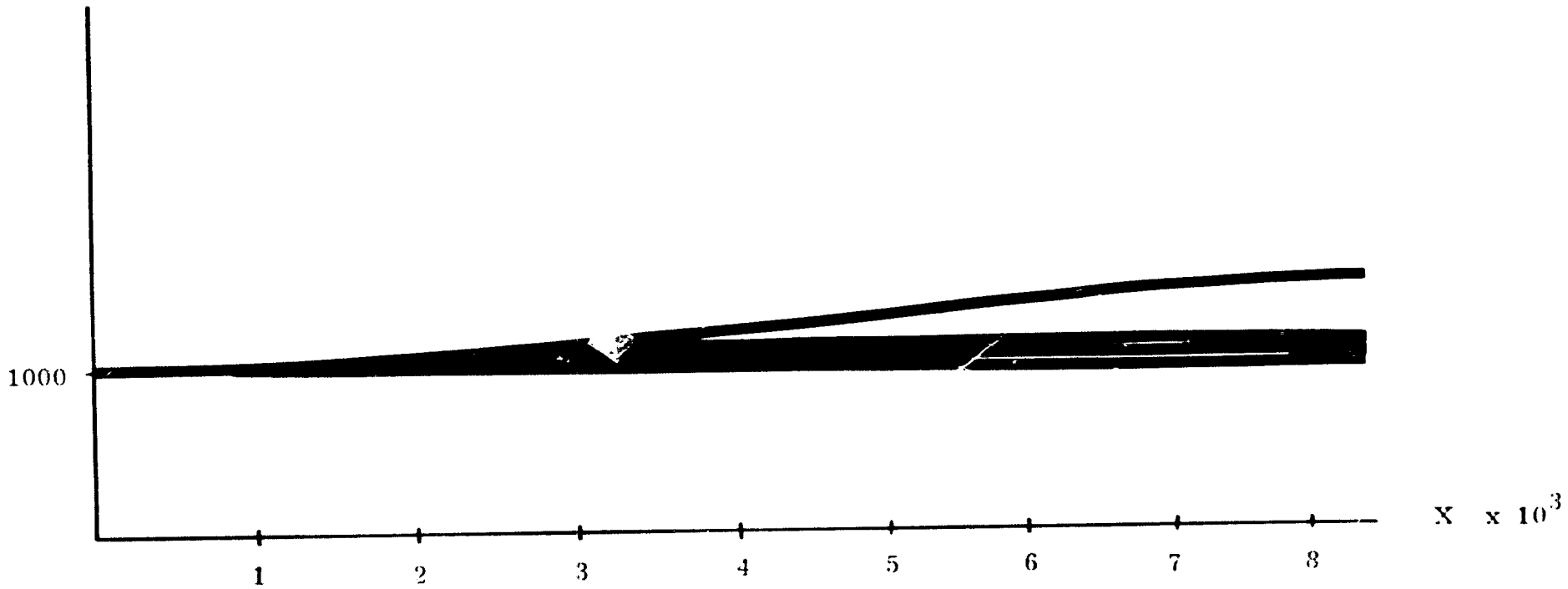

Fig. 5.17-2 Vertical control system responses to desired altitude changes of 0, 50, 100 and 500 ft showing the nonlinear character of the responses.

CHAPTER 6

ACQUISITION CONTROL SYSTEM

6.1 Introduction

The first phase of a landing sequence is a maneuver which changes the flight path from a linear course crossing the ILS center line at an angle ψ_a to a path coincident with the ILS center line (the value of ψ_a is nominally 45^o). The acquisition is normally initiated when the aircraft intersects a radius drawn from the localizer transmitter approximately $2\text{-}1/2^o$ off the localizer center as shown in Fig. 6.1-1. The threshold is usually detected using the ILS localizer signal.

The main performance criterion for acquisition is the rapidity with which the ILS beam is acquired. It is desirable to accomplish this result as quickly as possible for a number of reasons:

1. Rapid acquisition ensures that the flight path will be completely stabilized on the beam center line before the final phases of DECRAB and FLARE are initiated.
2. A reduction in acquisition time permits the aircraft to acquire the beam closer to the runway threshold reducing the time required to complete a landing.

A conventional acquisition control system is a linear position controller which utilizes position and derived velocity data from the ILS system to define the roll control variable. A lateral position control system of this type is described in Appendix A. Prior to the initiation of acquisition the aircraft is maintained on a linear course by the directional autopilot. When the aircraft crosses the preset ILS threshold discussed above, control is transferred to the ILS referenced linear position controller which retains vehicle control until the initiation of the terminal landing maneuvers described in Chapter 7.

While the simplicity of this system is very attractive, it displays a number of undesirable qualities.

1. Sensitivity to disturbances due to low open-loop gain.
2. Sensitivity of response characteristics to the beam location where ac-

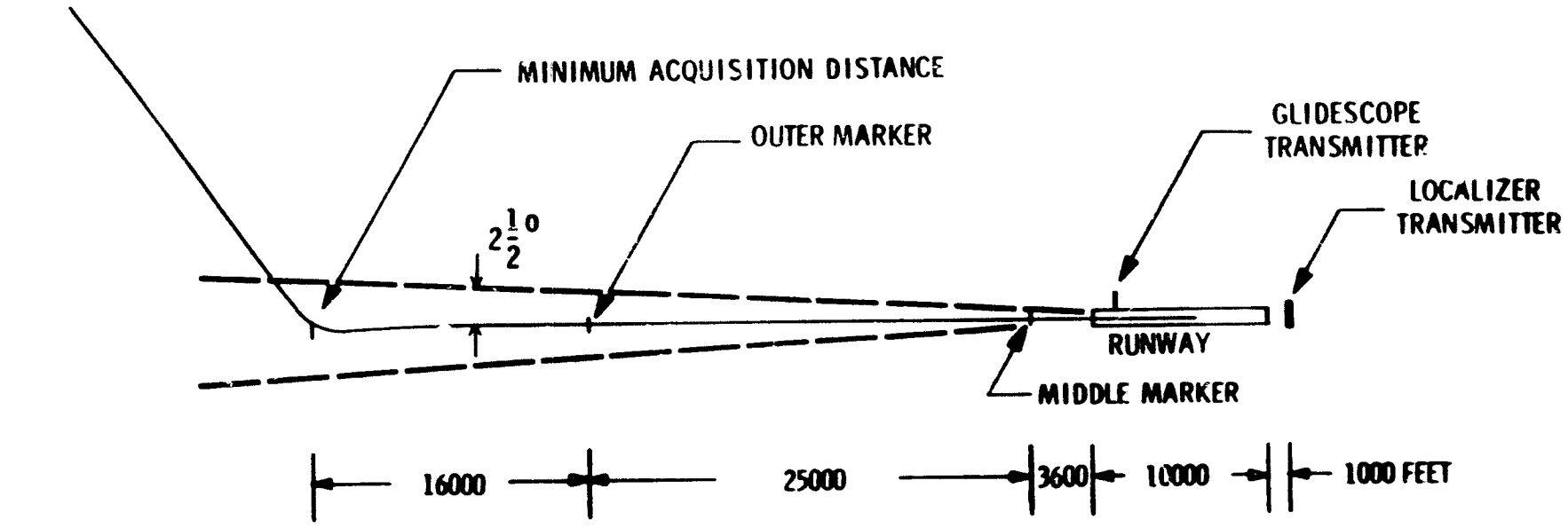

Fig. 6.1-1 Nominal geometrical relationships at the initiation of localizer acquisition.

quisition is initiated.

3. A large value of overshoot and a long settling time.

4. Excessive roll angle and roll angular rate.

As a result of these drawbacks, it was decided to approach the problem from an entirely new point of view based on the principles of TIME OPTIMAL CONTROL which is suggested by the criteria assigned to acquisition performance.

The key to the solution of this problem is the ability of the improved lateral control system to follow a trajectory in space with a high degree of precision. The object of this investigation is to utilize the theory of time optimal control to generate an improved trajectory which takes into account the limitations on the lateral control variable ϕ. The improved trajectory is applied as a reference input to the new lateral control system which then tracks it in a linear fashion. The result is a quasi-time-optimal acquisition system which provides:

1. Performance that is essentially independent of the direction, velocity and location of the initial path.

2. Minimum overshoot.

3. Automatic compensation for the effects of constant wind.

A simplified derivation of the properties of time-optimal lateral position control solutions is now presented.

6.2 Vehicle Equations

Acquisition of the ILS beam is primarily a vehicle lateral control problem. Such lateral control is achieved by modifying the roll angle of the aircraft. Assuming that the vehicle's turns are properly coordinated by the autopilot, the equation of motion may be simplified to:

$$\dot{\psi} = \frac{g \tan\phi}{v_p} \qquad (6.2\text{-}1)$$

$$\dot{y} = v_p \sin\psi \qquad (6.2\text{-}2)$$

where y is lateral deflection, ψ is the heading angle relative to the localizer reference plane, ϕ is the roll angle, g the gravitational constant and v_p is the path velocity. In order to ensure passenger comfort, additional limitations must be imposed on the control variable ϕ.

$$|\phi| \leq \phi_{max} \ (\approx 30 \text{ degrees}) \qquad (6.2\text{-}3)$$

$$|\dot{\phi}| \leq \dot{\phi}_{max} \ (\approx 10 \text{ degrees/sec}) \tag{6.2-4}$$

A state vector x may be associated with the system by setting:

$$\dot{x}_1 = \dot{u} \tag{6.2-5}$$

$$\dot{x}_2 = \frac{g \tan x_1}{v_p} \tag{6.2-6}$$

$$\dot{x}_3 = v_p \sin x_2 \tag{6.2-7}$$

where u is equal to ϕ. In vector notation Eqs (6.2-5) - (6.2-7) are written:

$$\dot{x} = f(x, \dot{u}) \tag{6.2-8}$$

The inclusion of $x_1 = \phi$ into the state vector x is necessary to account for the dynamics [Eq (6.2-4)] associated with ϕ and facilitates a direct solution of the minimal time control problem which may now be defined.

6.3 Definition of the Problem

Find a control $u \in C_0 (t, T)$,* which minimizes the integral performance index:

$$J = \int_t^T dt = T - t \tag{6.3-1}$$

subject to a fixed terminal state:

$$x(T) = 0 \tag{6.3-2}$$

the nonholonomic constraint:

$$\dot{x} = f(x, \dot{u}) \tag{6.3-3}$$

with the boundary condition:

$$x(t) = a \tag{6.3-4}$$

and the saturation constraints:

$$|x_1| \leq \phi_{max} \tag{6.3-5}$$

$$|\dot{u}| \leq \dot{\phi}_{max} \tag{6.3-6}$$

*The notation $u \in C_n (t, T)$ indicates that u is a member of the family of functions with continuous derivatives up to the nth order on the interval (t, T).

6.4 Solution by Application of the Minimum Principle

The class of problems defined above was among the first to interest researchers in the area of optimal control systems and was solved heuristically for linear second-order systems as early as 1950 by McDonald.[8] Since that time a large number of papers have appeared which enable the most complicated problems to be solved in theory.[9-14] The properties of minimal time controls are best illustrated as an application of L. S. Pontryagin's Minimum Principle[15, 16] which states that the Hamiltonian must be a minimum along any extremal of the problem posed above. The Hamiltonian for this particular problem is defined as follows.

Definition: The Hamiltonian of the systems of Eqs (6.3-1) and (6.3-3) is given by:

$$H = 1 + p' f \tag{6.4-1}$$

where p is the adjoint state vector associated with the vehicle equations and is defined by:

$$\dot{p} = -H_x \tag{6.4-2}$$

$$p(T) = k \tag{6.4-3}$$

where H_x is the gradient of the Hamiltonian with respect to x and k is an unknown terminal adjoint state.

A control solution is obtained by application of the Minimum Principle. Expansion of Eq (6.4-1) gives:

$$H = 1 + p_1 \dot{u} + \frac{p_2 g \tan x_1}{v_p} + p_3 v_p \sin x_2 \tag{6.4-4}$$

This expression is minimized by ensuring that the contribution resulting from the control is as negative as possible. Minimality is achieved if the control variable $\dot{u}$ is set equal to:

$$\dot{u} = -\dot{\phi}_{max} \mathrm{sgn}(p_1) \tag{6.4-5}$$

Thus the magnitude of the optimal roll angular rate is always equal to its maximum value whenever:

$$|x_1| \leq \phi_{max} \tag{6.4-6}$$

While the properties of the solution given in Eq (6.4-5) are quite clear, the problems associated with its actual computation are (usually) insuperable from a pratical point of view.

6.5 Generation of Time Optimal Controls

The computational difficulties associated with the realization of time mini-

mal control systems evolve from the boundary conditions imposed in Eqs (6.3-2), (6.3-4), and (6.4-3). Since knowledge is limited to the current state, x(t), an algorithm must be derived to define the unknown parameters p(T) and T if a solution is to be formed for the general case. This involves the solution of a two-point boundary value problem. The situation is further complicated by the nonlinear character of the vehicle equations of motion. Such problems may be solved by variational programming techniques. [17, 18] The computational techniques are, however, quite time consuming and are not currently feasible for most real-time control applications.

The difficulties described above are greatly diminished if the problem may be specialized in some sense. Such specialization is possible here since the initial value of ϕ is usually close to zero as a result of the linearity of the initial flight path. The condition $\phi_o = 0$ effectively collapses the problem dimensionality to two permitting a two-parameter set of switching characteristics to be generated.

A trajectory which displays some of the properties of the time-optimal solution described in Eqs (6.4-5) and (6.4-6) is shown in Fig. 6.5-1. The aircraft is initially on a linear path having an angle ψ_a relative to the runway center line. As the boundary at $y = y_{aqc}$ is crossed, the aircraft is rolled to an angle $\phi = -\phi_{aq}$ at a rate limited so that:

$$|\dot{\phi}| < \dot{\phi}_{aq} \leq \dot{\phi}_{max} \qquad (6.5\text{-}1)$$

At the conclusion of this maneuver the aircraft is on a path of constant radius. The aircraft continues to change direction until the boundary at y_{aqa} is reached, at which point it is rolled to level flight at a rate limited by Eq (6.5-1). It is apparent that a correct choice of the values y_{aqc} and y_{aqa} will lead to a final flight path tangent to the localizer center.

A set of switching boundaries, y_{aqc} and y_{aqa} which result in a terminal path along the localizer center may be generated using the geometrical parameters shown in Fig. 6.5-1. The following calculations are based on flight in a stationary air mass. The effects of constant components of wind are considered in a subsequent section. The initial heading angle and path velocity (in the absence of wind) are designated ψ_{aq}, $v_{aq} = v_{as}$.

The time required for the aircraft to roll from level flight to ϕ_{aq} degrees limited by Eq (6.5-1) is designated T_{aqa}. Knowledge of T_{aqa} permits the parameters associated with the terminal portion of the flight to be generated. These parameters y_{aqa}, x_{aqa}, $\delta\psi_{aq}$, C_{aq} and R_{aq} may be computed <u>a priori</u> and stored for later use.

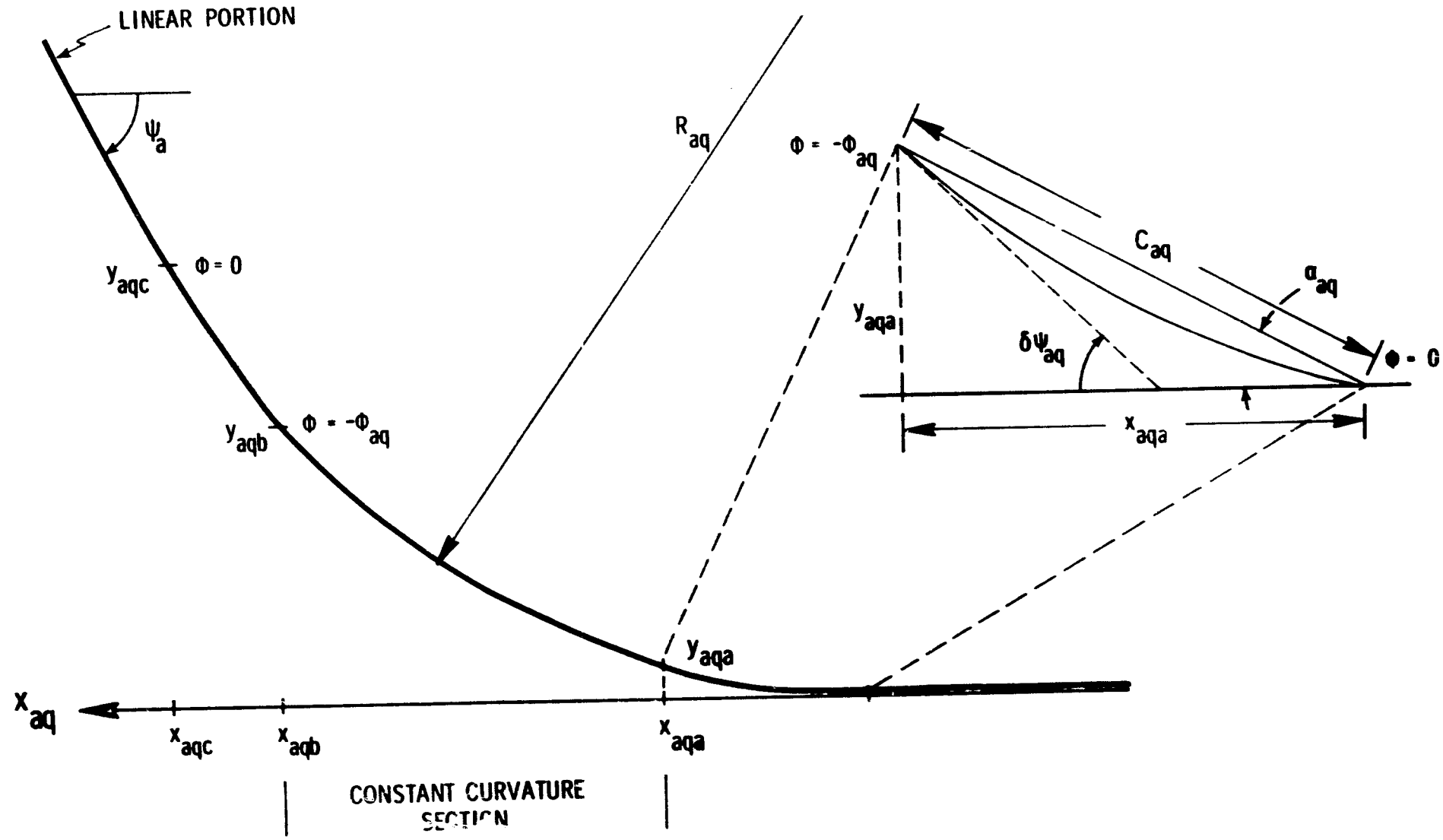

Fig. 6.5-1 Quasi-time optimal localizer acquisition trajectory.

$$\sigma\psi_{aq} = \int_0^{T_{aqa}} \frac{g \tan \phi}{v_{aq}} dt \qquad (6.5\text{-}2)$$

$$y_{aqa} = \int_0^{T_{aqa}} v_{aq} \sin \psi \, dt \qquad (6.5\text{-}3)$$

$$x_{aqa} = -\int_0^{T_{aqa}} v_{aq} \cos \psi \, dt \qquad (6.5\text{-}4)$$

$$\alpha_{aq} = \tan^{-1}\left(\frac{y_{aqa}}{x_{aqa}}\right) \qquad (6.5\text{-}5)$$

$$C_{aq} = \frac{x_{aqa}}{\cos(\alpha_{aq})} \qquad (6.5\text{-}6)$$

$$R_{aq} = \frac{v_{aq}}{g \tan(\phi_{aq})} \qquad (6.5\text{-}7)$$

where

$\delta\psi_{aq}$ is the change in heading angle which results when the aircraft rolls from banked flight ($\phi = -\phi_{aq}$) to level flight ($\phi = 0$) at a desired roll rate $\dot{\phi}_d = \dot{\phi}_{aq}$.

R_{aq} is the radius of curvature of the flight path when $|\phi| = \phi_{aq}$.

The other variables are defined in Fig. 6.5-1. The other switching boundaries may then be computed.

$$y_{aqb} = R_{aq}\left[\cos(\delta\psi_{aq}) - \cos(\psi_{aq} + \delta\psi_{aq})\right] \operatorname{sgn}(y_{\ell}) + y_{aqa} \qquad (6.5\text{-}8)$$

$$x_{aqb} = -R_{aq}\left[\sin(\delta\psi_{aq}) - \sin(\psi_{aq} + \delta\psi_{aq})\right] + x_{aqa} \qquad (6.5\text{-}9)$$

$$y_{aqc} = -C_{aq} \sin(\psi_{aq} + \alpha_{aq}) + y_{aqb} \qquad (6.5\text{-}10)$$

$$x_{aqc} = -C_{aq} \cos(\psi_{aq} + \alpha_{aq}) + x_{aqb} \qquad (6.5\text{-}11)$$

The time required to complete the acquisition maneuver is then:

$$T_{aq} = 2T_{aqa} + \frac{|\psi_{aq} + 2\delta\psi_{aq}|\ R_{aq}}{v_{aq}} \qquad (6.5\text{-}12)$$

It is apparent from Eqs (6.5-3) and (6.5-10) that the switching boundaries may be expressed in terms of two parameters v_{aq}, ψ_{aq}. The first variable v_{aq} is normally a constant so that the switching curves may be represented in two dimensions.

The point of intersection and the altitude of intersection with the ILS glide slope center line may now be computed:

$$x_{aq} = x - x_{aqc} - \frac{(y - y_{aqc})}{\tan\psi_{aq}} \qquad (6.5\text{-}13)$$

$$h_{aq} = -\alpha_{gs}\, x_{aq} \qquad (6.5\text{-}14)$$

where

α_{gs} is the inclination of the glide-slope center line relative to the horizontal (radians).

x_{aq} is the point on the x geographic axis where the acquisition maneuver is completed (ft).

h_{aq} is the altitude of the glide-slope beam at $x = x_{aq}$ (ft).

The modifications required to compensate for the effects of a constant wind are now investigated.

6.6 Compensation for a Constant Wind

The effects of steady components of wind produce significant changes in the flight path of a vehicle with respect to an earth-fixed reference frame. The availability of on-board inertial data permits the components of wind to be estimated to within a few knots. The components of wind velocity are obtained using the inertial system velocity information and the airspeed v_{as}.

$$w_x = \dot{x}_i - v_{as}\cos\theta\cos\psi \qquad (6.6\text{-}1)$$

$$w_y = \dot{y}_i - v_{as}\cos\theta\sin\psi \qquad (6.6\text{-}2)$$

where

w_x is the component of wind parallel to the runway (ft/sec).

w_y is the component of wind perpendicular to the runway (ft/sec).

v_{as} is the magnitude of aircraft's velocity relative to the air mass (ft/sec).

$\dot{x}_i$ is the x component of inertially-measured velocity (ft/sec).

$\dot{y}_i$ is the y component of inertially-measured velocity (ft/sec).

The heading ψ_{aq} and velocity v_{aq} in the absence of wind are then computed:

$$\psi_{aq} = \tan^{-1}\left[(\dot{y}_e - w_y)/(\dot{x}_e - w_x)\right] = \psi_b \qquad (6.6\text{-}3)$$

$$v_{aq} = v_{as} \qquad (6.6\text{-}4)$$

where ψ_b is the orientation of the longitudinal axis of the aircraft relative to the runway center line. Once ψ_{aq} and v_{aq} are known, the switching boundary y_{aqc} may be computed using the material in Section 6.4. The boundary must be modified to account for the drift of the aircraft perpendicular to the runway that is due to w_y.

$$y_{aqc} = y_{aqc} - w_y T_{aq} \qquad (6.6\text{-}5)$$

The point at which the vehicle acquired the beam is also modified:

$$x_{aq} = x_{aq} + w_x T_{aq} \qquad (6.6\text{-}6)$$

6.7 Acquisition Control System Synthesis

A schematic diagram of the acquisition control system is shown in Fig. 6.7-1. The reference trajectory y_m is generated by a model of the lateral vehicle characteristics. The nonlinear trajectory generator NTG_m provides a dynamic model which simulates the vehicle roll response subject to the constraints:

$$|\phi_m| \leq \phi_{aq} < \phi_{max} \qquad (6.7\text{-}1)$$

$$|\dot{\phi}_m| \leq \dot{\phi}_{aq} < \dot{\phi}_{max} \qquad (6.7\text{-}2)$$

$$|\ddot{\phi}_m| \leq \ddot{\phi}_{aq} < \ddot{\phi}_{max} \qquad (6.7\text{-}3)$$

The limitations on model response permit the vehicle to correct errors introduced by model inaccuracies and environmental disturbances. The input to the roll tra-

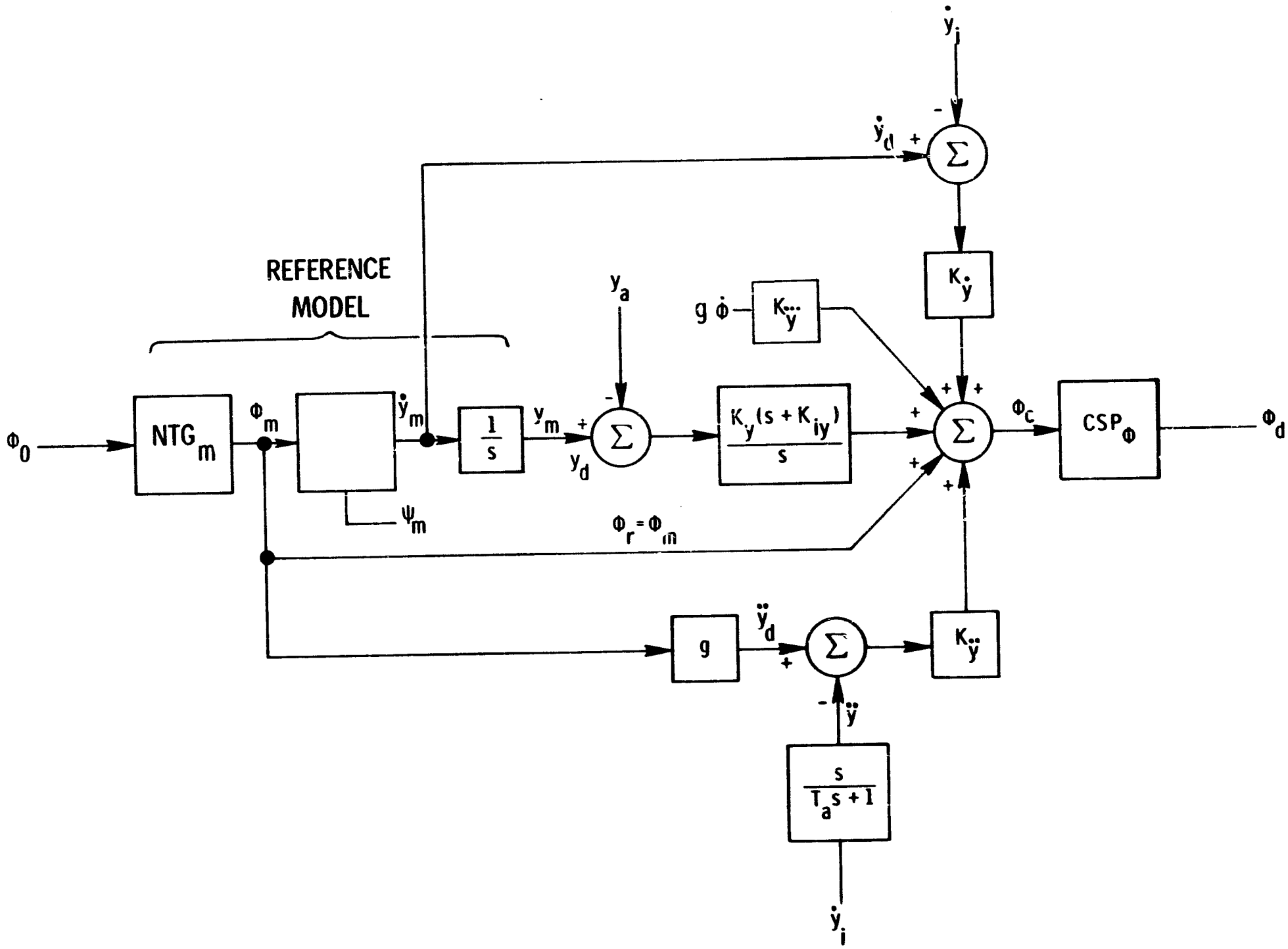

Fig. 6.7-1 Acquisition control system.

jectory generator is a control based on the time-optimal derivation presented in Section 6.5. The time T_{aqa} is redefined to equal the time required for NTG_m to roll from $\phi_m = 0$ to $\phi_m = \phi_{aq} - \delta\phi_{aq}$ where $\delta\phi_{aq}$ is approximately 0.5 degrees. The parameters associated with a quasi-time-optimal control are then computed using Eqs (6.5-2) to (6.5-14). The effects of wind are taken into account as indicated in Section 6.6. The equations of the vehicle model are chosen so that:

$$\dot{\psi}_m = \frac{g \tan \phi_m}{v_p} \tag{6.7-4}$$

$$\dot{y}_m = v_p \sin \psi_m + w_y \tag{6.7-5}$$

with the initial conditions:

$$y_m = y_{es}(t_0) \tag{6.7-6}$$

$$\psi_m = \psi(t_0) \tag{6.7-7}$$

where

t_0 is the time at which acquisition is initiated.

y_{es} is the best estimate of the position of the aircraft at $t = t_0$.

If an input of the form:

$$\phi_0 = 0 \qquad |y_{es}| > |y_{aqc}| \tag{6.7-8}$$

$$\phi_0 = -\phi_{aq} \operatorname{sgn}(y_{es}) \begin{cases} |y_{es}| < y_{aqc} \\ |\psi_m| > \delta\psi_{aq} \end{cases} \tag{6.7-9}$$

$$\phi_0 = 0 \qquad |\psi_m| < \delta\psi_{aq} \tag{6.7-10}$$

is applied to NTG_m, it is apparent that the trajectory of the model will be a quasi-time-optimal trajectory similar to that shown in Fig. 6.5-1. The aircraft is forced to follow this trajectory by constructing the commanded roll angle ϕ_c in the form:

$$\phi_c = \phi_m + K_y(y_m - y_a) + K_{\dot{y}}(\dot{y}_m - \dot{y}_i) + K_{\ddot{y}}\left(\ddot{y}_m - \frac{s}{T_a s + 1}\,\dot{y}_i\right) + K_{\dddot{y}} g\dot{\phi} \tag{6.7-11}$$

where

$$y_a = y_{es} + \int_{t_0}^{t} \dot{y}_i dt \tag{6.7-12}$$

As a result of the manner in which the model trajectory is generated, the actual path of the aircraft will correspond to the model trajectory with a high degree of precision.

The parameters associated with the acquisition control system are defined in Table 6.7-1.

6.8 Termination of the Acquisition Maneuver

At the end of the control sequence described in Section 6.5 the aircraft will be in a level flight on a straight path essentially parallel to the ILS localizer center. The major contribution to the distance between the path and the localizer is the error in the initial estimate y_{es} of y. At the termination of acquisition improved estimates of lateral position will be available from the algorithms described in Chapter 3. This information is utilized by transferring to a linear control mode using the system described in Section 5.8. The initial conditions of the trajectory generator NTG_y are set to:

$$y_d = \hat{y} \qquad (6.8\text{-}1)$$

$$\dot{y}_d = \hat{\dot{y}} \qquad (6.8\text{-}2)$$

to reflect the availability of more precise data. Lateral vehicle control is maintained by this linear system until the terminal maneuvers, DECRAB and FLAREOUT are initiated.

6.9 Acquisition Control System Responses

The response characteristics of the acquisition system are illustrated in Fig.(6.9-1). A family of responses corresponding to various values of initial heading angle appear in Fig.(6.9-2). The effects of a lateral wind component are illustrated in Fig.(6.9-3). These trajectories demonstrate the ability of the vehicle to follow the desired path precisely. Control system adaptation to modifications in heading angle and lateral wind is also illustrated.

Table 6.7-1 Acquisition Control System Parameters

GAINS		
K_y, $K_{\dot{y}}$, $K_{\ddot{y}}$, $K_{\dddot{y}}$, K_{iy}	Lateral position control system gains	see Table 5.8-1
CONSTANTS		
T_a	lateral acceleration filter time constant	see Table 5.8-1
SATURATION LIMITS	IMPOSED BY NTG_ϕ	IMPOSED BY NTG_m
ϕ	30.000 deg	20.000 deg
$\dot{\phi}$	10.000 deg/sec	7.500 deg/sec
$\ddot{\phi}$	10.000 deg/sec	7.500 deg/sec
NTG PARAMETERS		
ω_m	Model NTG natural frequency	8.660 rad/sec
ξ_m	Model NTG damping ratio	4.330

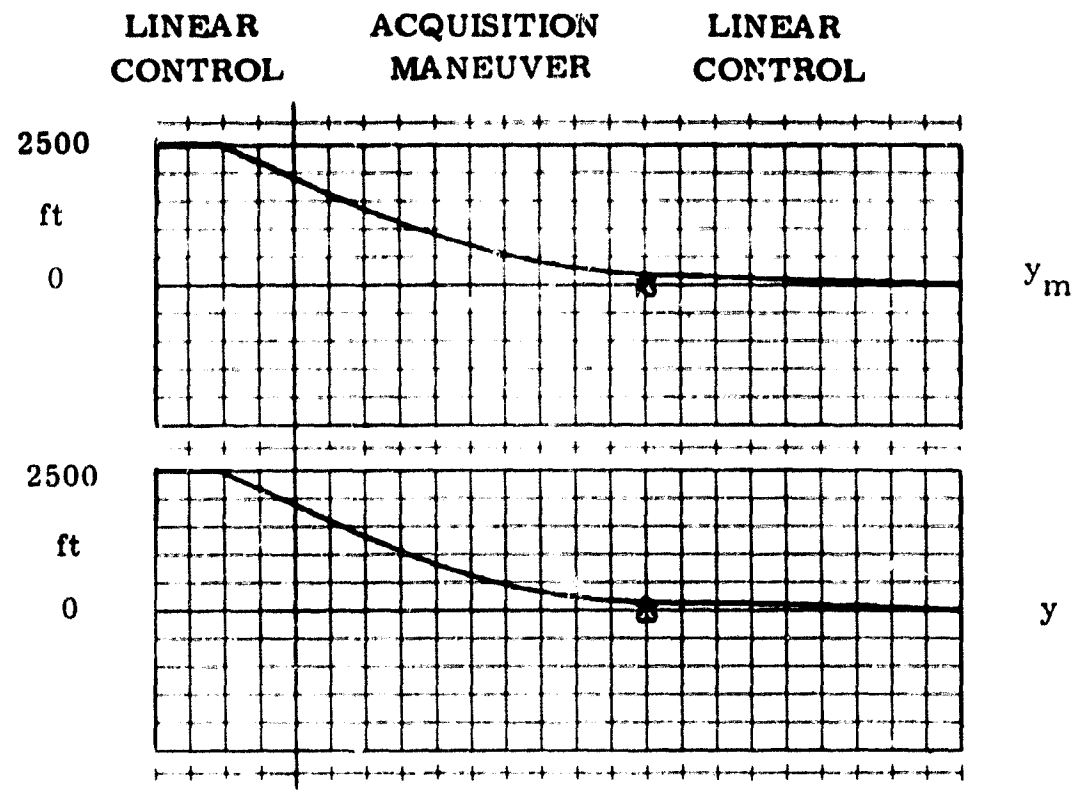

Fig. 6.9-1 Typical acquisition control system response showing the reference trajectory y_m, the actual path y and the roll angle ϕ . ($\psi_a = 45^o$).

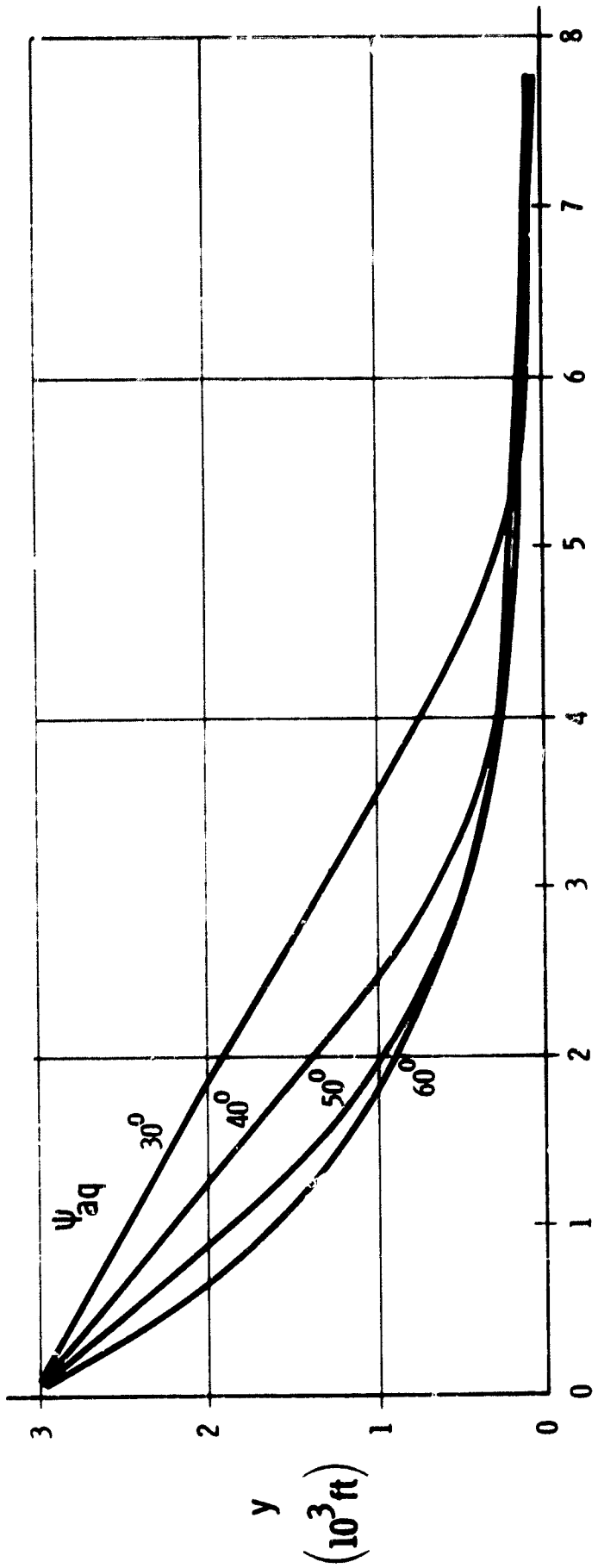

Fig. 6.9-2 Acquisition control system responses for various initial heading angles. These responses demonstrate ability to acquire the localizer beam from a broad range of initial flight path headings.

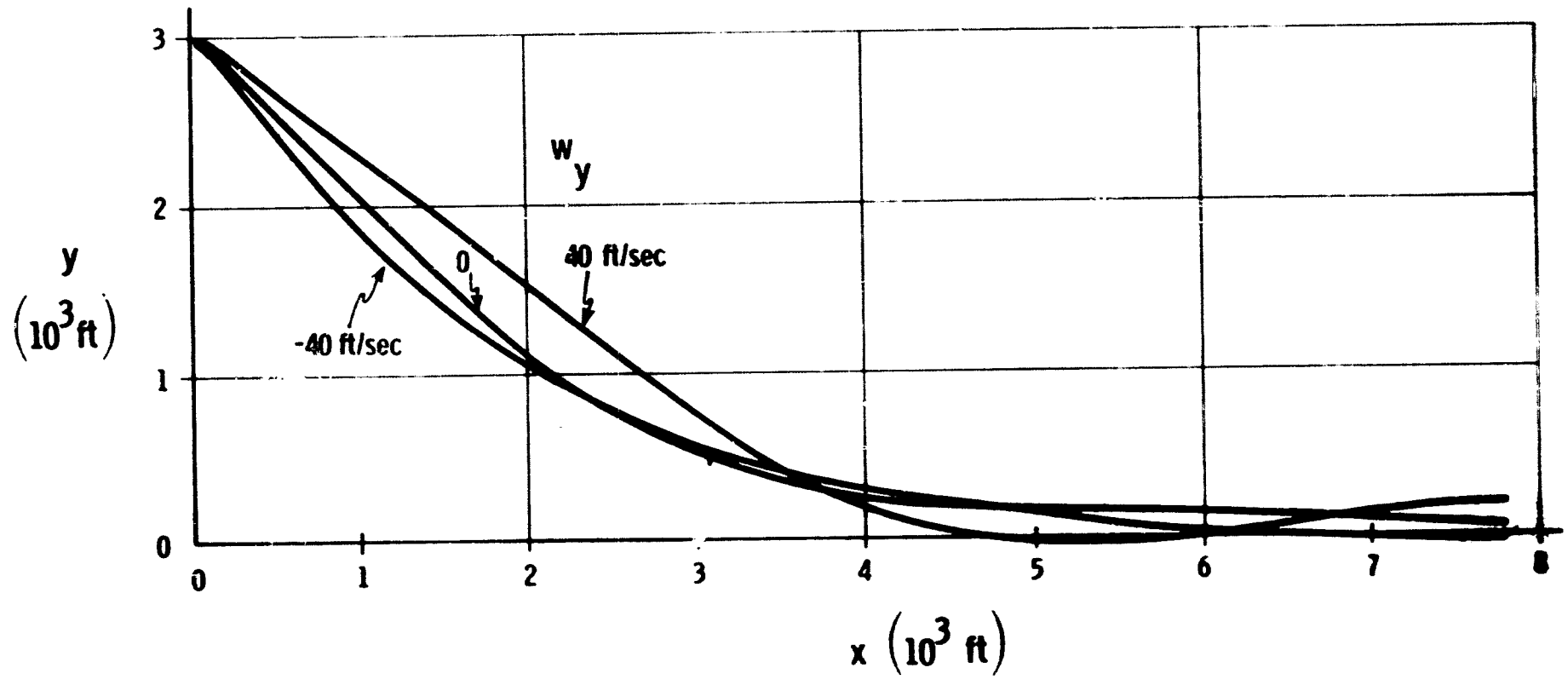

Fig. 6.9-3 The effect on a lateral component of wind on acquisition system response characteristics. The vehicle heading is 45^{o}. The ability to cope with strong crosswinds is an important advantage of the new acquisition control system.

CHAPTER 7

TERMINAL MANEUVER CONTROL SYSTEMS

7.1 Introduction

The final phase of an automatic landing requires the solution of a number of interesting control problems. During the terminal phase the aircraft must reduce its vertical component of velocity from a nominal value of 10 ft/sec to approximately 2.5 ft/sec. The velocity change ensures a landing velocity low enough to avoid structural damage or passenger discomfort while still providing a firm touchdown. Coincident with the above maneuver, the aircraft must align its longitudinal axis and its ground-referenced velocity vector as closely as possible with the center line of the runway. Two preliminary control system designs which are capable of achieving the above goals will now be described in detail.

7.2 Flareout Control

An important aspect of the control problem during the final phases of landing is flareout. The flareout maneuver is characterized by a departure from the glide-slope plane which defines the vertical flight path after termination of ACQUISITION, and by a reduction in vertical velocity from the value required to track the glide slope (10 ft/sec) to the nominal touchdown velocity (2.0 - 2.5 ft/sec).

The problem stands apart from the previous discussion as a result of the emphasis which must be placed on precise velocity rather than precise position control. To meet the touchdown velocity goal the primary loop is closed on vertical velocity. A secondary closure on acceleration is introduced to provide essential damping and improved velocity profile control. The velocity and acceleration loop gains are the same as those obtained in the section on vertical control system design. The flareout trajectory generator is a simple modification of the vertical profile generator. The complete system is delineated in Fig. 7.2-1. The structure is similar to that of the vertical control system. It will be noted that the trajectory generation technique is different; there is no loop closure on vertical position, and a proportional plus integral compensator with a gain equal to $K_{iz}^{\cdot}$

$$G_{iz} = \frac{s + K_{iz}^{\cdot}}{s} \qquad (7.2\text{-}1)$$

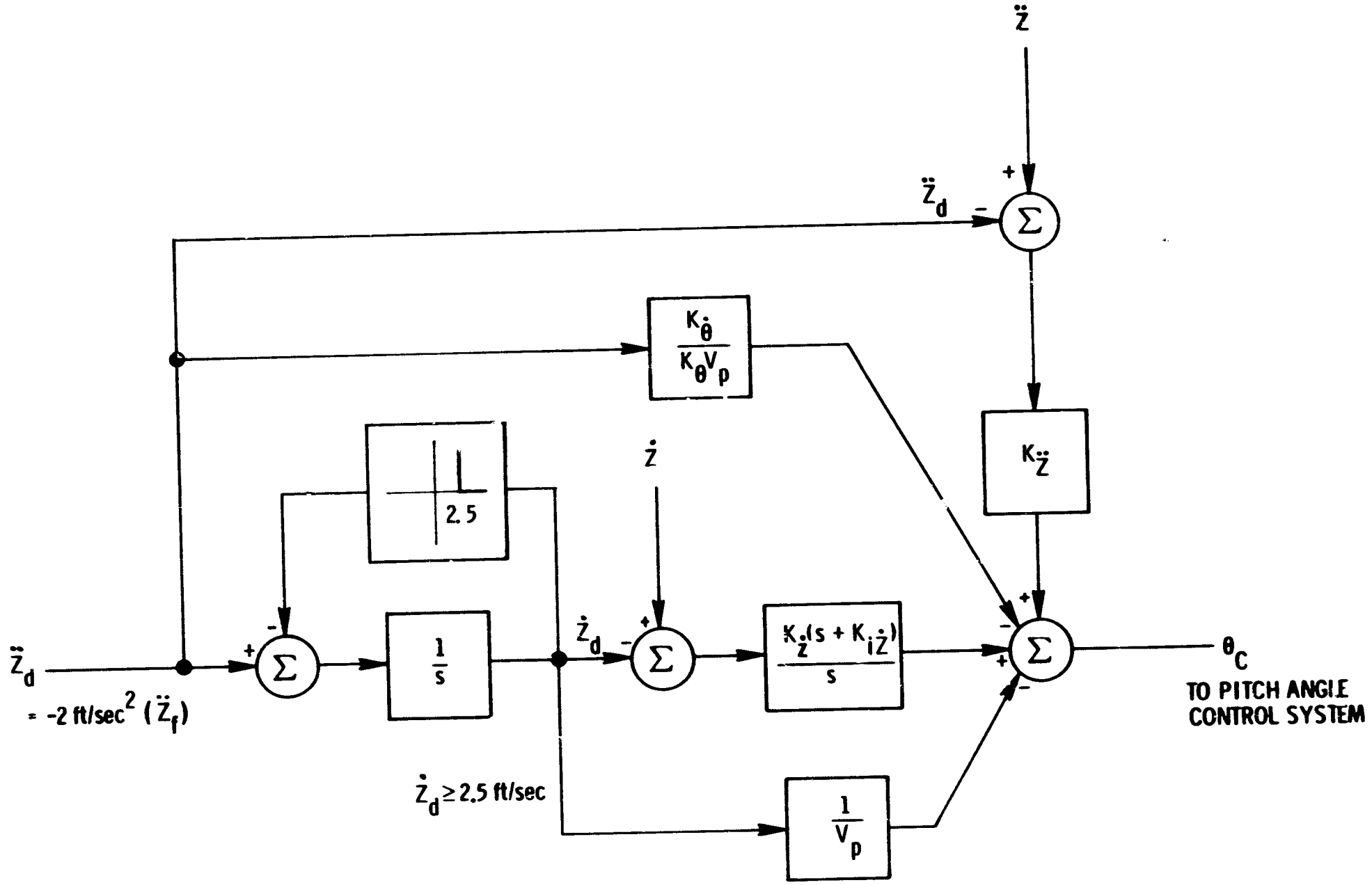

Fig. 7.2-1 The flareout control system.

has been introduced in the velocity control loop. The compensator provides a residual component of θ_c which is required to maintain a zero quiescent velocity error.

The limitations on elevator range and actuation rate define corresponding limits on pitch acceleration and acceleration rate as discussed in Section 2.3. The effector limitations also impose limits on vertical acceleration and acceleration rate. A satisfactory flare velocity profile must be obtained within the imposed kinematic limits. In addition, the trajectory must be tailored to ensure passenger comfort, which implies a low vertical acceleration. The equations of the selected trajectory have the form

$$\ddot{z}_d = \begin{cases} \ddot{z}_f & \dot{z}_d > \dot{z}_f \quad h < h_f \\ 0 & \dot{z}_d \leq \dot{z}_f \quad h < h_f \end{cases} \tag{7.2-2}$$

$$z_d = \frac{\ddot{z}_d (t - t_f)^2 + 2z_f}{2} \tag{7.2-3}$$

where

$h_f = -z_f$ is the altitude at which flare is initiated.

$\dot{z}_f$ = the desired vertical component of velocity at touchdown.

t_f = the time at which flare is initiated.

The time of initiation of the flareout maneuver can be determined by using the vehicle radio altitude. This method provides an accurate initiation although vertical errors of several feet are common. A small error in altitude results in a touchdown error given by the relationship

$$e_{td} \approx \dot{x} \frac{e_{ra}}{\dot{z}_f} \tag{7.2-4}$$

where

e_{td} is the longitudinal position error (feet).

e_{ra} is the radio altitude error (feet).

$\dot{x}$ is the ground velocity along the runway (ft/sec).

$\dot{z}_f$ is the desired vertical velocity at touchdown (ft/sec).

Additional error results from the effect of atmospheric disturbances close to the ground, although these effects are minimized by the magnitude of the vehicle

mass and the quality of the control system.

Responses of a typical maneuver are illustrated in Fig. 7.2-2. The parameters associated with the responses shown are

$$h_f = 100 \text{ ft} \tag{7.2-5}$$

$$\ddot{z}_f = 2 \text{ ft/sec}^2 \tag{7.2-6}$$

Some appreciation of the scale associated with the flareout maneuver may be obtained from Fig. 7.2-3 where attitude is plotted against distance along the runway center line.

7.3 Decrab Control

If a constant component of wind w_y exists perpendicular to the runway the approach along the glide-slope center line is executed with the aircraft crabbed into the wind so that its net ground velocity perpendicular to the localizer center line is zero. The required crab angle ψ_c at any instant in time t_c is given by

$$\psi_c = \tan^{-1}\left(\frac{w_y}{\dot{x}}\right) \tag{7.3-1}$$

In order to minimize undercarriage stress, it is important to place the aircraft on the runway with its velocity vector parallel to the longitudinal axis of the aircraft. The velocity vector should also be aligned with the runway center line to reduce runoff. To effect the required condition the aerodynamic properties of the vehicle are utilized. The lateral component of velocity may be written

$$\dot{y} \approx v_p \sin(\psi - \beta)\cos\theta \tag{7.3-2}$$

Thus if β is equal to ψ the lateral velocity is zero. This condition may be achieved for a short time by yawing the aircraft very rapidly as shown in Fig. 7.10-2. Thus if the crabbed aircraft is rapidly rotated through an angle ψ_c the velocity is

$$\begin{aligned} \dot{y} &\approx v_p \sin(\psi_c - \beta)\cos\theta \\ &\approx v_p \sin(\psi_c - \psi_c)\cos\theta \\ &= 0 \end{aligned} \tag{7.3-3}$$

7.4 Linear Analysis of a Decrab Control System

The touchdown conditions specified are achieved by controlling the aircraft heading ψ while maintaining a zero roll angle. The primary control is the rudder deflection δ_r. The transfer function relating heading rate r to rudder deflection δ_r is shown in Fig. 7.4-1. Deflection of the rudder produces a side force on the vertical stabilizer generating a moment about the z-axis. As heading rate increases

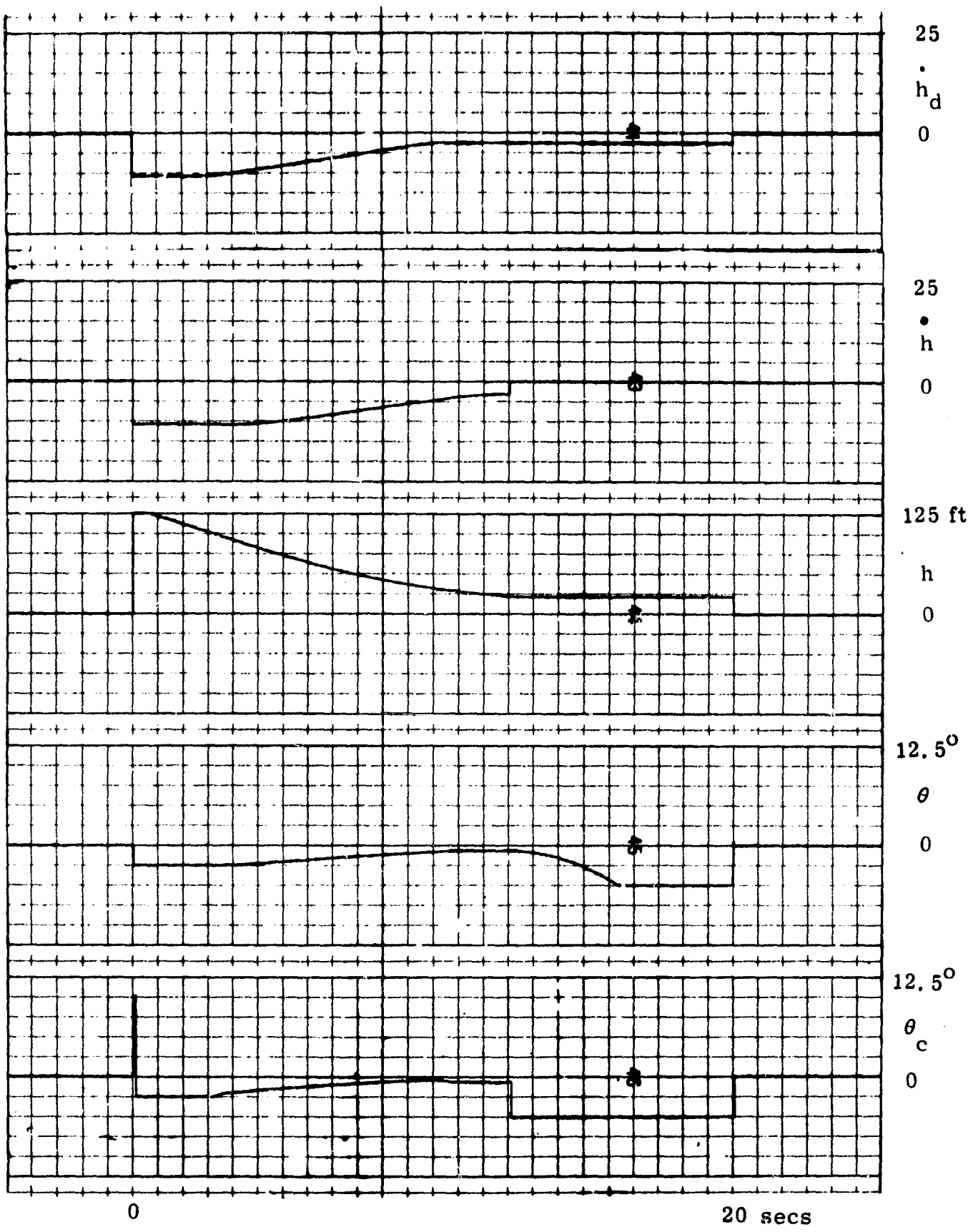

Fig. 7.2-2 Flareout control system response (h_c= 100 ft).

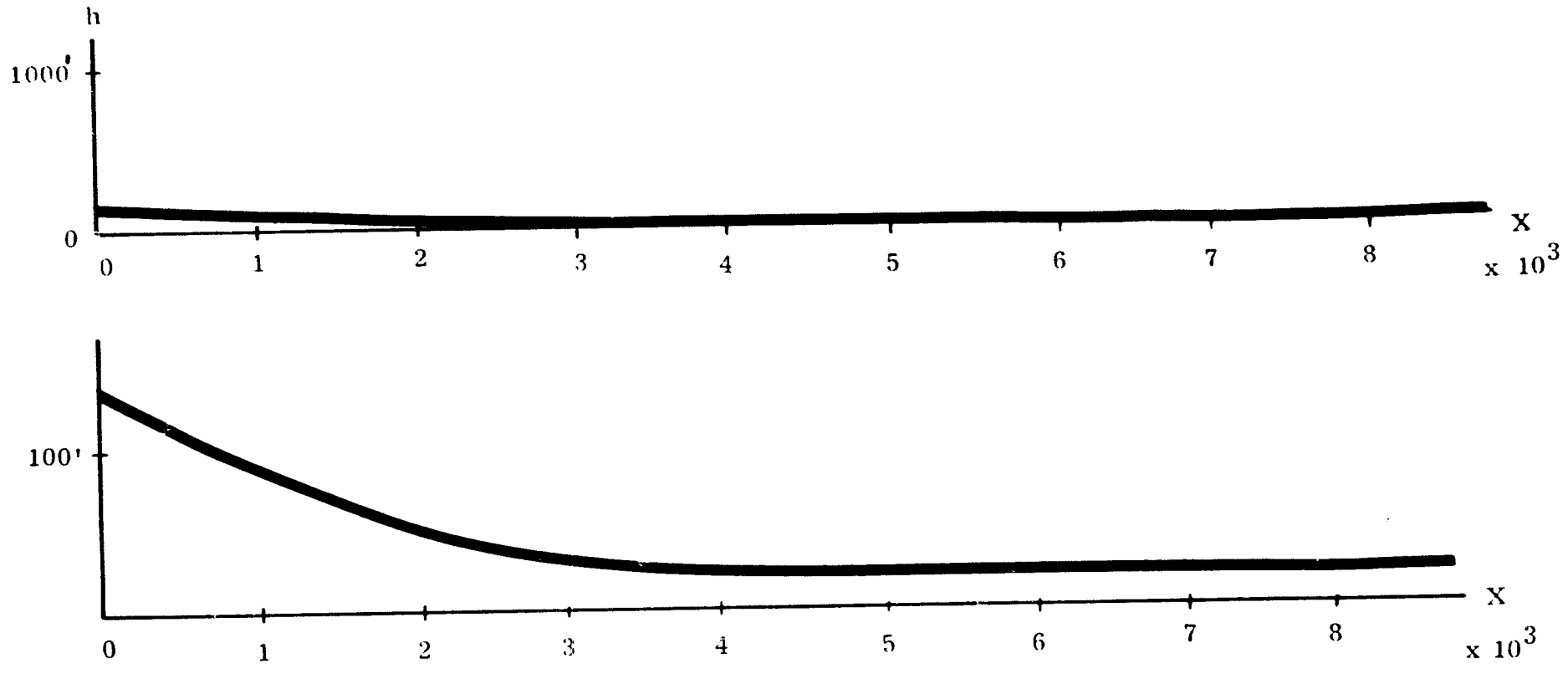

Fig. 7.2-3 The top figure displays altitude versus distance along the runway centerline during a typical FLAREOUT maneuver. In the bottom figure the altitude scale has been multiplied by 10 to exaggerate the path structure.

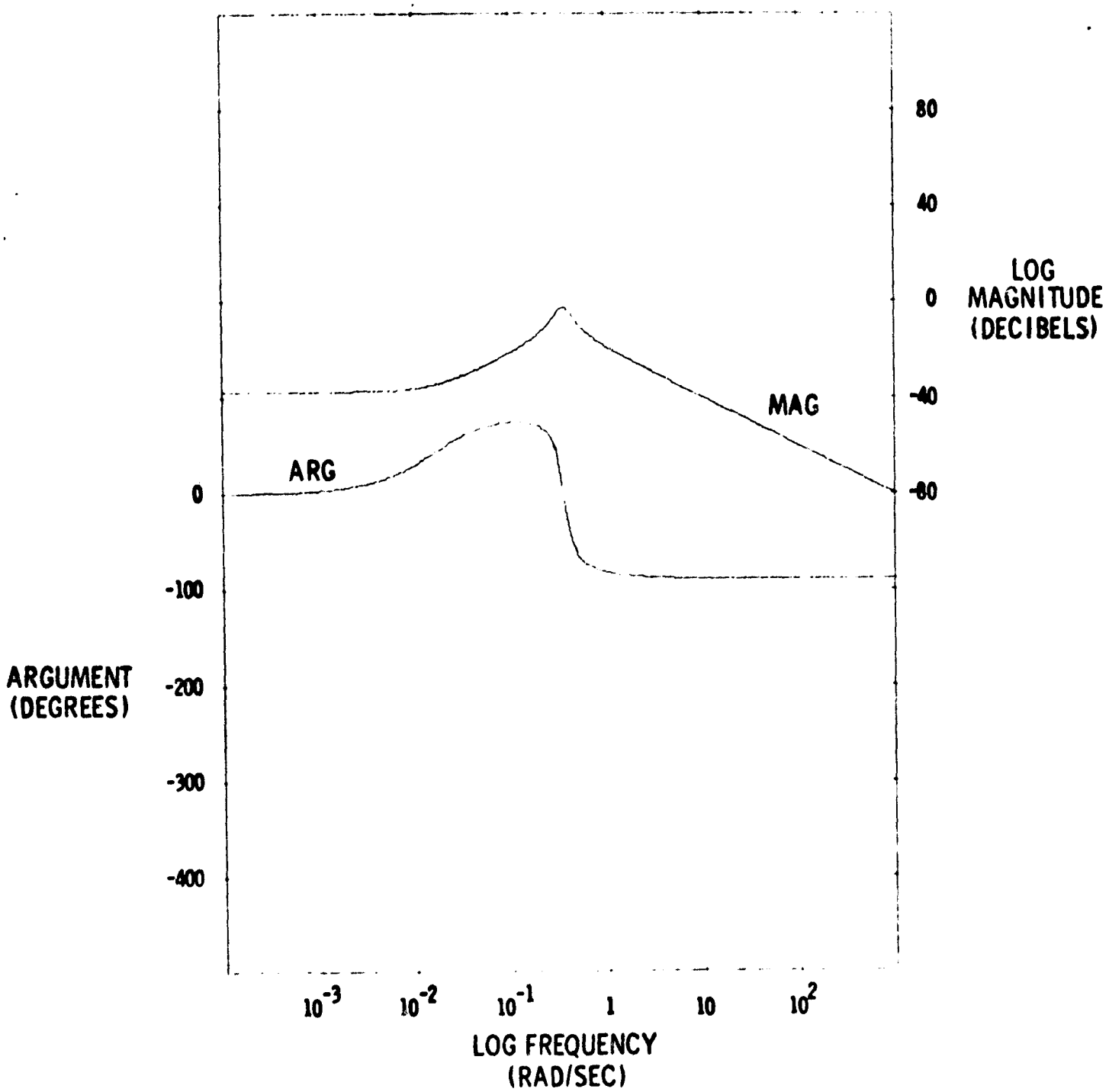

Fig. 7.4-1 Transfer function relating yaw rate to rudder deflection, $\left(-\frac{r}{\delta_r}\right)_{p=0}$

in response to this moment the effective force produced by the rudder decreases, eventually approaching zero for a fixed rudder deflection. Thus at high frequencies the rate r is proportional to the integral of the rudder deflection, while at low frequencies it is proportional to the derivative of rudder deflection.

The rudder effector is modeled by a simple first-order transfer function with a 0.05 second time constant. The linearized system is shown in Fig. 7.4-2 where

ψ_d is a desired heading angle (radians).

K_ψ and K_r are adjustable gains.

T_{rud} is the time constant associated with the simple first order model of the rudder actuator.

A loop closed on ψ satisfies the primary orientation requirement, while a second loop closed on rate r ensures satisfactory damping characteristics. The open and closed-loop transfer functions and linear step responses are shown in Figs. 7.4-3, 7.4-4 and 7.4-5.

7.5 Nonlinear Considerations for Decrab Control

As in the case of lateral and longitudinal control, it is important to consider the effects of magnitude and rate limitations on rudder deflection. These limitations are reflected in corresponding restrictions on maximum yaw acceleration and acceleration rate. It is desirable to operate the rudder as close to saturation as possible to achieve the fastest yaw response characteristics. The current design achieves this goal by utilizing a nonlinear trajectory generator (NTG_ψ) to control the heading rate and position. The trajectory generator is characterized by somewhat faster response characteristics than the vehicle-control system combination alone. This is an important point since it leads to a fast heading response without the high gains which would normally be required to achieve a high rate of response, thus avoiding sensor noise and stability problems.

7.6 Compensation for Steady-State Errors

As a result of the character of the transfer function relating β to δ_r, a constant value of rudder deflection is required to maintain a sideslip angle β. The rudder deflection may be written in the form

$$\delta_r \approx -C_d\beta \tag{7.6-1}$$

where C_d is a constant. Assuming that $\beta = -\psi_c$, it is apparent that

$$\delta_r = C_d\psi_c \tag{7.6-2}$$

at touchdown. The component of rudder deflection, Eq (7.6-2), is primarily

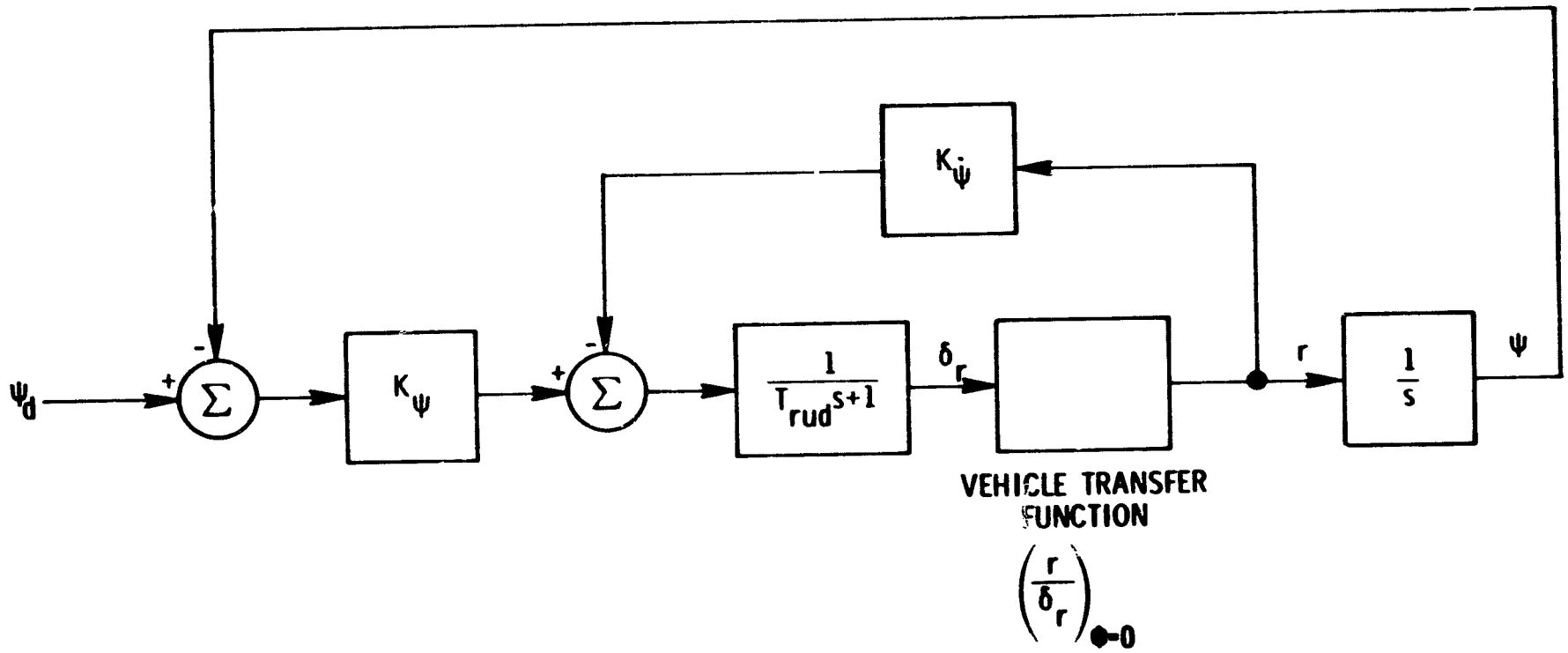

Fig. 7.4-2 Linearized model of a decrab control system.

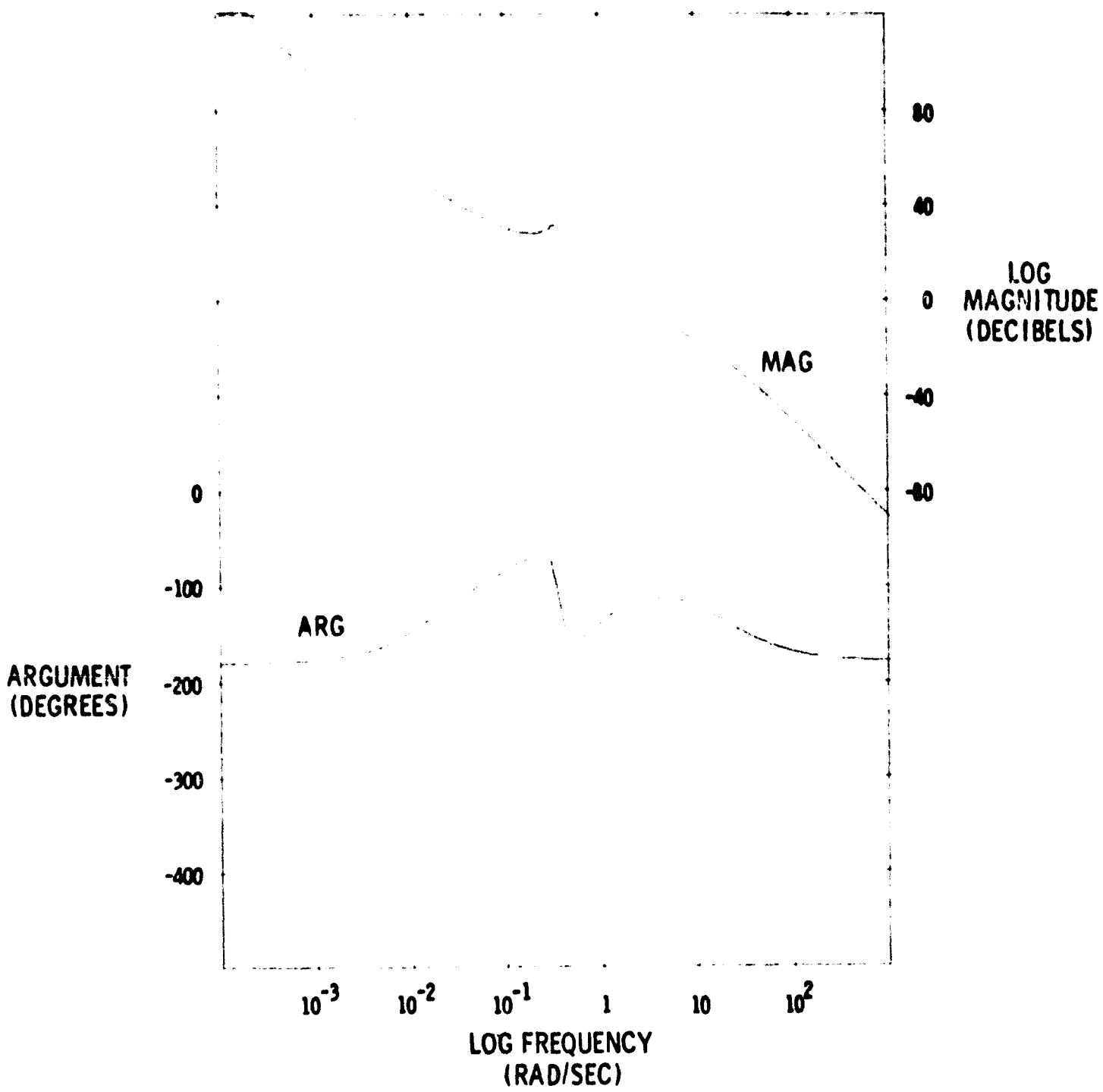

Fig. 7.4-3 Open-loop transfer function of linearized heading angle control system.

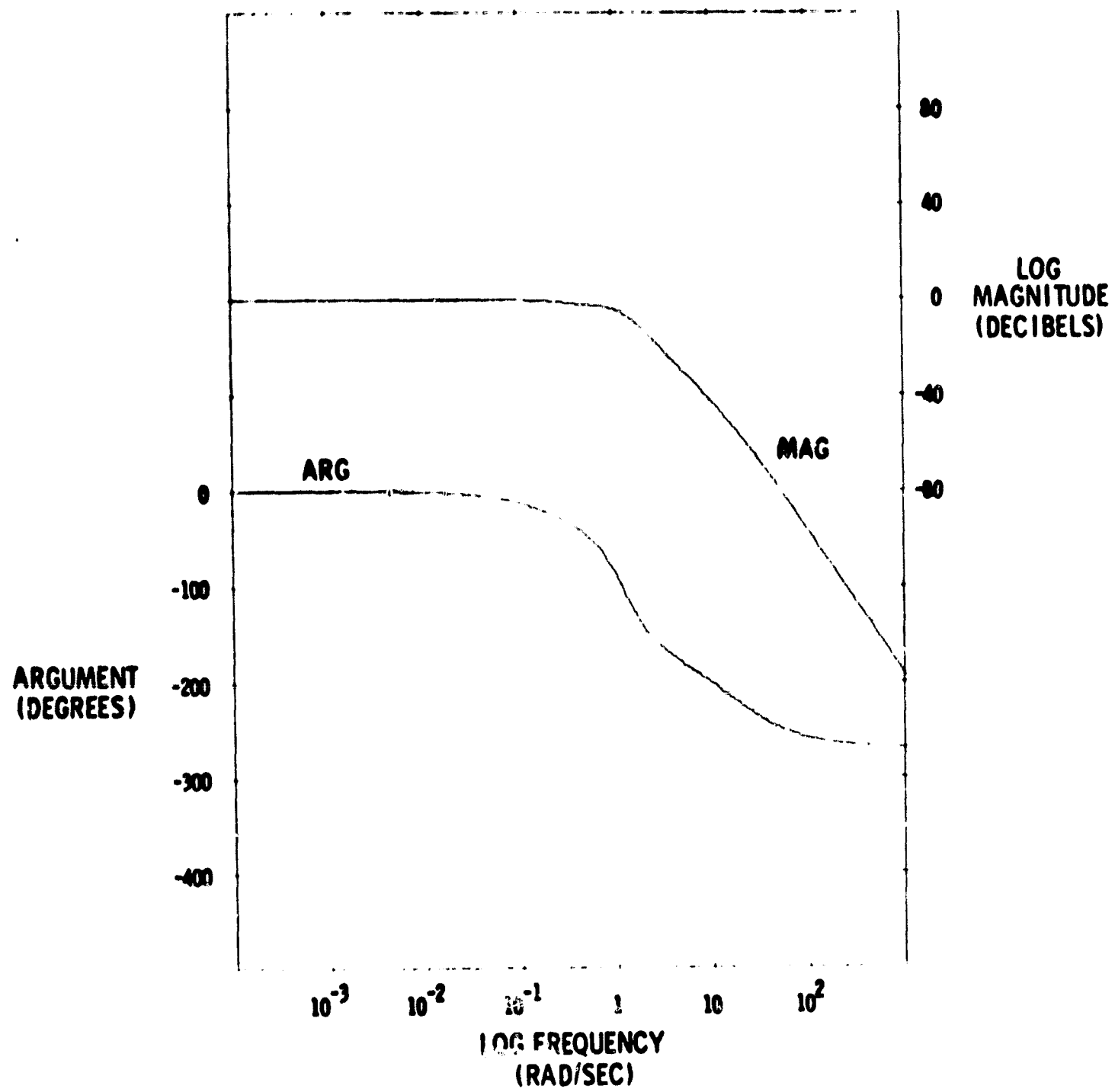

Fig. 7.4-4 Closed-loop transfer function of linearized heading angle control system.

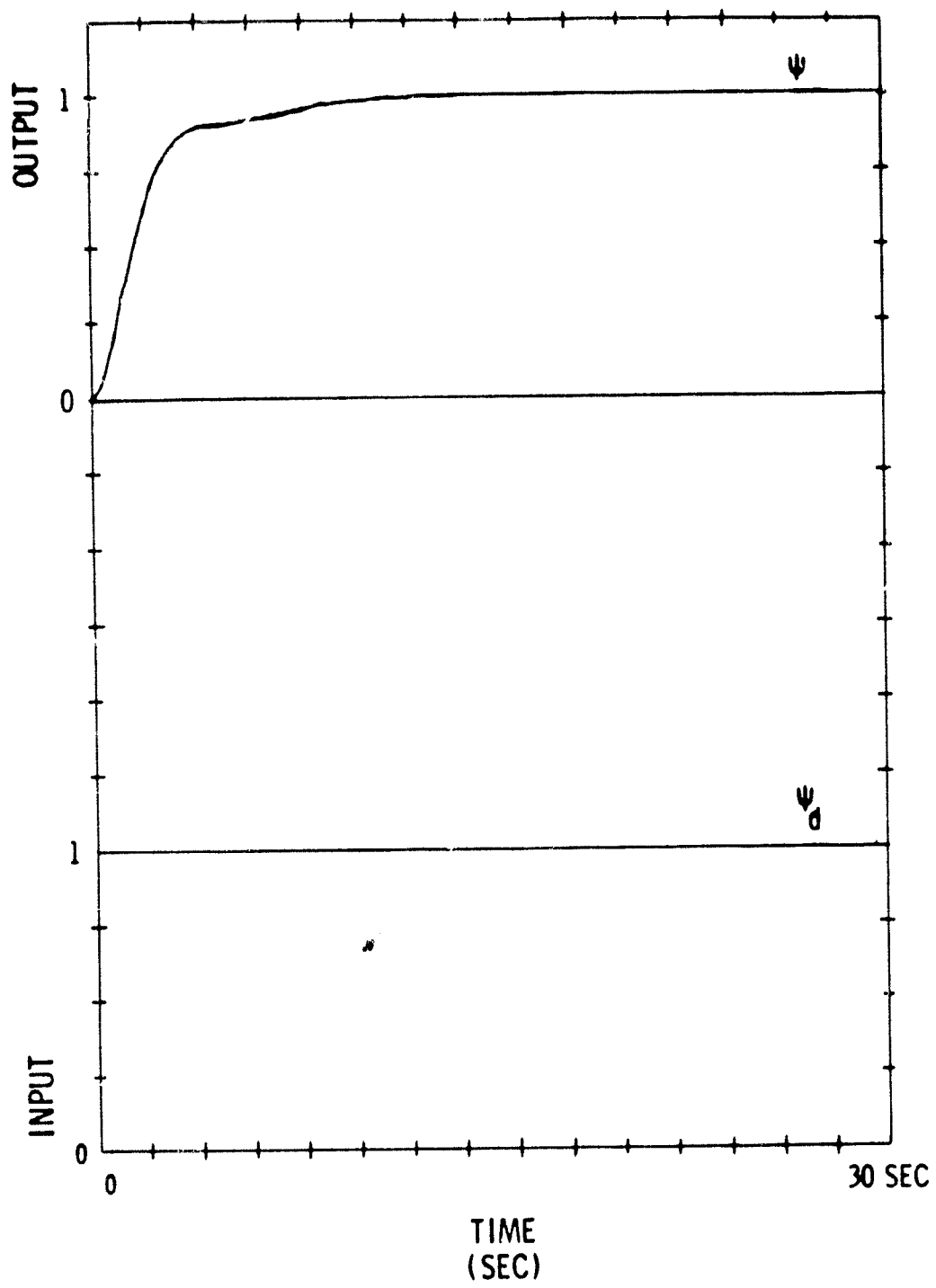

Fig. 7.4-5 Unit-step response of the linearized heading angle control system.

supplied by an error in heading angle

$$e_\psi = \frac{C_d \psi_c}{K_\psi} \tag{7.6-3}$$

The heading error is eliminated by introducing a proportional plus integral compensator with gain $K_{i\psi}$

$$G_{i\psi} = \frac{s + K_{i\psi}}{s} \tag{7.6-4}$$

as shown in Fig. 7.10-1, and the reference input

$$\delta_r = C_d \psi_c \tag{7.6-5}$$

The proportional plus integral compensator compensates for errors in Eq (7.6-2).

7.7 Heading Rate Feedforward Compensation

Precise heading rate control is achieved by comparing the actual heading rate r with the velocity $\dot{\psi}_d$ output from NTG_ψ. The final control law has the form

$$\delta_r = K_\psi \left(\frac{s + K_{i\psi}}{s} \right) (\psi_d - \psi) + K_{\dot{\psi}} (\dot{\psi}_d - \dot{\psi}) + C_d \psi_c \tag{7.7-1}$$

7.8 Yaw-Roll Decoupling

The yawing DECRAB maneuver introduces perturbations in the roll equation which will lead to an unacceptable roll angle if appropriate corrective measures are not taken. The slow response of the roll system does not permit compensation by roll feedback alone, and feedforward compensation techniques must be adopted. The relevant terms in the roll vehicle equation are

$$C_{\dot{p}}\dot{p} = C_{\dot{p}\beta}\beta + C_{\dot{p}r}r + C_{\dot{p}\delta_r}\delta_r + C_{\dot{p}\delta_a}\delta_a \tag{7.8-1}$$

where

C_{xy} is a constant relating variable x to variable y.
$C_{\dot{p}}$ is a constant.

Zero roll rate is achieved by manipulating the ailerons so that

$$(\delta_a)_d = \frac{-1}{C_{\dot{p}\delta_a}} (C_{\dot{p}\beta}\beta + C_{\dot{p}r}r + C_{\dot{p}\delta_r}\delta_r) \tag{7.8-2}$$

The sideslip angle β is not, in general, available from instrumentation. However, during the decrab maneuver

$$\beta \approx \psi_c - \psi \tag{7.8-3}$$

so that Eq (7.8-2) may be written

$$(\delta_a)_d = \frac{-1}{C_{\dot{p}\delta_a}}(C_{\dot{p}\beta}(\psi_c - \psi) + C_{\dot{p}r}r + C_{\dot{p}\delta_r}\delta_r) \qquad (7.8\text{-}4)$$

The lateral stablility augmentation system of the ILS is designed to achieve turn coordination by driving $\dot{\beta}$ to zero. This action is undesirable during decrab and is avoided by disabling the lateral SAS. Roll angle control is still desirable and is achieved by constructing the aileron command directly.

$$(\delta_a)_\phi = -K_\phi\phi - K_{\dot{\phi}}\dot{\phi} \qquad (7.8\text{-}5)$$

The total aileron command is generated by summing Eqs (7.8-4) and (7.8-5)

$$\delta_a = (\delta_a)_\phi + (\delta_a)_d \qquad (7.8\text{-}6)$$

7.9 Decrab Control System Configuration

A complete decrab control system is shown in Fig. 7.9-1, and the parameters are defined in Table 7.9-1. The nonlinear trajectory generator is described in detail in Section 4.3, while a typical Decrab response is shown in Fig. 7.9-2.

Table 7.9-1 Decrab Control System Parameters

GAINS		
K_ψ	Heading position gain	7.900
$K_{\dot{\psi}}$	Heading rate gain	15.800 sec
$K_{i\psi}$	Integral compensator gain	0.500
K_ϕ	Roll angle gain	1.000
$K_{\dot{\phi}}$	Roll-rate gain	2.000 sec
CONSTANTS		
c_d		-1.000

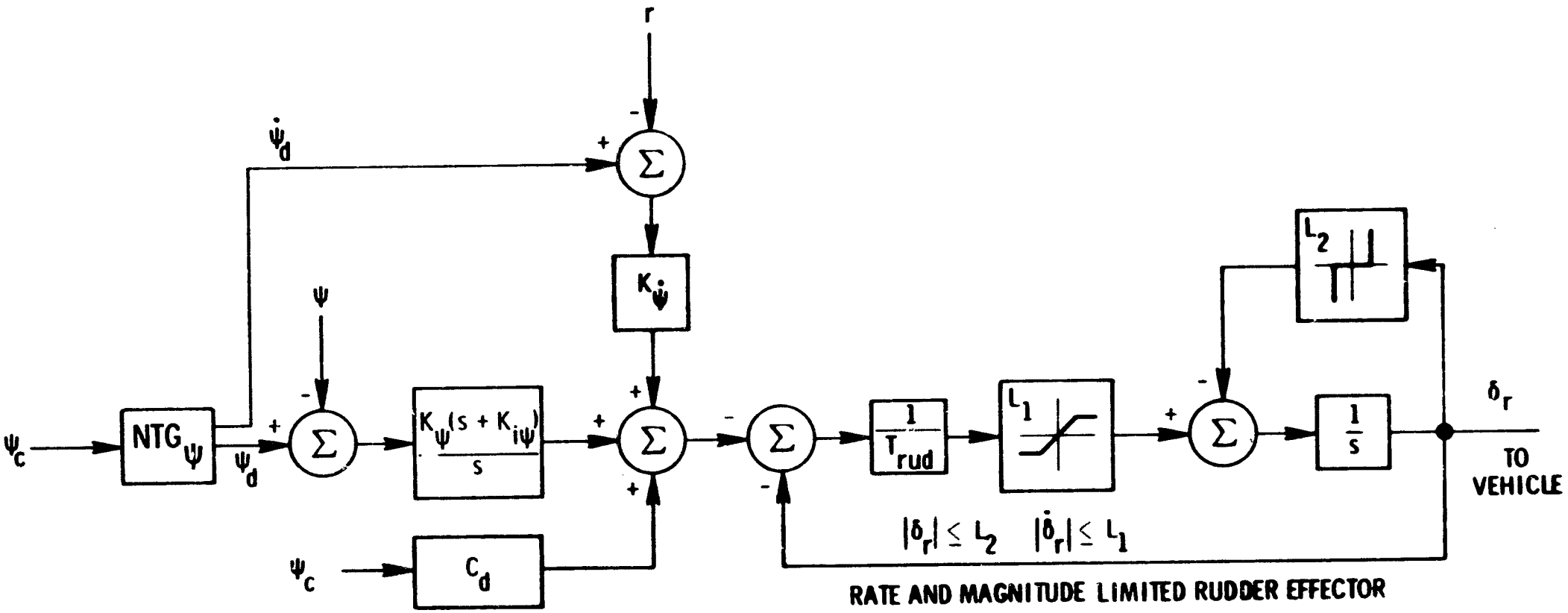

HEADING ANGLE CONTROL SYSTEM

Fig. 7. 9 -1 Decrab control system.

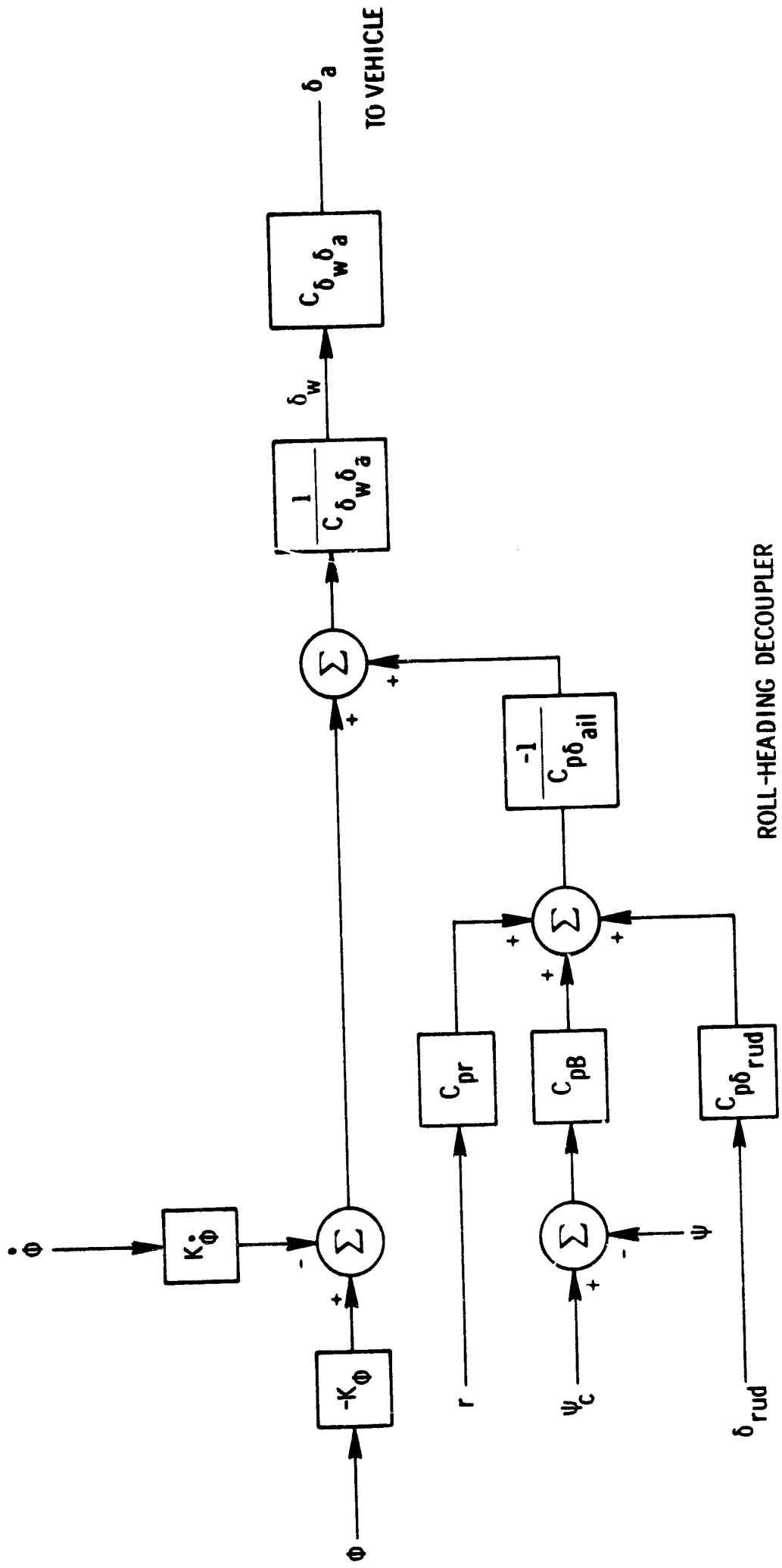

Fig 7. 9 -1 (cont) Decrab control system.

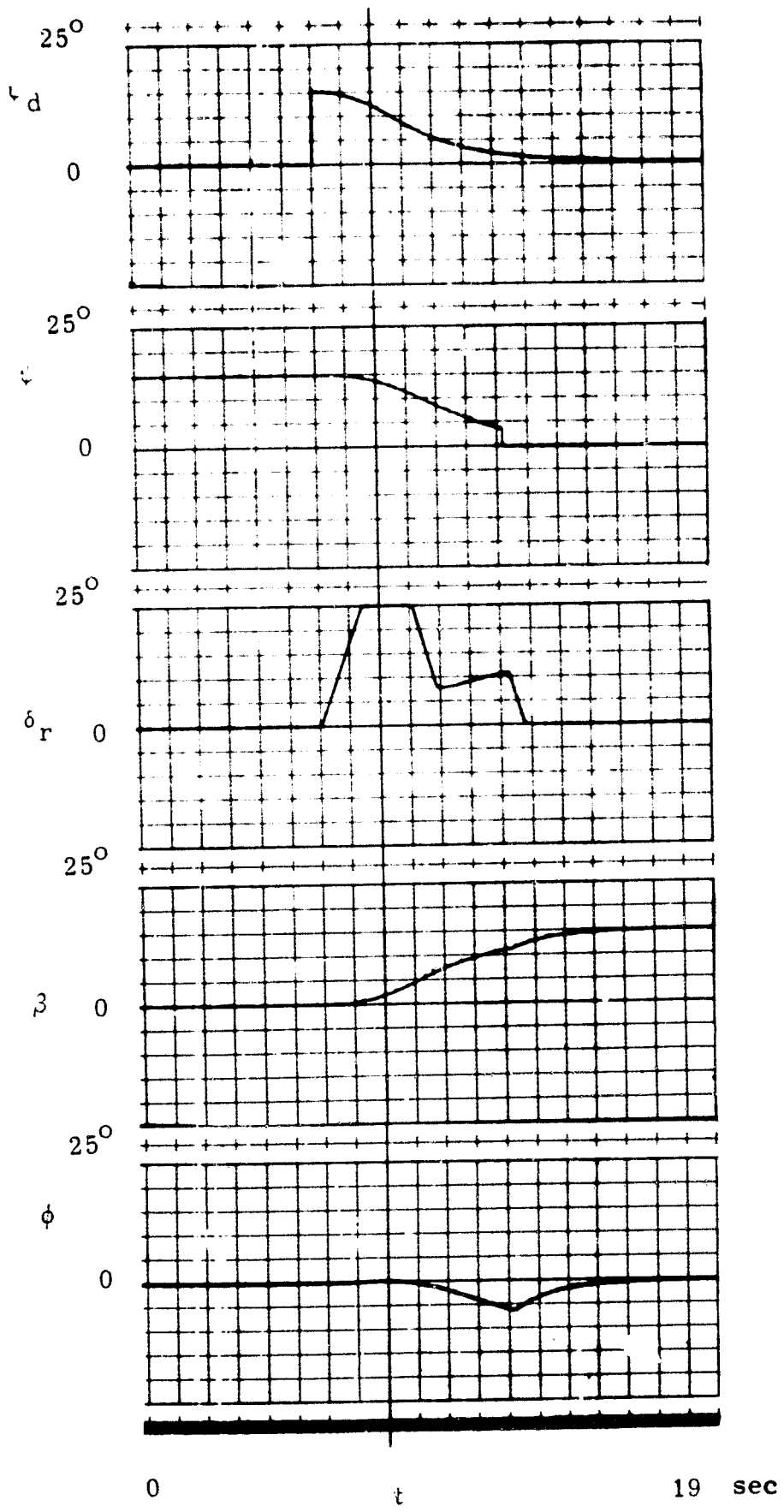

Fig. 7. 9-2 Typical decrab maneuver.

CHAPTER 8

VEHICLE EQUATIONS OF MOTION

8.1 Summary

In this chapter, the general equations of unsteady motion of the aircraft are initially presented without derivation. Partial linearization is then made as appropriate to the proposed simulation. The final set of vehicle equations as mechanized in the digital simulation appear in Section 8.5.

The evaluation of the aerodynamic forces and moments is presented in Section 8.4. It is based upon aerodynamic information which appears in Appendix E and was supplied by the Boeing Aircraft Company and the FAA.

8.2 Introduction

The aerodynamic information for the SST that has been made available by Boeing and the FAA is in classical stability derivative form with derivatives calculated, measured or contrived for one particular airspeed. Classical aircraft stability investigations are generally concerned with the response of an aircraft to control displacements or aerodynamic disturbances at discrete points in the flight velocity spectrum. There is generally no concern with gross uniform motion of the atmosphere rather, only aircraft response to gusts. In any event, there is no need to keep accurate track of the aircraft with respect to inertial space and usually no need to consider airspeed changes greater than a small perturbation from the reference state. For such analyses the use of linear aerodynamic coefficients such as the stability derivatives is well established.

Dynamic simulation of the aircraft in the approach must consider flight through an unsteady atmosphere - unsteady because of wind gradients, wind gusts and turbulence. The aircraft velocity control system holds the airspeed essentially constant, except where a programmed speed change is called for during the flare, for example, when the airspeed is reduced from the nominal approach speed of $1.3\,V_s$ to $1.2\,V_s$ at touchdown. To hold airspeed may require a significant inertial increment in response to a significant component of aerodynamic noise, where here significant is meant to indicate a value somewhat above that normally considered to be a "small perturbation." The important point is that the airspeed perturbation (the sum of the inertial velocity increment and the aerodynamic noise velocity increment) remains small, so that the use of the linear aerodynamic coefficients (calculated at the

nominal approach speed) is justified provided, of course, that the aerodynamic forces do not change very rapidly for any reason.

There are situations during the approach and landing where it may be necessary to consider the effect of a significant change in airspeed. Correction on the glide-slope to the nominal approach speed and the progressive speed reduction during the flare, are examples. Further, at high lift coefficients and particularly near the ground plane, the aerodynamics is nonlinear. The method of handling the aerodynamics in these cases is to include higher order terms in the aerodynamic model.

In Appendix F an extension of the linear aerodynamic model has been made to include second-order terms. Those finite second partial derivatives arising as a result of a significant change in airspeed are then derived as an extrapolation of the available aerodynamic information.

8.3 The Aircraft Nonlinear Equations of Motion

The general nonlinear equations of motion with respect to a set of axes fixed in the aircraft have been derived often in the literature, for example in ref (6), and consequently are presented here without derivation. They are as follows:

$$\underline{\text{LIFT}} \qquad Z + mg\cos\Theta\cos\Phi = m(\dot{W} + PV - QU) \tag{a}$$

$$\underline{\text{DRAG}} \qquad X - mg\sin\Theta = m(\dot{U} + QW - RV) \tag{b}$$

$$\underline{\text{SIDE FORCE}} \qquad Y + mg\cos\Theta\sin\Phi = m(\dot{V} + RU - PW) \tag{c}$$

$$\underline{\text{PITCH}} \qquad M = B\dot{Q} + RP(A - C) + E(P^2 - R^2) \tag{d}$$

$$\underline{\text{ROLL}} \qquad L = A\dot{P} - E\dot{R} + QR(C - B) - EPQ \tag{e}$$

$$\underline{\text{YAW}} \qquad N = -E\dot{P} + C\dot{R} + PQ(B - A) + EQR \tag{f}$$

EULER ANGLE RATE EQUATIONS

$$\dot{\Theta} = Q\cos\Phi - R\sin\Phi \tag{g}$$

$$\dot{\Phi} = P + Q\sin\Phi\tan\Theta + R\cos\Phi\tan\Theta \tag{h}$$

$$\dot{\Psi} = (Q\sin\Phi + R\cos\Phi)\sec\Theta \tag{i}$$

TRAJECTORY EQUATIONS

$$\dot{y}_A = U\cos\Theta\sin\Psi + V(\sin\Phi\sin\Theta\sin\Psi + \cos\Phi\cos\Psi) + W(\cos\Phi\sin\Theta\sin\Psi - \sin\Phi\cos\Psi) \tag{j}$$

$$\dot{x}_A = U\cos\Theta\cos\Psi + V(\sin\Phi\sin\Theta\cos\Psi - \cos\Phi\sin\Psi) + W(\cos\Phi\sin\Theta\cos\Psi + \sin\Phi\sin\Psi) \tag{k}$$

$$\dot{z}_A = -U\sin\Theta + V\sin\Phi\cos\Theta + W\cos\Phi\cos\Theta \tag{l}$$

(8-3-1)

The aircraft velocity vector, whose components along aircraft axes are U, V, W in the above equations, is with respect to an unaccelerated set of reference axes fixed in an air mass moving with the initial wind velocity components. The trajectory equations are also with respect to this set of axes.

The Euler angle set, defining the orientation of the aircraft, is shown in Fig. 8.3-1. The axes Ox_1, y_1, z_1 are parallel to the above set of reference axes.

Changes in the time-dependent variables from some reference state are now introduced, so that

$$U(t) = U_o + u(t)$$

$$V(t) = V_o + v(t)$$

$$W(t) = W_o + w(t)$$

$$P(t) = p_o + p(t)$$

$$Q(t) = q_o + q(t)$$

$$R(t) = r_o + r(t)$$

and

$$\Theta(t) = \theta_o + \theta(t)$$

$$\Phi(t) = \phi_o + \phi(t)$$

$$\Psi(t) = \psi_o + \psi(t)$$

The aerodynamic forces and moments (including thrust components) are

$$X(t) = X_o + \Delta X$$

$$Y(t) = Y_o + \Delta Y$$

$$Z(t) = Z_o + \Delta Z$$

$$L(t) = L_o + \Delta L$$

$$M(t) = M_o + \Delta M$$

$$N(t) = N_o + \Delta N$$

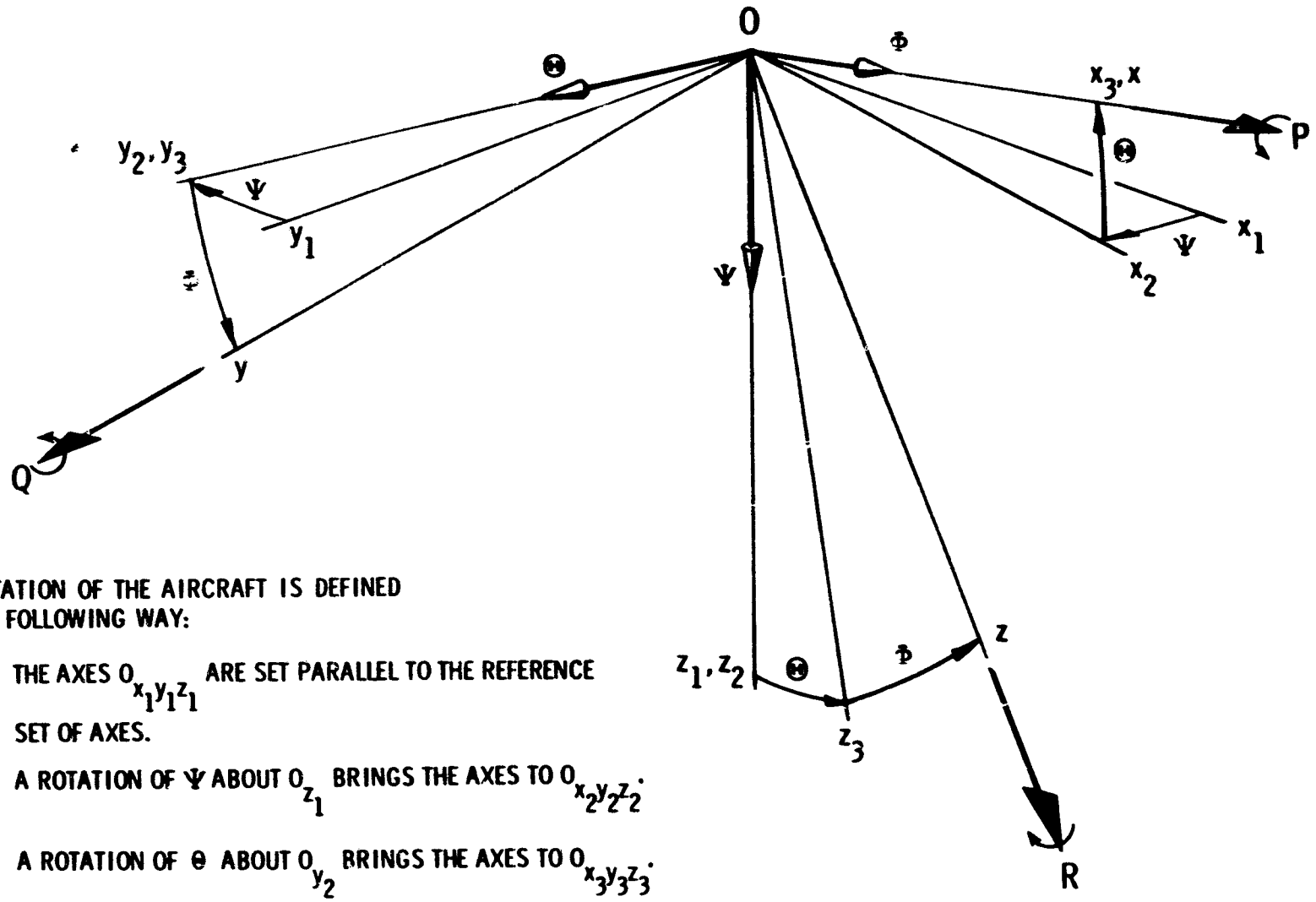

ORIENTATION OF THE AIRCRAFT IS DEFINED IN THE FOLLOWING WAY:

1) THE AXES $O_{x_1y_1z_1}$ ARE SET PARALLEL TO THE REFERENCE SET OF AXES.
2) A ROTATION OF Ψ ABOUT O_{z_1} BRINGS THE AXES TO $O_{x_2y_2z_2}$.
3) A ROTATION OF Θ ABOUT O_{y_2} BRINGS THE AXES TO $O_{x_3y_3z_3}$.
4) A ROTATION OF Φ ABOUT O_{x_3} BRINGS THE AXES TO THE FINAL POSITION, O_{xyz}.

Fig. 3.3-1 Euler angle set.

The effective aerodynamic perturbations should each be considered to be the sum of the component due to the rigid body response of the aircraft and the aerodynamic noise component so that, for example;

$$u(t) = u_i(t) + u_n(t)$$

$$v(t) = v_i(t) + v_n(t) \quad ,\text{etc.}$$

where u_n, v_n, . . . , are either known, assumed or calculated functions of time, and the u_i, v_i components represent the rigid-body responses of the vehicle whose values are determined from the vehicle equations of motion.

The effective aerodynamic perturbation quantities and their derivatives must necessarily be small for valid use of the linear aerodynamic model. This will be so for the major part of the simulation. When an airspeed change rather larger than the usual small perturbation must be considered, then the higher-order aerodynamics must be included. An example of the latter is investigation of longitudinal response to an airspeed change on the glide slope and during the flare.

Initial Reference State

The initial reference state is restricted to an unaccelerated atmosphere, defining $V_o = 0$. The use of a stability axis coincident with the initial aircraft velocity vector defines $W_o = 0$, and U_o is then the initial airspeed, v_p. The initial steady state and disturbed positions of the stability axes are shown in Fig. 3.3-2.

Roll, Pitch and Yaw

The initial values of roll, pitch and yaw rate are assumed zero.

$$p_o,\ q_o,\ r_o = 0$$

Aircraft Initial Attitude

The initial value of roll angle is assumed zero, while initial values of pitch attitude and azimuth may be nonzero.

$$\phi_o = 0; \quad \theta_o,\ \psi_o \text{ nonzero} \quad .$$

There are no further restrictions on the size of Θ, Φ, or Ψ.

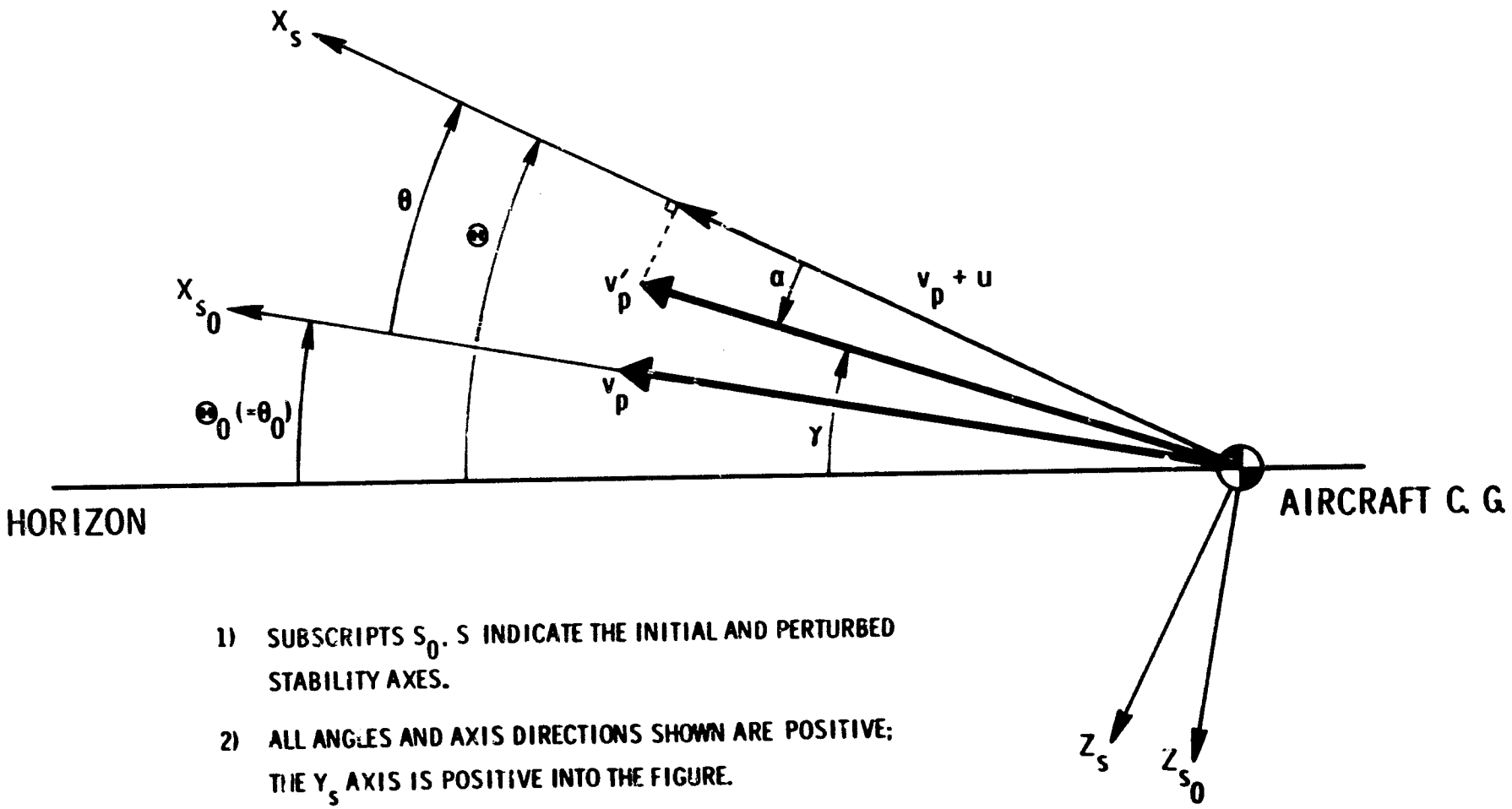

1) SUBSCRIPTS S_0, S INDICATE THE INITIAL AND PERTURBED STABILITY AXES.

2) ALL ANGLES AND AXIS DIRECTIONS SHOWN ARE POSITIVE; THE Y_s AXIS IS POSITIVE INTO THE FIGURE.

3) v_p IS THE INITIAL AIRCRAFT VELOCITY VECTOR DEFINING THE INITIAL POSITION OF THE STABILITY AXES.

Fig. 8.3-2 Initial steady state and disturbed stability axes.

Expansion of the Equations of Motion

The perturbed quantities are substituted into the equations of motion to give:

$$\underline{\text{LIFT}} \qquad Z_o + \Delta Z + mg \cos\theta \cos\phi = m\left[\dot{w}_i + p_i v_i - q_i u_i\right] \tag{a}$$

$$\underline{\text{DRAG}} \qquad X_o + \Delta X - mg \sin\theta = m\left[\dot{u}_i + q_i w_i - r_i v_i\right] \tag{b}$$

$$\underline{\text{SIDE FORCE}} \qquad Y_o + \Delta Y + mg \cos\theta \sin\phi = m\left[\dot{v}_i + r_i U_o + r_i u_i - p_i w_i\right] \tag{c}$$

$$\underline{\text{PITCH}} \qquad M_o + \Delta M = B\dot{q}_i + r_i p_i (A - C) + E(p_i^2 - r_i^2) \tag{d}$$

$$\underline{\text{ROLL}} \qquad L_o + \Delta L = A\dot{p}_i - Er_i + q_i r_i (C - B) - p_i q_i E \tag{e}$$

$$\underline{\text{YAW}} \qquad N_o + \Delta N = -E\dot{p}_i + C\dot{r}_i + p_i q_i (B - A) + q_i r_i E \tag{f}$$

(8.3-2)

The reference flight condition is extracted by setting the perturbation quantities equal to zero:

$$Z_o + mg \cos\theta_o = 0$$

$$X_o - mg \sin\theta_o = 0$$

$$Y_o = 0$$

$$M_o = 0$$

$$L_o = 0$$

$$N_o = 0$$

Substitution for the reference forces and moments in Eq 8.3-2 and neglect of second-order terms gives:

$$\underline{\text{LIFT}} \qquad -mg \cos\theta_o\left[1 - \sec\theta_o \cos\theta \cos\phi\right] + \Delta Z = m\left[\dot{w}_i + p_i v_i - q_i U_o - q_i u_i\right] \tag{a}$$

$$\underline{\text{DRAG}} \qquad -mg \cos\theta_o\left[\sec\theta_o \sin\theta - \tan\theta_o\right] + \Delta X = m\left[\dot{u}_i - r_i v_i\right] \tag{b}$$

$$\underline{\text{SIDE FORCE}} \qquad \Delta Y + mg \cos\theta \sin\phi = m\left[\dot{v}_i + r_i U_o + r_i u_i\right] \tag{c}$$

$$\underline{\text{PITCH}} \qquad \Delta M = B\dot{q}_i \tag{d}$$

$$\underline{\text{ROLL}} \qquad \Delta L = A\dot{p}_i - E\dot{r}_i \tag{e}$$

$$\underline{\text{YAW}} \qquad \Delta N = -E\dot{p}_i + C\dot{r}_i \tag{f}$$

(8.3-3)

8.4 The Aerodynamic Forces and Moments

A general force or moment change about the reference flight condition is represented by a Taylor series expansion:

$$\Delta \text{ Force (or Moment)} = g'x + 1/2\ x' Ax + \text{higher-order terms}$$

where g is the vector of first-order partial derivatives (the stability derivatives) and A is the matrix of second-order derivatives. The vector x represents the perturbation quantities and the aircraft control deflections.

For the major part of the simulation, the second-and higher-order terms may be neglected.

Investigation of aircraft response to a significant airspeed change along the glide slope or during the flare requires inclusion of the second-order term. In this case the only component of the state that exceeds the small perturbation limitation is the airspeed. This means that the matrix A need have finite elements only for those derivatives with respect to the velocity component along the flight path.

All derivatives with respect to acceleration quantities have been omitted except some with respect to $\dot{\alpha}$. The terms omitted are either negligibly small or zero.

The derivatives associated with changes due to ground effect, viz.

$$X_h,\ Z_h,\ M_h,\ \left(M_{l\alpha}\right)_h$$

are discontinuous functions, zero above a specific height, finite and constant below that height.

Force and Moment Changes Due to a Change in Thrust

The aircraft is assumed to have a velocity control system that holds the airspeed essentially constant or drives the airspeed according to some predetermined program as, for example, during the flare maneuver. The controller will generate a delta thrust which will result in force and moment changes. These terms have been included with the aerodynamic force and moment perturbation terms to give a total delta force or moment.

The Linear, Quasi-Steady Aerodynamic Model

The first term of the Taylor series expansion, constituting the linear aerodynamic model, is now further expanded.

For the lift, drag and pitching moment equations, the x vector is given by:

$$x = \left\{u, \alpha, \dot{\alpha}, q, \delta_e, \delta_{ae}, \delta_t, \delta_{sd}, \delta_c, \Delta T, <\Delta h>\right\}$$

and for the yaw moment, rolling moment and side force equations, the x vector is given by:

$$x = \left\{\beta, p, r, \dot{p}, \dot{r}, \delta_a, \delta_s, \delta_r, \delta_t\right\}$$

The g vectors are given by:

LIFT $$g = \left\{Z_u, Z_\alpha, Z_{\dot{\alpha}}, Z_q, Z_{\delta_e}, Z_{\delta_{ae}}, Z_{\delta_t}, Z_{\delta_{sd}}, Z_{\delta_c}, \sin\alpha_\epsilon, Z_h\right\}$$

DRAG $$g = \left\{X_u, X_\alpha, 0, 0, 0, 0, 0, X_{\delta_{sd}}, 0, \cos\alpha_\epsilon, X_h\right\}$$

SIDE FORCE $$g = \left\{Y_\beta, Y_p, Y_r, 0, 0, Y_{\delta_a}, Y_{\delta_s}, Y_{\delta_r}, Y_{\delta_t}\right\}$$

PITCH $$g = \left\{M_u, M_\alpha, M_{\dot{\alpha}}, M_q, M_{\delta_e}, M_{\delta_{ae}}, M_{\delta_t}, M_{\delta_{sd}}, M_{\delta_c}, z_\epsilon, \left(M_h + \left[M_{lc}\right]_h\right)\right\}$$

ROLL $$g = \left\{L_\beta, L_p, L_r, 0, L_{\dot{r}}, L_{\delta_a}, L_{\delta_s}, L_{\delta_r}, L_{\delta_t}\right\}$$

YAW $$g = \left\{N_\beta, N_p, N_r, N_{\dot{p}}, 0, N_{\delta_a}, N_{\delta_s}, N_{\delta_r}, N_{\delta_t}\right\}$$

where $\alpha = w/v_p$, $\beta = v/v_p$ and $\left[M_{lc}\right]_h = M_{lc}\left[K_{ge}/\Delta h\right]$

All the above derivatives are evaluated at the reference flight condition. The nondimensional form of the derivatives in the above expressions are usually referred to as the "stability derivatives" in classical aircraft stability analysis. A listing of the stability derivatives represents the conventional characterization of the aircraft aerodynamics for some particular flight condition.

For the stability derivatives to appear explicitly in the equations of motion, it is necessary to nondimensionalize the derivative terms.

Non-Dimensionalization of the Derivative Terms

Let the following non-dimensional coefficients be defined by:

$$\mu = \frac{m}{\rho S l}$$

$$i_A = \frac{A}{\rho S l^3}$$

$$i_B = \frac{B}{\rho S l^3}$$

$$i_C = \frac{C}{\rho S l^3}$$

$$i_E = \frac{E}{\rho S l^3}$$

$t^* = \frac{l}{v_p}$, the non-dimensional time

where l is the characteristic length;

lift, drag and pitch equations, $l = \frac{c_R}{2}$

yaw, roll and side force equations, $l = \frac{b}{2}$

and let

$$\alpha_i = \frac{w_i}{v_p} \quad , \quad \alpha_n = \frac{w_n}{v_p}$$

$$\beta_i = \frac{v_i}{v_p} \quad , \quad \beta_n = \frac{v_n}{v_p}$$

and recall that

$$mg \cos \theta_o = -Z_o = L_o, \text{ the initial aircraft lift}$$

and

$$mg \sin \theta_o = (mg \cos \theta_o) \tan \theta_o = L_o \tan \theta_o$$

Introducing into Eq 8.3-3 the expressions for the aerodynamic terms, including the above relationships and newly defined variables, and finally dividing the force equations by $1/2\rho v_p^2 S$ and the moment equations by $\rho v_p^2 S l$ results in the following aircraft equations of motion in which the nondimensional stability derivatives now appear explicitly.

EULER ANGLE RATE EQUATIONS

$$\dot{\Theta} = q_i \cos\Phi - r_i \sin\Phi$$

$$\dot{\Phi} = p_i + q_i \sin\Phi \cdot \tan\Theta + r_i \cos\Phi \cdot \tan\Theta$$

$$\dot{\Psi} = (q_i \sin\Phi + r_i \cos\Phi) \sec\Theta$$

TRAJECTORY EQUATIONS

$$\dot{x}_A = (v_p + u_i) \cos\Theta \cos\Psi + v_p\beta_i (\sin\Phi \sin\Theta \cos\Psi - \cos\Phi \sin\Psi)$$
$$+ v_p(\alpha_i) [\cos\Phi \sin\Theta \cos\Psi + \sin\Phi \sin\Psi]$$

$$\dot{y}_A = (v_p + u_i) \cos\Theta \sin\Psi + v_p\beta_i (\sin\Phi \sin\Theta \sin\Psi + \cos\Phi \cos\Psi)$$
$$+ v_p(\alpha_i) [\cos\Phi \sin\Theta \sin\Psi] - [\sin\Phi \cos\Psi]$$

$$\dot{z}_A = -(v_p + u_i) \sin\Theta + v_p\beta_i (\sin\Phi \cos\Theta) + v_p(\alpha_i) [\cos\Phi \cos\Theta]$$

where

$$\Phi(t) = \phi_o + \phi(t)$$

$$\Psi(t) = \psi_o + \psi(t)$$

$$\Theta(t) = \theta_o + \theta(t)$$

8.6 Table of Coefficients

Let

$$a = \left(\frac{c_R}{2v_p}\right)$$

$$e = \left(\frac{b}{2v_p}\right)$$

$$d = \left(\frac{1}{v_p}\right)$$

C	Coefficient	C	Coefficient
1	$-2\mu_{1n}\cdot ad$	20	$\frac{\Delta C_m}{\Delta h}$
2	$[-C_{x_u} - 2C_{L_o} \tan \theta_o]d$	21	$\frac{K_{ge}}{\Delta h}$
3	$-C_{x_\alpha}$	22	C_{22}
5	$2\mu_{1t}\ e$	23	C_{23}
6	C_{y_β}	24	$[C_{z_{\dot\alpha}} - 2\mu_{1n}]a$
7	$[C_{y_r} - 2\mu_{1t}]e$	25	$-C_{z_\alpha}$
8	$C_{y_p}\ e$	26	$[-2\mu_{1n} - C_{z_q}]a$
9	C_{L_o}	27	$[2C_{L_o} - C_{z_u}]d$
10	$C_{y_{\delta_s}}$	29	$[-C_{z_{\delta_e}} - C_{z_{\delta_t}}]$
11	$C_{y_{\delta_r}}$	30	$-C_{z_{\delta_{ae}}}$
12	$C_{y_{\delta_t}}$	31	$-\frac{\Delta C_z}{\Delta h}$
13	$i_B a^2$	32	C_{32}
14	$C_{m_u}\ d$	33	$i_A\cdot b^2$
15	C_{m_α}	34	C_{l_β}
16	$C_{m_{\dot\alpha}}\ a$	35	$C_{l_r}\cdot e$
17	$C_{m_q}\ a$	37	$i_E\cdot e^2$
18	$[C_{m_{\delta_e}} + C_{m_{\delta_t}}]$	38	$C_{l_{\delta_a}}$
19	$C_{m_{\delta_{ae}}}$	39	$C_{l_{\delta_s}}$

C	Coefficient	C	Coefficient
40	$C_{l_{\delta_t}}$	55	$C_{m_{\delta_c}}$
41	$C_{l_{\delta_r}}$	64	$-2\mu_{1t}{}^{e}$
42	$i_C{}^{b^2}$	65	$-2\mu_{1t}{}^{ed}$
43	C_{n_β}	66	$2\mu_{1t}{}^{e}$
44	$C_{n_p}{}^{e}$	67	$-2\mu_{1n}{}^{ad}$
45	$i_E{}^{e^2}$	69	$-\cos\alpha_\epsilon$
46	$C_{n_r}{}^{e}$	70	$\frac{z_e}{c_R}$
47	$C_{n_{\delta_a}}$	71	$\sin\alpha_\epsilon$
48	$C_{n_{\delta_s}}$	72	$C_{y_r}{}^{e}$
49	$C_{n_{\delta_r}}$	73	$\frac{v_p^2}{\mu_{1t}\,b}$
50	$C_{n_{\delta_t}}$		
51	$-C_{x_{\delta_{sd}}}$		
52	$-C_{z_{\delta_{sd}}}$		
53	$-C_{z_{\delta_c}}$		
54	$C_{m_{\delta_{sd}}}$		

K	Coefficient	K	Coefficient
1	$[-C_{x_u} - 2C_{L_o} \tan\theta_o]\, d$	11	$-C_{z_q}\, a$
2	$-C_{x_\alpha}$	12	$[2C_{L_o} - C_{z_u}]d$
3	C_{y_β}	13	$-C_{z_{\dot{\alpha}}}$
4	$C_{y_r}\, e$	14	C_{l_β}
5	$C_{y_p}\, e$	15	$C_{l_p}\, e$
6	$C_{m_u}\, d$	16	$C_{l_r}\, e$
7	C_{m_α}	17	C_{n_β}
8	$C_{m_{\dot{\alpha}}}\, a$	18	$C_{n_p}\, e$
9	$C_{m_q}\, a$	19	$C_{n_r}\, e$
10	$-C_{z_\alpha}$		

Notes on Sections 8.5 and 8.6

1. Auxiliary elevator and tip (elevon) control angles do not appear explicitly in the equations for longitudinal response because they have the same magnitude as the primary elevator angle, and all three work in unison for longitudinal control. The associated stability derivatives are consequently combined, except for that of the auxiliary elevator which must be handled independently to account for its restriction to negative (up) angles.
2. The F*, F**, X* are discontinuous functions operating on the ground effect terms.
3. Direct lift spoiler and canard terms are included, although they are not functional controls of the Phase II SST primarily studied in this report. They are included so that the characteristics of later aircraft configurations may be directly incorporated without simulation modification.

4. The second-order aerodynamic and noise terms are written separately, as they are in the actual simulation. They may then be ignored if not required without unnecessarily complicating the computations.

5. Note that some coefficients, originally numbered, have been subsequently dropped and do not appear in the table of coefficients.

8.7 Atmospheric Noise

Atmospheric turbulence can be characterized by an exponential auto-correlation function $\phi(\tau)$ with a characteristic constant, a, chosen to fit the actual turbulence data. The associated spectral density is then given by:

$$\Phi(\omega) = \frac{2}{\pi} \int_0^\infty \phi(\tau) \cos \omega\tau \, d\tau$$

let $$\phi(\tau) = \sigma^2 e^{-|\tau|a}$$

then $$\Phi(\omega) = \frac{2}{\pi} \sigma^2 \int_0^\infty e^{-|\tau|a} \cos \omega\tau \, d\tau$$

$$= \frac{2\sigma^2 a}{\pi} \quad \frac{1}{\omega^2 + a^2} \qquad (8.7\text{-}1)$$

Now it is known that by "shaping" continuous white noise with filters it is possible to obtain a continuous output with certain desired properties. In this case it is desired to reproduce the above spectral density of atmospheric turbulence.

Let white noise be applied to a low-pass filter having the transfer function

$$F(p) = \frac{1}{p + a}$$

let the input autocorrelation function be

$$\phi_i(\tau) = Q^2 \delta(\tau)$$

then the power spectral density is

$$\Phi_i(\omega) = \frac{Q^2}{2\pi}$$

the output power spectral density is

$$\Phi_o(\omega) = |F|^2_{p = i\omega} \Phi_i(\omega)$$

$$= \frac{Q^2}{2\pi} \frac{1}{\omega^2 + a^2} \qquad (3.7\text{-}2)$$

In comparing the above result with that obtained before for the power spectral density of atmospheric turbulence, it is seen that

1. the filter time constant is related to the characteristic constant, a, governing the exponential autocorrelation function of the turbulence and that
2. the magnitude of input white noise is related to both the intensity σ and characteristic constant of the turbulence.

So

$$\sigma^2 = \frac{Q^2}{4a}$$

Let the white noise be replaced by a time series N having a flat spectrum over the bandwidth of the filter. Let the time series have

1. uniform time intervals Δt.
2. a constant value over each time interval.
3. uncorrelated random values in each time interval.
4. mean-square value v^2.

It can be shown that

$$\Phi_N(\omega) \approx \frac{v^2 \Delta t}{2\pi} \; ; \; \omega << \frac{1}{\Delta t}$$

then

$$\frac{v^2 \Delta t}{2\pi} = \frac{Q^2}{2\pi}$$

$$v^2 = \frac{Q^2}{\Delta t} = \frac{4a\sigma^2}{\Delta t}$$

the time series has

$$m\,(N) = 0$$

$$\text{sigma}\,(N) = \sqrt{\frac{4a\sigma^2}{\Delta t}}$$

A new random number ψ is chosen every Δt seconds with

$$m\,(\psi) = 0$$

$$\text{sigma}\,(\psi) = 1$$

then

$$N = \text{sigma}\,(N)\,\psi$$

Taking N through the filter,

$$\dot{n} = -na + N \qquad (8.7\text{-}3)$$

where $\frac{1}{a}$ is the filter time constant.

Atmospheric Turbulence Model

It was assumed that the atmospheric velocity field could be approximated as homogeneous, isotropic turbulence and that the turbulent field was "frozen", that is, the velocity varied from point to point in space but was constant in time.

The one-dimensional spectrum function for atmospheric turbulence, widely accepted (see refs (6) and (21)), is given by

$$\Phi(\Omega) = \frac{2\sigma^2 L}{\pi} \cdot \frac{1}{1 + (L\Omega)^2} \qquad (8.7\text{-}4)$$

where

Ω = component wave number, $\frac{2\pi}{\lambda}$, rad ft^{-1}

λ = component wave length, ft

L = integral scale of the turbulence, ft

σ = root mean square gust velocity, ft sec^{-1}

The characteristic constant associated with the turbulence is given by

$$a = \frac{v_p}{L} \quad \text{sec}^{-1}$$

and

$$\omega = v_p \Omega \quad \text{rad sec}^{-1}$$

where v_p is the aircraft airspeed.

Substituting for the various quantities in Eq 8.7-4 returns

$$\Phi(\omega) = \frac{2\sigma^2 a}{\pi} \cdot \frac{1}{\omega^2 + a^2} \qquad (8.7\text{-}1)$$

Estimation of Turbulence Integral Scale Length and Intensity

At low levels, the turbulence resembles that in boundary layers adjacent to rough surfaces and is strongly affected by the terrain. The scale and intensity are a function of height above the ground and in general the field is neither homogeneous nor isotropic. Etkin, in ref (21) reported on a number of measurements indicating that the scale factor may be approximated by

$$L = 0.9\, h$$

up to 1000 ft altitude. Etkin, also in ref (21), gave a semi-empirical formula for the variation of intensity with height and ground roughness under unstable meteorological conditions;

$$\sigma = 0.226 \frac{\bar{v}}{\log \frac{h}{h_o}}$$

where

$\bar{v}$ = mean wind at height h

h_o = characteristic roughness length

Typical values for h_o are

low trees, h_o = 10 ft

crops, h_o = 1 ft

water, snow field, h_o = 0.1 ft

Despite the fact that at low levels the turbulence is neither truly isotropic nor homogeneous, such a model is probably the only acceptable one to use at the moment. It will, in any case, be more realistic than a discrete gust model.

Generation of the Aerodynamic Noise

The three gust velocity components are uncorrelated inputs but each assumed to have the same power spectrum given by Eq 8.7-4 . They are concurrently generated by entering the random number series ψ at different starting points.

Both the turbulence intensity and its characteristic constant are functions of altitude and so continually change as the aircraft descends down the glide slope.

Let the uncorrelated velocity component noise outputs of the shaping filters be given by

$$n_1,\ n_2,\ n_3$$

and let there be one additional function, n_4.

Then the aerodynamic noise is given by

$$u_n = n_1$$

$$\alpha_n = n_2/v_p$$

$$\beta_n = \dot{n}_3/v_p$$

$$\dot{\alpha}_n = \dot{n}_2/v_p$$

$$q_n = -\dot{n}_2/v_p$$

$$r_n = \dot{n}_3/v_p$$

$$p_n = \dot{n}_4/v_p$$

and there is correlation between

α_n and q_n

β_n and r_n

α_n and $\dot{\alpha}_n$

The treatment is restricted to the range of gust wavelengths for which the influence of the gust gradients is adequately accounted for by the use of equivalent rates of pitch, roll and yaw. That is, the wavelength is such that the gust gradient is essentially constant over a characteristic length of the aircraft. So the response to only part of the spectrum of atmospheric turbulence can be calculated by this method. In Fig. 8.7-1 the assumed turbulence spectrum has been plotted; then the portion of the spectrum omitted is to the right of the dotted line. This can be seen by admitting the smallest wavelength to be

$$\lambda = 8l$$

where l is a characteristic length of the aircraft.

Let $l \approx 120$ ft.

$\lambda = 960$ ft.

$$\Omega = \frac{2\pi}{\lambda} = .0066$$

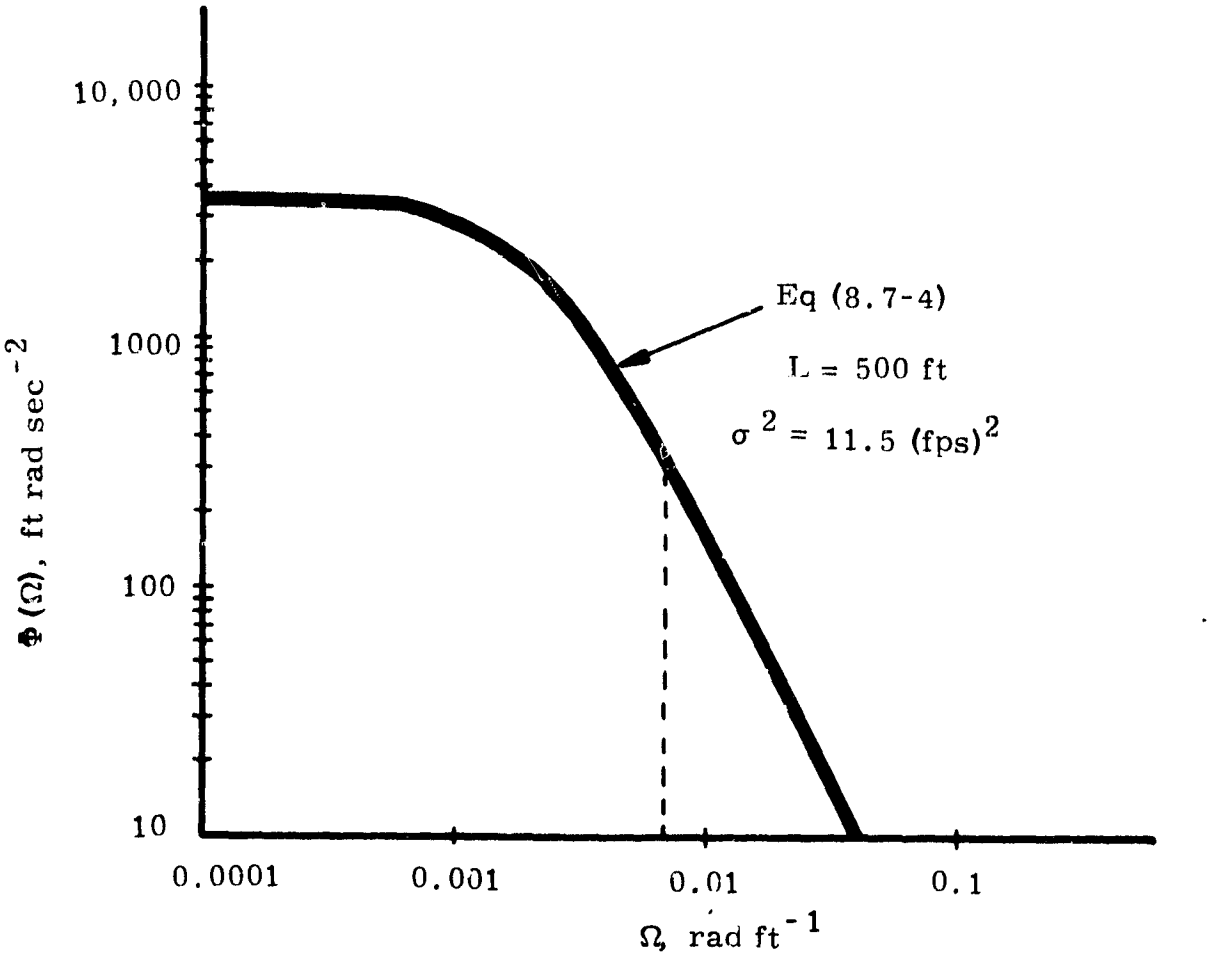

Fig. 8.7-1 Power spectral density for atmospheric turbulence.

The time constant of a linear filter designed to attenuate the smaller wavelengths is then given approximately by

$$\tau = \frac{1}{\omega} = \frac{1}{V_p \Omega}$$

$$= 0.63 \text{ sec.}$$

The portion of the spectrum omitted is small and Etkin in refs (6) and (21) indicates that its influence on the rigid aircraft response is negligible. He shows that most of the effects of interest in the response of a rigid aircraft will be predicted with sufficient accuracy with the above approximation. The neglected portion of the spectrum excites primarily the aircraft flexible modes.

To generate the rolling moment noise it was assumed that there were no contributions from u_n and β_n (although in reality, there are) so that the total contribution was given by the spanwise variation of w_n, that is, by $\frac{\partial w_n}{\partial y}$. The additional uncorrelated noise n_4 was used to generate p_n.

Wind Gradient

The wind gradient contribution to the aerodynamic noise is superimposed on the turbulence contributions generated above. Only u_n and β_n are involved.

The wind gradient model presently assumed is a simple linear reduction from the mean wind speed at 1000 feet to half that value at ground level. A more realistic parabolic reduction could easily be incorporated so as to better simulate the stronger gradients close to the ground.

8.8 Notation

X, Y, Z	components of the external aerodynamic force on the aircraft, resolved along stability axes
M, L, N	components of the external aerodynamic moment on the aircraft, resolved along stability axes
X_o, Y_o, Z_o	initial steady-state values of X, Y, Z
M_o, L_o, N_o	initial steady-state values of M, L, N
$\Delta X, \Delta Y, \Delta Z$	changes in X, Y, Z from the initial steady state
$\Delta M, \Delta L, \Delta N$	changes in M, L, N from the initial steady state
P, Q, R	components of the aircraft angular velocity about the stability axes.
p_o, q_o, r_o	initial steady-state values of P, Q, R
p, q, r	perturbations in P, Q, R

8.8 Notation (Cont)

p_i, q_i, r_i	components of effective aerodynamic perturbations in p, q, r due to aircraft inertial response.
p_n, q_n, r_n	components of effective aerodynamic perturbations in p, q, r due to aerodynamic noise.
V_s	aircraft stalling speed, ft/sec
U, V, W	components of the aircraft velocity vector, with respect to the unaccelerated reference frame, resolved along fixed aircraft stability axes.
u_o, v_o, w_o	initial steady-state values of U, V, W
u, v, w	perturbations in U, V, W
u_i, v_i, w_i	components of effective aerodynamic perturbations in u, v, w due to aircraft inertial response.
u_n, v_n, w_n	components of effective aerodynamic perturbations in u, v, w due to aerodynamic noise.
Θ, Φ, Ψ	Euler angle set
θ_o, ϕ_o, ψ_o	initial steady-state values of Θ, Φ, Ψ
θ, ϕ, ψ	perturbations in Θ, Φ, Ψ
A, B, C	moments of inertia about the x, y, z stability axes, slug-ft^2
D	product of inertia $\int$ yz dm, stability axes, slug ft^2
E	product of inertia $\int$ xz dm, stability axes, slug ft^2
F	product of inertia $\int$ xy dm, stability axes, slug ft^2
I_{xx}, I_{yy}, I_{zz}	moments of inertia about the x, y, z aircraft body axes, slug-ft^2
I_{xz}	product of inertia $\int$ xz dm, aircraft body axes, slug-ft^2
x_A, y_A, z_A	aircraft displacement with respect to the unaccelerated frame of reference
m	mass of the aircraft, slugs
g	acceleration due to gravity

8.8 Notation (Cont)

M_{lc}	pitching moment due to longitudinal control
K_{ge}	factor, multiplying the pitching moment due to longitudinal control in ground effect
h	height of the aircraft c.g. above the ground
δ_e	primary elevator control deflection angle, rad
δ_{ae}	auxiliary elevator control deflection angle, rad
δ_t	tip (elevon) control deflection angle, rad
δ_s	spoiler control deflection angle, rad
δ_{sd}	direct lift spoiler control deflection angle, rad
δ_c	canard control deflection angle, rad
δ_a	aileron control deflection angle, rad
δ_w	pilot's wheel control deflection angle, rad
δ_r	rudder control deflection angle, rad
ΔT	change in thrust from the initial steady state
α_ϵ	angle between the thrust line and aircraft longitudinal body axis
z_ϵ	vertical displacement of thrust line from the aircraft c.g.
c_R	reference root chord, ft
b	reference wing span, ft
S	reference wing area, ft^2
ρ	air density, slugs ft^{-3}

CHAPTER 9

SUMMARY AND CONCLUSIONS

9.1 Design Concepts and Performance Criteria

The preceding chapters have introduced and developed a comprehensive approach to the design of an improved automatic landing system. The approach has been based on the application of five new design concepts as follows:

1. Inertial stabilization of the aircraft control system.
2. Inertial filtering of the ILS reference beams.
3. Nonlinear trajectory generation.
4. Command signal processing.
5. Generalized trajectory control.

and on the interaction of these concepts with

6. Open-loop gain maximization.

Items 1 and 2 are concerned with the introduction of new (inertially-measured) information into the control system. Items 3, 4 and 5 are nonlinear control concepts designed to produce improved performance in the sense of the criteria given below. Item 6 is a design parameter having a critical effect upon performance.

The general criteria of performance that have been adopted are the following:

1. Sensitivity to environmental disturbances.
2. Accuracy of flight relative to a desired reference trajectory.
3. Control effector activity caused by noise.
4. Physical limitations imposed by the aircraft structure.
5. Human factors.

In this chapter some of the quantitative results of the design approach are summarized.

9.2 Comparisions

To evaluate the quality of the new control systems that have been designed,

a comprehensive set of digital simulations of the vehicle and control systems has been undertaken. The simulations encompassed:

1. A simplified aircraft as described in Chapter 2.
2. A detailed model of the SST using information provided by the FAA and the Boeing Company.

Comparisions of systems involving the introduction of inertial information utilized the simplified model. Other comparisions utilized the SST model.

To provide an adequate basis for evaluation of the new control system designs, a parallel study was made to design control system configurations of conventional type. An effort was made to optimize the conventional designs to provide a fair comparison. A detailed description of the conventional system designs appears in Appendix A.

9.3 Reduction of ILS Beam Noise

The most serious source of noise in the automatic landing systems considered in this study is ILS beam noise. Fluctuations of the localizer and glide-slope center planes from their desired locations are the result of reflections from uneven features on the ground illuminated by the glide slope and localizer antennas. This problem is handled in conventional systems by introducing simple lags into the signal path as discussed in Appendix A. While the noise level is satisfactorily reduced by the introduction of lags, undesirable effects on the dynamic response characteristics of the vehicle are generated as well. Inertially-measured position and velocity are essentially free of high-frequency noise; however, the accumulation of errors, especially in position, due to gyro drift precludes the direct application of inertially-measured variables after a flight of several hours. The inertially-stabilized system employs estimation procedures which utilize ILS data to correct errors in the position and velocity provided by the inertial system. The corrected inertial data is applied to the control system as reference information. Lagged acceleration is obtained by applying a suitable operator to the accelerometer outputs.

A comparison illustrating the effect of using corrected inertial data was obtained for the lateral position control system. The vehicle response was subject to an initial 400 ft lateral position error, ILS beam noise and initial errors of the inertial system. The top curve in Fig. 9.3-1 shows the roll control variable for the simplified conventional system described in Chapter 2. The lower curve illustrates roll for an inertially-stabilized system. A three-fold reduction in peak roll is achieved using the improved information in spite of the fact that the gains of the inertially-stabilized system are considerably higher than

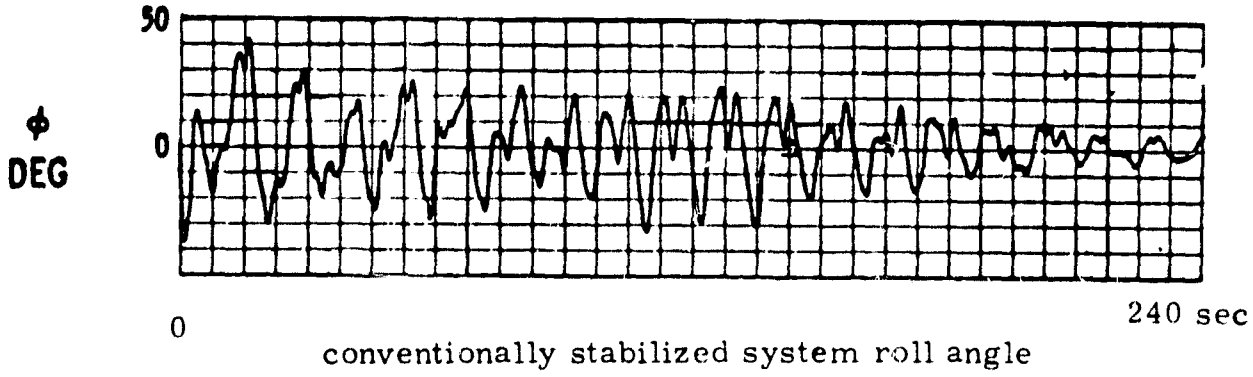

conventionally stabilized system roll angle

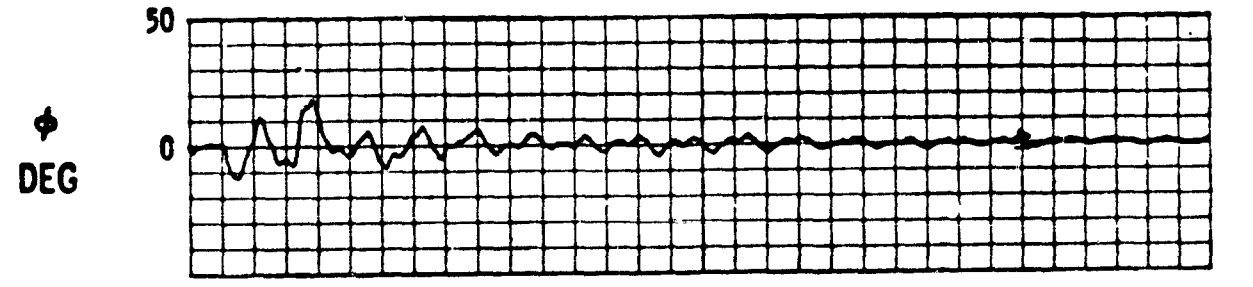

inertially-stabilized system roll angle

Fig. 9.3-1 The application of corrected inertial information reduces the effect of ILS localizer beam bending noise on the lateral control variable ϕ .

the conventional system gains. The lateral position trajectories corresponding to the roll inputs shown in Fig. 9.3-1 are illustrated in Fig. 9.3-2 . Corrected inertial stabilization leads to a smoother trajectory which improves passenger comfort and pilot confidence.

9.4 Increasing Open-Loop Gain

The application of inertial reference information allows the position and velocity feedback gains to be increased. In addition, it is possible to close control loops on lateral and vertical acceleration which provide superior cancellation of external disturbances. The gains for the conventional and inertially-stabilized lateral and vertical position control systems are shown in Table 9.4-1. As a result of the increase in gain and the closure of the acceleration loops, an improvement in sensitivity to disturbances was obtained.

The primary disturbance input to the vehicle equations describing lateral motion is the noise component of sideslip angle β_n. This variable is shown in Fig. 9.4-1. Application of this signal, and the less important components of noise, to the stabilized vehicle results in the velocity responses shown in Fig. 9.4-2 and the position responses shown in Fig. 9.4-3. The new design reduces the velocity excursions by a factor of approximately 2. The lateral position error, which is caused by wind shear, is reduced by a factor of 4 at 200 ft altitude. One remarkable characteristic of the inertially-stabilized system is a reduction in control variable amplitude. Roll-angle amplitude is reduced by a factor of approximately 3. This is surprising, as the reduction is coupled with an improvement in control quality.

The most important disturbance input in the vertical plane is the noise component in angle of attack, α_n. Application of this signal, the slideslip angle β_n in Fig. 9.4-1 and the other components of noise result in the velocity responses shown in Fig. 9.4-5 and the vertical trajectories shown in Fig. 9.4-6. Inertial stabilization reduces the vertical velocity range by approximately 0.6. A corresponding improvement is noted in vertical position error. Some improvement is also apparent in the amplitude of the control variable in Fig. 9.4-7.

9.5 Flight Trajectory Synthesis

The shape of the flight path in response to a desired alteration is an important consideration when a controlled system is subject to saturation constraints imposed by effector limits, and/or human factors. Effector saturation should be avoided to minimize control sensitivity to disturbances as discussed in Section 4.3. Operation within the constraints dictated by human factors is obviously an essential design goal.

The trajectory followed by the conventional systems described in Appendix A is determined by the values of the adjustable velocity and position gains. A worst-case approach was used to determine the set of gains which yield satisfactory response throughout the normal operating range. The path followed by the vehicle with the improved control system is relatively independent of the choice of position, velocity and acceleration gains. The vehicle closely follows a trajectory generated by the nonlinear trajectory generators (NTG_y and NTG_z), thus permitting independent selection of gains and trajectory characteristics. The trajectory design reflects the dynamic properties of the control system and the limits imposed by the effector characteristics and human factors.

A comparison between the linear response characteristics of the conventional lateral position control system and the nonlinear responses of the improved system is shown in Fig. 9.5-1. The maximum value of roll angle during these responses is shown in Fig. 9.5-2. The limit imposed by passenger comfort is exceeded when the conventional system responds to position errors larger than 1000 ft. This problem is usually treated by limiting the roll-angle command directly. This results in open-loop behavior whenever ϕ_c saturates.

The ability of the improved system to follow a desired trajectory is utilized to improve the performance during the localizer acquisition phase of the landing. During acquisition the aircraft must transfer from a linear path inclined relative to the localizer reference plane to a trajectory in the plane. The conventional system achieves this result by controlling the vehicle position relative to the plane in a linear fashion. While beam acquisition is achieved, the values of roll angle are quite large (up to 50^o). The new acquisition control system based on the theory of time-optimal control improves response characteristics, while imposing the restriction ($|\phi| < 30^o$), as shown in Fig. 9.5-3. The quasi-time-optimal paths terminate on trajectories parallel to the localizer reference plane. Coincidence is achieved by transferring to the normal lateral position control mode discussed in Chapter 5.

9.6 Areas for Further Investigation

The preceding sections in Chapter 9 have presented some of the major contributions embodied in the work completed to date. These results are still of a preliminary nature and will undoubtedly be further refined before publication of the final report. Further work is required in the following areas:

1. Integration of the inertial system errors and the estimation process with the complete SST model.
2. Vertical control system design improvement to achieve more precise vertical trajectory control.

Table 9.4-1 Lateral and Vertical Position Control System Gains for the Comprehensive SST Simulation

SYSTEM	POSITION GAIN deg/ft	VELOCITY GAIN deg/ft/sec	ACCELERATION GAIN deg/ft/ sec^2	INTEGRAL COMPENSATOR GAIN sec
LATERAL POSITION CONTROL SYSTEMS				
CONVENTIONAL SYSTEM	0.0205	0.410		0.005
INERTIALLY STABILIZED SYSTEM	0.051	0.510	1.02	0.020
VERTICAL POSITION CONTROL SYSTEMS				
CONVENTIONAL SYSTEM	0.041	0.205		0.005
INERTIALLY STABILIZED SYSTEM	0.063	0.246	0.157	0.010

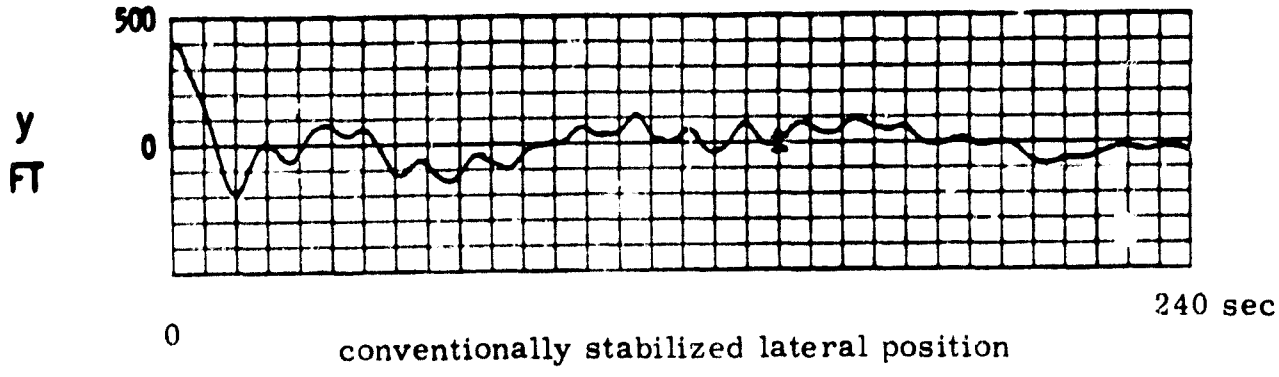

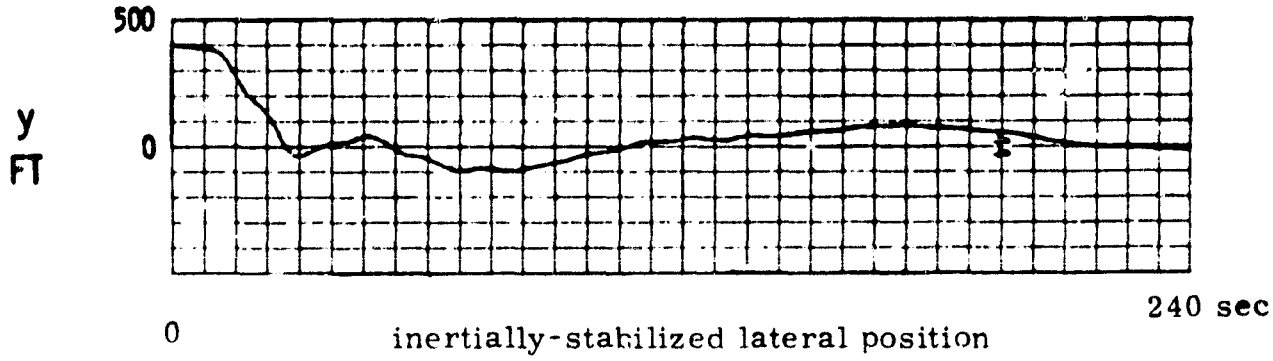

Fig. 9.3-2 The reduction of angular noise in roll using updated inertial data results in a smoother, more accurate lateral trajectory.

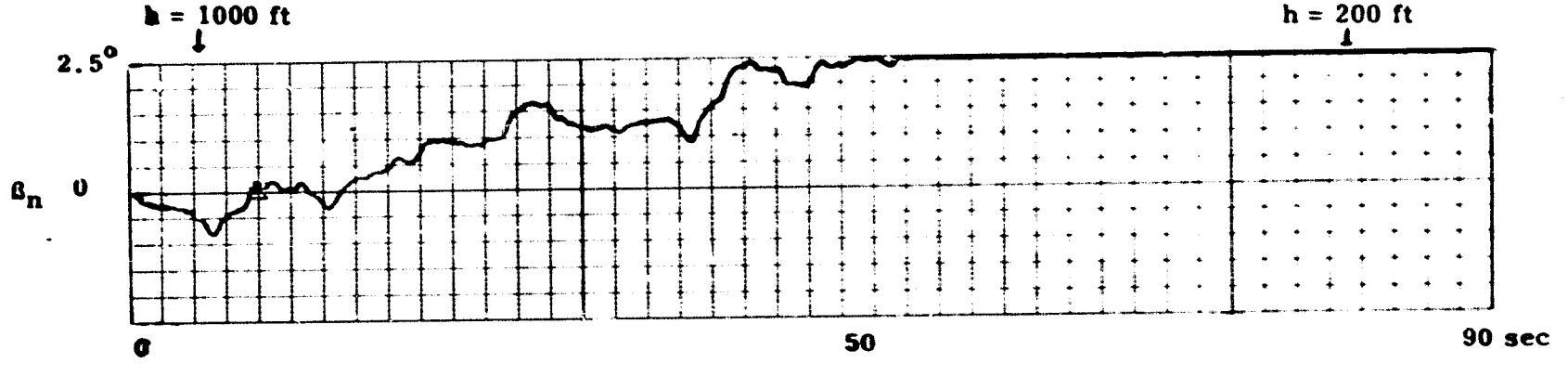

slideslip angle noise component

Fig 9.4-1 Lateral gusts of a random nature and wind gradients (2.5 ft/sec/100 ft starting at 1000 ft) produce a noise component in the sideslip angle and resulting aerodynamic disturbances on the vehicle. The wind gradient is an altitude-sensitive component which increases as altitude decreases eventually driving β_n off scale.

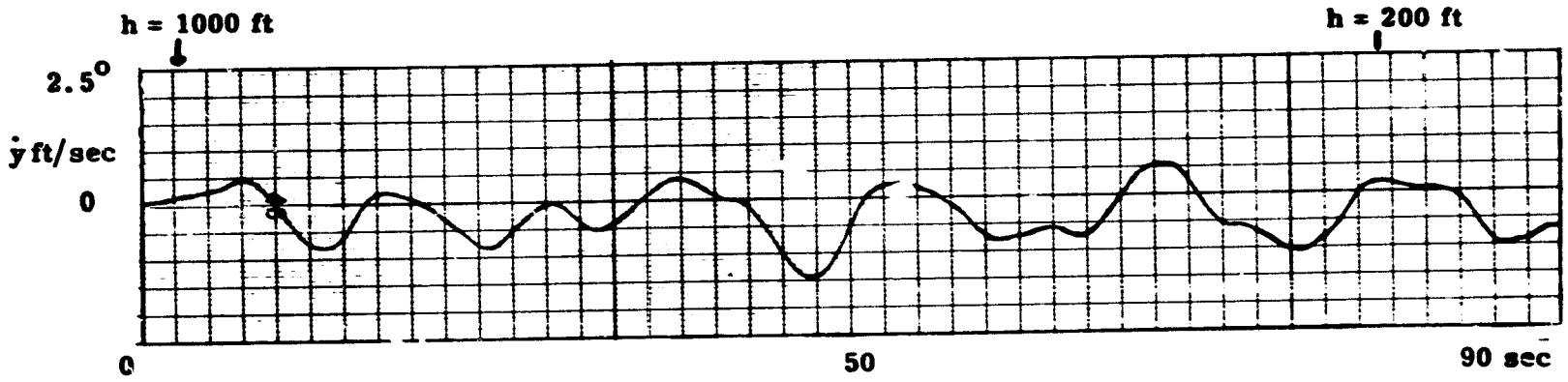

conventionally stabilized lateral velocity

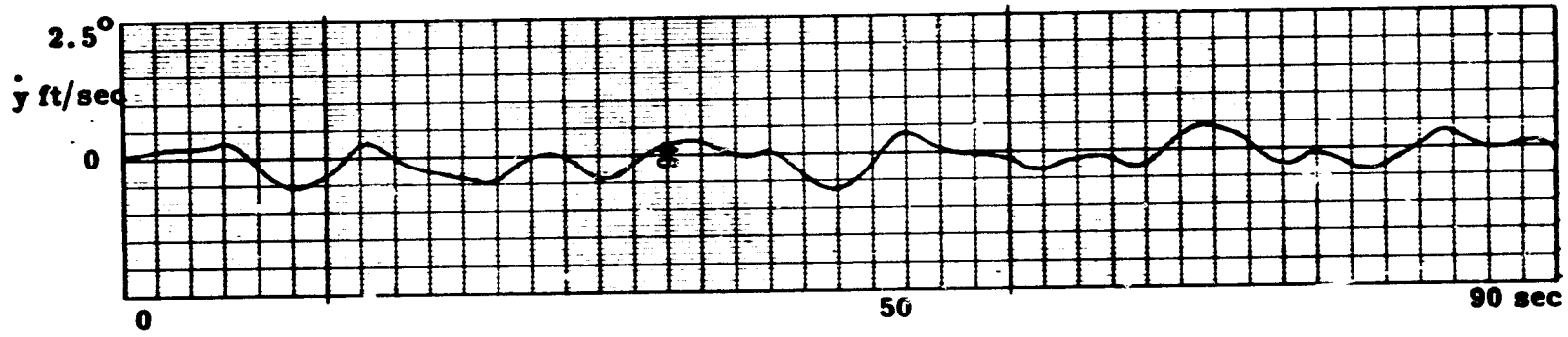

inertially-stabilized lateral velocity

Fig. 9.4-2 Inertial stabilization results in a reduction in the maximum deviation in lateral velocity from gusts and wind shear.

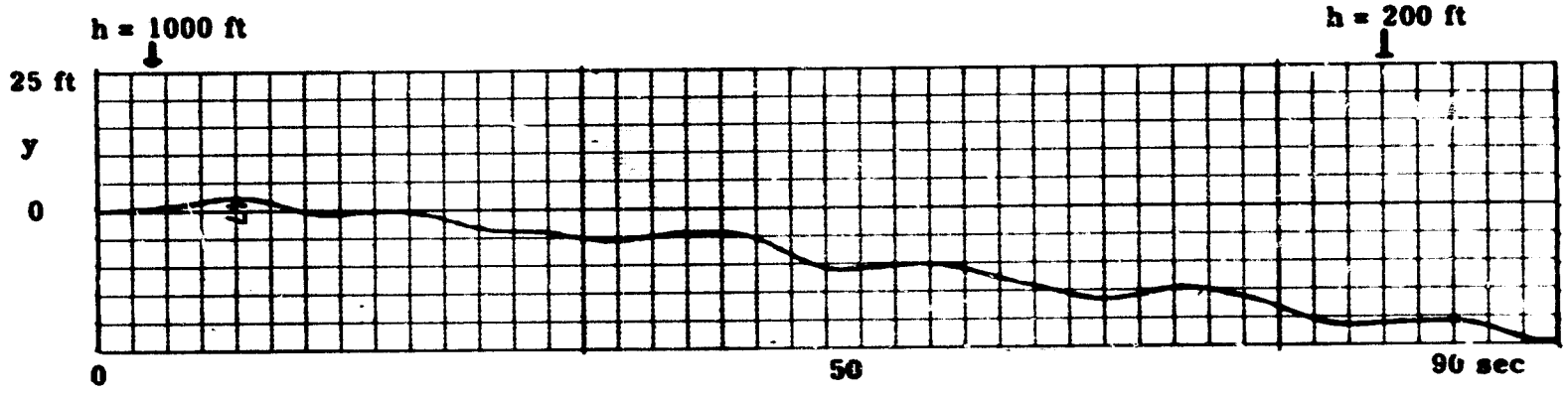

conventionally stabilized lateral position

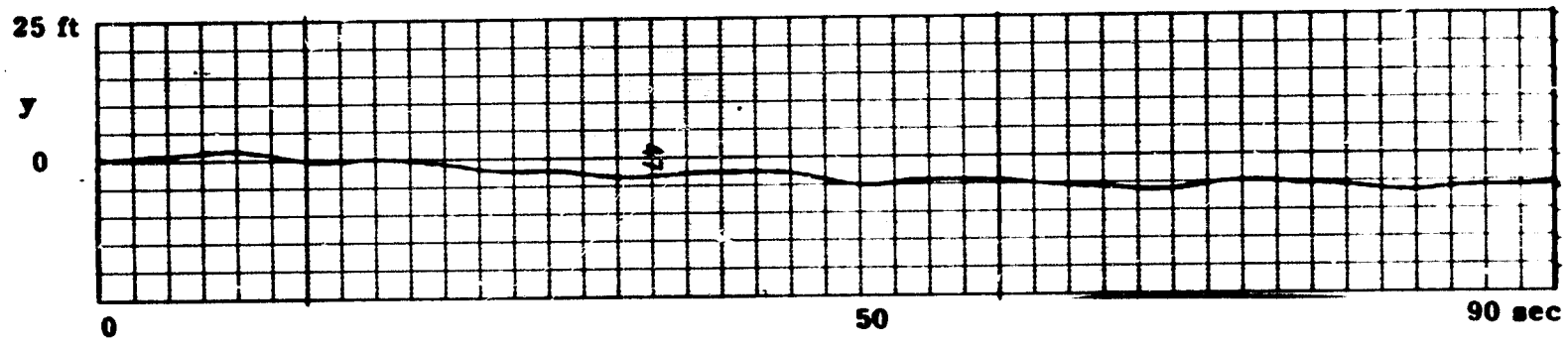

inertially-stabilized lateral position

Fig. 9.4-3 The linear wind gradient results in an error in lateral position which is eventually driven to zero by the proportional plus integral compensator. Error diminishment is not apparent in the case of the conventional system because of the low gain associated with the integrator.

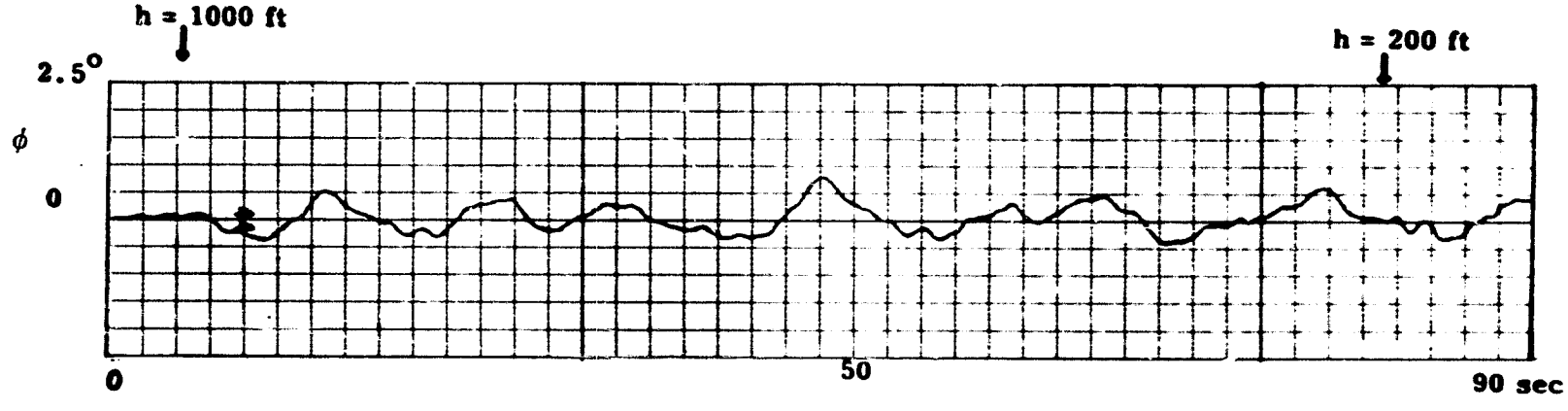

conventionally stabilized system roll angle

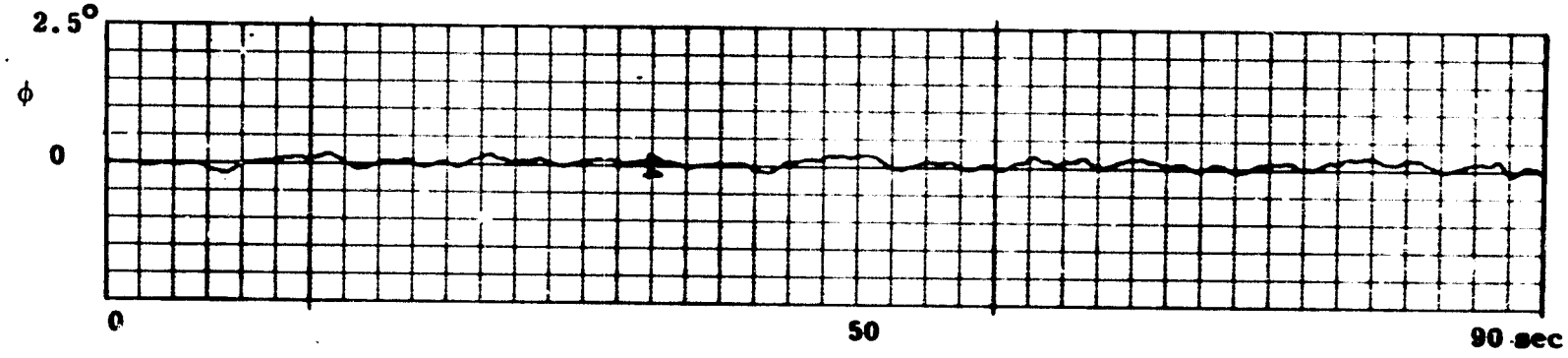

inertially-stabilized system roll angle

Fig. 9.4-4 Aircraft roll angle versus time. The inertially-stabilized control system results in a marked reduction in roll amplitude.

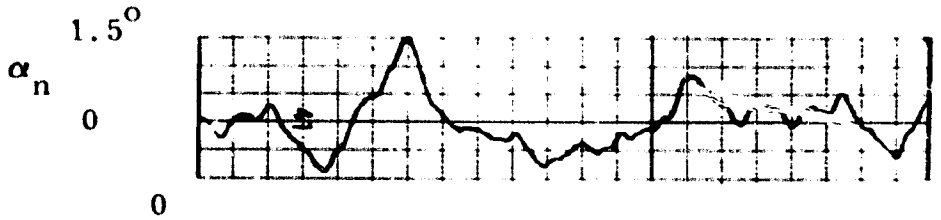

angle of attack noise component

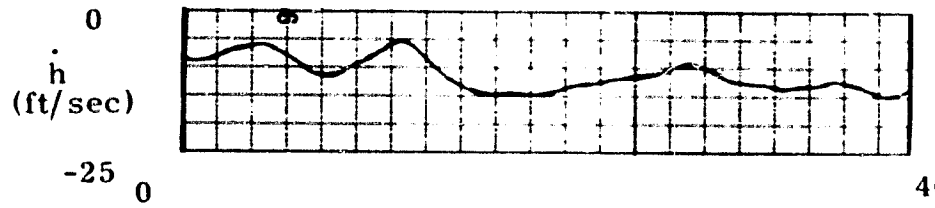

conventionally stabilized vertical velocity

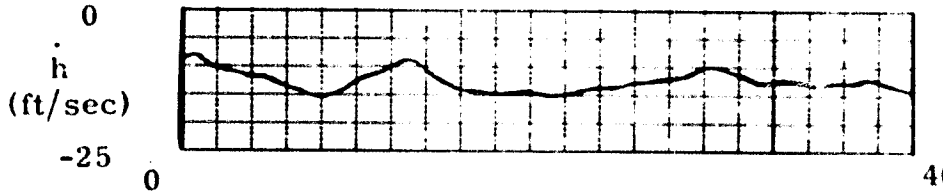

inertially-stabilized vertical velocity

Fig. 9.4-5 Inertial stabilization results in a reduction in the vertical velocity variation due to disturbances acting on the vehicle.

angle of attack noise component

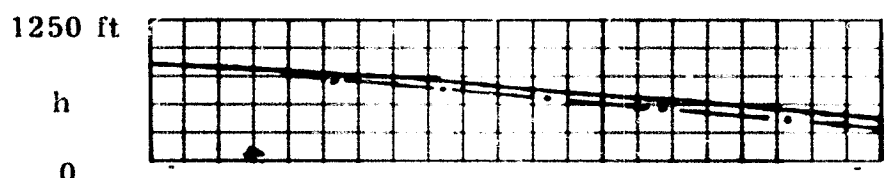

conventionally stabilized vertical position

—— · —— desired; ——— actual

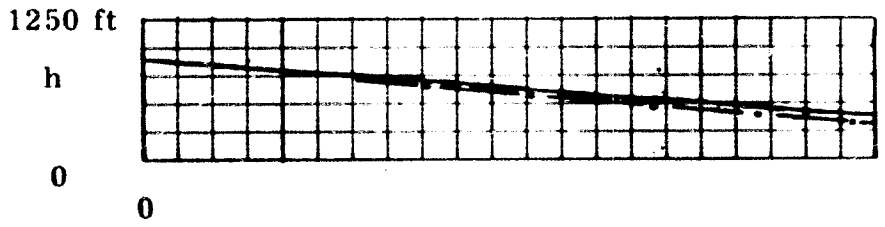

inertially-stabilized vertical position

—— · —— desired; ——— actual

Fig. 9.4-6 The inertially-stabilized vertical control system reduces the error between the desired and actual vertical paths.

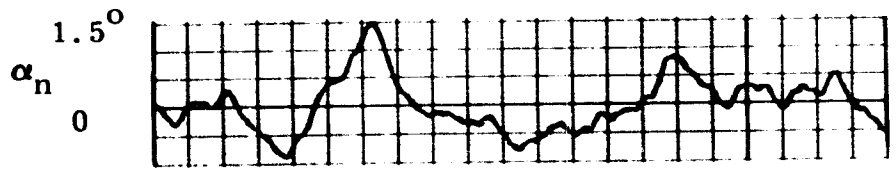

angle of attack noise component

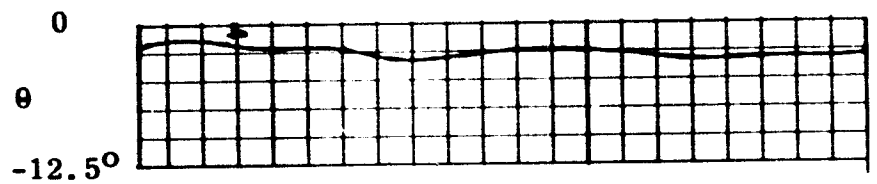

conventionally stabilized pitch angle

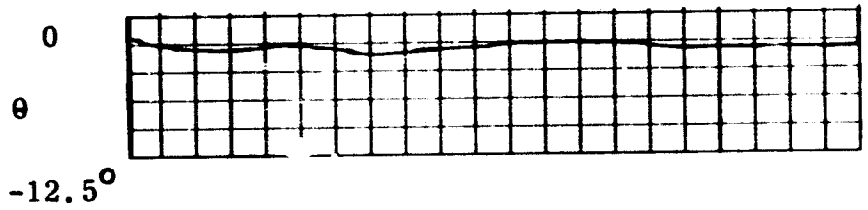

inertially-stabilized pitch angle

Fig. 9.4-7 The inertially stabilized system utilizes a smaller control variable range to achieve superior control.

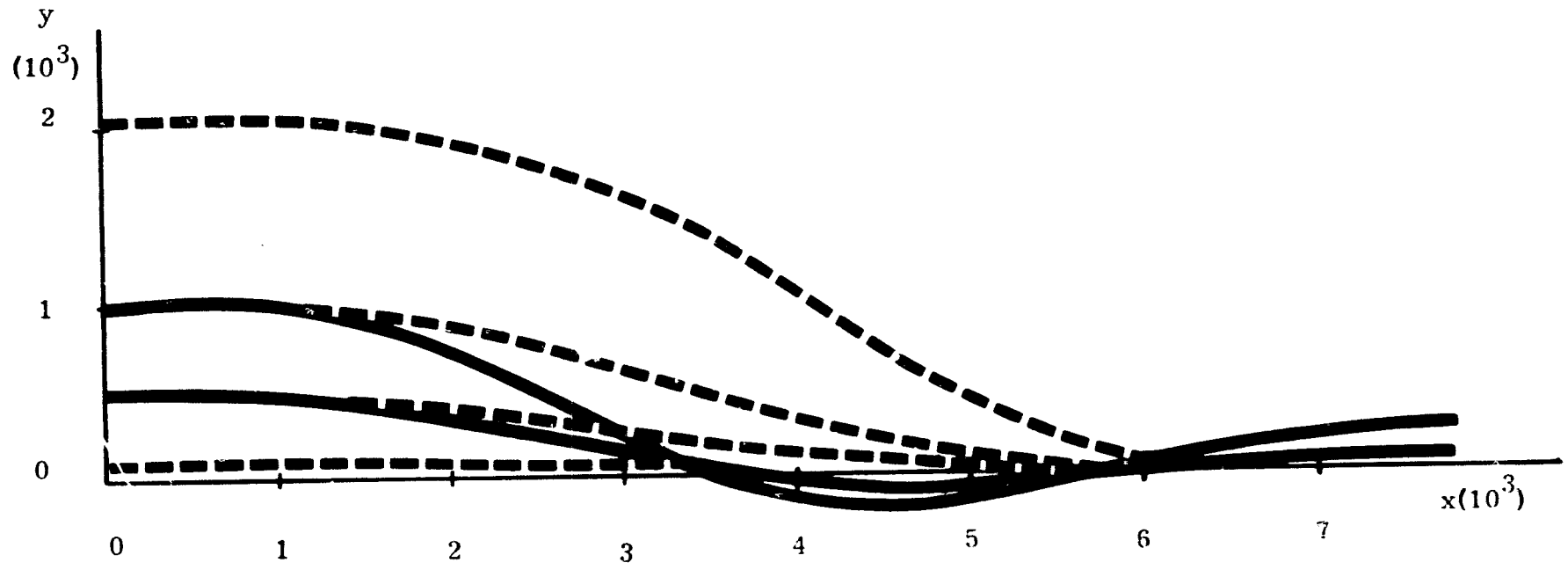

Fig. 9.5-1 Typical conventional and new (dotted lines) lateral control system responses to an initial y displacement ($\dot{y} = 0$). The conventional system response to a 2000 ft error is not shown because the maximum permissible roll angle (30^{o}) was exceeded.

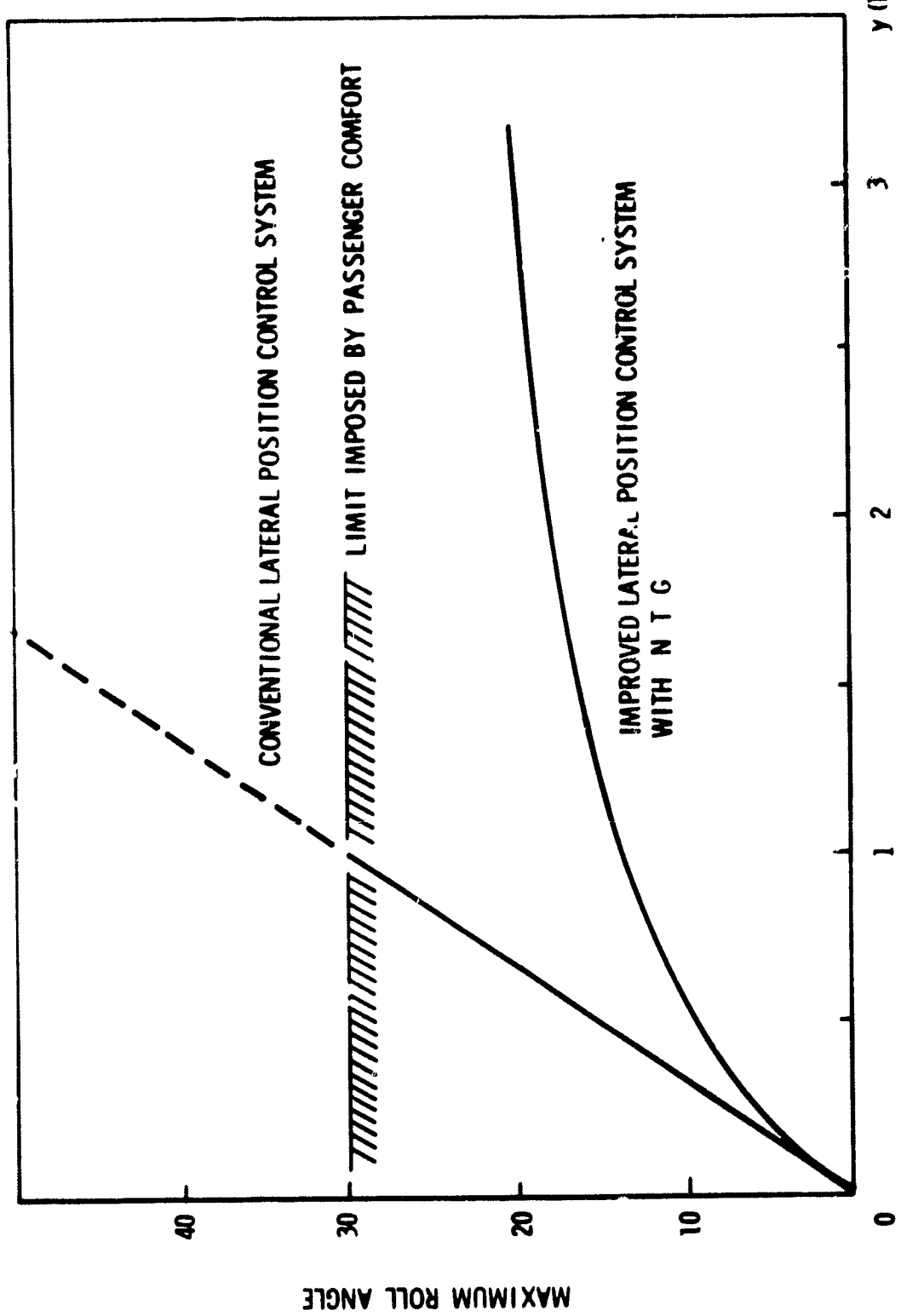

Fig. 9.5-2 Maximum roll angle experienced during ing response to an initial lateral position error.

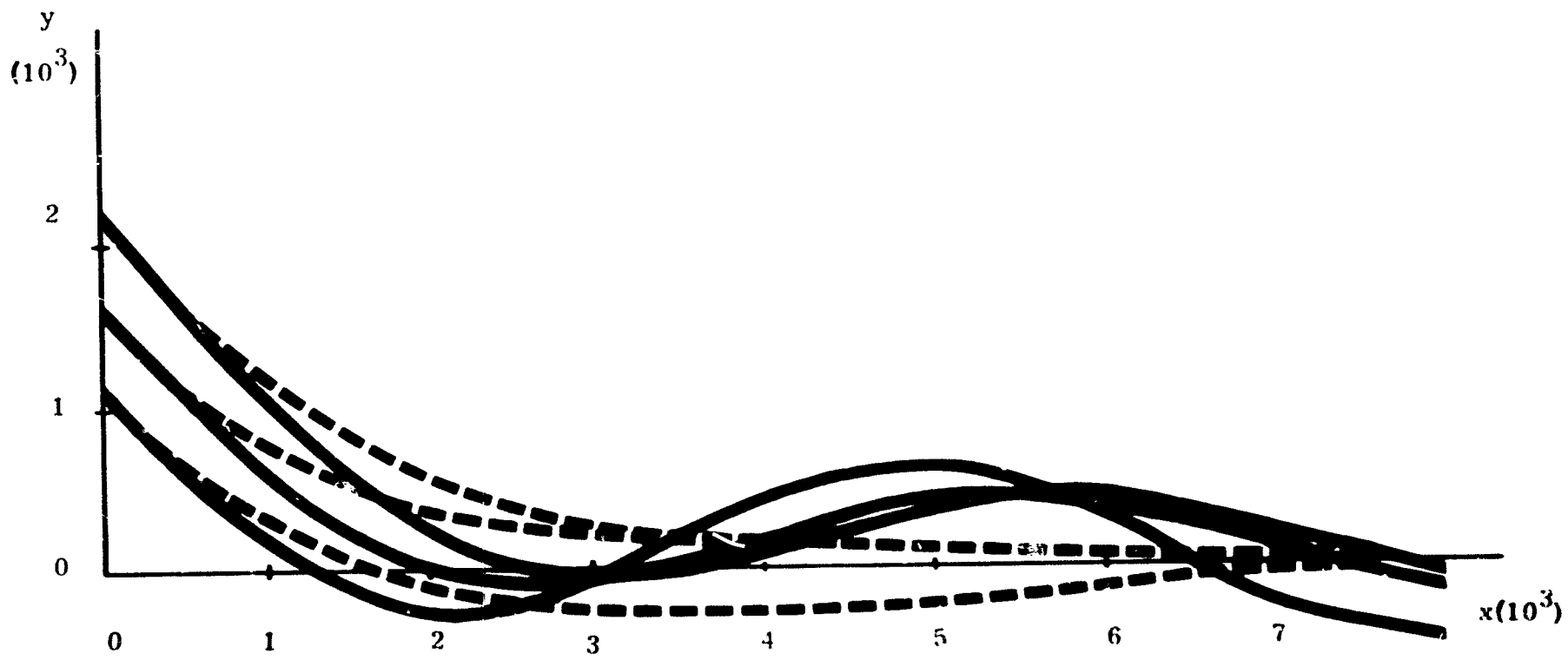

Fig. 9.5-3 Conventional and quasi-time optimal (dotted line) acquisition system responses: The acquisition maneuver is initiated at 1000, 1500, and 2000 ft from the localizer center. The initial path inclination angle is 45^{o}.

3. Decrab trajectory optimization to improve overall decrab performance.
4. Flareout control system redesign to incorporate improvements in the vertical control system.
5. Rollout control system development.
6. Optimal landing abort control.

In addition to the above points which deal specifically with landing problems, many practical questions in the areas of displays, data processing, flight test planning, reliability and failure detection provide a wide scope for further investigations in automatic landing alone. Ultimately, the work should be broadened to encompass automatic takeoff, traffic pattern control and all the other flight activities in the terminus area.

APPENDIX A

A. 1 Introduction

The most common type of automatic landing system uses information derived from the ILS localizer and glide-path receivers to provide the position error data required for acquisition and flight along the reference line defined by the intersection of the ILS localizer and glide-slope center planes. Conventional systems provide essentially linear position control relative to this reference line. This appendix describes lateral and vertical control system designs which are based on the conventional approach.

A. 2 Conventional Lateral Position Control System

In the lateral channel the coupler output provides the reference input to the roll autopilot. Roll angle serves as the lateral control variable, since the heading rate $\dot{\psi}$ is roughly proportional to roll angle ϕ

$$\dot{\psi} = \frac{g \tan \phi}{v_p} \qquad \text{(A. 2-1)}$$

and the lateral velocity y is proportional to heading angle relative to the path (in the absence of a cross wind).

$$\dot{y} = v_p \sin \psi \qquad \text{(A. 2-2)}$$

where g is the gravitational constant and v_p is the path velocity. A schematic diagram of a conventional LATERAL control system is shown in Fig. A. 2-1 where:

K_y is an adjustable position feedback gain.

$K_{\dot{y}}$ is an adjustable rate feedback gain.

K_{iy} is the integral compensator gain.

T_r is the ILS Receiver Time Constant.

T_v is the velocity lead network time constant.

d_{loc} is the estimated distance to the localized antenna.

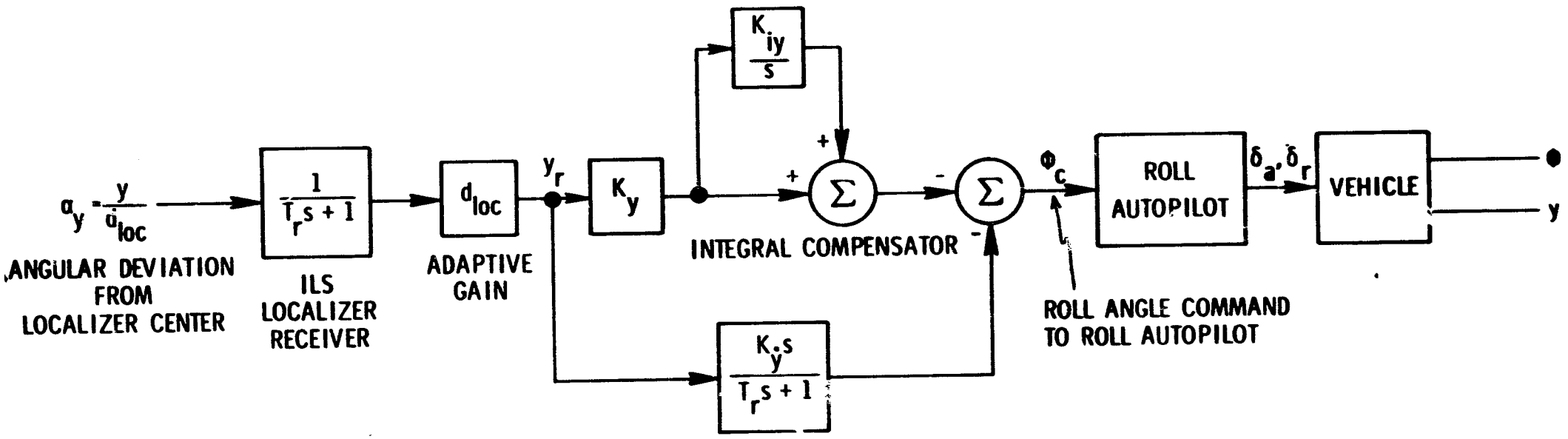

Fig. A.2-1 Conventional lateral position control system.

Position information relative to the localizer beam center is obtained by multiplying the angular deviation (radians) provided by the localizer receiver by the distance d_{loc} to the localizer antenna. This position information is multiplied by the gain K_y to close the position control loop.

The integral compensator operates on y to provide a roll command which maintains the correct crab angle when the aircraft is operated in a varying cross wind as well as correcting for any individual errors in trim.

The lead network generates a signal proportional to the rate of change of lateral position y. This signal provides dynamic response compensation as indicated above. This compensation may be augmented by heading feedback due to the relation in Eq (A. 2-2).

The open-loop transfer characteristics of the control system are shown in Fig. A. 2-2, which uses the linearized vehicle transfer functions in Appendix B, the roll angle control system in Section 5. 3 and the parameter values in Table A. 3-1. The closed-loop transfer function is shown in Fig. A. 2-3. A linearized response appears in Fig. A. 2-4.

A. 3 Conventional Vertical Position Control System

Vertical position control is achieved by applying the output of the vertical coupler as a reference input to the pitch autopilot as shown in Fig. A. 3-1 where

K_z is an adjustable position feedback gain.

$K_{\dot{z}}$ is an adjustable velocity feedback gain.

K_{iz} is an adjustable integral compensator gain.

T_r is the ILS receiver time constant.

T_v is the velocity lead network time constant.

d_{gs} is the estimated distance to the glide-slope antenna.

α_{gs} is the angular deviation from the glide-path center.

z_{gs} is the vertical coordinate of the glide-path center.

x is the distance to the glide-slope antenna.

z is the vertical distance between the aircraft and the glide-path center.

The vertical component of velocity $\dot{z}$ is approximately proportional to the pitch θ.

$$\dot{z} \approx -v_p\theta$$

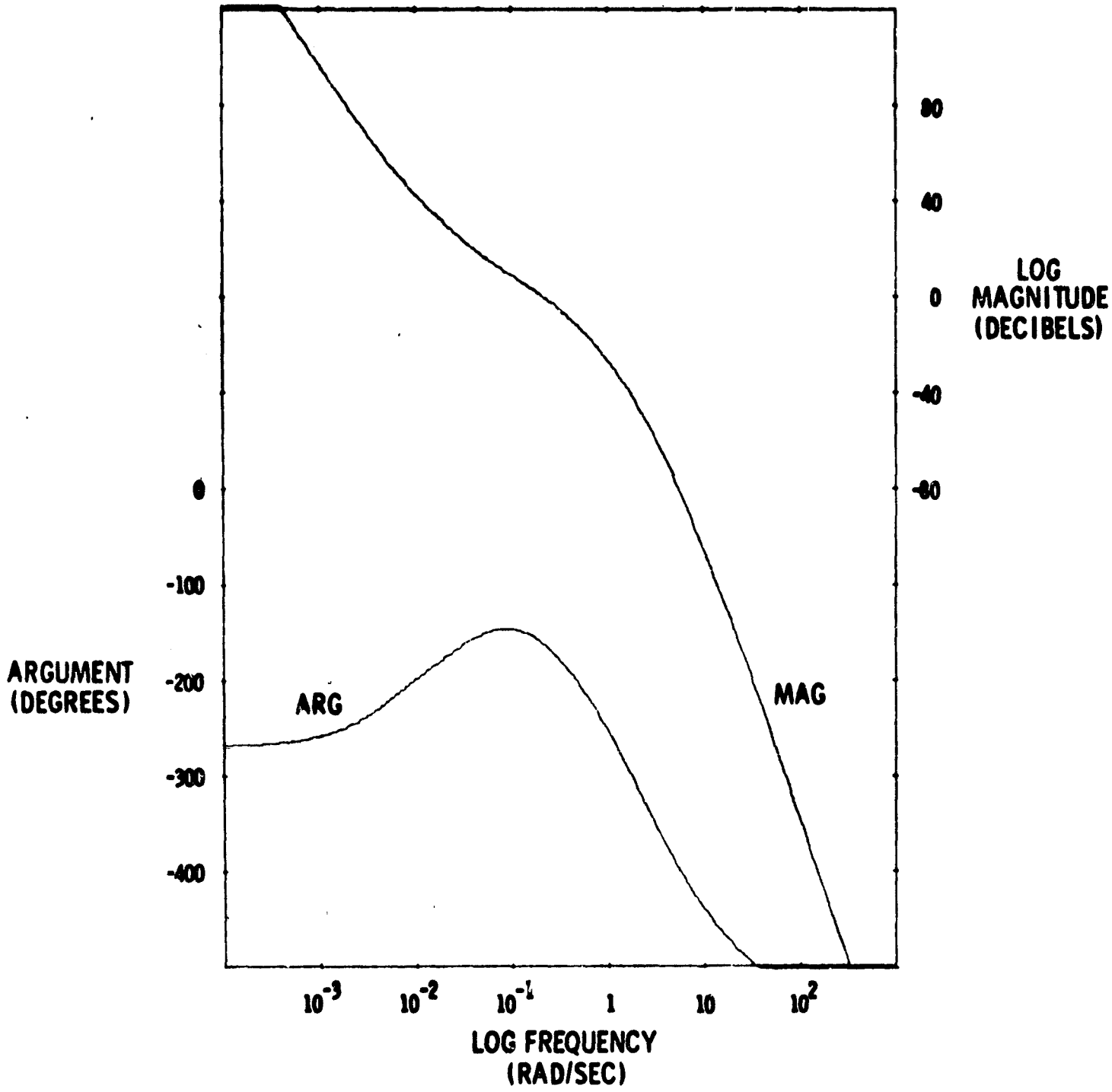

Fig. A.2-2 Open-loop transfer function of a conventional lateral position control system.

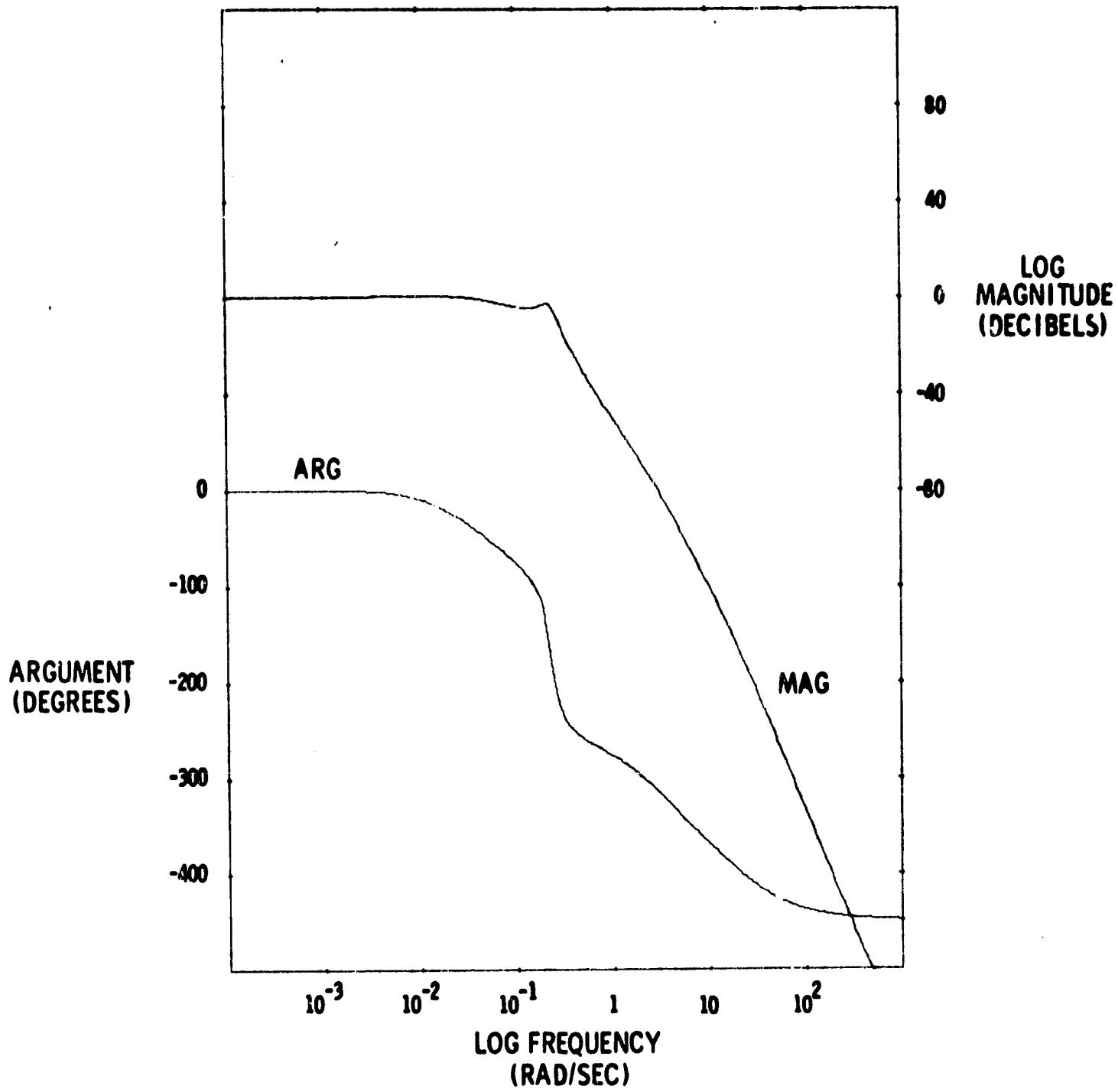

Fig. A.2-3 Closed-loop transfer function $\frac{y}{y_d}$ for a conventional lateral position control system.

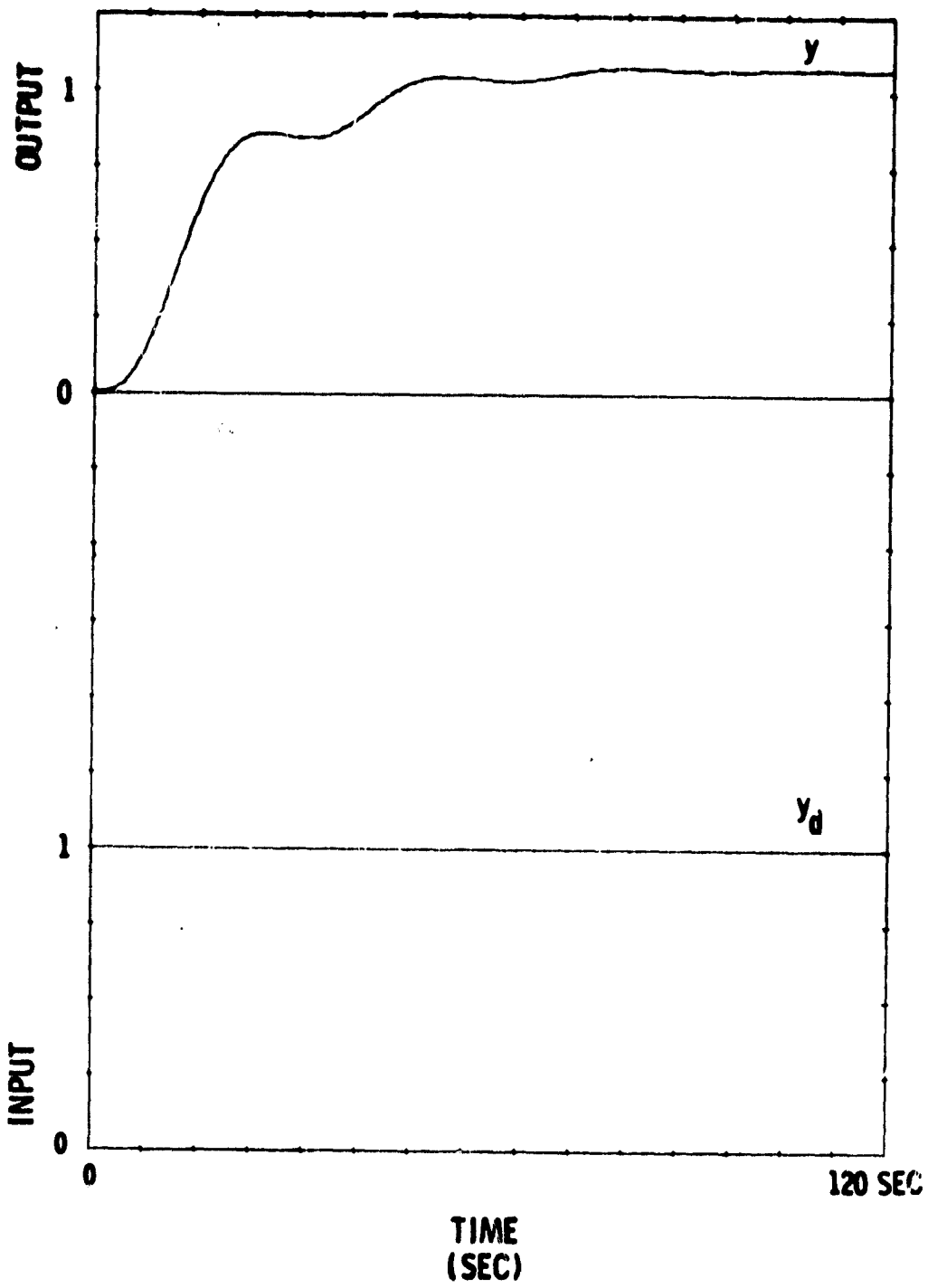

Fig. A.2-4 Unit-step response of the linearized conventional lateral position control system.

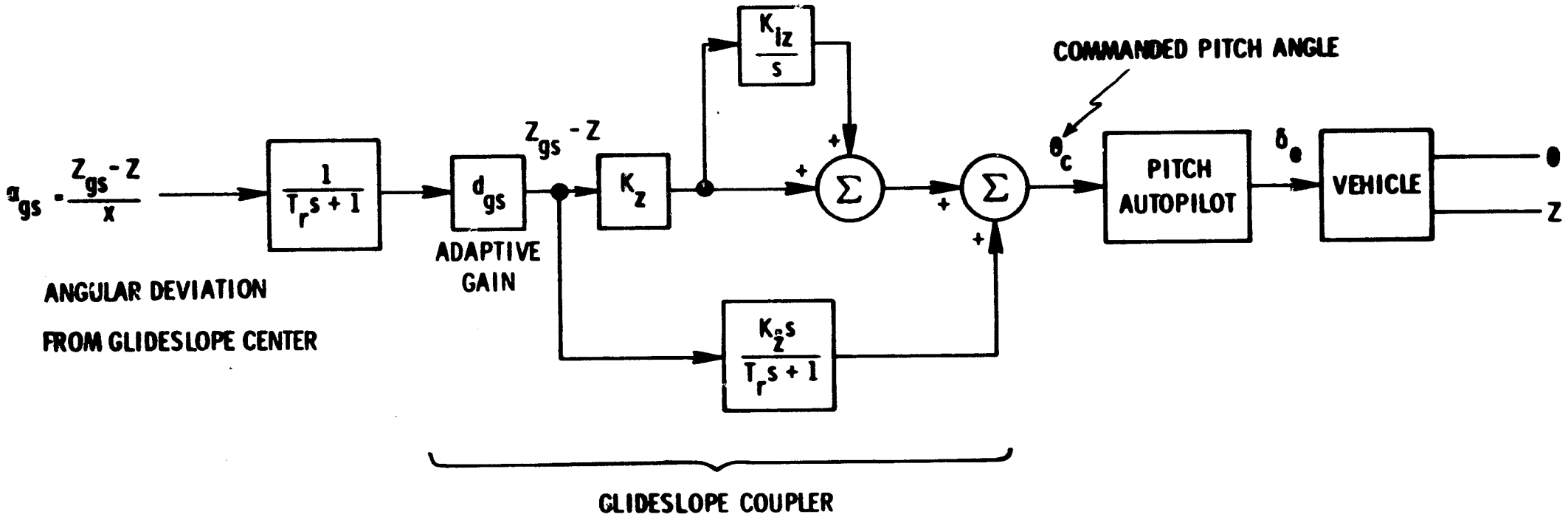

Fig. A.3-1 Conventional vertical position control system.

The vertical distance between the aircraft and the glide-path center is obtained by multiplying the angular deviation (radians) from the ILS glide-slope receiver by the estimated distance to the glide-slope transmitter. This is then multiplied by a gain K_z to close the position loop.

The integral compensator provides the constant component of θ which is required for flight down an inclined path with zero position error as well as correcting for trim. The velocity lead network provides a signal proportional to the rate of change of vertical position for dynamic compensation.

The open-loop transfer function of the control system is shown in Fig. A.3-2 and is generated using the vehicle transfer function in Section C.5, the pitch angle control system in Section 5.11 and the parameter values in Table A.3-1. The closed-loop transfer function is shown in Fig. A.3-3, and the unit-step response of the linear model appears in Fig. A.3-4.

Table A.3-1 Parameter Values for Conventional ILS Coupler

GAINS		
K_y	lateral position gain	0.0205 deg/ft
$K_{\dot{y}}$	lateral velocity gain	0.410 deg/ft/sec
K_{iy}	y intrgral compensator gain	0.005 sec
K_z	vertical position gain	0.041 deg/ft
$K_{\dot{z}}$	vertical velocity gain	0.205 deg/ft/sec
K_{iz}	z integral compensator gain	0.005 sec
CONSTANTS		
T_r	ILS receiver time constant	0.40 secs
T_v	velocity filter time constant	1.00 secs

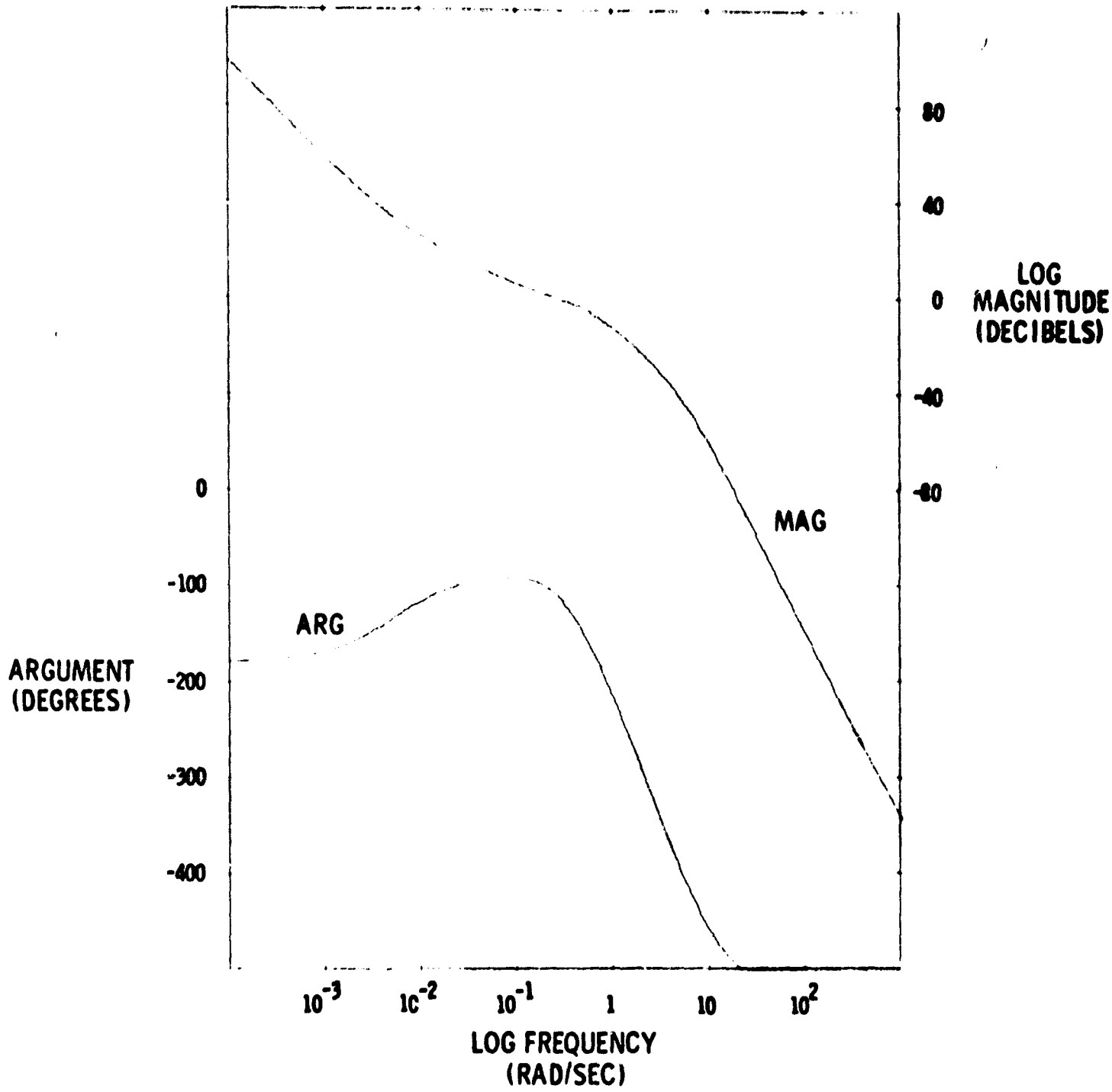

Fig. A.3-2 Open-loop transfer function of a conventional vertical position control system.

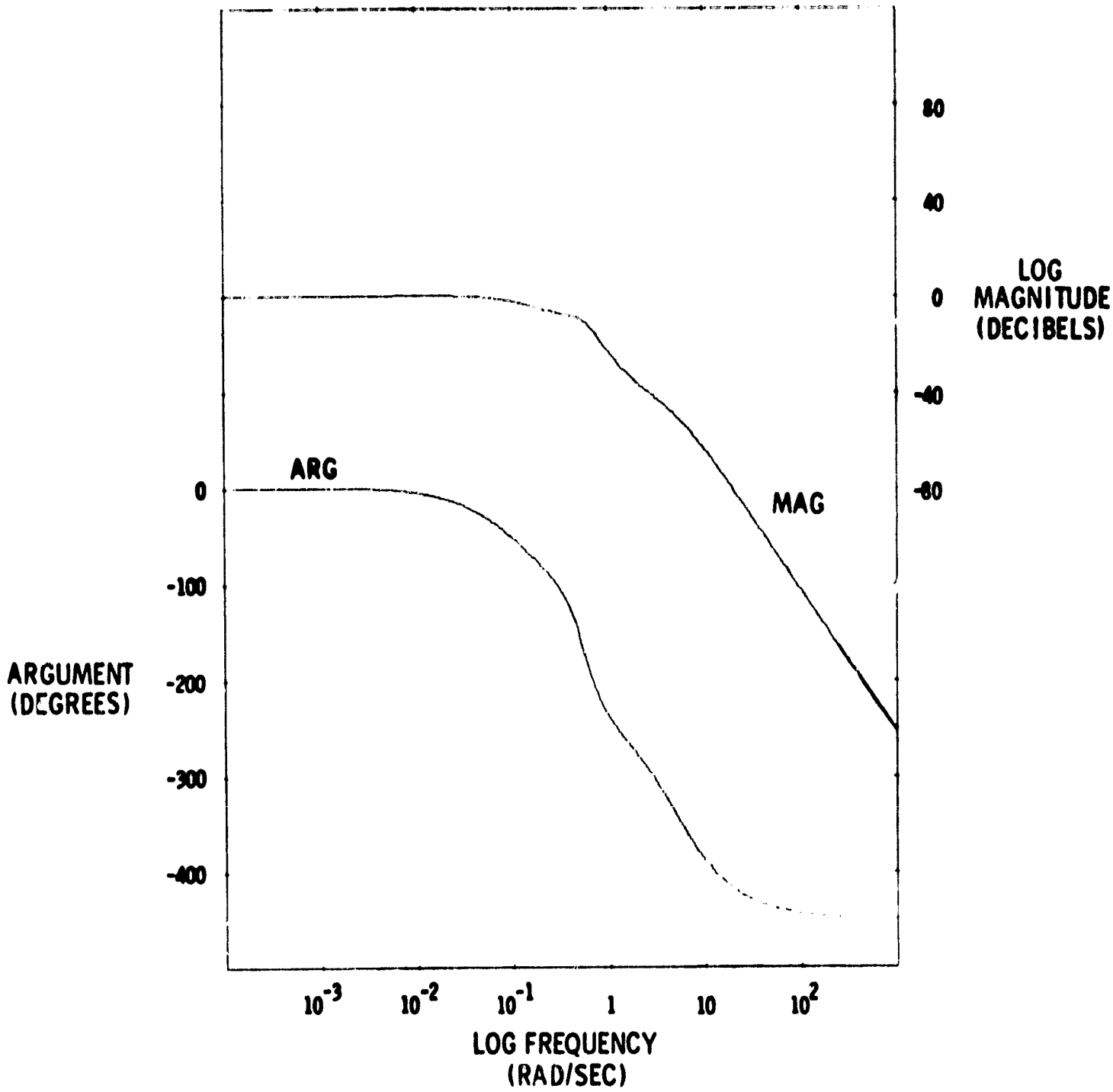

Fig. A.3-3 Closed-loop transfer function $\frac{z}{z_d}$ of a conventional vertical position control system.

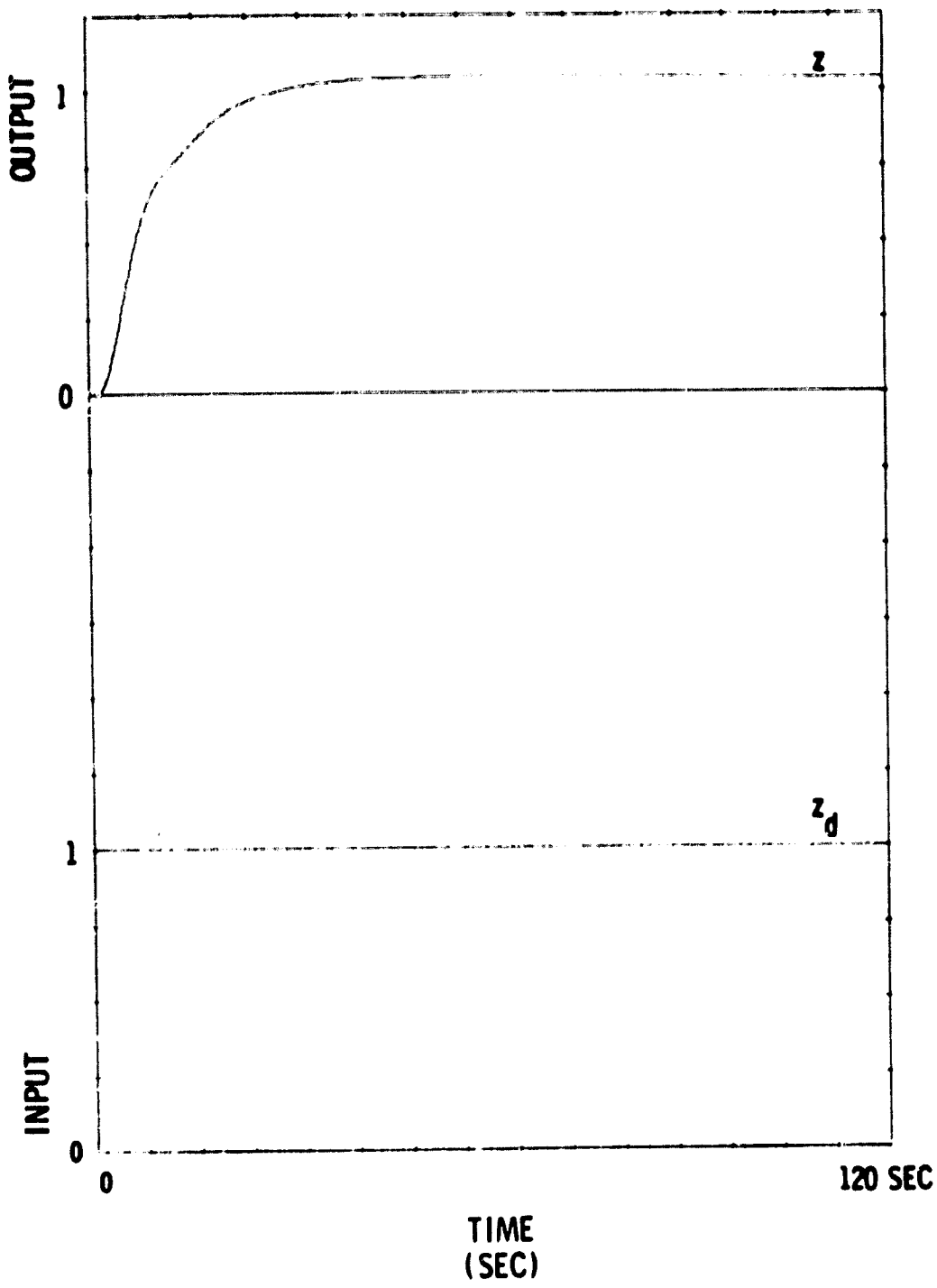

Fig. A.3-4 Unit-step response of the linearized conventional vertical position control system .

APPENDIX B

KALMAN FILTER THEORY

B.1 Introduction

This appendix contains an exposition of Kalman Filter Theory sufficient for the application of the theory that is made in Chapter 3. The references on which the following discussion is based are refs (24) and (25) by Battin, Levine and Brock, respectively.

The problem to be considered may be defined as follows:

A system state vector x satisfies the differential equation

$$\dot{x} = f(t)\ x + n \qquad \text{(B. 1-1)}$$

where n is white noise. A vector z, accessible to measurement, is sampled periodically. The vector z is related to x by

$$z = H(t)\, x + u \qquad \text{(B. 1-2)}$$

where u, the error of measurement, is uncorrelated from sample to sample.

At time t an estimate $\hat{x}'$ of x is assumed to be available. Following a measurement of z at time t, an improved estimate $\hat{x}$ is computed. The estimation process is designed so that the expectation of the sum of the squares of the estimation errors of the state variables $\mathcal{E}\left[(\hat{x} - x)_T(\hat{x} - x)\right]$ is a minimum. The expectation is assumed to be taken over an ensemble of systems characterized by the same parameters as the actual system at hand.

B.2 Derivation of the Estimation Equations

At time t an estimated state vector $\hat{x}'$ is available, and a measurement z is made. Let $\hat{z}'$ be the best estimate of z prior to making the measurement. Then

$$\hat{z}' = H\hat{x}' \qquad \text{(B. 1-3)}$$

since u is unknown. It is assumed that an improved estimate $\hat{x}$ is given by the linear relationship

$$\hat{x} = \hat{x}' + w(z - \hat{z}') \qquad \text{(B. 1-4)}$$

where w is an appropriate weighting factor. Substitution of Eq (B.1-3) into Eq (B.1-4) yields

$$\hat{x} = \hat{x}' + w(z - H\hat{x}') \tag{B.1-5}$$

The estimation error is

$$e = \hat{x} - x \tag{B.1-6}$$

$$= \hat{x}' + w(z - H\hat{x}') - x$$

$$= (\hat{x}' - x) - wH(\hat{x}' - x) + wu$$

$$= e' - wHe' + wu \tag{B.1-7}$$

The covariance matrix E is defined as an expectation of the product ee_T.

$$E = \mathcal{E}(ee_T) \tag{B.1-8}$$

Note that E is a square matrix, whereas the quantity to be minimized, $\mathcal{E}(e_T e)$, is a scalar equal to the trace of E.

The product ee_T is

$$ee_T = e'e'_T - wHe'e'_T - wue'_T - e'e'_T H_T w_T + wHe'e'_T H_T w_T$$

$$- wue'_T H_T w_T + e'u_T u_T - wHe'u_T w_T + wuu_T w_T \tag{B.1-9}$$

Since u is uncorrelated with either x or $\hat{x}'$

$$\mathcal{E}(ue'_T) = \mathcal{E}(e'u_T) = 0 \tag{B.1-10}$$

Let

$$\mathcal{E}(uu_T) = R \tag{B.1-11}$$

Then

$$E = E' - wHE' - E'H_T w_T + wHE'H_T w_T + wRw_T$$

$$= E' - wHE' - (wHE')_T + w(HE'H_T + R)w_T \tag{B.1-12}$$

The trace of this equation is

$$trE = tr\left[E' - 2wHE' + w(HE'H_T + R)w_T\right] \tag{B.1-13}$$

The increment of trE is

$$\delta \text{tr}\, E = \text{tr}\left[-2\delta w H E' + \delta w (H E' H_T + R) w_T + w(H E' H_T + R)\delta w_T\right] \qquad \text{(B. 1-14)}$$

Since E' and R are symmetric by definition

$$\delta \text{tr}\, E = 2\,\text{tr}\left[-\delta w H E' + \delta w (H E' H_T + R) w_T\right]$$

tr E will be stationary when δtrE = 0 for an arbitrary increment δw and this condition is satisfied when

$$0 = HE' + (HE'HH_T + R)\, w_T$$

Therefore

$$w = E'H_T(HE'H_T + R)^{-1} \qquad \text{(B. 1-15)}$$

and Eq (B. 1-5) becomes

$$\hat{x} = \hat{x}' + E'H_T(HE'H_T + R)^{-1}(z - H\hat{x}') \qquad \text{(B. 1-16)}$$

The equation for updating the covariance matrix, following the measurement, is obtained by substitution of (B. 1-15) into (B. 1-12)

$$E = E' - E'H_T(HEH_T + R)^{-1}HE' \qquad \text{(B. 1-17)}$$

Between measurements, both $\hat{x}$ and E must be extrapolated forward in time. Since n is unknown, the best estimate of the state vector between measurements is given by

$$\dot{\hat{x}} = F\hat{x} \qquad \text{(B. 1-18)}$$

A differential equation satisfied by E, between measurements, can be derived as follows:

$$e = \hat{x} - x \qquad \text{(B. 1-19)}$$

$$\dot{e} = \dot{\hat{x}} - \dot{x}$$

$$= F\hat{x} - Fx - n$$

$$= Fe - n$$

Also

$$\begin{aligned} E &= \mathcal{E}(ee_T) \\ \dot{E} &= \mathcal{E}(e\dot{e}_T + \dot{e}e_T) \\ &= \mathcal{E}(ee_T F_T + Fee_T - en_T - ne_T) \end{aligned} \tag{B. 1-20}$$

The expectation of the product en_T is

$$\begin{aligned} \mathcal{E}(en_T) &= \mathcal{E}(\hat{x}n_T - xn_T) \\ &= \mathcal{E}(-xn_T) \end{aligned} \tag{B. 1-21}$$

since $\hat{x}$ does not depend on the noise since the last measurement. Furthermore, x can be expressed in the form

$$x(t) = \int_{t_o}^{t} [Fx(\tau) + n(\tau)]\, d\tau + x(t_o)$$

and

$$x(t)n_T(t) = \int_{t_o}^{t} [Fx(\tau)\, n(t) + n(\tau)\, n(t)]\, d\tau + x(t_o)n_T(t)$$

Since

$$t \geq \tau \text{ and } t > t_o$$

$$\mathcal{E} \int_{t_o}^{t} s(\tau)\, n_T(t)\, dt = 0$$

and

$$\mathcal{E}\, x(t_o)\, n_T(t) = 0$$

It follows that

$$\mathcal{E}\, x(t)\, n_T(t) = \mathcal{E} \int_{t_o}^{t} n(\tau)\, n_T(t)\, dt \tag{B. 1-22}$$

Since n is white noise, it is characterized by an autocorrelation function

$$\mathcal{E}\, n(\tau)\, n(t) = Q\delta(\tau - t) \qquad \text{(B. 1-23)}$$

By the formal properties of the delta function

$$\mathcal{E} \int_{t_o}^{t} x(\tau)\, n_T(t)\, d\tau = \frac{1}{2} Q$$

Similar considerations applied to Eq (B. 1-20) yield the result

$$\dot{E} = FE + EF_T + Q \qquad \text{(B. 1-24)}$$

APPENDIX C

C.1 Derivation of Linear Vehicle Transfer Functions

The most useful techniques for analyzing and synthesizing control systems are based on the theory of linear systems. In order to apply these techniques, the basically nonlinear vehicle equations are linearized about the nominal operating state as shown in Chapter 8. This procedure results in a set of six coupled linear differential equations which describe the behavior of the perturbations u, β, α, p, q and r. The forcing inputs to this set of equations are perturbations in the control surface deflections. These transfer functions are now derived.

C.2 Lateral Vehicle Transfer Functions

The vehicle equations which describe the behavior of the vehicle in the lateral body axis are

$$C_{\dot{\beta}}\dot{\beta} = C_{\dot{\beta}\beta}\beta + C_{\dot{\beta}p}p + C_{\dot{\beta}\phi}\phi + C_{\dot{\beta}r}r + C_{\dot{\beta}\delta_r}\delta_r \qquad (C.2\text{-}1)$$

$$C_{\dot{p}}\dot{p} = C_{\dot{p}\beta}\beta + C_{\dot{p}r}r + C_{\dot{p}\delta_r}\delta_r + C_{\dot{p}\delta_a}\delta_a \qquad (C.2\text{-}2)$$

$$C_{\dot{r}}\dot{r} = C_{\dot{r}\beta}\beta + C_{\dot{r}r}r + C_{\dot{r}p}p + C_{\dot{r}\delta_r}\delta_r + C_{\dot{r}\delta_a}\delta_a \qquad (C.2\text{-}3)$$

where C_{xy} is a constant coefficient relating the variable x to the variable y. The constant C_x is a multiplier for the variable x. Two cases are considered

$$1. \quad \beta = \dot{\beta} = 0 \qquad (C.2\text{-}4)$$

$$2. \quad \phi = p = \dot{p} = 0 \qquad (C.2\text{-}5)$$

The first case depicts the conditions of coordinated flight which persist during ILS acquisition and extend to the point of acquisition and the terminal maneuvers. The second is important during the DECRAB where a change in heading is desired while level flight is maintained.

C.3 Coordinated Flight Transfer Functions

In coordinated flight a change in heading direction is achieved by rolling the vehicle using the ailerons δ_a as the primary control. Aileron deflections produce a yawing moment which results in an undesirable sideslip angle, β. Additional con-

tributions to β result from the roll rate p, roll angle ϕ and heading rate r. An accumulation of a slip angle β is prevented by deflecting the rudder. The required rudder deflection which satisfies Eq (C.2-4) is

$$\delta_r = -C_{\dot{\beta}\delta_r}^{-1} \left(C_{\dot{\beta}r} r + C_{\dot{\beta}p} + C_{\dot{\beta}\phi} \left(\frac{p}{s}\right) \right) \qquad \text{(C.3-1)}$$

where s is the complex variable. Equations (C.3-1) and (C.2-4) are utilized to eliminate δ_r and β from Eqs (C2-2) and (C.2-3).

$$C_{\dot{r}}sr = C_{\dot{r}r} r + C_{\dot{r}p} p + C_{\dot{r}\delta_a} \delta_a - \frac{C_{r\delta_r}}{C_{\beta\delta_r}} \left[C_{\dot{\beta}r} r + C_{\dot{\beta}p} + C_{\dot{\beta}\phi} \left(\frac{p}{s}\right) \right] \qquad \text{(C.3-2)}$$

$$C_{\dot{p}}sp = C_{\dot{p}r} r + C_{\dot{p}p} p - \frac{C_{\dot{p}\delta_r}}{C_{\dot{\beta}\delta_r}} \left[C_{\dot{\beta}r} r + C_{\dot{\beta}p} p + C_{\dot{\beta}\phi} \left(\frac{p}{s}\right) \right] + C_{p\delta_a} \delta_a \qquad \text{(C.3-3)}$$

Equations (C.3 2) and (C.3 3) are then rewritten in the form

$$G_{rr} r + G_{rp} p = G_{r\delta_a} \delta_a \qquad \text{(C.3-4)}$$

$$G_{pr} r + G_{pp} p = G_{p\delta_a} \delta_a \qquad \text{(C.3-5)}$$

where G_{rr}, G_{rp}, $G_{r\delta_a}$, G_{pr}, G_{pp} and $G_{p\delta_a}$ are polynomials in the complex variable s.

Defining the characteristic polynomial

$$G_{cy} = G_{rr} G_{pp} - G_{pr} G_{rp} \qquad \text{(C.3-6)}$$

the desired transfer functions may be written

$$\left(\frac{r}{\delta_a}\right)_{\beta=0} = \frac{G_{r\delta_a} G_{pp} - G_{p\delta_a} G_{rp}}{G_{cy}} \qquad \text{(C.3-7)}$$

$$\left(\frac{p}{\delta_a}\right)_{\beta=0} = \frac{G_{rr}G_{p\delta_a} - G_{pr}G_{r\delta_a}}{G_{cy}} \qquad \text{(C. 3-8)}$$

Magnitude and phase response characteristics of Eqs (C. 3-7) and (C. 3-8) are shown in Figs. C. 3-1 and C. 3-3 respectively. The corresponding time domain responses to a step input are shown in Figs. C. 3-2 and C. 3-4.

C. 4 Decrab Control Transfer Functions

During the DECRAB maneuver the aircraft is yawed about the z body axis while maintaining a zero roll angle. The primary effector is rudder deflection δ_r which produces a large yaw acceleration. Coupling in the vehicle equations simultaneously generates a roll moment which is countered by operating the ailerons δ_a. The necessary aileron deflection δ_a which satisfies Eq (C. 2-5) is

$$\delta_a = -C_{\dot{p}\delta_a}^{-1}\left[C_{\dot{p}\beta}\beta + C_{\dot{p}r}r + C_{\dot{p}\delta_r}\delta_r\right] \qquad \text{(C. 4-1)}$$

This relationship is used to eliminate δ_r, ϕ and p from Eqs (C. 2-1) and (C. 2-3) to yield

$$C_{\dot{r}}sr = C_{\dot{r}\beta}\beta + C_{\dot{r}r}r + C_{\dot{r}\delta_r}\delta_r - \frac{C_{\dot{r}\delta_a}}{C_{\dot{p}\delta_a}}\left[C_{\dot{p}\beta}\beta + C_{\dot{p}r}r + C_{\dot{p}\delta_r}\delta_r\right] \qquad \text{(C. 4-2)}$$

$$C_{\dot{\beta}}s\beta = C_{\dot{\beta}\beta}\beta + C_{\dot{\beta}r}r + C_{\dot{\beta}\delta_r}\delta_r \qquad \text{(C. 4-3)}$$

where s is the complex variable. Equations (C. 4-2) and (C. 4-3) may be written in the form

$$G_{rr}r + G_{r\beta}\beta = G_{r\delta_r}\delta_r \qquad \text{(C. 4-4)}$$

$$G_{\beta r}r + G_{\beta\beta}\beta = G_{\beta\delta_r}\delta_r \qquad \text{(C. 4-5)}$$

where G_{rr}, G_{rp}, $G_{r\delta_r}$, $G_{\beta r}$, $G_{\beta\beta}$ and $G_{\beta\delta_r}$ are polynomials in s. The characteristic polynomial is defined

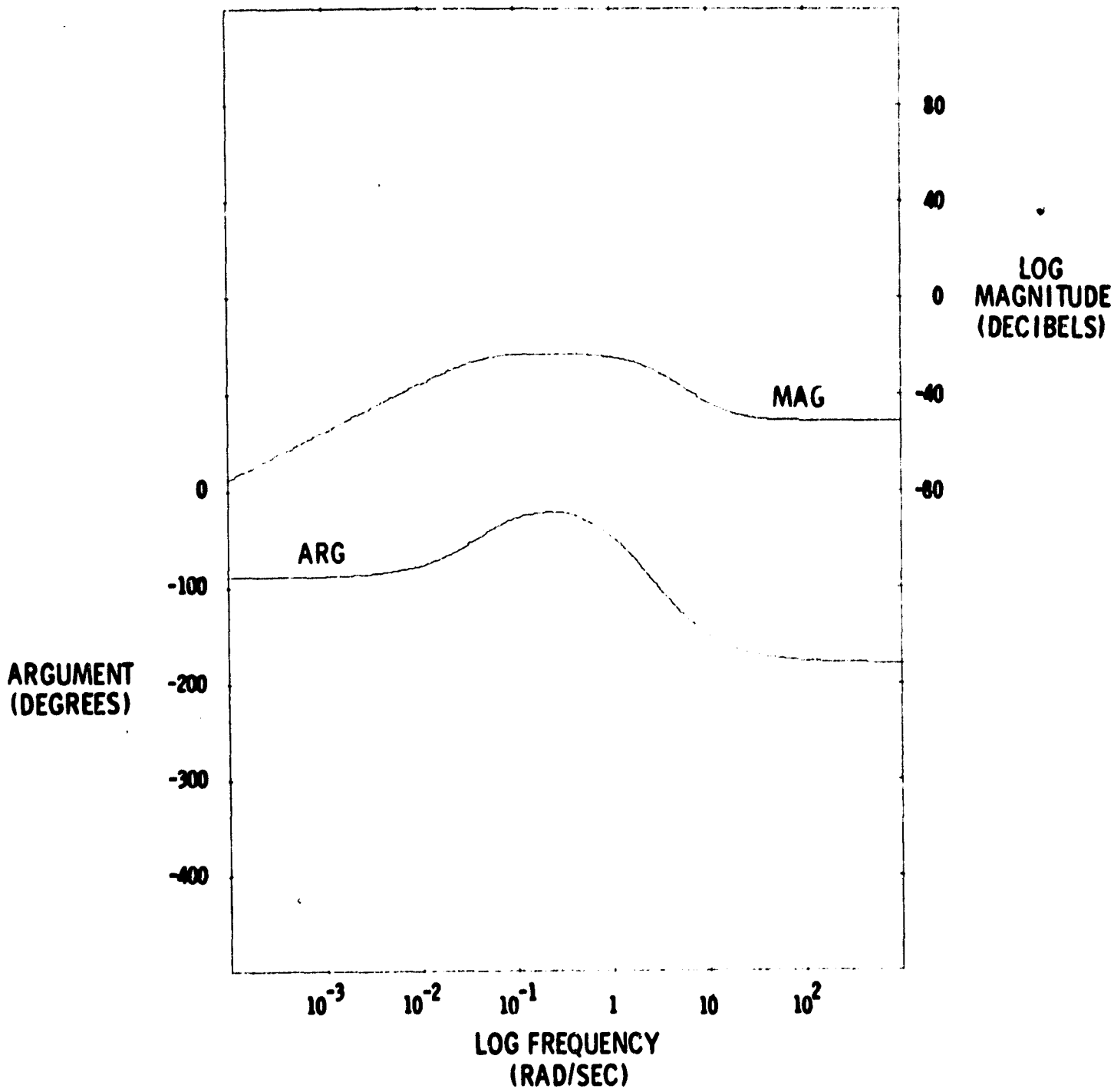

Fig. C.3-1 Magnitude and phase characteristics of $\left(\frac{-r}{\delta_a}\right)_{\beta = 0}$

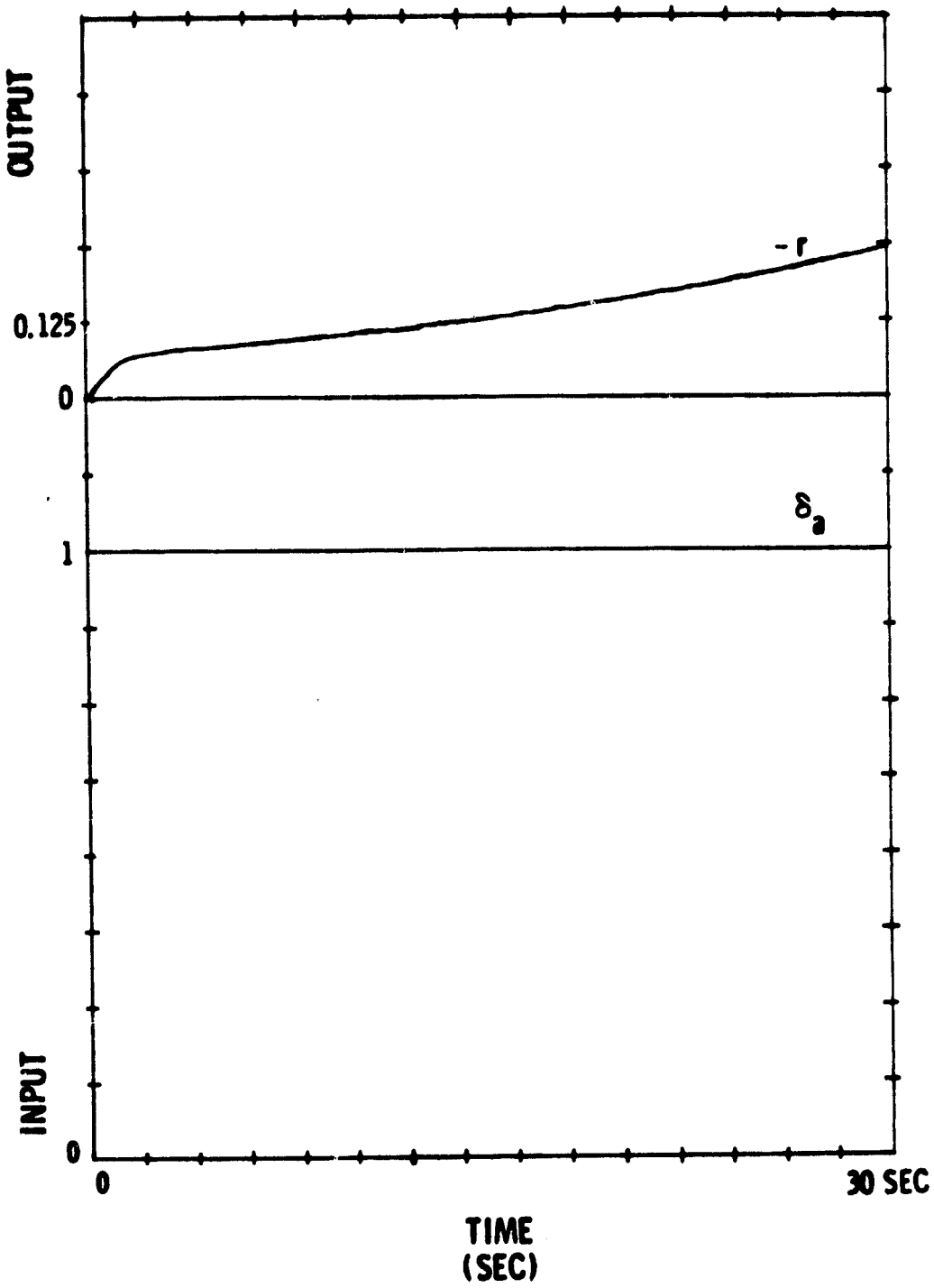

Fig. C.3-2 Heading rate response to a step aileron input ($\beta = 0$).

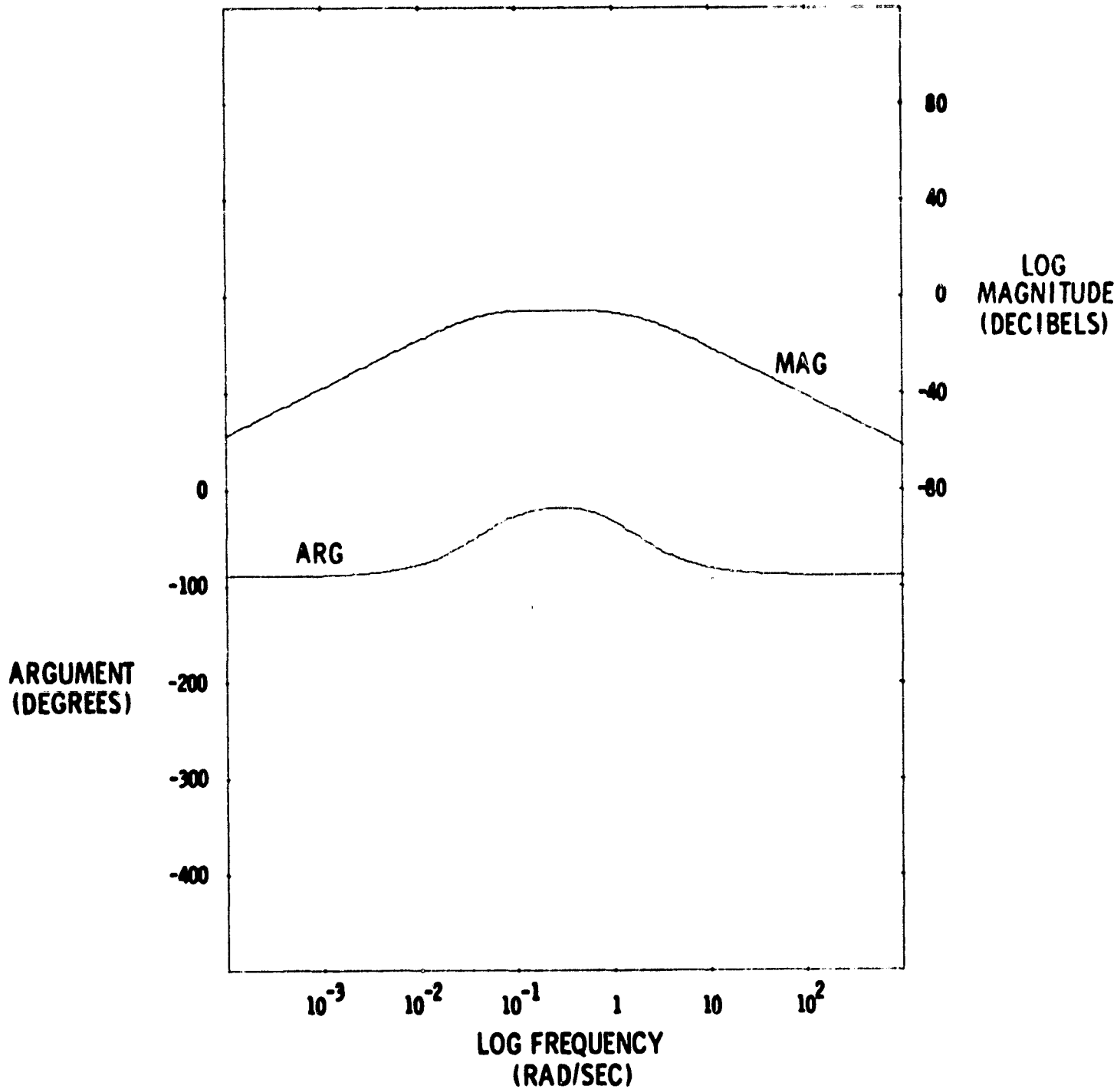

Fig. C.3-3 Magnitude and phase characteristics of $\left(\frac{p}{\delta_a}\right)_{\beta = 0}$

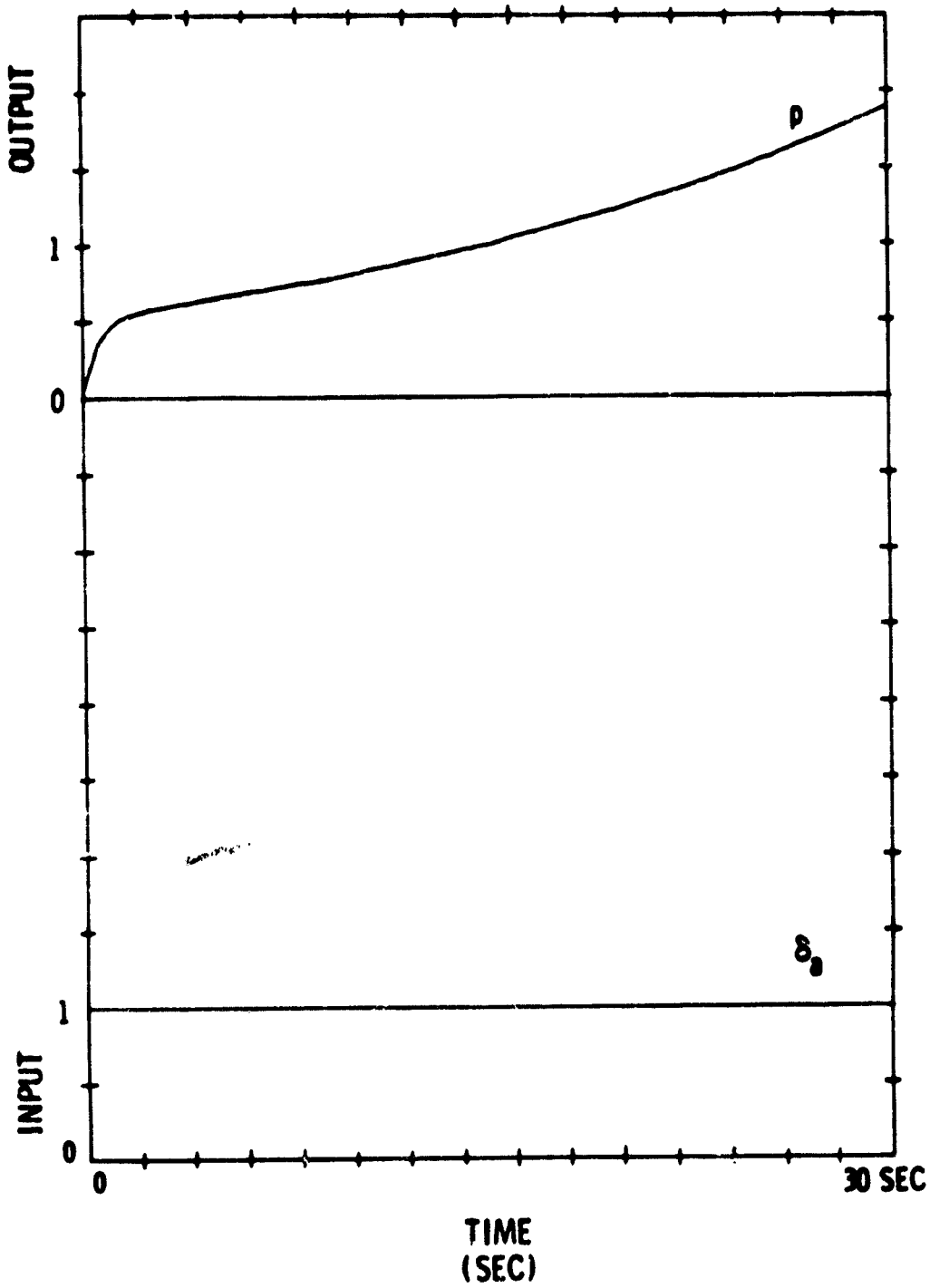

Fig. C.3-4 Roll rate response to a step aileron input ($\beta = 0$).

$$G_{cyu} = G_{rr}G_{\beta\beta} - G_{\beta r}G_{r\beta} \tag{C.4-6}$$

A solution of Eqs (C.4-4) and (C.4-5) may then be written

$$\left(\frac{r}{\delta_r}\right)_{p=0} = \frac{G_{r\delta_r}G_{\beta\beta} - G_{\beta\delta_r}G_{r\beta}}{G_{cyu}} \tag{C.4-7}$$

$$\left(\frac{\beta}{\delta_r}\right)_{p=0} = \frac{G_{rr}G_{\beta\delta_r} - G_{\beta r}G_{r\delta_r}}{G_{cyu}} \tag{C.4-8}$$

Magnitude and phase response characteristics of Eqs (C.4-7) and (C.4-8) are shown in Figs. C.4-1 and C.4-3 respectively. Corresponding step input responses are shown in Figs. C.4-2 and C.4-4.

C.5 Longitudinal Transfer Functions

The longitudinal variables u, α, q are related by a coupled set of linear differential equations.

$$C_{\dot{u}}\dot{u} = C_{\dot{u}u}u + C_{\dot{u}\alpha}\alpha + C_{\dot{u}\theta}\theta + C_{\dot{u}\delta_s}\delta_s \tag{C.5-1}$$

$$C_{\dot{\alpha}}\dot{\alpha} = C_{\dot{\alpha}u}u + C_{\dot{\alpha}\alpha}\alpha + C_{\dot{\alpha}q}q + C_{\dot{\alpha}\theta}\theta + C_{\dot{\alpha}\delta_e}\delta_e \tag{C.5-2}$$

$$C_{\dot{q}}\dot{q} = C_{\dot{q}u}u + C_{\dot{q}\alpha}\alpha + C_{\dot{q}q}q + C_{\dot{q}\delta}\delta_e \tag{C.5-3}$$

Vehicle control in the vertical plane is achieved by manipulating the elevators δ_e to achieve a change in q and α. The change in the x body component of speed u is assumed to be zero as a result of control affected by changing the engine thrust. The coupling effects of thrust into q and α are ignored for the moment. Setting u = 0, the three longitudinal equations reduce to

$$C_{\dot{q}}\dot{q} = C_{\dot{q}\alpha}\alpha + C_{\dot{q}q}q + C_{\dot{q}\delta_e}\delta_e \tag{C.5-4}$$

$$C_{\dot{\alpha}}\dot{\alpha} = C_{\dot{\alpha}\alpha}\alpha + C_{\dot{\alpha}q}q + C_{\dot{\alpha}\theta}\theta + C_{\dot{\alpha}\delta_e}\delta_e \tag{C.5-5}$$

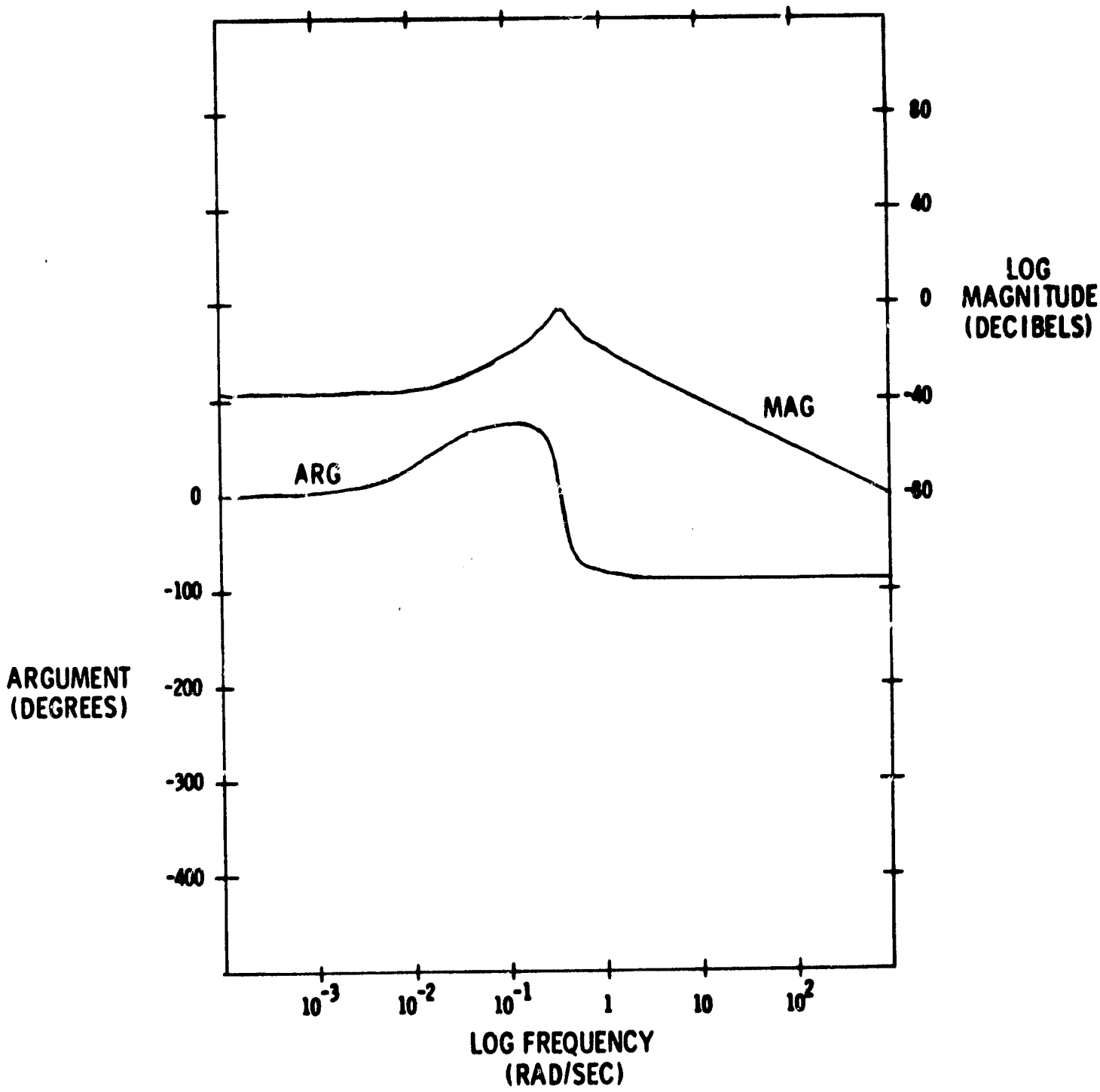

Fig. C.4-1 Magnitude and phase characteristics of $\left(\frac{-r}{\delta}\right)_{r/p\,=\,0}$.

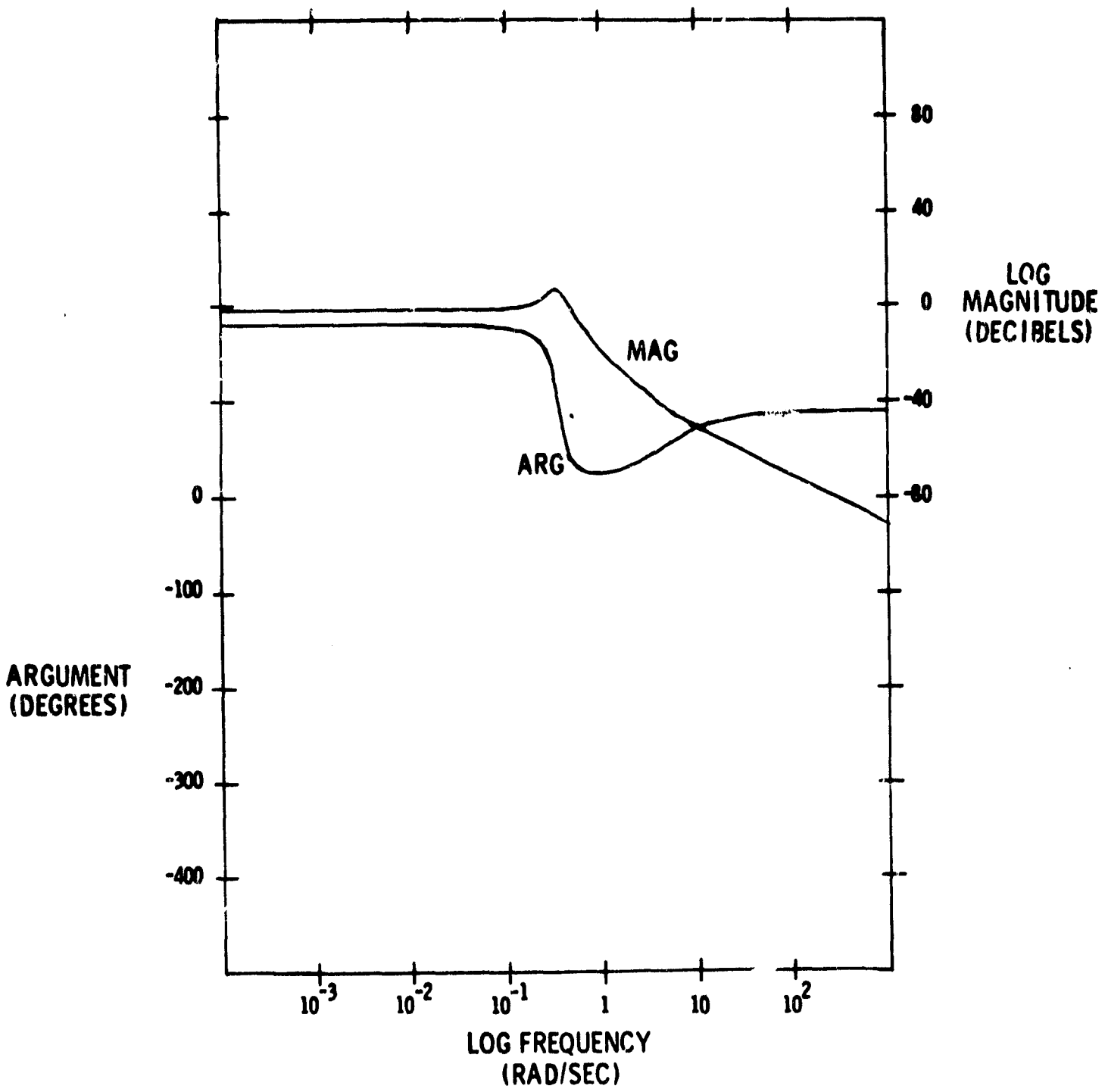

Fig. C.4-3 Magnitude and phase characteristics of $\left(\frac{\beta}{\delta_r}\right)_{p=0}$.

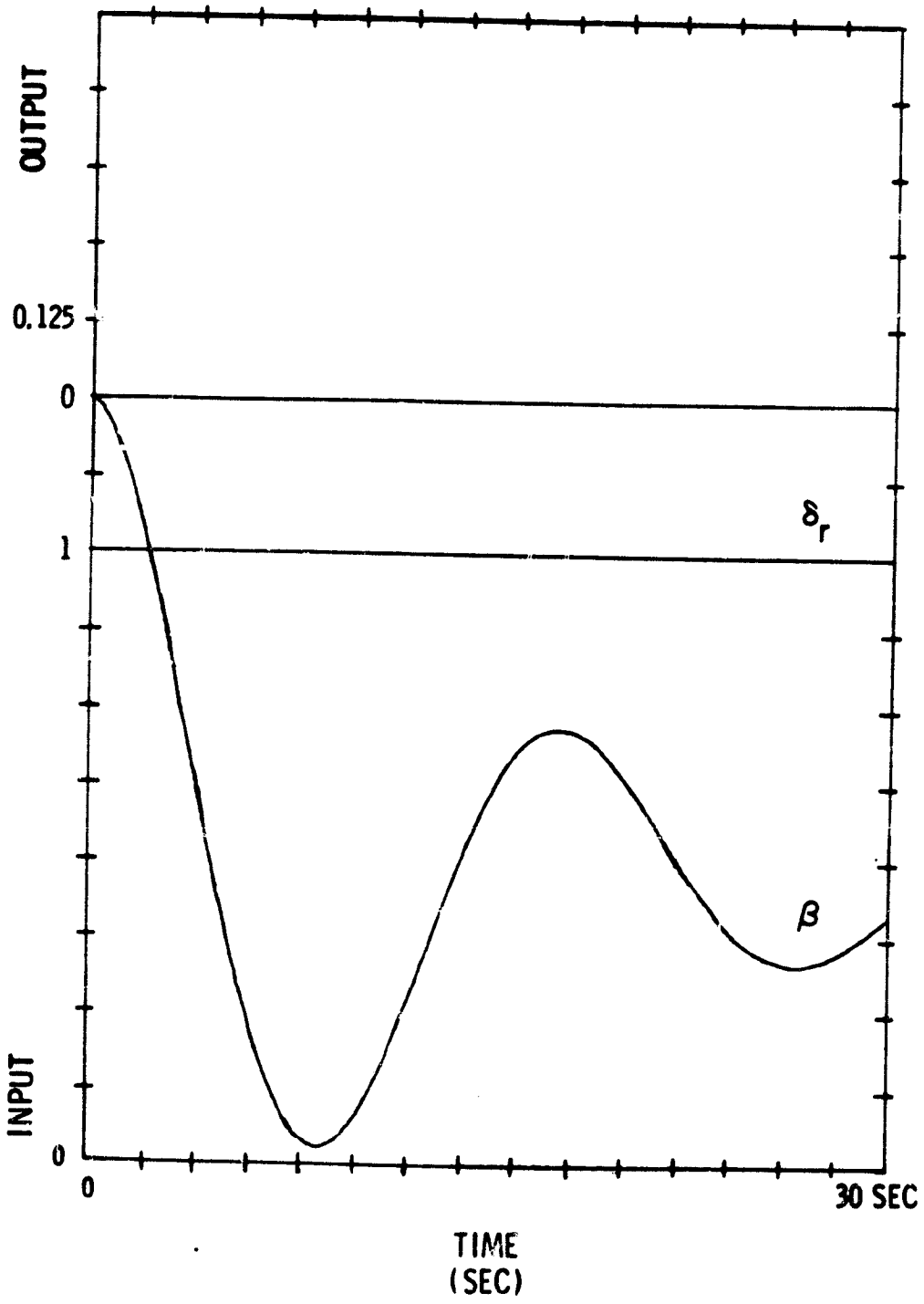

Fig. C.4-4 Vehicle slideslip angle response to unit rudder deflection.

Equations (C.5-1) and (C.5-2) may be rewritten in the form

$$G_{qq}q + G_{q\alpha}\alpha = G_{q\delta_e}\delta_e \qquad \text{(C.5-6)}$$

$$G_{\alpha q}q + G_{\alpha\alpha}\alpha = G_{\alpha\delta_e}\delta_e \qquad \text{(C.5-7)}$$

where G_{qq}, $G_{q\alpha}$, $G_{q\delta_e}$, $G_{\alpha q}$, $G_{\alpha\alpha}$ and $G_{\alpha\delta_e}$ are polynomials in s. Defining the characteristic polynomial

$$G_{cz} = G_{qq}G_{\alpha\alpha} - G_{\alpha q}G_{q\alpha} \qquad \text{(C.5-8)}$$

permits a simultaneous solution of (C.5-3) and (C.5-8) for the transfer functions

$$\left(\frac{q}{\delta_e}\right)_{u=0} = \frac{G_{q\delta_e}G_{\alpha\alpha} - G_{\alpha\delta_e}G_{q\alpha}}{G_{cz}} \qquad \text{(C.5-10)}$$

$$\left(\frac{\alpha}{\delta_e}\right)_{u=0} = \frac{G_{qq}G_{\alpha\delta_e} - G_{\alpha q}G_{q\delta_e}}{G_{cz}} \qquad \text{(C.5-11)}$$

Phase and magnitude response characteristics of (C.5-10) and (C.5-11) are shown in Figs. C.5-1 and C.5-3 respectively. Corresponding unit step responses appear in Figs. C.5-2 and C.5-4.

C.6 Numerical Values of Vehicle Transfer Functions

The numerical values of the coefficients in the vehicle transfer functions were generated by a digital computer and are shown below. While the transfer functions describe the vehicle precisely they may not be in reduced form (i.e., the numerator and denominator polynomials may contain common factors).

$$\left(\frac{r}{\delta_a}\right)_{\beta=0} = \frac{0.0219s - 0.0000356s^2 - 0.000141s^3}{-0.0135 + 0.301s + 0.268s^2 + 0.0505s^3}$$

$$\left(\frac{p}{\delta_a}\right)_{\beta=0} = \frac{0.168s + 0.0443s^2}{-0.0135 + 0.301s + 0.268s^2 + 0.0505s^3}$$

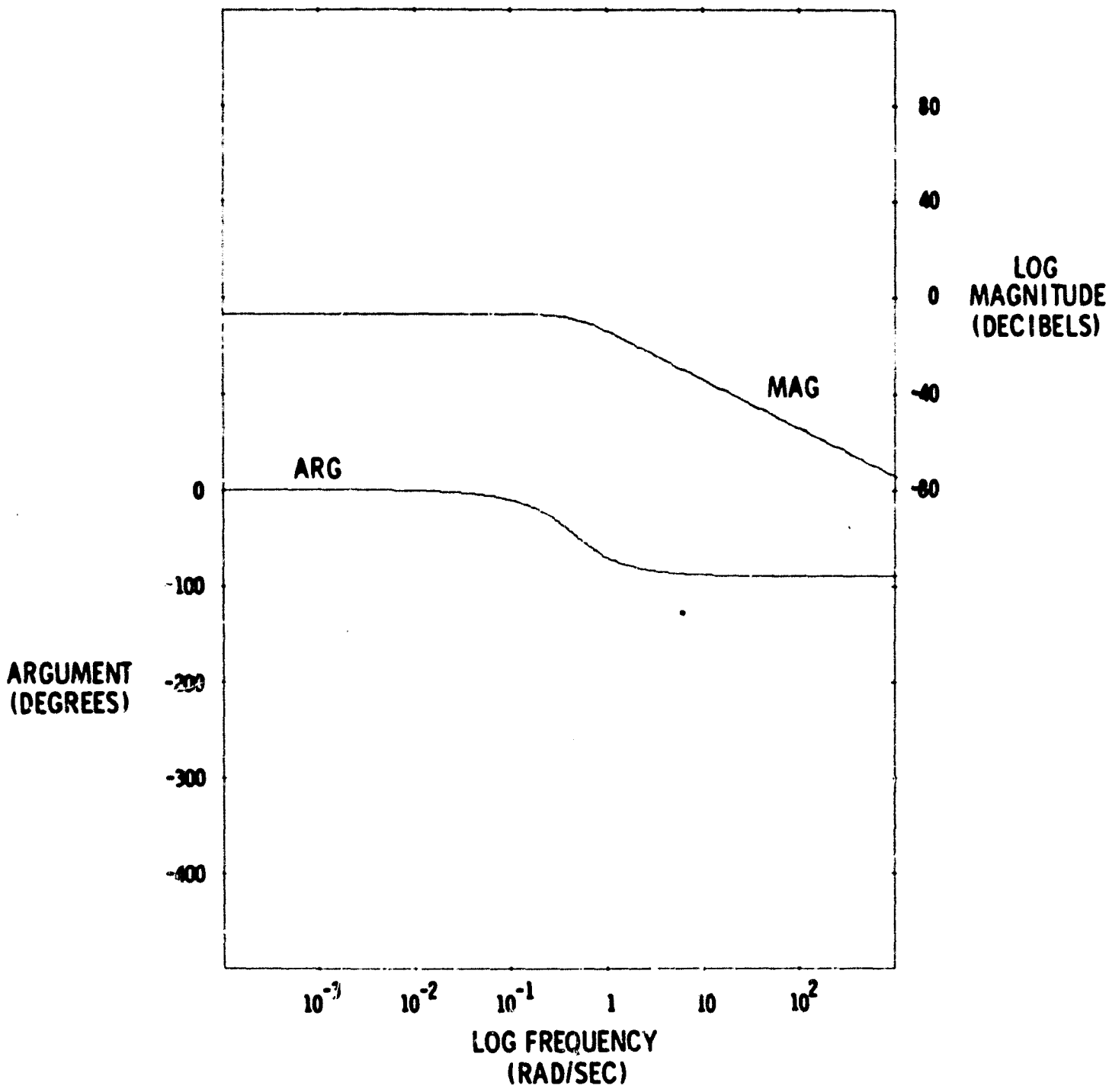

Fig. C.5-1 Magnitude and phase characteristics of $\left(\frac{-q}{\delta_e}\right)_{u=0}$

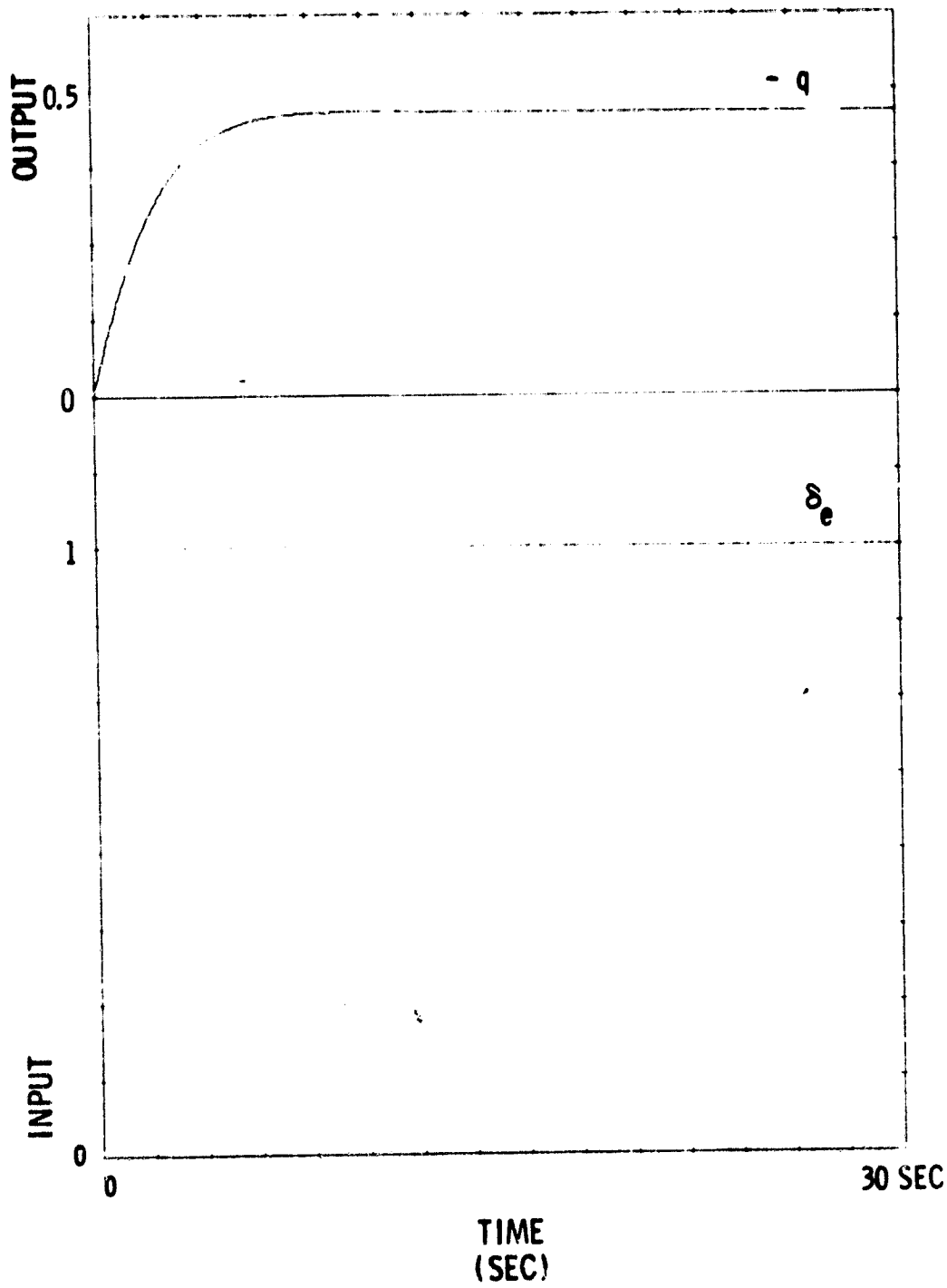

Fig. C.5-2 Vehicle pitch rate response to a unit-step elevator input.

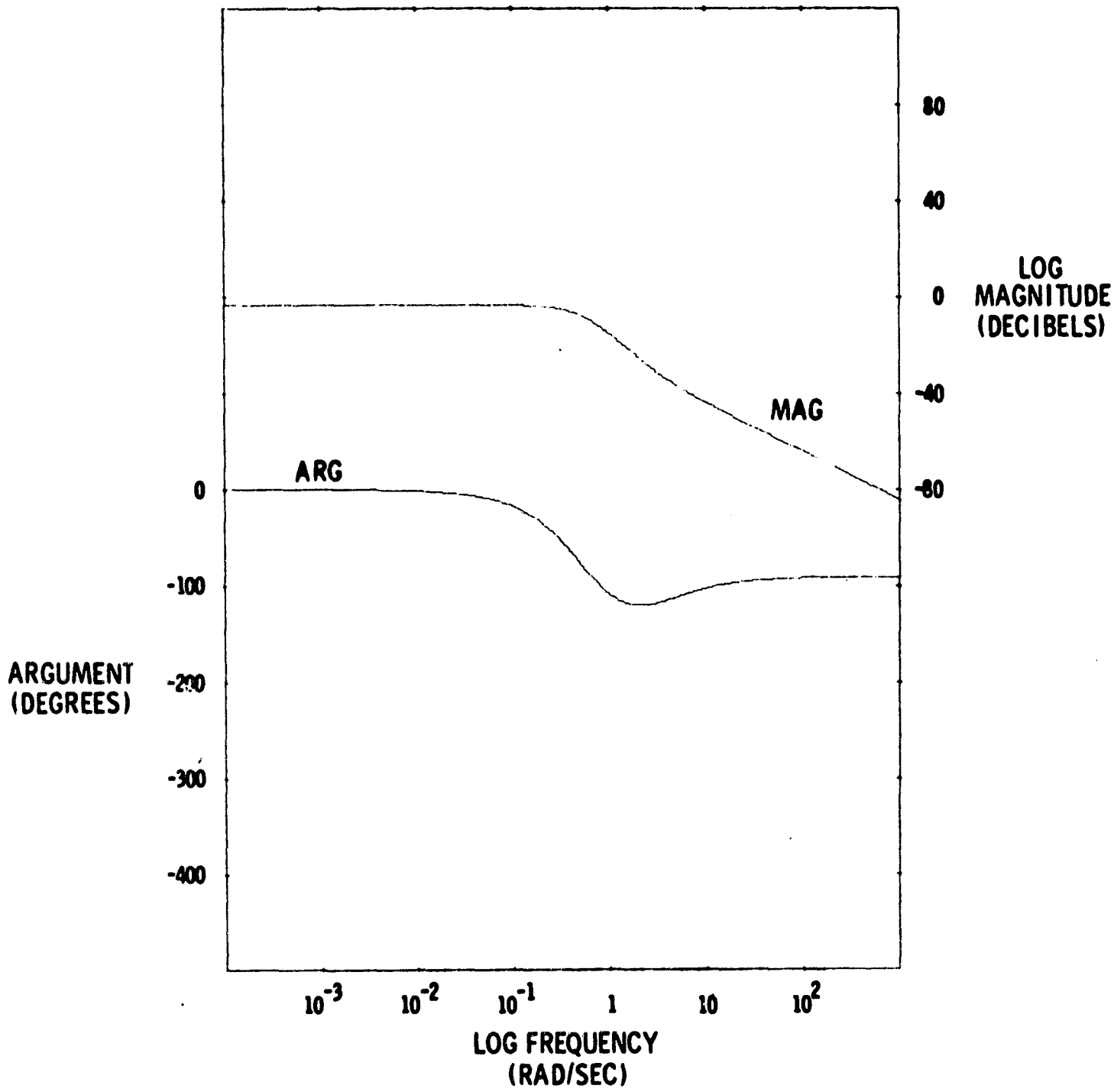

Fig. C.5-3 Magnitude and phase characteristics of $\left(\frac{-\alpha}{\delta_e}\right)_{u=0}$

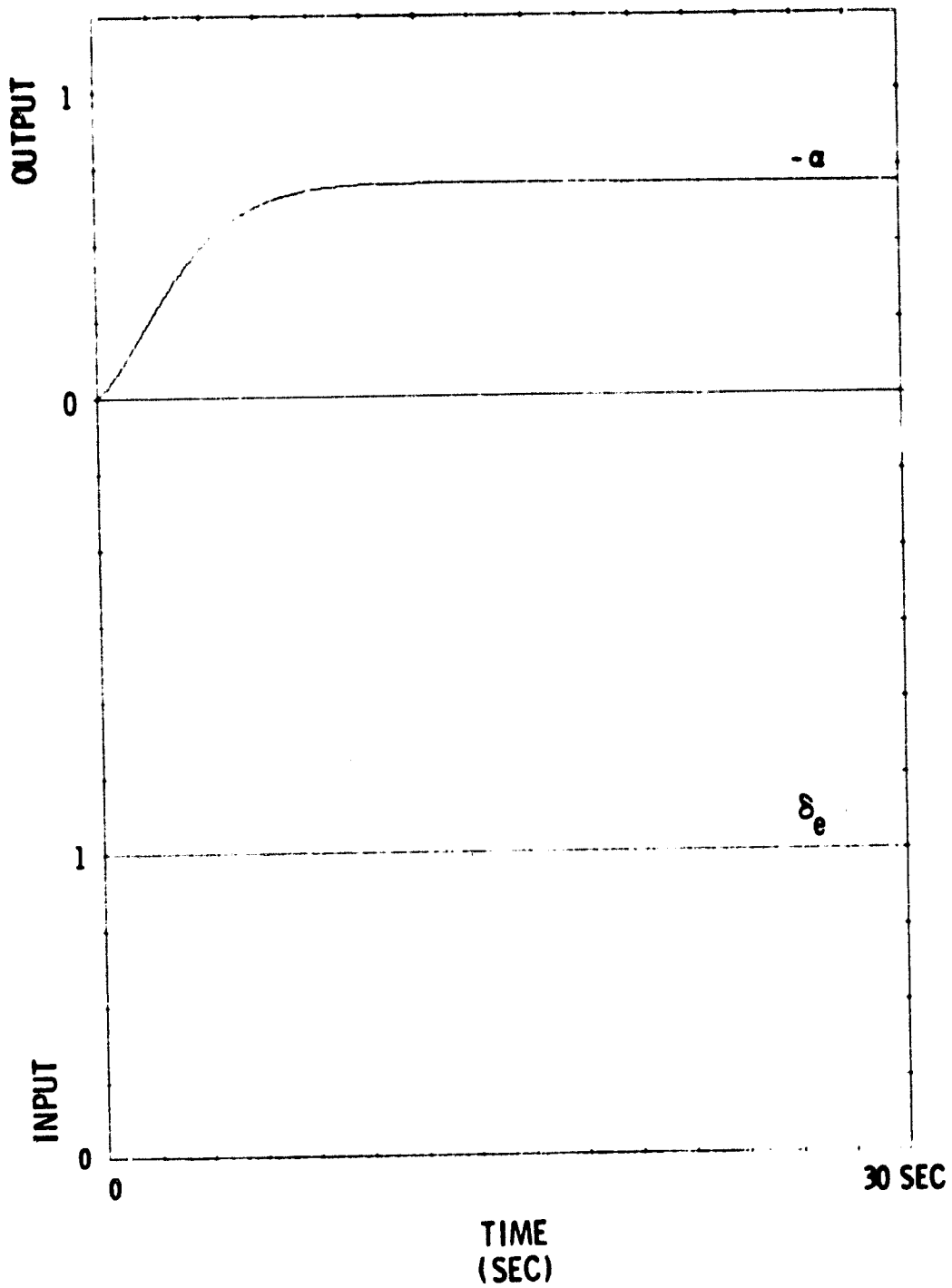

Fig. C.5-4 Vehicle α response to a step input in elevator deflections.

$$\left(\frac{r}{\delta_r}\right)_{p=0} = \frac{-0.00485 \cdot 0.285s}{0.371 + 0.376s + 2.892s^2}$$

$$\left(\frac{\beta}{\delta_r}\right)_{p=0} = \frac{+0.290 + 0.0766s}{0.371 + 0.376s + 2.892s^2}$$

$$\left(\frac{q}{\delta_e}\right)_{u=0} = \frac{+0.244 + 0.368s}{-0.528 - 1.797s - 1.866s^2}$$

$$\left(\frac{\alpha}{\delta_e}\right)_{u=0} = \frac{+0.368 + 0.116s}{-0.528 - 1.797s - 1.866s^2}$$

APPENDIX D

D. 1 Digital Simulation of an Automatic Landing System

The theoretical control system designs derived in Chapters 3 to 5 were validated by digital computer simulation of the SST and its automatic control system. Digital to analog conversion permitted the direct recording of solutions generated by the computer.

The system of differential equations describing the vehicle, vehicle stability augmentation system, autopilot and automatic landing system were written in the form

$$\dot{x} = f(x, m) \tag{D. 1-1}$$

where

- x is a vector describing the system which is not necessarily a state vector.
- $\dot{x}$ is a vector of derivatives.
- m is a set of control inputs such as desired vertical position and velocity for example. $\dim(m) \leq \dim(x)$.

The vectors x and $\dot{x}$ are subject to magnitude limits of the form

$$|x| < L_x \tag{D. 1-2}$$

$$|\dot{x}| < L_{\dot{x}} \tag{D. 1-3}$$

and a boundary condition

$$x(0) = a \tag{D. 1-4}$$

A solution of (D. 1-1) may be obtained by direct integration from the boundary value (D. 1-4). A simplified block diagram of a simulation is shown in Fig. (D. 1-1).

Integration step size is an important consideration in the construction of a digital simulation. Several factors play an important role in step size selection.

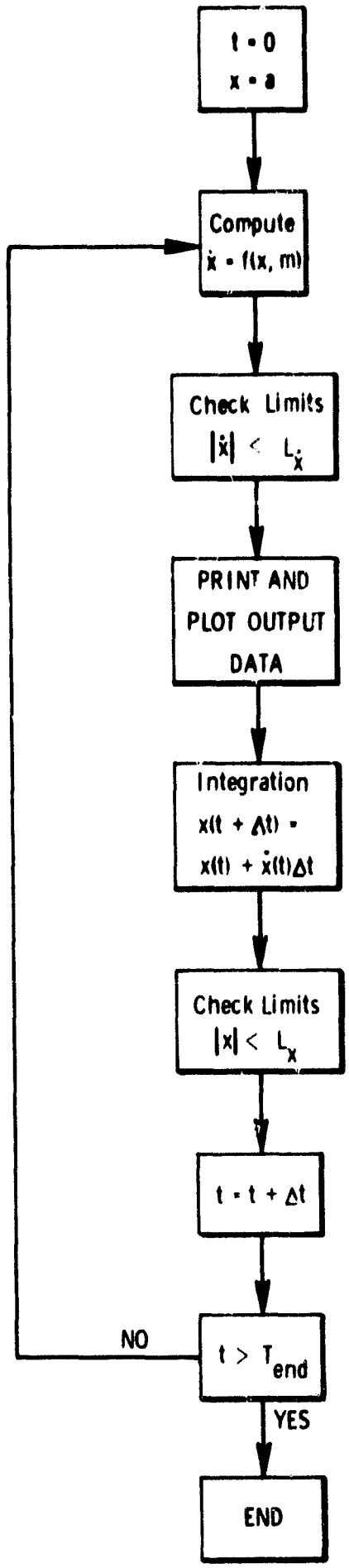

Fig. D.1-1 Simplified block diagram of a simplified digital simulation.

1. Solution accuracy.

2. Integration law.

3. Order of the largest coupled system of differential equations in D. 1-1.

Step size is normally reduced until a further reduction does not yield a significant improvement in accuracy. An integration law with improved convergence characteristics usually permits an increase in step size. An upper bound on step size is often determined by the order of the largest independent set of coupled differential equations.

The computer programs were written in FORTRAN II. The computations were performed using a Scientific Data Systems 930 computer. (16 thousand 24-bit words of random access memory, 2 μsec cycle time). The size of the program may be inferred from Fig. D. 1-2. The selected step size was 0.020 seconds. This yielded a simulation which generates a solution at a speed approximately 1/10 real time.

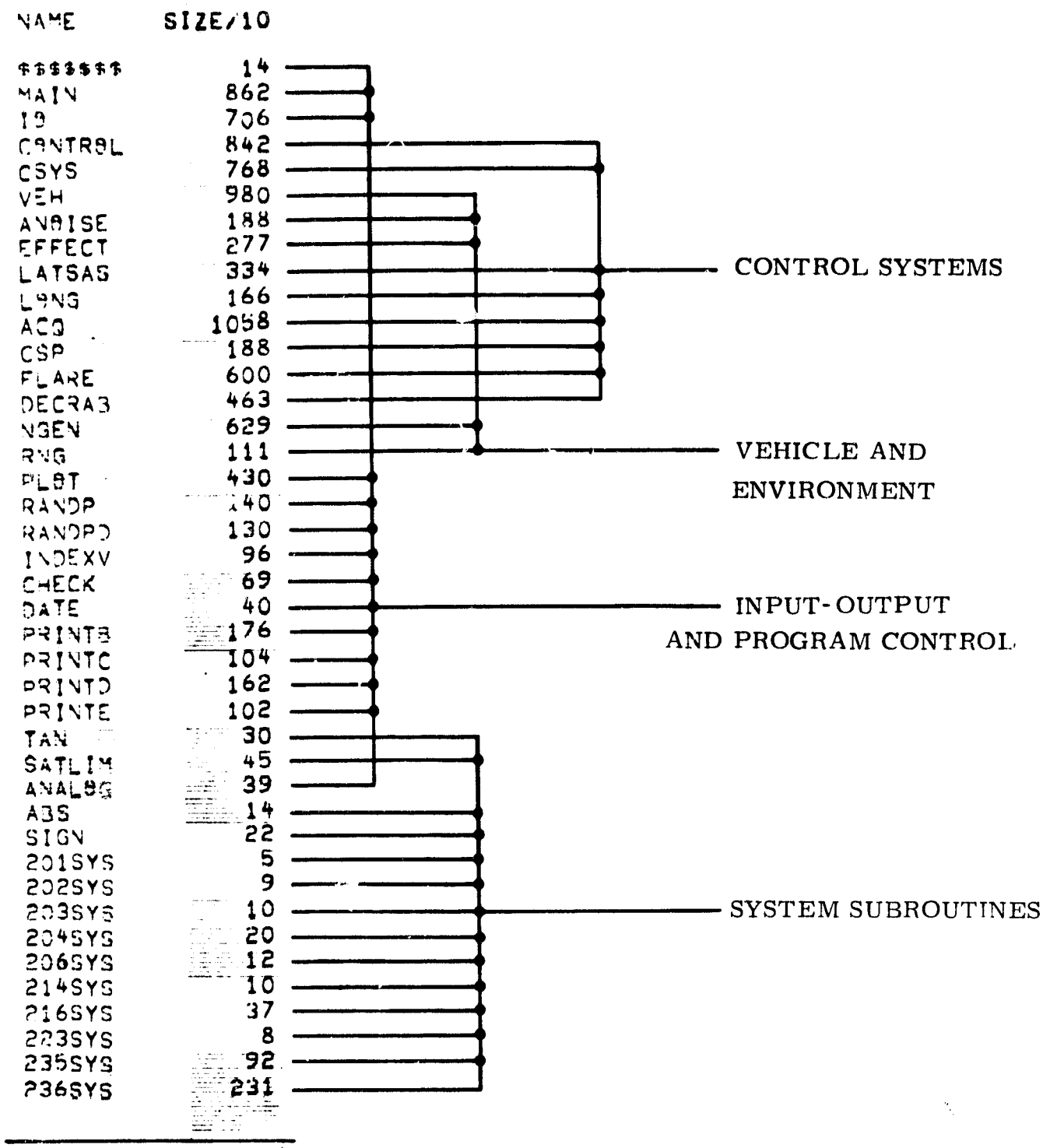

TOTAL	11231
COMMON STORAGE	1593
TOTAL	12824

Fig. D.1-2 Computer memory requirements.

APPENDIX E

E. 1 Introduction

The following aerodynamic information was supplied by the Boeing Aircraft Company and the FAA as appropriate to the Boeing B-2707 SST - Phase IIC (refs (19, 20)).

The aerodynamic information is for the aircraft in the landing approach configuration. Additional derivatives required were analytically evaluated as in Section E. 4.

Ground effect data appears in Section E. 5.

Table E.1-1 Landing Approach Configuration of the Boeing B-2707 SST

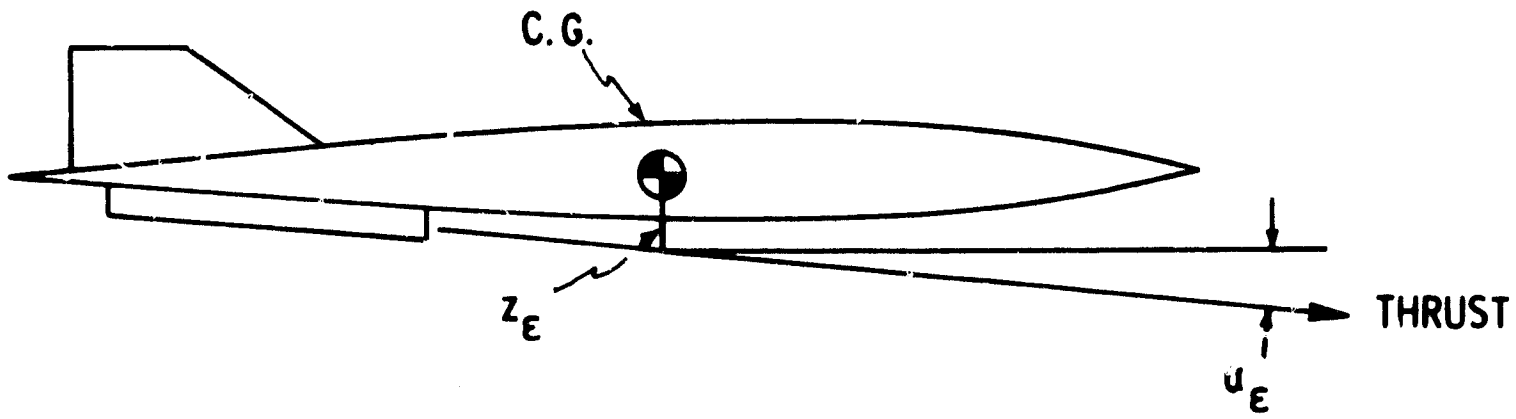

MOMENT OF INERTIA ABOUT THE BODY AXIS $\sim 10^6$ SLUG·FT^2	GEOMETRY	TRIM CONDITIONS
I_{xx} = 4.27	S_{gross} = 9000 ft^2	α_{trim} = 0.8 deg
I_{yy} = 40.2	c_R = 158.0 ft	$\delta_{e\,trim}$ = 0.5 deg
I_{zz} = 44.2	b = 105.7 ft	$C_{L_{trim}}$ = 0.602
I_{xz} = 0.25	z_ϵ = 2.65 ft	$C_{D_{trim}}$ = 0.0945
	ϵ = 0.75 deg	

FLIGHT CONDITIONS	
G.W.	= 381,000 lb.
Mass	= 1.18 x 10^4 slugs
C.G. Loc	= 61.1 % c_R
$\Lambda_{l.e.}$	= 30°
Flap Setting (landing)	30°
h	= sea level, ft
v_{cal}	= 144 knots
γ_o	= -3.0°
v_p	= 224 ft/sec
q	= 71 lb/ft^2
Mach no.	= 0.219

Table E.1-2 Stability Derivatives for Boeing B-2707 SST - Phase IIC in the Landing Approach Configuration

	DRAG	LIFT				PITCH					
	C_{D_α}	C_{L_α}	$C_{L_{\delta e}}$	$C_{L_{\delta ae}}$	$C_{L_{\delta t}}$	C_{m_α}	$C_{m_{\dot{\alpha}}}$	C_{mq}	$C_{m_{\delta e}}$	$C_{m_{\delta ae}}$	$C_{m_{\delta t}}$
RAD.$^{-1}$	0.29	3.152	0.132	0.0625	0.156	-0.043	-0.10	-0.33	-0.0363	-0.0172	-0.043

	ROLL							
	C_{l_β}	C_{l_p}	C_{l_r}	$C_{l_{\delta r}}$	$C_{l_{\delta a}}$	$C_{l_{\delta s}}$	$C_{l_{\delta t}}$	$C_{l_{\delta w}}$
RAD.$^{-1}$	-0.159	-0.547	0.211	0.00372	0.0693	0.0696	0.0407	0.0647

	YAW							
	$C_{n_{\dot{\beta}}}$	C_{n_p}	C_{n_r}	$C_{n_{\delta r}}$	$C_{n_{\delta a}}$	$C_{n_{\delta s}}$	$C_{n_{\delta t}}$	$C_{n_{\delta w}}$
RAD.$^{-1}$	0.0837	-0.0812	-0.239	-0.063	-0.0017	0.0063	-0.00344	0.00315

	SIDE FORCE						
	C_{Y_β}	C_{Y_p}	C_{Y_r}	$C_{Y_{\delta r}}$	$C_{Y_{\delta s}}$	$C_{Y_{\delta t}}$	$C_{Y_{\delta w}}$
RAD.$^{-1}$	-0.229	0.177	0.054	0.12	-0.00011	-0.0143	-0.00007

MAXIMUM DEFLECTION ANGLES AND RATES							
	δ_e	δ_{ae}	δ_t	δ_a	δ_s	δ_w	δ_r
DEG.	±30	-30	±30	±25	±45	±75	±25
DEG./SEC	25	25	25	50	60	-	25

E.2 Additional Aerodynamic Derivatives

Additional aerodynamic derivatives required were analytically derived in the following way:

$$C_{x_u} = -2(C_{D_o} + C_{L_o}\theta_o) - M \cdot \frac{\partial C_D}{\partial M}$$

where M is the Mach number

$$C_{x_\alpha} = C_{L_o} - \left(\frac{\partial C_D}{\partial \alpha}\right)_o$$

$$C_{z_u} = -\frac{M^2}{1 - M^2} \cdot C_{L_o}$$

$$C_{z_\alpha} = -(C_{L_\alpha} + C_{D_o})$$

$$[C_{z_q}]_{tail} = C_{m_q} \cdot \frac{c_R}{l_t}$$

where l_t is the tail moment arm

$$C_{z_{\dot\alpha}} = C_{m_{\dot\alpha}} \cdot \frac{c_R}{l_t}$$

$$C_{m_u} = M \cdot \frac{\partial C_m}{\partial M}$$

Landing Approach Flight Condition

C_{x_u}	C_{x_α}	C_{z_u}	C_{z_α}	C_{z_q}	$C_{z_{\dot\alpha}}$	C_{m_u}	C_{D_o}	$\frac{\partial C_D}{\partial M}$	l_t
-0.106	0.312	-0.0303	-3.235	-0.847	-0.335	-0.00142	0.0833	0.0113	47 feet

E.3 Lift, Drag and Pitching Moment Changes Due to Ground Effect

$$\frac{\Delta C_m}{\Delta h} = -0.000825 \qquad h \leq 63 \text{ ft}$$

$$= 0 \qquad h > 63 \text{ ft}$$

$$\frac{K_{ge}}{\Delta h} = 0.0076 \qquad h \leq 50 \text{ ft}$$

$$= 0 \qquad h > 50 \text{ ft}$$

$$\frac{\Delta C_D}{\Delta h} = -0.00475 \qquad h \leq 80 \text{ ft}$$

$$= 0 \qquad h > 80 \text{ ft}$$

$$\frac{\Delta C_z}{\Delta h} = -0.00313 \qquad h \leq 80 \text{ ft}$$

$$= 0 \qquad h > 80 \text{ ft}$$

Ground Effect Coefficients:

	C_{22}	C_{23}	C_{32}
Feet	50	63	80

APPENDIX F

F. 1 Aerodynamic Force and Moment Corrections

In this Appendix the second-order aerodynamic force and moment corrections, to account for a significant change in airspeed, are developed.

The second partial derivatives are elements of the A matrices involved in the second-order terms of the Taylor series expansions of the aerodynamic force and moment changes. There is, of course, a unique A matrix for each equation of motion.

Assuming that u is the only component of state exceeding the small perturbation restriction, then the only second partial derivatives that need be calculated are those taken at least once with respect to u, the change in airspeed along the X-axis. All the other elements of the A matrices may be put equal to zero. Then the only equations involved will be DRAG, LIFT and PITCH.

Following are the second partial derivatives that must be evaluated.

DRAG

$$X_{uu},\ X_{\alpha u},\ X_{\delta_{sd} u}$$

LIFT

$$Z_{uu},\ Z_{\alpha u},\ Z_{\dot{\alpha} u},\ Z_{qu},\ Z_{\delta_e u},\ Z_{\delta_{ae} u},\ Z_{\delta_t u},\ Z_{\delta_{sd} u},\ Z_{\delta_c u}$$

PITCH

$$M_{uu},\ M_{\alpha u},\ M_{\dot{\alpha} u},\ M_{qu},\ M_{\delta_e u},\ M_{\delta_{ae} u},\ M_{\delta_t u},\ M_{\delta_{sd} u},\ M_{\delta_c u}$$

To estimate these derivatives, the first partial derivatives were evaluated over the expected speed range and the results plotted in Figs. F. 1-1, F. 1-2 and F. 1-3. The aerodynamic information contained in refs (19, 20) together with analytic formulae of Appendix E, were used to evaluate the first partial derivatives.

Reference (20) indicated that the stability derivative with respect to elevator control, $C_{z_{\delta_e}}$, was approximately constant over the limited speed range. In the absence of better information, it was assumed that the non-dimensional stability derivatives with respect to auxiliary elevator and tip controls were also constant over the limited speed range.

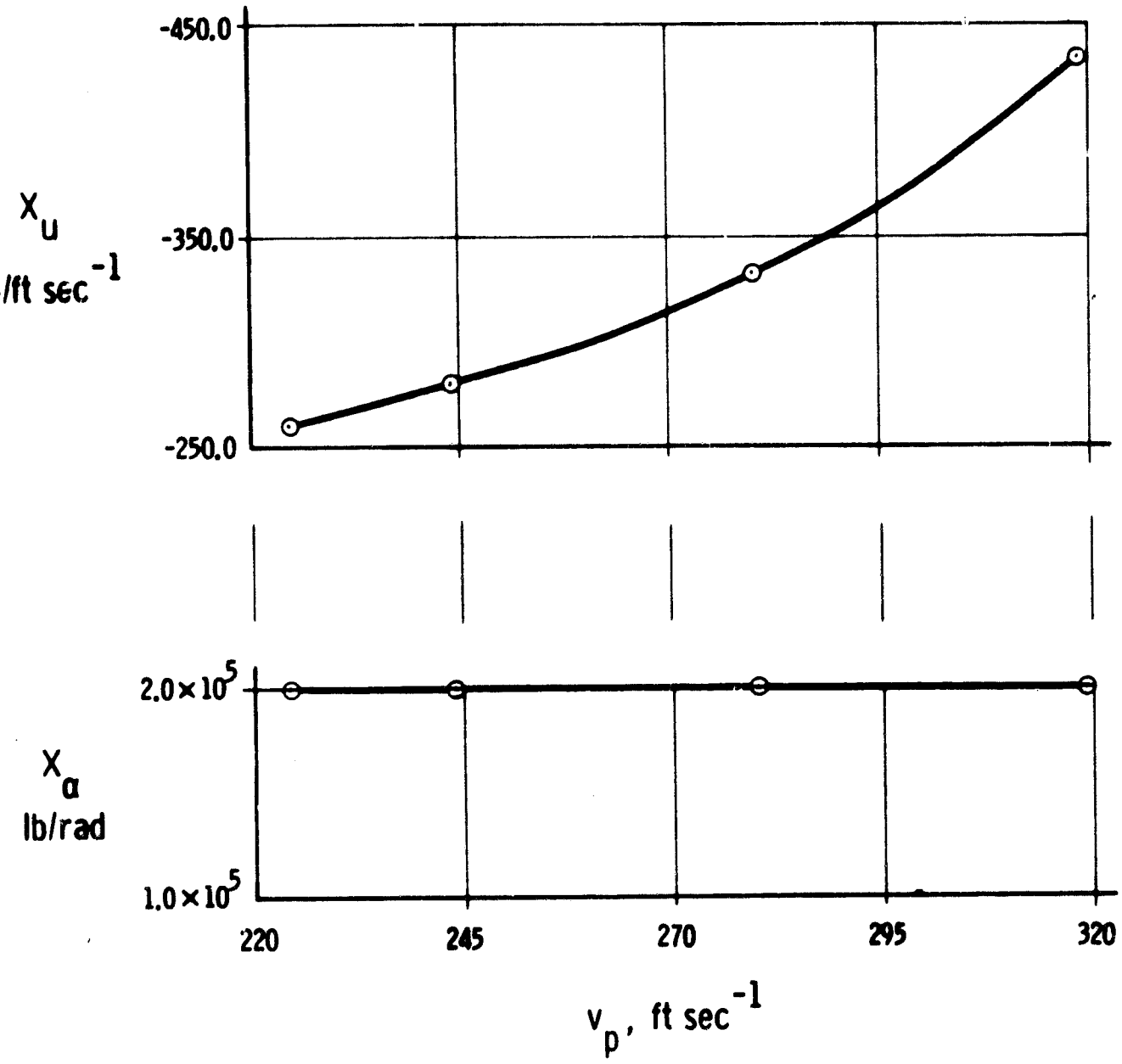

Fig. F-1-1 Variation of X_u, X_α with airspeed, v_p.

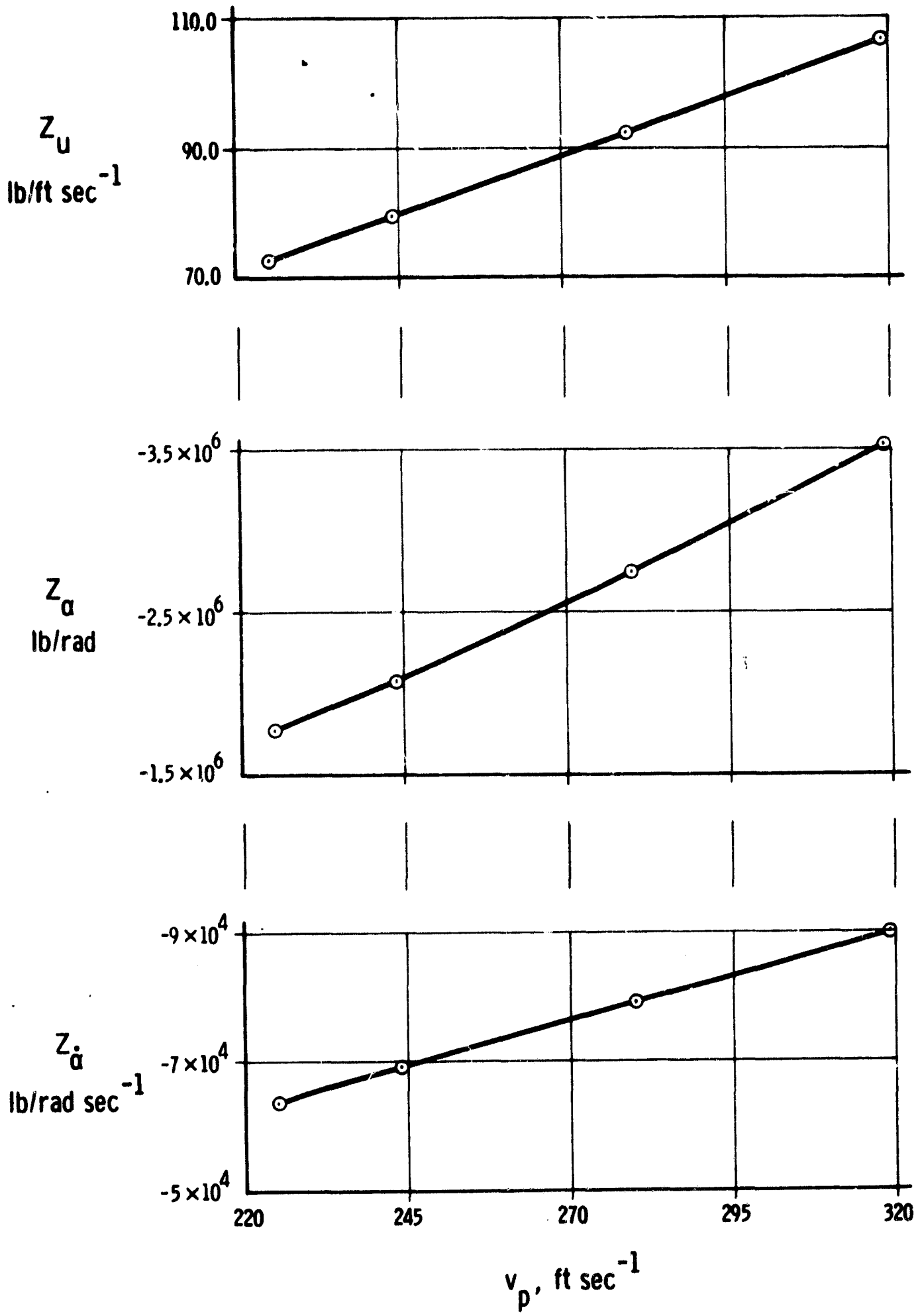

Fig. F. 1-2 Variation of Z_u, Z_α, $Z_{\dot{\alpha}}$ with airspeed, v_p

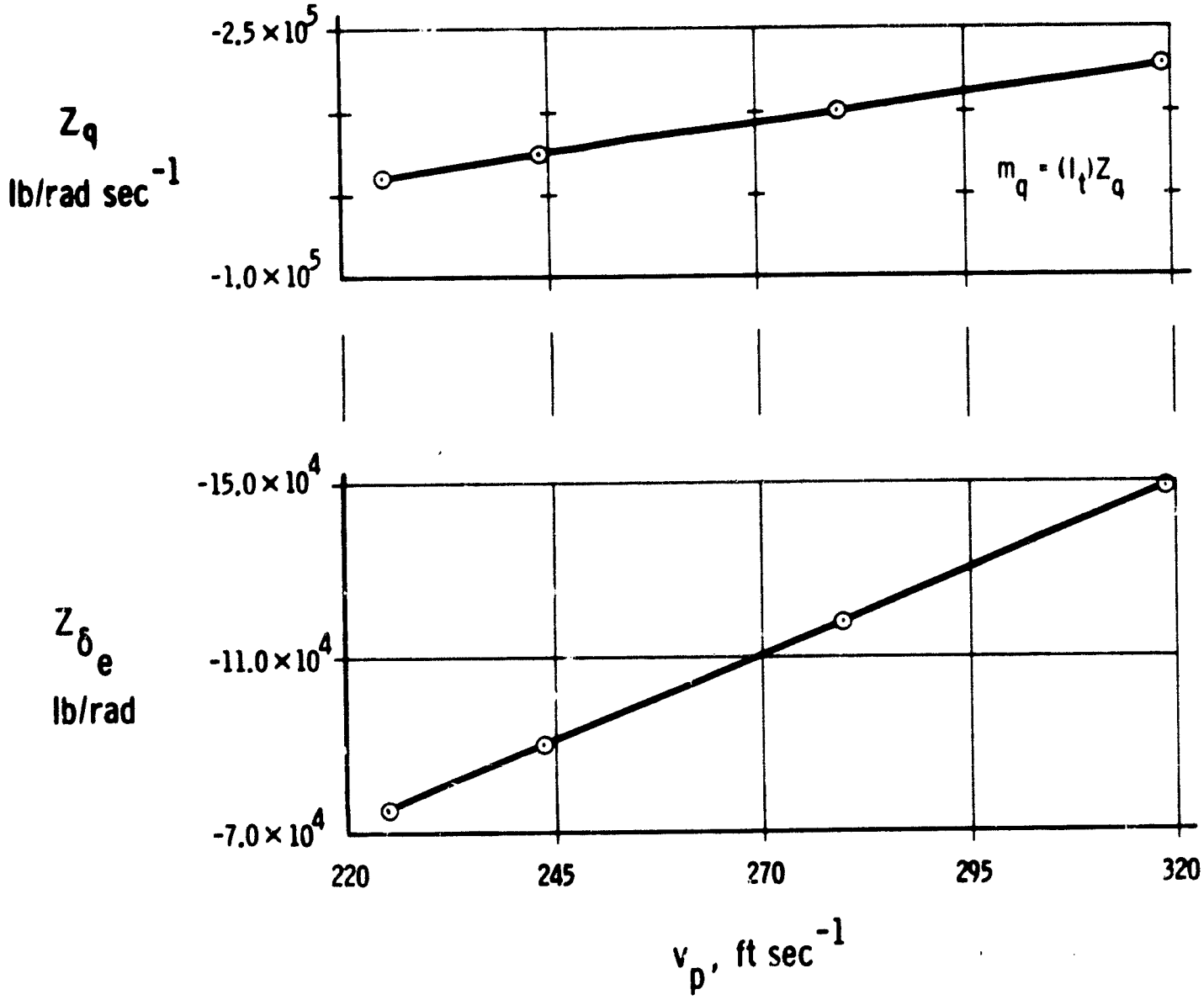

Fig. F. 1-2 (Cont) Variation of Z_q, Z_{δ_e} with airspeed, v_p

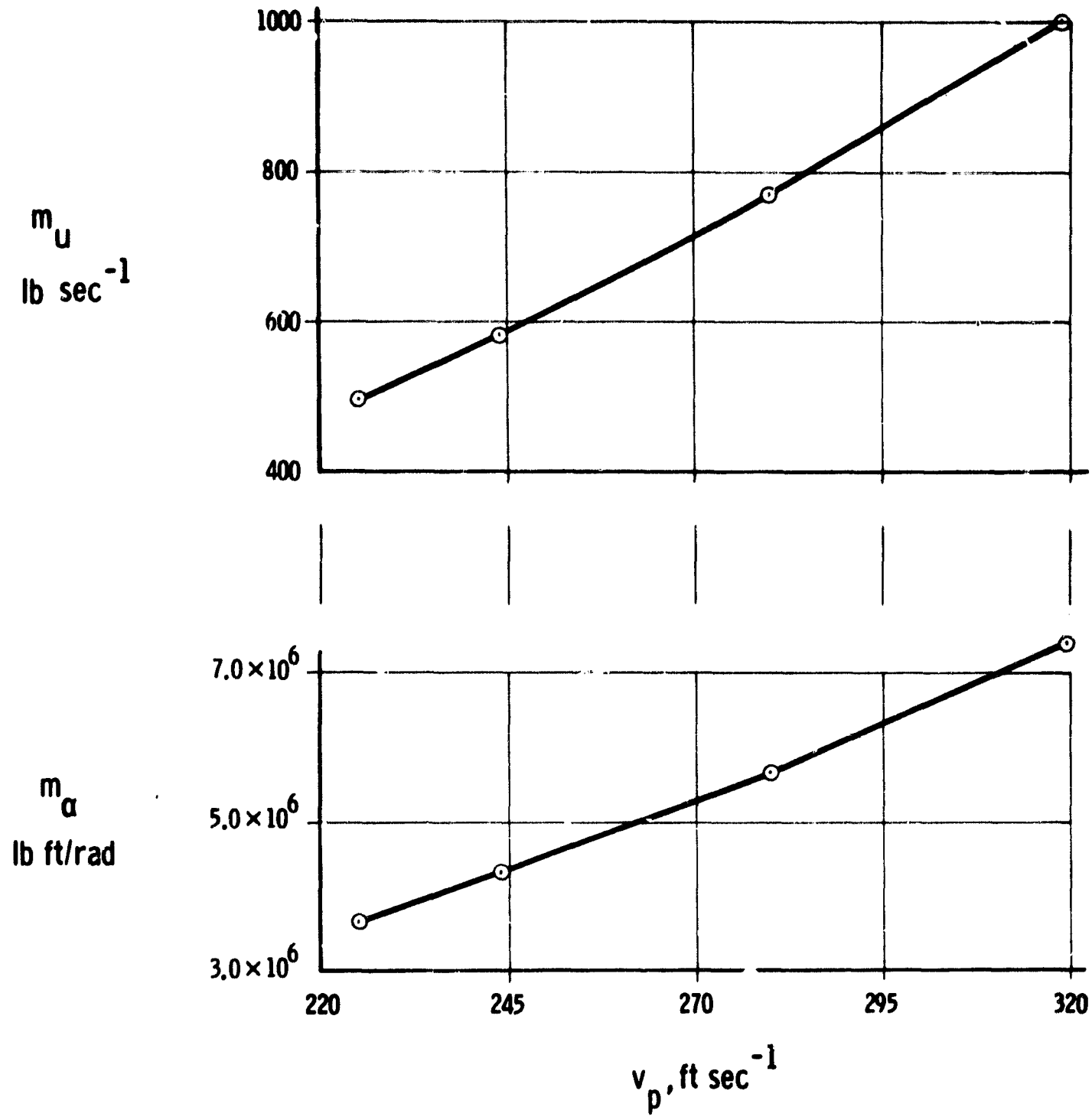

Fig. F. 1-3 Variation of M_u, M_α with airspeed, V_p

REFERENCES

1 Vice, J. R. and Muir, J. C., Final Report - Evaluation of the BLEU Automatic Landing System, FAA Report AD 600829 December 1963.

2 Analog Computer Study of a Category III ILS, Airborne and Ground Equipment Standards, The Bendix Corporation - Eclipse-Pioneer Division FAA Project No. AD 1091, September 1964.

3 Standard Performance Criterion for Autopilot/Coupler Equipment, Radio Technical Commission for Aeronautics Paper No. 31-63/ DO-118 March 14, 1963.

4 Analytical Study of ILS Beam Characteristics for the Systems Research and Development Service, The Bendix Corporation, Eclipse-Pioneer Division. Appendix to ref 3.

5 Blakelock, J. H., Automatic Control of Aircraft and Missiles, John Wiley and Sons, 1965.

6 Etkin, B., Dynamics of Flight, Stability and Control, John Wiley and Sons, 1959.

7 Broxmeyer, C., Inertial Navigation Systems, McGraw Hill, 1964.

8 McDonald, D., "Nonlinear Techniques for Improving Servo Performance," Proceedings of the National Electronics Conference 1950, pp. 400-421.

9 Hopkins, A. M., "A Phase Plane Approach to the Compensation of Saturating Servomechanisms," Transactions of the AIEE, 1951, pp. 631-639.

10 Neiswander, R. S. and MacNeal, R. H., "Optimization of Nonlinear Control Systems by Means of Nonlinear Feedbacks," Transactions of the AIEE, 1953, Part 2.

11 Bogner, I. and Kazda, L. F., "An Investigation of the Switching Criteria for Higher Order Contactor Servomechanisms," Transactions of the AIEE, 1964, Part 2, pp. 118-127.

12 Chang, S. S. L., "Optimum Switching Criteria for Higher Order Contactor Servomechanisms," Transactions of the AIEE, 1955, Part 2, pp. 273-276.

REFERENCES (Cont)

13 Kalman, R. D., "Analysis and Design Principles of Second and Higher Order Saturating Servomechanisms," Transactions of the AIEE, 1955, Part 2, pp. 294-310.

14 Neiswander, R. S., "An Experimental Treatment of Nonlinear Servomechanisms," Transactions of the AIEE, 1956, Part 2, pp. 308-316.

15 Rozonoer, L. I., "L. S. Pontryagin Maximum Principle in the Theory of Optimum Systems," Automatika i Telemekhanika, Vol. 20, Nos. 10-12, November 1959.

16 Pontryagin, L. S., Boltyanskii, V. G., Gamkrelidze, R. V., and Mishehenko, E. F., The Mathematical Theory of Optimal Processes, John Wiley and Sons, 1963.

17 Bryson, A. E. and Ho, Y. C., Optimal Programming, Estimation, and Control, Mimeographed lecture notes, Harvard University, February 1965.

18 Merriam, C. W., Optimization Theory and the Design of Feedback Control Systems, McGraw-Hill, 1964.

19 Boeing letter 9-7310-00-11, November 1967.

20 Willich, W., "B-2707 Stability Derivatives as Mechanized in the Phase IIC Full Mission Profile Simulation," Boeing Report No. D6A10485-1, November 1966, Revision to the above report, No. 2707-AERO-5, January 1967.

21 Etkin, B., "Theory of the Flight of Airplanes in Isotropic Turbulence - Review and Extension," AGARD Report No. 372, April 1961.

22 Kalman, R. E., "A New Approach to Linear Filtering and Prediction Problem," Journal of Basic Engineering, Transactions of the ASME, March 1960.

23 Kalman, R. E. and Bucy, R. S., "New Results in Linear Filtering and Prediction Theory," Journal of Basic Engineering, Transaction of the ASME, March 1961

24 Battin, R. H., "A Statistical Optimizing Navigation Procedure for Space Flight," Report R-341, M. I. T. Instrumentation Laboratory, Cambridge, Mass., May 1962.

25 Brock, L. D., "Application of Statistical Estimation to Navigation Systems," Report R-414, M. I. T. Instrumentation Laboratory, Cambridge, Mass., June 1965.